frontiers | Research Topics

Innovative immunotherapy strategies for enhanced treatment of Hodgkin and non-Hodgkin lymphomas

Edited by
Michael John Robertson, Eric Vivier and Penny Fang

Published in
Frontiers in Immunology

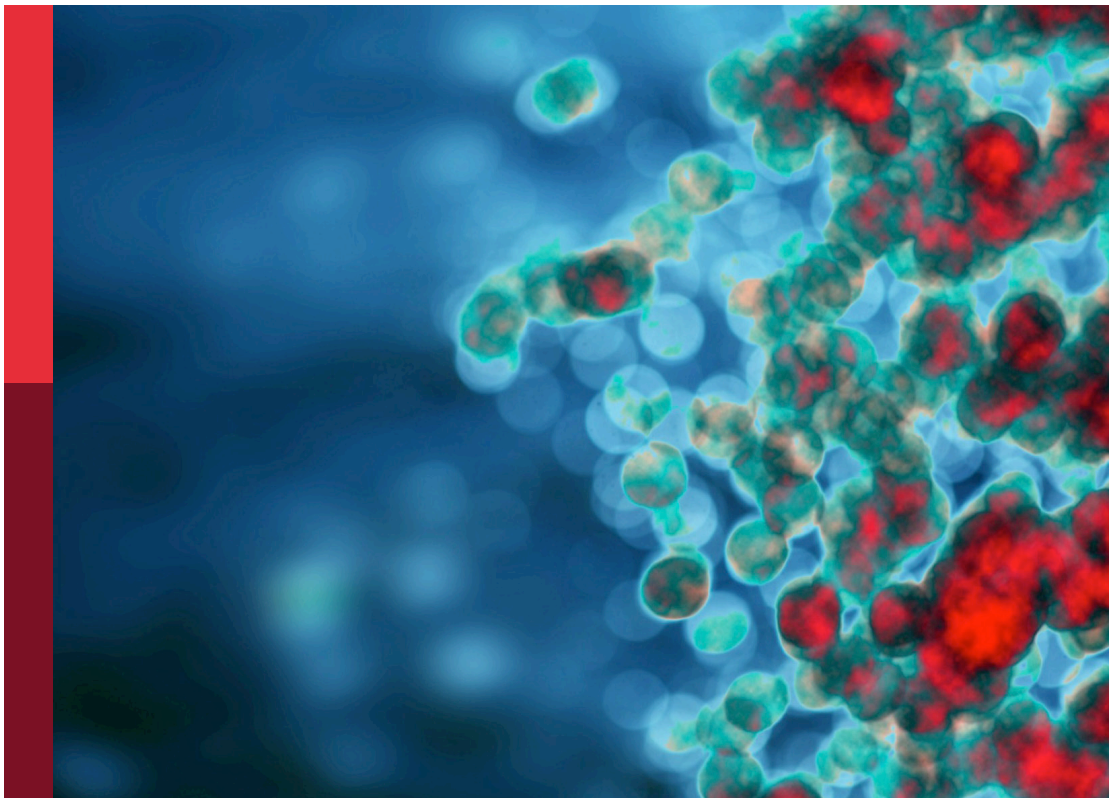

ISSN 1664-8714
ISBN 978-2-8325-6536-0
DOI 10.3389/978-2-8325-6536-0

Generative AI statement
Any alternative text (Alt text) provided alongside figures in the articles in this ebook has been generated by Frontiers with the support of artificial intelligence and reasonable efforts have been made to ensure accuracy, including review by the authors wherever possible. If you identify any issues, please contact us.

About Frontiers

Frontiers is more than just an open access publisher of scholarly articles: it is a pioneering approach to the world of academia, radically improving the way scholarly research is managed. The grand vision of Frontiers is a world where all people have an equal opportunity to seek, share and generate knowledge. Frontiers provides immediate and permanent online open access to all its publications, but this alone is not enough to realize our grand goals.

Frontiers journal series

The Frontiers journal series is a multi-tier and interdisciplinary set of open-access, online journals, promising a paradigm shift from the current review, selection and dissemination processes in academic publishing. All Frontiers journals are driven by researchers for researchers; therefore, they constitute a service to the scholarly community. At the same time, the *Frontiers journal series* operates on a revolutionary invention, the tiered publishing system, initially addressing specific communities of scholars, and gradually climbing up to broader public understanding, thus serving the interests of the lay society, too.

Dedication to quality

Each Frontiers article is a landmark of the highest quality, thanks to genuinely collaborative interactions between authors and review editors, who include some of the world's best academicians. Research must be certified by peers before entering a stream of knowledge that may eventually reach the public - and shape society; therefore, Frontiers only applies the most rigorous and unbiased reviews. Frontiers revolutionizes research publishing by freely delivering the most outstanding research, evaluated with no bias from both the academic and social point of view. By applying the most advanced information technologies, Frontiers is catapulting scholarly publishing into a new generation.

What are Frontiers Research Topics?

Frontiers Research Topics are very popular trademarks of the *Frontiers journals series*: they are collections of at least ten articles, all centered on a particular subject. With their unique mix of varied contributions from Original Research to Review Articles, Frontiers Research Topics unify the most influential researchers, the latest key findings and historical advances in a hot research area.

Find out more on how to host your own Frontiers Research Topic or contribute to one as an author by contacting the Frontiers editorial office: frontiersin.org/about/contact

Innovative immunotherapy strategies for enhanced treatment of Hodgkin and non-Hodgkin lymphomas

Topic editors

Michael John Robertson — Indiana University Bloomington, United States

Eric Vivier — INSERM U1104 Centre d'immunologie de Marseille-Luminy (CIML), France

Penny Fang — University of Texas MD Anderson Cancer Center, United States

Citation

Robertson, M. J., Vivier, E., Fang, P., eds. (2025). *Innovative immunotherapy strategies for enhanced treatment of Hodgkin and non-Hodgkin lymphomas*. Lausanne: Frontiers Media SA. doi: 10.3389/978-2-8325-6536-0

Table of contents

frontiers | Frontiers in Immunology

TYPE Editorial
PUBLISHED 20 June 2025
DOI 10.3389/fimmu.2025.1642505

OPEN ACCESS

EDITED AND REVIEWED BY
Peter Brossart,
University of Bonn, Germany

*CORRESPONDENCE
Michael J. Robertson
mjrobert@iu.edu

RECEIVED 06 June 2025
ACCEPTED 10 June 2025
PUBLISHED 20 June 2025

CITATION
Robertson MJ, Vivier E and Fang P (2025) Editorial: Innovative immunotherapy strategies for enhanced treatment of Hodgkin and non-Hodgkin lymphomas. *Front. Immunol.* 16:1642505. doi: 10.3389/fimmu.2025.1642505

Editorial: Innovative immunotherapy strategies for enhanced treatment of Hodgkin and non-Hodgkin lymphomas

Michael J. Robertson[1]*, Eric Vivier[2] and Penny Fang[3]

[1]Indiana University Melvin and Bren Simon Comprehensive Cancer Center, Indianapolis, IN, United States, [2]Centre d'Immunologie de Marseille-Luminy, Marseille, France, [3]Department of Radiation Oncology, The University of Texas MD Anderson Cancer Center, Houston, TX, United States

KEYWORDS

lymphoma, immunotherapy, CAR (chimeric antigen receptor) T-cell therapy, immune checkpoint inhibitors, monoclonal Abs

Editorial on the Research Topic
Innovative immunotherapy strategies for enhanced treatment of Hodgkin and non-Hodgkin lymphomas

Immunotherapy is a major component of current cancer treatment. Rituximab, one of the first efficacious immunotherapies for cancer, remains integral to treatment regimens for B cell lymphomas. Recent advances include approval of CD19-directed chimeric antigen receptor (CAR) T-cell therapies and CD20 x CD3 bispecific antibodies for relapsed and refractory B cell lymphomas (1, 2). Furthermore, immune checkpoint inhibitors (ICI) and CD30 antibody-drug conjugates have significantly improved treatment outcomes for classic Hodgkin lymphoma (cHL) (2). However clinical results remain suboptimal and further improvement in therapeutic options is needed. The seven original research articles, two case reports, and review article in this Research Project survey promising novel strategies for treatment of lymphoma.

Several articles investigate new approaches for CAR T-cell therapy. Efficacy of CAR T-cell therapy could be enhanced by use of CAR T-cells directed at more than one target antigen (3). Huang et al. and Luo et al. describe the safety and efficacy of dual CD20/CD30- and CD19/CD22-directed autologous CAR T-cells for treatment of aggressive B cell lymphomas. The patient in the report of Huang et al. had diffuse large B cell lymphoma (DLBCL) that had transformed from low-grade follicular lymphoma. The patient had durable complete response after CD20/CD30-directed CAR T-cell therapy even though the malignant cells expressed CD30 only weakly and partially. CD30 antibody-drug conjugate brentuximab vedotin has significant activity in DLBCL irrespective of CD30 expression (4). CD30 could be expressed by tumor cells at levels below the limit of detection by routine immunohistochemistry but sufficient to mediate antitumor activity. CD30-targeted agents could also affect tumor cells indirectly by modifying the tumor microenvironment. The patient did not experience cytokine release syndrome (CRS) or immune effector cell-associated neurotoxicity syndrome (ICANS).

Luo et al. took a sequential approach to treat a patient with refractory Burkitt lymphoma. High-dose chemotherapy and autologous peripheral blood stem cell

transplantation was done to reduce tumor bulk and as lymphodepletion, followed by infusion of CD19/CD22-directed CAR T-cells. Maintenance treatment with anti-PD-1 antibody tislelizumab was given after the patient achieved complete response. In addition to employing a dual targeting extracellular domain, the third generation CAR used in this study had a novel intracellular signaling domain that included a CD3 zeta motif and costimulatory elements of CD28 and TLR2.

After apheresis has been done to collect autologous lymphocytes, bridging therapy is often needed to prevent rapid disease progression while awaiting production of CAR T-cells (5). Radiotherapy may offer advantages compared to chemotherapy for bridging therapy (5, 6). Ruan et al. have investigated the feasibility and potential mechanism of action of hyper-fractionated radiotherapy as bridging treatment prior to CD19-directed CAR T-cell therapy. Hyper-fractionated radiotherapy was safe and effective and, within limitations of an uncontrolled study, did not appear to affect incidence of CRS or ICANS. Exploratory studies suggested that bridging radiotherapy may have immunomodulatory effects.

Non-viral gene transfer techniques have been explored as an alternative to retroviral or lentiviral vectors for production of CAR T-cells. Transposon DNA plasmids (such as Sleeping Beauty and piggyBac) have significant advantages, including reduced production costs and immunogenicity compared to viral vectors, but are limited by lower transduction efficiency (7). Mucha et al. describe a novel procedure for non-viral production of CAR T-cells involving piggyBac transposons and irradiated allogeneic feeder cells. This approach allowed large scale production of clinical grade CD19-directed autologous CAR T-cells that were used successfully in clinical trials.

ICI have shown impressive activity for treatment of cHL and primary mediastinal large B cell lymphoma, but efficacy of ICI for most other types of non-Hodgkin lymphoma has been limited. Ricard et al. studied ICI-based treatment of angioimmunoblastic T-cell lymphoma (AITCL). The tumor microenvironment of AITCL often contains EBV-infected immunoblasts that promote overexpression of PD-L1 (8). Furthermore, mutations in genes regulating DNA methylation, including *TET2* and *DNMT3A*, are seen in peripheral T cell lymphomas, including AITCL (8, 9). Therefore Ricard et al. used hypomethylating agent 5-azacytidine together with ICI nivolumab to treat patients with AITCL. Treatment was well tolerated and overall response rate was 78%.

Ruggeri et al. examined expression of serine/threonine kinase CK2 in cHL. CK2a was overexpressed in cHL cell lines and Reed-Sternberg cells of patients with cHL. Silmitasertib, an inhibitor of CK2α, caused apoptosis of cHL cell lines and decreased expression of PD-L1. Thus CK2a may be a target for innovative therapies of cHL.

Rituximab, a type I chimeric CD20 monoclonal antibody (mAb) of IgG1 isotype, has revolutionized the treatment of B cell lymphomas. The mechanism of action of rituximab is complex and may involve antibody-dependent cellular phagocytosis (ADCP) by monocytes and macrophages, antibody-dependent cellular cytotoxicity by NK cells, and complement-dependent cytotoxicity. Nguyen et al. show that a CD20 mAb of IgG2 isotype (rituximab-IgG2) can enhance ADCP induced by different isotypes of rituximab and other therapeutic mAb. Rituximab-IgG2 augments ADCP in part by causing downregulation of CD47 on lymphoma cells. Rituximab-IgG2 also induced more apoptosis of lymphoma cells than rituximab-IgG1 or rituximab-IgG3.

Fan et al. investigated the causal relationship between metabolites, immune cell phenotypes, and risk of lymphoma and chronic lymphocytic leukemia (CLL) in Mendelian randomization analysis. Several metabolites and immune cell phenotypes were associated with different subtypes of lymphoma. However, evidence that immune cell phenotype was responsible for the effect of metabolites on risk of lymphoma was found only for DLBCL and CLL.

Wang et al. conducted a retrospective study of clinical characteristics of marginal zone lymphoma (MZL) and its response to treatment in the era of immunotherapy. MZL is a low-grade B cell lymphoma with three subtypes: extranodal MZL of mucosa-associated lymphoid tissue (MALT lymphoma), nodal MZL, and splenic MZL (10). Among 265 newly diagnosed patients with MZL reported by Wang et al., 66% had MALT lymphoma and the remaining cases were about equally distributed between nodal and splenic MZL. Overall response rates did not differ between patients receiving rituximab plus chemotherapy versus obinutuzumab plus chemotherapy. However, in a subgroup analysis of 51 patients with high tumor burden the overall response rate favored obinutuzumab over rituximab. This observation requires confirmation in prospective studies with larger numbers of patients that have high tumor burden.

Primary large B cell lymphomas of immune-privileged sites include primary DLBCL of the central nervous system (PCNSL), primary vitreoretinal DLBCL (PVRL), and primary testicular DLBCL (PTL). These aggressive lymphomas were grouped together in the 5th Edition of the World Health Organization Classification of Lymphoid Neoplasms based on their common biological features (11). Wang et al. have reviewed the epidemiology, pathogenesis, prognosis, and therapy of PCNSL, PVRL, and PTL. They discuss several novel therapeutic approaches involving small molecule inhibitors, antibody-drug conjugates, bispecific antibodies, and CAR-T cells for treatment of these challenging diseases. Finally, one should also consider the development of Natural Killer cell engagers which are in clinical trial in non-Hodgkin B cell lymphomas (12).

Author contributions

MR: Writing – review & editing, Writing – original draft. EV: Writing – review & editing. PF: Writing – review & editing.

Conflict of interest

The authors declare that the research was conducted in the absence of any commercial or financial relationships that could be construed as a potential conflict of interest.

The author(s) declared that they were an editorial board member of Frontiers, at the time of submission. This had no impact on the peer review process and the final decision.

Generative AI statement

The author(s) declare that no Generative AI was used in the creation of this manuscript.

Publisher's note

References

1. Haydu JE, Abramson JS. The rules of T-cell engagement: current state of CAR T cells and bispecific antibodies in B-cell lymphomas. *Blood Adv*. (2024). doi: 10.1182/bloodadvances.2021004535

2. Atallah-Yunes SA, Robertson MJ. Current and emerging monoclonal antibodies, antibody-drug conjugates, and bispecific antibodies in treatment of lymphoma. *Leuk Res Rep*. (2022). doi: 10.1016/j.lrr.2022.100319

3. Canedo GO, Roddie C, Amrolia PJ. Dual-targeting CAR T cells for B-cell acute lymphoblastic leukemia and B-cell non-Hodgkin lymphoma. *Blood Adv*. (2025). doi: 10.1182/bloodadvances2024013586

4. Bartlett NL, Hahn U, Kim W-S, Fleury I, Laribi K, Bergua J-M, et al. Brentuximab vedotin combination for relapsed diffuse large B-cell lymphoma. *J Clin Oncol*. (2025) 43:1061–72. doi: 10.1200/JCO-24-02242

5. Pinnix CC, Gunther JR, Dabaja BS, Strati P, Fang P, Hawkins MC, et al. Bridging therapy prior to axicabtagene ciloleucel for relapsed/refractory large B-cell lymphoma. *Blood Adv*. (2020). doi: 10.1182/bloodadvances.2020001837

6. Saifi O, Lester SC, Breen WG, Rule WG, Lin Y, Bennani NN, et al. Incorporating radiation with anti-CD19 chimeric antigen receptor T-cell therapy for relapsed/refractory non-Hodgkin lymphoma: a multicenter consensus approach. *Am J Hematol*. (2024) 99:124–34. doi: 10.1002/ajh.27155

7. Moretti A, Ponzo M, Nicolette CA, Tcherepanova IY, Biondi A, Magnani CF. The past, present, and future of non-viral CAR T cells. *Front Immunol*. (2022) 13. doi: 10.3389/fimmu.2022.867013

8. Lage LA, Culler HF, Reichert CO, Coelho da Siqueira SA, Pereira J. Angioimmunoblastic T-cell lymphoma and correlated neoplasms with T-cell follicular helper phenotype: from molecular mechanisms to therapeutic advances. *Front Oncol*. (2023) 13. doi: 10.3389/fonc.2023.1177590

9. Atallah-Yunes SA, Robertson MJ, Dave UP. Epigenetic aberrations and targets in peripheral T-cell lymphoma. *Clin Lymph Myeloma Leuk*. (2022) 22:659–65. doi: 10.1016/j.clml.2022.04.015

10. Cheah CY, Seymour JF. Marginal zone lymphoma: 2023 update on diagnosis and management. *Am J Hematol*. (2023) 98:1645–57. doi: 10.1002/ajh.27058

11. Alaggio R, Amador C, Anagnostopoulos I, Attygalle AD, Araujo IB, Berti E, et al. The 5th edition of the world health organization classification of haematolymphoid tumours: lymphoid neoplasms. *Leukemia*. (2022). doi: 10.1038/s41375-022-01620-2

12. Demaria O, Habif G, Vetizou M, Gauthier L, Remark R, Chiossone L, et al. A tetraspecific engager armed with a non-alpha IL-2 variant harnesses natural killer cells against B cell non-Hodgkin lymphoma. *Sci Immunol*. (2024) 9(101):eadp3720. doi: 10.1126/sciimmunol.adp3720

frontiers | Frontiers in Immunology

TYPE Original Research
PUBLISHED 14 May 2024
DOI 10.3389/fimmu.2024.1393485

OPEN ACCESS

EDITED BY
Michael John Robertson,
Indiana University Bloomington, United States

REVIEWED BY
Elisabetta Dondi,
Université Sorbonne Paris Nord, France
Richard Eric Davis,
University of Texas MD Anderson Cancer Center, United States

*CORRESPONDENCE
Andrea Visentin
andre.visentin@aopd.veneto.it
Livio Trentin
livio.trentin@unipd.it

RECEIVED 29 February 2024
ACCEPTED 25 April 2024
PUBLISHED 14 May 2024

CITATION
Ruggeri E, Frezzato F, Mouawad N, Pizzi M, Scarmozzino F, Capasso G, Trimarco V, Quotti Tubi L, Cellini A, Cavarretta CA, Ruocco V, Serafin A, Angotzi F, Danesin N, Manni S, Facco M, Piazza F, Trentin L and Visentin A (2024) Protein kinase CK2α is overexpressed in classical hodgkin lymphoma, regulates key signaling pathways, PD-L1 and may represent a new target for therapy.
Front. Immunol. 15:1393485.
doi: 10.3389/fimmu.2024.1393485

Protein kinase CK2α is overexpressed in classical hodgkin lymphoma, regulates key signaling pathways, PD-L1 and may represent a new target for therapy

Edoardo Ruggeri[1], Federica Frezzato[1], Nayla Mouawad[1], Marco Pizzi[2], Federico Scarmozzino[2], Guido Capasso[1], Valentina Trimarco[1], Laura Quotti Tubi[1], Alessandro Cellini[1], Chiara Adele Cavarretta[1], Valeria Ruocco[1], Andrea Serafin[1], Francesco Angotzi[1], Nicolò Danesin[1], Sabrina Manni[1], Monica Facco[1], Francesco Piazza[1], Livio Trentin[1]* and Andrea Visentin[1]*

[1]Hematology Unit, Department of Medicine (DIMED), University of Padova, Padova, Italy, [2]Surgical Pathology and Cytopathology Unit, Department of Medicine, University of Padova, Padova, Italy

Introduction: In classical Hodgkin lymphoma (cHL), the survival of neoplastic cells is mediated by the activation of NF-κB, JAK/STAT and PI3K/Akt signaling pathways. CK2 is a highly conserved serine/threonine kinase, consisting of two catalytic (α) and two regulatory (β) subunits, which is involved in several cellular processes and both subunits were found overexpressed in solid tumors and hematologic malignancies.

Methods and results: Biochemical analyses and *in vitro* assays showed an impaired expression of CK2 subunits in cHL, with CK2α being overexpressed and a decreased expression of CK2β compared to normal B lymphocytes. Mechanistically, CK2β was found to be ubiquitinated in all HL cell lines and consequently degraded by the proteasome pathway. Furthermore, at basal condition STAT3, NF-kB and AKT are phosphorylated in CK2-related targets, resulting in constitutive pathways activation. The inhibition of CK2 with CX-4945/silmitasertib triggered the de-phosphorylation of NF-κB-S529, STAT3-S727, AKT-S129 and -S473, leading to cHL cell lines apoptosis. Moreover, CX-4945/silmitasertib was able to decrease the expression of the immuno-checkpoint CD274/PD-L1 but not of CD30, and to synergize with monomethyl auristatin E (MMAE), the microtubule inhibitor of brentuximab vedotin.

Conclusions: Our data point out a pivotal role of CK2 in the survival and the activation of key signaling pathways in cHL. The skewed expression between CK2α and CK2β has never been reported in other lymphomas and might be specific for cHL. The effects of CK2 inhibition on PD-L1 expression and the synergistic combination of CX-4945/silmitasertib with MMAE pinpoints CK2 as a high-impact target for the development of new therapies for cHL

KEYWORDS

classical hodgkin lymphoma, anti-CD30, MMAE, CK2, PD-L1

Introduction

Classical Hodgkin's lymphoma (cHL) is an uncommon malignancy of the lymphatic system, usually affecting young adults (1, 2). Although the treatment of patients with cHL has improved with the combination or the sequential use of drugs targeting CD30 [such as the anti-CD30 monoclonal antibody conjugated with the monomethyl auristatin E (MMAE) brentuximab vedotin] and immune checkpoint PD-1 inhibitors (such as pembrolizumab and nivolumab) with chemotherapy, the outcome of double or triple refractory patients is still poor. Therefore, new targeted therapies with innovative mechanisms of action and new drug combinations are urgently needed (3–5). The mononuclear Hodgkin's cells alongside the prominent presence of large, bi- or multinucleated Reed-Sternberg (HRS) cells, which account for less than 2% of the total tumor bulk, display a constitutive pattern of activated signaling pathways due to EBV infection, microenvironment interaction and gene mutations that drive to activation of among others, NF-κB (nuclear factor kappa B), JAK/STAT3 (Janus Kinase/Signal transducer and activator of transcription factor 3), and PI3K/Akt (Phosphoinositide 3-kinase/RACα serine/threonine protein kinase) pathways (6). For some of these pathways clinically inhibitors have already been developed and used in different hematological malignancies [i.g., PI3K/Akt inhibitors (7) or JAK1/2 inhibitor (8–10)]. Additionally, these oncogenic pathways regulate the expression of PD-L1 (programmed death ligand 1). Through its interaction with PD-1, PD-L1 assumes a pivotal role in modulating mechanisms related to immunosuppression and T-cell exhaustion (5).

Protein CK2 is a constitutively active and highly conserved serine/threonine kinase, that has reached increasing visibility as a potential pharmacological target (5, 11). Structurally, CK2 is a tetrameric holoenzyme, composed of two catalytic α and/or α′, and two regulatory β subunits, in the possible configurations α2β2, αα′β2, or α′2β2 (12). The CK2 α and β dimers may also be present as dimer which seems to associated with distinct and specific functions (13). It is well documented that CK2 is involved in a wide range of biological processes, such as cell proliferation, differentiation, apoptosis and DNA damage repair (14, 15). Our group has demonstrated that both CK2α and CK2β subunits are overexpressed in acute leukemias, multiple myeloma and non-Hodgkin lymphomas (15–18). CK2 mediates the phosphorylation of NF-κB p65 (RelA) directly on Serine 529 (S529), of STAT3 on S727 and of AKT on S129, promoting the survival of neoplastic cells as well as drug resistance (19).

In this study we investigated the expression of CK2α and CK2β in a panel of HL cell lines and HL patient samples, analyzed CK2 mediated activation of survival signaling pathways and investigated the capability of inhibiting CK2 with the ATP-competitive inhibitor CX-4945/Silmitasertib along with MMAE to trigger HRS cell apoptosis and assess PD-L1 expression levels. These findings present a novel potential target to overcome resistance or to increase MMAE cytotoxicity.

Methods

Cell cultures and treatments

L-428, L-540, HDLM-2, and KM-H2 HL cell lines were kindly provided from Prof. Carmelo Carlo-Stella from Humanitas Hospital (Milan, Italy). The expression of the immuno-phenotypic markers of the HL lines is reported in the Supplementary Table S1. Testing for Mycoplasma infection was carried at a monthly basis. As positive controls, we used Kasumi-1 cells, an M2 acute myeloid leukemia cell line (Liebniz Institute Germane Collection of Microorganism and Cell Cultures DSMZ, Germania). Healthy donor B cells, serving as the normal control, were isolated from buffy-coat using EasySep™ kits (STEMCELL Technologies, USA). Two×10^6 cells for each HL cell line were resuspended in 1ml of appropriate culture medium and plated in 12/24-well plates. Cells were incubated at different time points (24, 48, and 72 hours) with medium only or with CX-4945/Silmitasertib 0, 5, 10, and 15μM (provided from Selleck Chemicals, Munich - Germany) or with MMAE 5nM (20) (monomethyl auristatin E; Selleck Chemicals). For specific experiments HL cell lines were also treated (2x10^6/ml) with the proteasome inhibitor Bortezomib (BTZ) 10nM up to 36 hours (Selleck Chemicals).

Flow cytometry

Aliquots of 100×10^5 HL cell lines were harvested, washed in PBS 1x, and incubated for 10 min in the dark at room temperature and co-stained with the following antibodies: CD20 (APC-H7 conjugated), CD30 (PE conjugated) (Becton Dickinson; Franklin Lakes, NJ, USA), CD274/PD-L1 (PE-Cy7 conjugated, Fisher Scientific; Hampton, NH, USA). After incubation with antibody, cells were washed with PBS and analyzed by the flow cytometry. For each sample, 20,000 events were acquired and analyzed using the FACSCanto II™ A cytometer and data were processed using the DIVA Software (Becton Dickinson). For each antibody the mean fluorescence intensity was reported as compared to the untreated condition.

Evaluation of apoptosis

Apoptosis of different cell samples (pathological cells from different HL cell lines, normal B lymphocytes) were assessed using the Annexin V/Propidium Iodide (PI) staining (Apoptosis Detection Kit, Valter Occhiena, Turin, Italy), and by detection of PARP cleavage in western blotting (21).

Assessment of drug concentration-effect and calculation of the combination index

L-428, L-540, HDLM-2, and KM-H2 HL cell lines were plated into 48 well plates (2×10^5 cells/ml) in appropriate culture medium. CX-4945, MMAE were added at different concentrations: CX-4945 ranging from 1μM to 25μM and of MMAE ranging from 0.05nM to 10nM for 72h alone or in combination. Cell viability was measured through Trypan blue exclusion dye assay. The concentration of the single drug able to kill the 50% of cells (EC50) was determined by fitting the dose-response curve utilizing the Prism 7 software (GraphPad Software Inc. La Jolla, CA, USA). To calculate the Combination Index, cells were treated with a combination of CX-4945 and MMAE using the method of constant ratio drug combination proposed and described by Chou and Talalay (22).

Western blot and antibodies

Whole cell extracts (WCE) were obtained by RIPA Lysis and extraction buffer (Tris-HCL 20mmol/l, NaCl 150mmol/l, EDTA 5.0mmol/l, Niaproof 1.5%, Na3VO4 1.0mmol/l, SDS 0.1%, Thermo Fisher Scientific, Waltham, MA, USA), added with protease inhibitors (Halt Protease Inhibitor Cocktail, Thermo Fisher Scientific), phosphatase inhibitors (Phosphatase Inhibitor Cocktail, Thermo Fisher Scientific), and EDTA (Thermo Fisher Scientific) on ice. Nuclear and cytoplasmic Subcellular Fractionation were prepared using a commercial kit (Thermo Scientific, Rockford, IL, USA). The supernatant was quantified by BCA protein quantification assay (Thermo Fisher Scientific). Equal amounts of protein sample were added to 3× Red loading sample buffer (Cell Signaling Technology, Danvers, USA) and boiled for 5 min. Western blotting was conducted according to standard protocols (23). Briefly, 15 to 25 μg of WCE or nuclear and cytoplasmic fractions were subjected to SDS-PAGE, transferred to Nitrocellulose/PVDF membranes and immunoblotted with the following primary antibodies: anti-Akt-Ser129or anti-Akt-Ser473 (Cell Signaling), anti-Akt, anti-STAT3-Ser727, anti-STAT3 (Abcam, Cambridge, UK), anti-CK2β and anti-CK2α (kindly provided by Prof. Maria Ruzzene, University of Padova), anti-NF-κB-Ser529 (p65) (Cell Signaling), anti-NF-κB-p65 (Abcam), anti-PARP (Cell Signaling), mono- and polyubiquitinylated protein conjugates (Enzo Life Science Ltd, Exeter, UK), anti-β-actin (Sigma-Aldrich, St. Louis, MO), anti-α-tubulin (Sigma Aldrich), anti-GAPDH (Cell Signaling). Detection was performed using chemiluminescence reaction (ECL, Euroclone, Milan, Italy). Images were acquired using the Amersham Imager 600 (GE Healthcare; Chicago, IL, USA), the protein bands were scanned and quantified by densitometry, using the Image J program (Github, San Francisco, USA).

Immunoprecipitation

HL cell lines (L-540, L-428, HDLM-2, KM-H2) were lysed in Blast R™ Lysis Buffer by Signal-Seeker™ Kit (Cytoskeleton-Thermofisher Scientific) and the enriched total ubiquitinated proteins from HL cell line lysates were pulled out by an affinity beads system. Ubiquitinated protein fractions were obtained from 1mg total protein lysates. After extensive washes in IP buffer the immunocomplex was resuspended in Laemmli buffer with β-mercaptoethanol and processed for WB analysis.

Confocal microscopy analysis

Aliquots of the different cell samples (pathological cells from different HL cell lines and normal B lymphocytes from healthy subjects) were collected, washed and plated on poly-L-lysine coated slides for 15 min at RT. Cells were then fixed in 4% paraformaldehyde for 10min, washed twice with PBS 1x and permeabilized with 0,1% Triton X-100 (Sigma-Aldrich) for 4 min (24). Before staining, non-specific protein binding were blocked by incubating the slides for at least 30 min in 2% BSA. Cells were then stained with antibodies against CK2α and CK2β (the same used for WB) and DAPI for nuclear staining, washed three times with PBS and incubated with anti-mouse-Alexa488 secondary antibody for 30 minutes in the dark. Slides were mounted with cover slips and fluorescence was detected using the UltraView LCI confocal system (Perkin Elmer; Waltham, MA, USA) equipped with a fluorescence filter set for excitation at 488 and 360nm.

Tissue microarray

Tissue microarrays were prepared from cases with adequate diagnostic material, as previously reported (25). In details, tumor areas enriched in HRS cells were selected and 3 tissue cores (diameter=1 mm) were obtained from each donor block. Appropriate positive and negative controls were also included.

The tissue microarray was prepared by using the Galileo TMA CK3500 arrayer (Integrated System Engineering; Milan – Italy. Immunohistochemical staining for CK2α (EP1963Y, Epitomics, CA, USA) and CK2β (PA5-27416, ThermoFisher, Massachusetts, USA) were performed in duplicate. Antigen retrieval was performed with heat/ethylenediamine-tetra-acetic acid (EDTA) in an automated immunostainer (University Hospital of Padova). All cases with discordant immunohistochemical results were assessed in joint sessions at the microscope by two haemato-pathologists. The positivity for CK2α and CK2β were graded as: 0 = negative; 1 = positive <30% of HRS; 2 = positive 30-60% HRS or week-moderate intensity; 3 = positive >60% HRS or strong diffuse intensity. The clinical features, including age, sex and therapies of the 25 analyzed patients are summarized in Supplementary Table S2. Inclusion criteria were diagnosis of cHL before 2000 and having signed the informed consent. This part of the study was conducted according to the declaration of Helsinki, approved by the ethic committee of the Padova University Hospital (protocol # 4,089/AO/17) and informed consents were collected.

Quantitative real-time PCR

Total cellular RNA was extracted from the four HL cell lines, Kasumi, and purified healthy B lymphocytes, using the RNeasy Mini Kit (Qiagen, Germany). cDNA was generated by Reverse Transcription System (Promega, USA). SYBR Green (FastStart Universal SYBR Green Master, ROX) real-time polymerase chain reaction (RT-PCR) was carried out in a Sequence Detection System 7000 (Applied Biosystem) with the ABI PRISM 7000 software (AppliedBiosystems, Foster City, CA). The primers used are the following: *CSNK2A1* (CK2α): Forward 5′-3′ GTTTGGGTTGTAT GCTGGCA and Reverse 5′-3′ TTTCGAGAGTGTCTGCCCAA; *CSNK2A2* (CK2α'): Forward 5′-3′ CGACCATCAACAGAGAC TGACTG and Reverse 5′-3′ GTGAGACCACTGGAAAGCAC AG; *CSNK2B* (CK2β): Forward 5′-3′ TCCTTACCAACCGTGGC ATC and Reverse 5′-3′ CATGCACTTGGGGCAGTAGA; *ACTIN* (β-actin): Forward 5′-3′ CCAGCTCACCATGGATGATG and Reverse 5′-3′ ATGCCGGAGCCGTTGTC.

Statistical analysis

Statistical analyses were performed using Prism 7 (GraphPad Software Inc. La Jolla, CA, USA) for paired Student's *t* test, *Kruskall-Wallis*, and *Mann-Whitney Test*, *Wilcoxon matched-pairs signed rank test*. Data are reported as mean ± standard deviation (SD). $p<0.05$ or less were considered statistically significant.

Results

CK2 subunits are unbalanced in cHL

We assessed expression of CK2 subunits in cHL cell lines. By WB, we found that all the four HL-derived cell lines L-428, L-540, KM-H2 and HDLM-2 expressed higher levels of the catalytic subunit CK2α than normal B lymphocytes (Figure 1A). As positive control, we stained protein extracts from Kasumi-1 cell line, which notably shows high expression levels of both the CK2 subunits (26). The median densitometry of CK2α/Tubulin for each cell lines was 0.46 ± 0.05 ($p=0.0250$), 0.51 ± 0.10 ($p=0.0285$), 0.86 ± 0.05 ($p=0.0005$), 0.89 ± 0.05 ($p=0.0044$) and 0.26 ± 0.09 for L-428, HDLM-2, L-540, KM-H2 and normal B-cell from heathy donors (Figures 1A, B). The median CK2α/Tubulin ratio in HL cell lines was 2.7-fold higher than healthy B lymphocytes ($p=0.0044$) (Figure 1B). Conversely, the non-catalytic subunit CK2β was found to be expressed at lower levels as compared to normal B lymphocytes ($p<0.05$) (Figure 1A). The median densitometry of CK2β/Tubulin was 0.07 ± 0.03 ($p<0.0001$), 0.20 ± 0.02 ($p<0.0001$), 0.31 ± 0.10 ($p=0.0009$), 0.47 ± 0.10 ($p=0.0025$) and 0.98 ± 0.09 for L-428, HDLM-2, L-540, KM-H2 and B-cell from heathy donors (Figures 1A, C). The median CK2β/Tubulin ratio in HL cell lines was 3.8-fold fewer than B lymphocytes ($p=0.0040$) (Figure 1C).

Immunofluorescence experiments (Figure 1D) revealed a strong and diffuse signal for CK2α in HL cells, while CK2β exhibited a lower intensity signal, particularly in the KM-H2 and HDLM-2 cell lines. CK2α seems to be localized both in the nucleus and cytosol of HRS cells, including the formation of discrete foci, as observed in the L-428 and KM-H2 cell lines. Instead, CK2β exhibits a diffuse and weak signal with a less distinct localization which hampers the quality of picture. In order to determine the subcellular distribution of α and β subunits more precisely in HL cell lines, we analyzed subcellular protein fractions, unveiling the presence of CK2α in both the nuclear and cytosolic compartments of HL cell lines. In contrast, CK2β predominantly localizes to the cytosol but exhibits a faint representation in the nuclear compartment of the L-540 and L-428 cell lines (Figure 1E).

To assess whether the dysregulation among CK2 subunits was linked to alterations in CK2 mRNA levels, we performed RT-PCR analysis on the mRNA of CK2 catalytic (α - *CSNK2A1* and α^{I} - *CSNK2A2*) and regulatory (β - *CSNK2B*) subunits. The mRNA levels in HL lines were then compared to those observed in control B lymphocytes. We observed statistically significant differences only for the CSNK2A1 gene, specifically in the L-428 ($p<0.01$) and L-540 ($p<0.0001$) cell lines (Supplementary Results, Supplementary Figure S2C).

CK2 subunits are skewed in patients with HL

We performed a tissue microarray of neoplastic lymph nodes derived from 25 patients with cHL (Supplementary Table S3) and 5 with reactive adenopathies to evaluate the expression and localization of CK2 subunits in primary HL specimens. As shown in Figure 1F, G and Supplementary Figures S1A–C, we observed that 71% of patients strongly expressed CK2α in HRS cells (i.e., grade 3), while 29% were at grade 2 and 4% at grade 1 but no one was grade 0. Conversely, no patient expressed CK2β at grade 3, 67% of HL patients expressed CK2β at grade 2, 21% at grade 1 and 17% at grade zero (Figures 1F, G). Moreover CK2α was expressed

10.3389/fimmu.2024.1393485

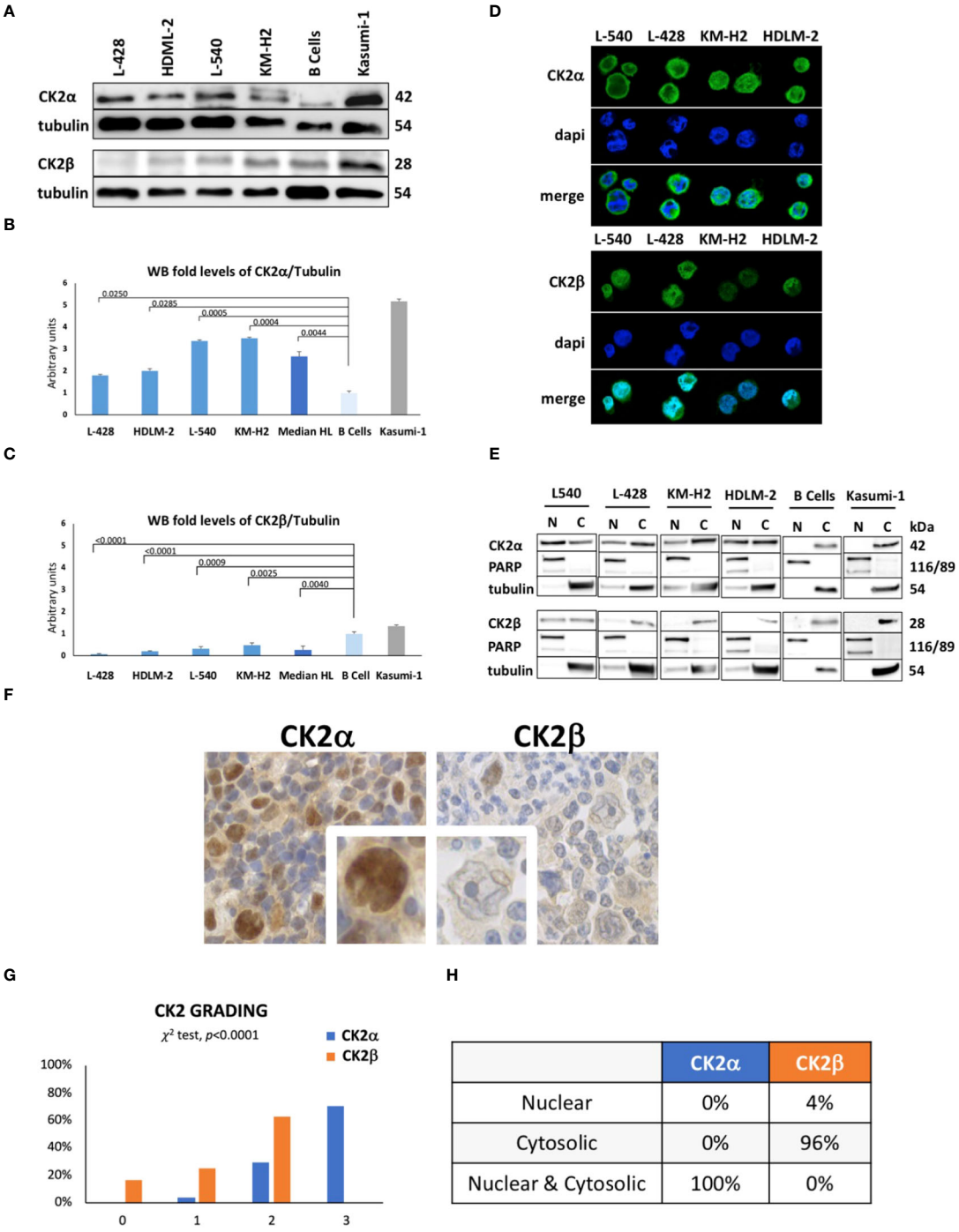

	CK2α	CK2β
Nuclear	0%	4%
Cytosolic	0%	96%
Nuclear & Cytosolic	100%	0%

FIGURE 1
Protein expression levels of CK2 alpha (α) and beta (β) subunits in HL cell lines. Representative WB analysis **(A)**, and the corresponding densitometric values **(B, C)** are reported as mean ± SD of n= 3 independent experiments. α-Tubulin was used as the loading control. (L-428, HDLM-2, L-540, KM-H2 are HL cell lines; B cell are healthy lymphocytes purified from three different buffy coats; Kasumi-1, a cell line model of acute myeloid leukemia, was used ad positive control). Above the histogram bars **(B, C)**, the *p*-value is reported. In the upper-right part of the figure confocal microscopy is shown **(D)**. The experiment was performed in different preparations for each HL cell line; the α and β subunits of CK2 were detected using green fluorescence (Alexa Fluor 488), nuclei were visualized through blue staining (DAPI), and the merge for each CK2 subunit is shown. Images were collected with 40X magnification, Scale bars = 15μm. Cell Fractionation was performed on the four HL cell lines, healthy B cells (normal control), and Kasumi-1 cell line as positive controls. WB reports α and β subunits of CK2, PARP (Poly (ADP-ribose) polymerase) used as nuclear marker, α-Tubulin as cytosolic marker. The image reports a representative case of three independent experiments **(E)**. Expression and localization of CK2 α and β subunits assessed by tissue microarray performed in neoplastic lymph nodes from 25 patients and 5 reactive adenopathy **(F)**. Representative case of CK2 expression in patient-derived Hodgkin and Reed-Sternberg (HRS) cells. CK2α appears to be localized in both the nucleus and cytoplasm of HRS cells. Expression of CK2 subunits according to the grading level **(G)**, and description of their cellular localization **(H)**. Positivity was graded as: 0 = negative; 1 = positive <30% of HRS; 2 = positive 30-60% HRS or week-moderate intensity; 3 = positive >60% HRS or strong diffuse intensity.

bothin the nucleus and the cytosol of all HRS, while CKβ was found in the cytosol in 96% of cases but in the nucleus only in 1 patient (p<0.0001) (Figure 1H, Supplementary Figures S1A–C) confirming our above-mentioned findings (Figures 1D, E). We also compared the clinical characteristics of our HL patients with the grading of CK2 subunits expression, but we did not find any correlation between age, gender, histological subtypes, interim 18-FDG PET-CT results, or relapsed cases. However, higher CK2β levels (i.e., grade 2) were associated with shorter progression free survival (PFS) than patient displaying lower levels (i.e., grade 0-1) (p=0.0421, Supplementary Figure S2A).

CK2β subunit undergoes proteasome-dependent degradation

To elucidate the mechanisms accounting for the downregulation of CK2β, we investigated whether CK2β was degraded by the proteasome. For this purpose, we treated HL cell lines *in vitro* with 10nM Bortezomib (BTZ) for 36 h. Inhibition of the proteasome resulted in an increase of the CK2β subunit protein levels compared to the untreated condition in the HL cell lines (Figures 2A, B). To further investigate this issue, all polyubiquitinated proteins from both the untreated and treated conditions were subjected to purification

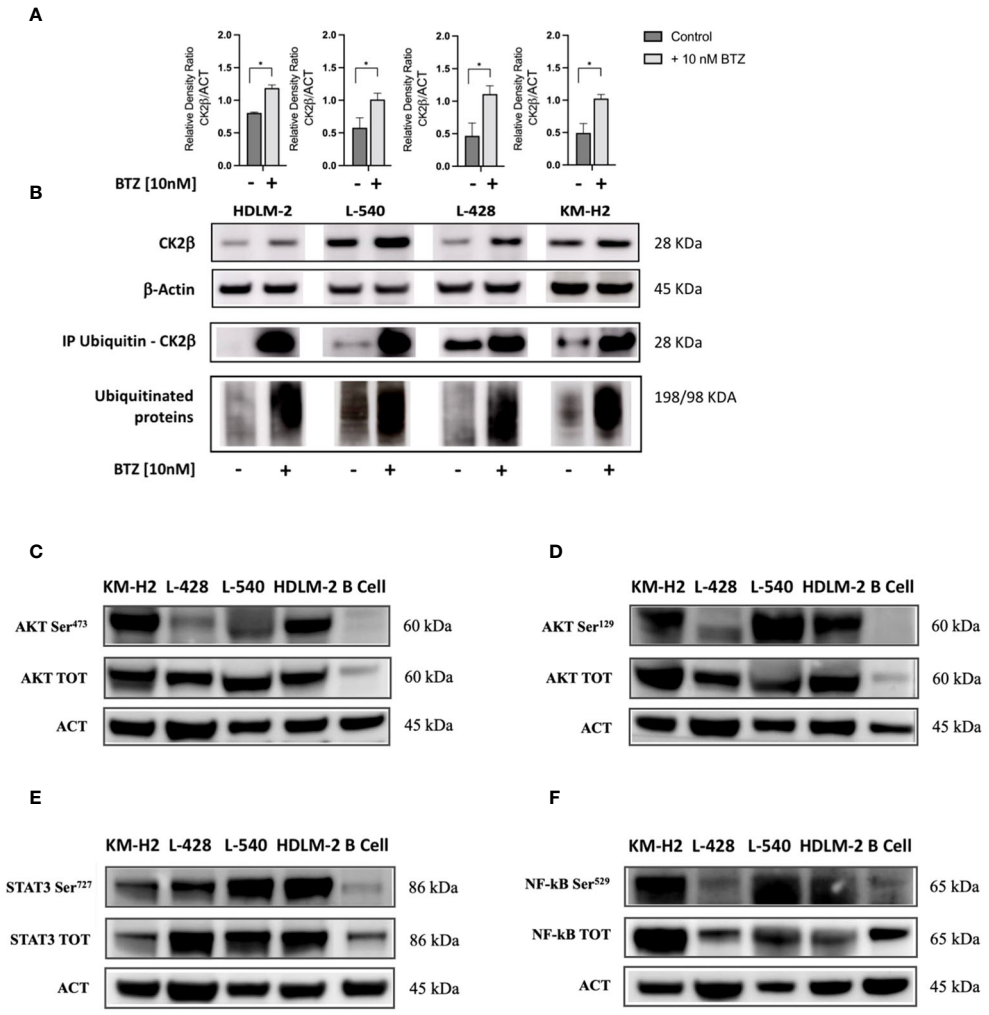

FIGURE 2
Western blotting analysis of ubiquitinated CK2β and phosphorylation levels of different CK2 targets. **(A)**. Relative densitometry of CK2β subunit with/without treatment of Bortezomib (BTZ) 10nM for 36h. **(B)** Representative WB. The proteins were immunoprecipitated, and all polyubiquitinated proteins were purified using a Ubiquitin detection kit. The immunocomplexes were then loaded onto an SDS-PAGE gel and subsequently analyzed using an anti-CK2β antibody. The results of proteasome inhibition were evaluated using the anti-poly ubiquitinated proteins (poly-Ubi) as positive control. For each condition, total cell lysates were loaded in SDS-PAGE and probed with anti-CK2β. * indicates p<0.05 (*Mann-Whitney test*), ACT: β-Actin; BTZ: Bortezomib. Representative WB of the main signaling pathways overexpressed in HL cell lines sustained by CK2 activity compared to the normal B lymphocytes **(C–F)**. The images depict phosphorylation levels at the Serine residue targeted by CK2α, and their corresponding total proteins for: AKT-S473 **(C)**, AKT-S129 **(D)**, STAT3-S727 **(E)**, and NF-kB (p65) S529 **(F)**. Densitometry for phosphorylated/total protein, total/β-Actin protein, and phosphorylated/β-Actin protein ratios are shown alongside each representative WB picture. β-Actin was used as the loading control. Analysis reports the mean ± SD of n = 3 independent experiments. * indicates p< 0.05 (*unpaired t test*).

using specific affinity beads. The enriched protein samples were analyzed by WB, revealing a pronounced presence of polyubiquitinated CK2β in the BTZ-treated condition, strongly indicating proteasome-dependent degradation of β subunits in HL cell lines (Figure 2B). To verify if the proteasome was effectively inhibited, we assessed the nonspecific increase in polyubiquitin residues through WB, which demonstrated a marked increase of ubiquitinated proteins across a broad range of molecular weights, as expected. (Figure 2B).

CK2 targets are phosphorylated

By means of WB analysis, we confirmed the overexpression of AKT, STAT3, and NF-kB (p65) as compared to their normal B cell counterparts (see Figures 2C–F). As depicted in the representative WB images, we found higher levels of both the whole protein and of the phosphorylated counterpart at the phosphorylation target sites of CK2α. Specifically, CK2 can phosphorylate AKT on Serine 473 (AKT S473, Figure 2C) by recruiting the mTOR2 complex (27) and directly phosphorylates AKT on Serine 129 (AKT S129, Figure 2D), NF-kB p65 on Serine 529 (NF-kB S529, Figure 2E), and STAT3 on Serine 727 (STAT3 S727, Figure 2F). These molecules exhibited phosphorylation at CK2-related residues under basal conditions, as compared to normal B lymphocytes. Protein phosphorylation levels diverged across different cell lines, reflecting the clinical heterogeneity observed in patients with HL. In addition, AKT, STAT3, and NF-kB (p65) were significantly more expressed in HL cell lines compared to normal B cells ($p<0.05$ unpaired Student's *t* test, Figures 2C–F). Densitometric values have been summarized in Supplementary Table S4.

CK2 modulates the expression of PD-L1 but not of CD30

CD30 and PD-L1/CD274 are known to be expressed on the cell membrane of HRS cells, while CD20 is usually absent. According to data coming from the literature, in HRS the locus of the gene CD274, that is mapped on chromosome 9 is usually amplified (5). Moreover, STAT3, NF-kB, and AKT molecular pathways can regulate the expression PD-L1 gene (5, 28, 29). Considering the role of CK2 in activating all these proteins within cHL cell lines, we examined whether CK2 could potentially affect PD-L1 expression. To delve into this question, we treated HRS cell lines with CK2α-specific inhibitor CX-4945/silmitasertib at a concentration of 10μM for 24h and 48h and we assessed expression of CD20, CD30 and PD-L1. We found a decrease in the mean fluorescence intensity (MFI) of PD-L1 after treatment with CX-4945 in HL cell lines, while no significant changes were observed for CD20 and CD30 (Figure 3A and Supplementary Figures S2B). Specifically, after 24 hours of treatment, the decrease of CD274/PD-L1 MFI was 46.0% ($p<0.05$), 51.4% ($p<0.01$), 29.0% ($p<0.05$), and 29.6% ($p<0.05$), for HDLM-2, L-428, L-540, and KM-H2, respectively, as compared to untreated conditions. Similarly, after 48 hours of treatment, the CD274/PD-L1 MFI decreased of 31.3% ($p<0.05$) for HDLM-2, 50.0% ($p<0.01$) for L-428, 55.7% ($p<0.01$) for L-540, 42.6% ($p<0.01$) for KM-H2, compared to untreated conditions (Mann-Whitney test, Figure 3A). The downregulation of PD-L1 was also confirmed by WB analysis (Figures 3B, C). The PD-L1 expression values, determined through protein densitometry and normalized to β-actin, align with flow cytometry results, confirming a substantial reduction in protein levels following treatment with the CK2 inhibitor. Specifically, after 24 hours of culture, the PD-L1/β-actin ratios shifted from 1.17 ± 0.14, 0.85 ± 0.07, 1.74 ± 0.5, and 0.82 ± 0.06 under untreated conditions to 0.53 ± 0.08, 0.74 ± 0.02, 0.4 ± 0.11, and 0.60 ± 0.03 after treatment with CX-5945 at 10 μM, respectively, for L-428, L-540, KM-H2, and HDLM-2 cell lines. Specifically, HL cell lines L-428 and HDLM-2 displayed a significant difference in the means of the experimental triplicates, with $p<0.05$ and $p<0.01$, respectively (unpaired t test). The association between CK2 and PD-L1 became more evident after 48 hours of treatment. The PD-L1/β-actin ratios shifted from fold change values of 0.83 ± 0.08, 1.0 ± 0.1, 0.90 ± 0.25, and 0.90 ± 0.06 to values of 0.36 ± 0.01, 0.4 ± 0.18, 0.30 ± 0.12, and 0.25 ± 0.01, respectively, following treatment with CX-4945/silmitasertib at 10 μM for the L-428, L-540, KM-H2, and HDLM-2 cell lines. Once again, the L-428 and HDLM-2 cell lines exhibited a treatment-related difference that was statistically significant ($p<0.01$ and $p<0.001$, respectively, unpaired t test).

CK2 inhibition triggers HL apoptosis

Since CK2 is known to sustain pro-survival signals in cancer cells, we examined the effect of its chemical inhibition in HL cell line. Treatment with CX-4945/silmitasertib resulted in time- and dose-dependent apoptosis, as confirmed through Annexin V/Propidium Iodide flow cytometry testing (Figures 4A, B, *Kruskal-Wallis's test*, $p<0.05$). For all the four HL cell lines, the percentage of viable cells exhibited a proportional decrease, starting from a dose of 5μM, in comparison to DMSO-treated cells ($p<0.05$). Notably, *in vitro* treatment with silmitasertib at 10μM concentration for 48 hours reduced the number of viable HL cells by half (Figure 4A). Furthermore, to elucidate the mechanisms underlying silmitasertib-induced apoptosis, we exposed HL cell lines to increasing doses of silmitasertib for 24 hours. This treatment resulted in the cleavage of PARP, a recognized marker of apoptosis (Figure 4B). Furthermore, that after 24 hours of cell treatment with CX-4945 (at concentrations of 5μM and 10μM), there was a significant decrease in the phosphorylation levels of AKT-S473 (Figure 4C), AKT-S129 (Figure 4D), STAT3-S727 (Figure 4E), and NF-kB-S529 (Figure 4F).

CK2 inhibition boosts the activity of MMAE

Since CD30 levels were not affected after CK2 inhibition (Supplementary Figure S2B), we subsequently proceeded to investigate whether CX-4945/silmitasertib might enhance the effectiveness of this innovative therapy. Specifically, we investigated whether CK2 inhibition could enhance the

10.3389/fimmu.2024.1393485

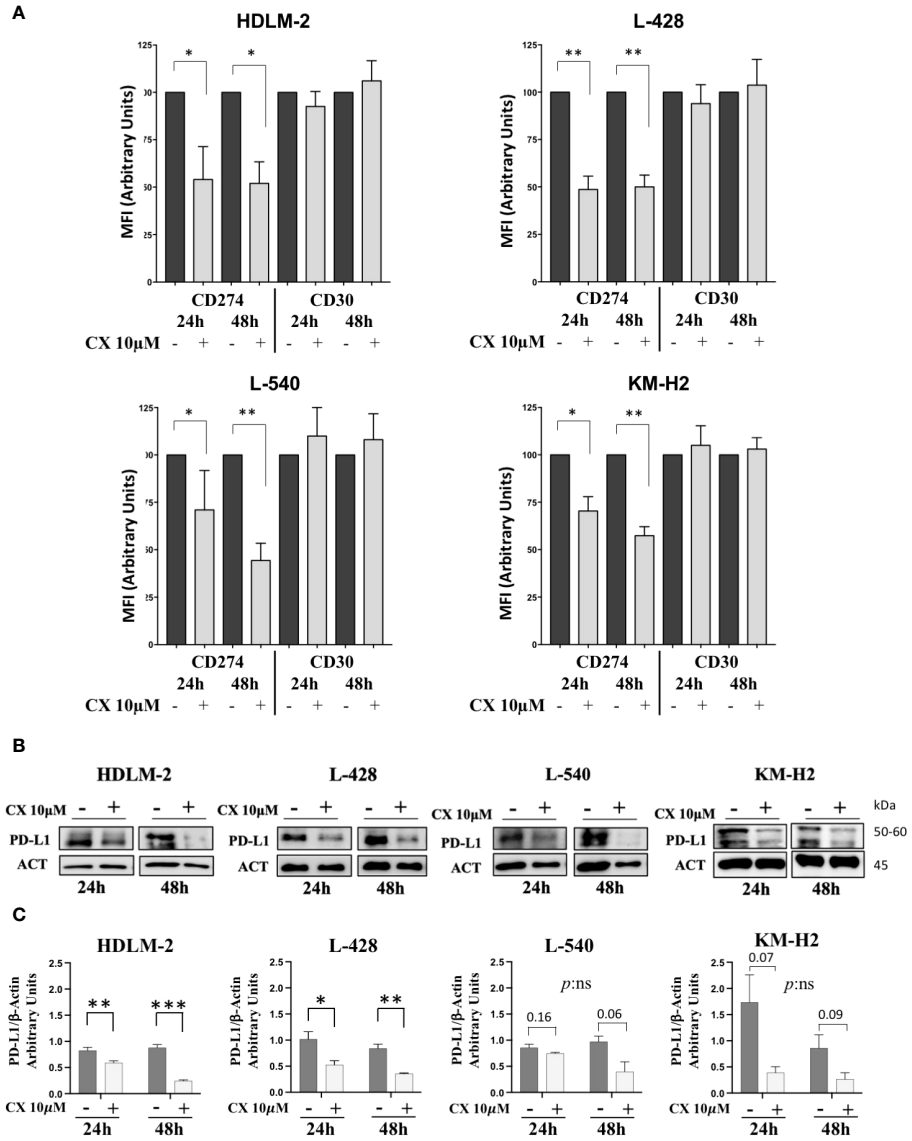

FIGURE 3
CD30 and CD274/PD-L1 expression assessment. In panel **(A)**, histograms depict the mean fluorescence intensity (MFI) of CD274 (PD-L1) and CD30 expression in the four HL cell lines, with or without 10μM CX-4945 treatment for 24 and 48 hours (three independent experiments, Student *t* test) CX: CX-4945. Only the viable cells were gated in the MFI analyses of PD-L1 or CD30 and normalized to their untreated condition. **(B)** Representative WB and **(C)** WB analysis of PD-L1 expression levels. HL cell lines were treated with or without 10μM CX-4945, for 24 and 48 hours. Densitometric values are reported as mean ± SD of n= 3 independent experiments, *Unpaired t test*. CX: CX-4945, ACT: β-Actin. *p<0.05, **p<0.01, ***p<0.001.

cytotoxicity of MMAE, the microtubule inhibitor conjugated to the anti-CD30 monoclonal antibody brentuximab vedotin.

To this aim, HL cell lines were treated with 5μM CX-4945 and 5nM MMAE, according to the literature (20), or a combination of both drugs for either 24 or 48 hours duration. As shown in Figure 5A, combination of CX-4945+MMAE significantly decreased the proportion of viable cells in comparison to MMAE. After 24 hours of *in-vitro* treatment, the percentage of viable cells, i.e. AV- PI-, decreased from 90.1%, 87.3%, 87.9%, and 94.8% with MMAE alone to 82.7% (p=0.12), 70.6% (p<0.05), 63.3% (p<0.05), and 85.9% (p<0.05) when treated with CX-4945 + MMAE in L428, L540, HDLM-2, and KM-H2, respectively (determined by the Wilcoxon matched-pairs signed rank test, Figure 5A). After 48 hours of treatment the rate of alive cells decreased from 79%, 62.2%, 66.5%, and 80.3% with MMAE alone to 64.3% (p=0.052), 51.8% (p=0.051), 48.4% (p<0.05), and 75.5% (p<0.05) with CX-4945 +MMAE in L428, L540, HDLM-2, and KM-H2, respectively (*Wilcoxon matched-pairs signed rank test*, Figure 5A). The cell lines tested responded differently to the combination treatment of CX-4945 and MMAE. Specifically, KM-H2 and L-428 cells exhibited the lowest sensitivity, whereas HDLM-2 cells demonstrated the highest sensitivity to the combination treatment. The increased apoptotic effect resulting from the combination of CX-4945 and MMAE was further supported by

10.3389/fimmu.2024.1393485

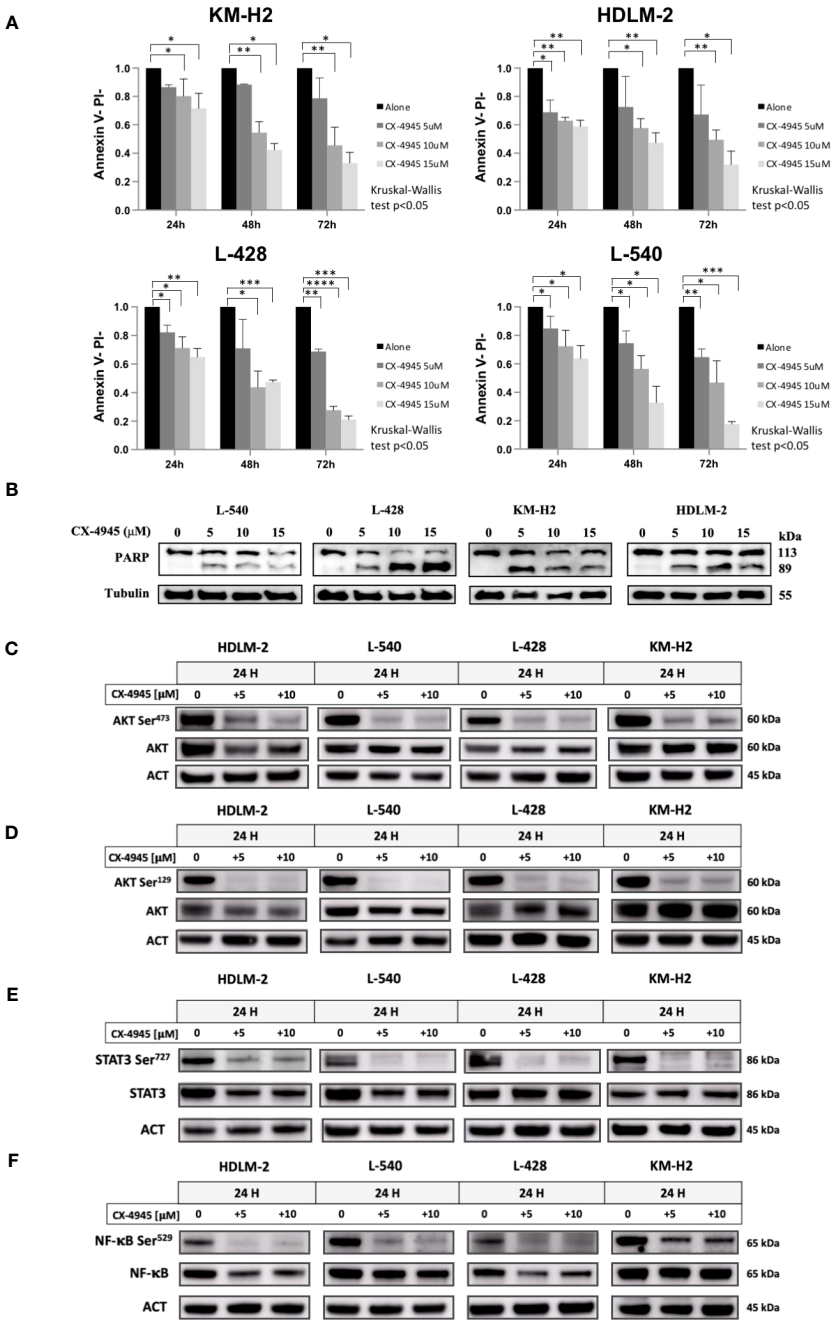

FIGURE 4
Apoptotic Effect of CX-4945 in HL Cell Lines. Apoptosis was detected through Annexin V propidium iodide (PI) assay by flow cytometry. Histograms illustrate the percentage of viable cells (Annexin V^{neg}/PI^{neg}) for each HL cell line after treatment with 5μM, 10μM, and 15μM CX-4945 at different time points (24, 48, and 72 hours). *p<0.05, **p<0.01, ***p<0.001, and ****p<0.0001 compared to the untreated cell population, *Kruskal-Wallis's test* **(A)**. Qualitative WB was performed using anti-PARP to highlight apoptosis induction in all four HL cell lines. Protein lysates, obtained after 48 hours of treatment with 0, 5, 10, and 15μM CX-4945, are presented. α-Tubulin was used as the loading control (experimental duplicate) **(B)**. WB illustrate the impact of CK2 inhibition with CX-4945 on CK2 substrates in the four HL cell lines. WBs depict phosphorylation levels on CK2 Serine targets, with and without CX-4945 treatment, along with corresponding total protein levels. The panels illustrate phosphorylation levels on AKT S473 **(C)**, AKT S129 **(D)**, STAT3 S727 **(E)**, and NF-κB at S529 **(F)** at 0, 5, and 10μM CX-4945 after 24 hours of treatment (experimental duplicate). ACT: β-Actin.

WB analysis, revealing a decreased full-length PARP band and an increased cleaved protein band compared to cells treated exclusively with MMAE.

The possible synergism between CX-4945 and MMAE in reducing cell viability was evaluated using the Chou-Talalay method through the evaluation of trypan blue exclusion. The EC50 for each cell lines of the single treatment (CX-4945 or MMAE) and the EC50 for the drugs used in combination are reported in Figure 5B. The combination effect analyses identified that the combination index values were all below 1 for each cell line,

10.3389/fimmu.2024.1393485

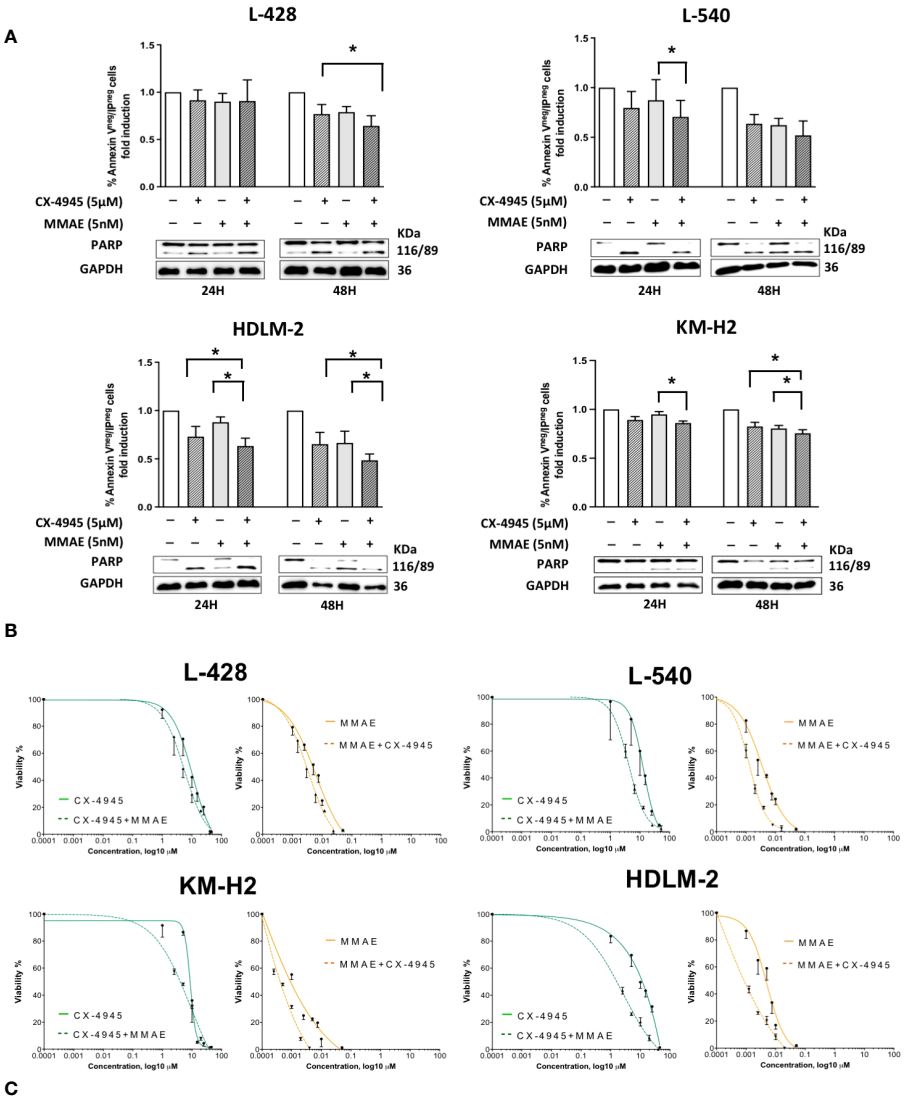

Table 2.

	EC50 [μM]		EC50 [nM]		
	CX-4945	CX-4945 + MMAE	MMAE	MMAE + CX-4945	CI
L-428	10.54	5.1	6.15	3.36	0.91
L-540	13.02	4.14	3.55	1.27	0.78
KM-H2	8.76	3.91	0.82	0.18	0.67
HDML-2	11.87	2.59	5.12	0.07	0.23

FIGURE 5
Apoptotic effect of CX-4945 alone or in combination with MMAE in Hodgkin lymphoma cell lines. HL cells lines were treated for 24 and 48 hours with CX-4945 and/or MMAE or the combination of both drugs. Apoptosis was detected through Annexin V propidium iodide (PI) assay by flow cytometry. Histograms shows alive non-apoptotic cells (Annexin V^{neg}/PI^{neg}). *Wilcoxon matched-pairs signed rank test* was used to compared paired data **(A)**. A qualitative WB (n=2), placed beneath each histogram, shows the cleavage of PARP protein expression in response to the heightened levels of apoptosis induced by the pharmacological treatments. In the middle panel **(B)** dose response curves of L-428, L-540, KM-H2, and HDLM-2 cell lines incubated for 72h with increasing concentrations of CX-4945 (green curves), and MMAE (orange curves) or their combination (dotted curves) are reported. Cell viability was assessed by trypan-blue exclusion assay. The curves were generated by maintaining a constant 1:1 ratio between the respective EC50 concentrations of CX-4945 and MMAE. In the lower panel **(C)**, EC50 values of CX-4945 and MMAE, used alone or in combination in L-428, L-540, KM-H2, and HDLM-2 cell lines incubated as in **(B)**. A combination index (CI) < 1 means a synergistic effect. Experiments were performed in triplicate. *$p<0.05$. *Wilcoxon matched-pairs signed rank test*.

indicating a synergistic cytotoxic effect between CX-4945 and MMAE. In particular, the obtained combination indexes were 0.91, 0.78, 0.67, and 0.23 for L-428, L-540, KM-H2, and HDLM-2, respectively (Figure 5C).

Discussion

In this work, we characterized the role of protein kinase CK2 in cHL. In recent years, CK2 is emerging as an increasingly interesting

target in hematological malignancies, being a key player in the regulation of proliferation, angiogenesis, secretion of growth factors, invasiveness and resistance to therapies (12). Previously, we and other groups demonstrated that both CK2α and CK2β were overexpressed and essential for neoplastic cell growth. Inhibition of CK2 triggered apoptosis in neoplastic cells of multiple myeloma (30), acute leukemias (26), and non-Hodgkin lymphomas (18, 25), without a significant impact on normal lymphocytes (31). However, the role of CK2 in cHL is unknown and has not been investigated yet.

In this study we demonstrated that CK2α was overexpressed in HL cell lines as compared to normal B-lymphocytes as assessed by WB and confocal microscopy. These data were also confirmed by IHC on primary samples of cHL patients, confirming that the catalytic α subunit was highly expressed, while the CK2β subunit was expressed at lower intensity. This aspect is remarkable, since, to our knowledge, cHL is the first hematological malignancy with an imbalance between α and β subunits. The expression of CK2α or β did not correlate with histological variants, age, stage, and outcome, suggesting that this unbalance expression of CK2α or β occurs in almost all cases and is likely to play a role in cHL development. Additionally, RT-qPCR analysis revealed a significant difference in mRNA expression levels only for the α subunits in the L-428 and L-540 cell lines when compared to healthy B cells. Therefore, we hypothesized that this unbalance could be the result of post-translational events in cHL. We investigated whether CK2β could be degraded by the proteasome. Consequently, we therefore immunoprecipitated all polyubiquitinated proteins following proteasome inhibition with bortezomib and assessed the presence of CK2β by immunoblotting. We observed an increase in the intensity of the CK2β subunit upon inhibiting the proteasome in all HL cell lines, indicating its degradation via the proteasome-dependent pathway. In line with our findings, recent studies have demonstrated that CK2 is active in the absence of the regulatory β subunit and that CK2β subunit influences substrate specificity, since there are proteins whose phosphorylation is specifically catalyzed by either the free α catalytic subunits, such as Akt S129, or CK2 holoenzyme through its N-terminal acid loop (32–34). In the latter case, CK2β acts as a docking platform for downstream substrates (35).

Of interest, our group has recently reported the first B-cell specific knockout mouse of CK2β, showing NOTCH2-mediated increase of marginal zone B cells and a decrease of follicular B cells (16). In addition, B cells lacking CK2β have an impaired signaling downstream to the B-cell receptor, toll-like receptor and CD40 (16). Since HRS are likely derived from crippled CD30+ germinal center B lymphocytes rescued by apoptosis, we can speculate that a skewed expression of CK2 subunits might be present also in CD30+ B cells or might be necessary for acquired the Hodgkin-phenotype as compared with other lymphomas where usually both subunits are overexpressed (25, 36).

Furthermore, pivotal signaling molecules in cHL, namely NF-kB, PI3K/AKT and STAT3, showed higher levels of their total protein compared to the control and were found to be phosphorylated at CK2 specific targets and therefore constitutively activated. Since AKT, NF-kB and STAT3 play a central role in HL, their basal phosphorylation suggests an important role of CK2 mediating a pro-survival function in HL (Figures 2C–F).

The CK2α inhibitor CX-4945/silmitasertib demonstrated a significant increase in *in vitro* apoptosis in the cHL cell lines tested, demonstrating a time- and dose-dependent response. Mechanistically, CX-4945 administration led to a decrease in the phosphorylation of the CK2 targets AKT, NF-kB and STAT3. Furthermore, PD-L1 receptor overexpression is known to be one of the main mechanisms by which HRS cells elude the immune response. PD-L1 gene is known to be amplified in most cases of cHL (37) and regulated by STAT3 and NF-κB transcription factors, both of which are activated by CK2 (11, 15). Our data demonstrate for the first time a novel CK2 mediated regulation of PD-L1 (CD274) in HL, since CK2 chemical inhibition with CX-4945 leads to the downregulation of PD-L1, possibly mediated through the impairment of STAT3 and NF-κB transcriptional activity. These findings suggest a potential indirect contribution of CK2 in inducing T-cell exhaustion and, consequently, contributing to an immunosuppressive microenvironment in HL.

The importance of targeting more pathways at the same time is highlighted by phase I-II clinical trials evaluating the clinical activity of JAK2 and/or PI3K inhibitors in relapsed refractory patients with HL (8, 38). A phase 1 dose-escalation/expansion study evaluated the safety and efficacy of dezapelisib, a new selective PI3Kδ inhibitor, as monotherapy or in combination with itacitinib, a selective JAK1 inhibitor, in adult patients with relapsed B-cell lymphomas. The combination of itacitinib and dezapelisib provided promising activity, resulting in an ORR of 67% in cHL compared to 29% in monotherapy (38). These clinical findings support the potential effectiveness of combining more pathway inhibitors as a relevant treatment strategy for highly pretreated HL patients. Accordingly, targeting CK2 would simultaneously switch off three key relevant survival signaling pathways. To this regard, we have also observed a synergistic effect between CX-4945/Silmitasertib and MMAE, a microtubule-disrupting agent conjugated with the anti-CD30 monoclonal antibody brentuximab vedotin. Although the CD30 overexpression is a common hallmark of HL and BV/MMAE has demonstrated clinical efficacy in the treatment of naive and relapsed patients, a small subset of triple refractory patients with cHL is emerging; therefore, it is of crucial importance to introduce potential pharmacological combinations to enhance therapy effectiveness. Silmitasertib (39) is a promising orally bioavailable selective inhibitor of protein kinase CK2. Despite CK2 significant impact on the human phosphoproteome, the inhibition of this kinase has been well tolerated in Phase I clinical trials (40). CX-4945 does not impinge on CD30 expression levels on the cell membrane as elucidated by the dose-response curves in each HL cell line tested in the present manuscript. Our data demonstrated that the mean EC50 value for individual treatments (CX-4945 or MMAE) undergoes a notable reduction upon their concomitant administration. This implies a prospective improvement in treatment tolerability, even at lower doses, all while upholding a precisely targeted cytotoxic effect designed to impair the tumor cell growth. Several *in vitro* studies like Martins et al. (41) in chronic lymphocytic leukemia, or Manni et al. (18) in mantle cell lymphoma, suggest that combination therapies with CX-

potentially increase treatment response, particularly for drug-refractory patients. Furthermore, the inhibition of CK2 might contribute to achieve a synergistic treatment effect, even when used in combination with checkpoint inhibitors.

In this study, we have provided strong evidence that, in accordance with the paradigm known as "non-oncogene dependence" (18, 42), overexpression of CK2α is believed to be responsible for pivotal mechanisms of cell proliferation and survival also in cHL.

Conclusions

We herein have demonstrated that cHL is likely the first hematological malignancy to exhibit an aberrant expression of CK2 subunits, with CK2α being overexpressed and CK2β downregulated in HRS cells, both in HL cell lines and primary lymph nodes from cHL patients. HRS cells exhibit a pronounced dependency on CK2α activity, since *in vitro* treatment with CX-4945/silmitasertib led to the dephosphorylation of AKT-S129 and S473, NF-κB-S529, and STAT3-S727, ultimately resulting in synthetic lethality in HL. Moreover, CX-4945 induced the downregulation of PD-L1/CD274, but not of CD30, and displayed a synergistic response with MMAE, which might have a relevant clinical implication. Further studies on CK2 protein will improve our understanding on HL pathogenesis.

Data availability statement

The raw data supporting the conclusions of this article will be made available by the authors, without undue reservation.

Ethics statement

The studies involving humans were approved by ethic committee of the Padova University Hospital (protocol # 4,089/AO/17). The studies were conducted in accordance with the local legislation and institutional requirements. The participants provided their written informed consent to participate in this study. Written informed consent was obtained from the individual(s) for the publication of any potentially identifiable images or data included in this article.

Author contributions

ER: Data curation, Formal analysis, Investigation, Methodology, Validation, Writing – original draft. FF: Data curation, Formal analysis, Investigation, Methodology, Conceptualization, Project administration, Supervision, Writing – review & editing. NM: Formal analysis, Investigation, Methodology, Supervision, Writing – review & editing. MP: Formal analysis, Investigation, Methodology, Writing – review & editing, Data curation. FS: Data curation, Formal analysis, Investigation, Methodology, Writing – review & editing, Supervision. GC: Formal analysis, Writing – review & editing. VT: Data curation, Formal analysis, Investigation, Methodology, Supervision, Writing – review & editing, Conceptualization. LQT: Data curation, Formal analysis, Investigation, Methodology, Supervision, Writing – review & editing. AC: Data curation, Formal analysis, Investigation, Methodology, Writing – review & editing. CC: Data curation, Formal analysis, Investigation, Methodology, Writing – review & editing. VR: Data curation, Formal analysis, Investigation, Methodology, Writing – review & editing, Project administration. AS: Data curation, Formal analysis, Investigation, Methodology, Writing – review & editing. FA: Data curation, Formal analysis, Investigation, Methodology, Writing – review & editing. ND: Data curation, Formal analysis, Investigation, Methodology, Writing – review & editing. SM: Data curation, Formal analysis, Investigation, Methodology, Writing – review & editing, Supervision, Validation, Visualization. MF: Methodology, Supervision, Visualization, Writing – review & editing, Project administration. FP: Methodology, Project administration, Supervision, Visualization, Writing – review & editing, Investigation, Resources, Validation. LQ: Project administration, Resources, Supervision, Visualization, Writing – review & editing, Funding acquisition. AV: Writing – review & editing, Conceptualization, Data curation, Formal analysis, Funding acquisition, Investigation, Methodology, Project administration, Resources, Software, Supervision, Validation, Visualization, Writing – original draft.

Funding

The author(s) declare financial support was received for the research, authorship, and/or publication of this article. This work was supported by funding from the Italian Association against Leukaemia-lymphoma and Myeloma (AIL), the Italian Association for Cancer Research (AIRC) IG-25024 to LT, Progetti di Rilevanza Nazionale PRIN PNRR (P2022PSMX4) to AS, the ONLUS 'Ricerca per Credere nella Vita' (RCV) odv, Padua, Italy. ER received a fellowship by AIL. The funders had no role in the study design, data collection and analysis, decision to publish or preparation of the manuscript. Open Access funding provided by Università degli Studi di Padova (University of Padua, Open Science Committee).

Acknowledgments

The authors gratefully acknowledge Prof. Carmelo Carlo-Stella (IRCCS Humanitas research Hospital) for kindly providing the HL cell lines used to perform the experiments in this project and Prof. Maria Ruzzene (University of Padua), for initially providing us CK2α antibody for WB.

Conflict of interest

AV and LT participated to scientific board organized and received travel grant by Takeda.

The remaining authors declare that the research was conducted in the absence of any commercial or financial relationships that could be construed as a potential conflict of interest.

The author(s) declared that they were an editorial board member of Frontiers, at the time of submission. This had no impact on the peer review process and the final decision.

Publisher's note

Supplementary material

The Supplementary Material for this article can be found online at: https://www.frontiersin.org/articles/10.3389/fimmu.2024.1393485/full#supplementary-material

References

1. Yung L, Linch D. Hodgkin's lymphoma. *Lancet*. (2003) 361:943–51. doi: 10.1016/S0140-6736(03)12777-8

2. Brice P, de Kerviler E, Friedberg JW. Classical Hodgkin lymphoma. *Lancet*. (2021) 398:1518–27. doi: 10.1016/S0140-6736(20)32207-8

3. Aldinucci D, Borghese C, Casagrande N. For of the immunosuppressive microenvironment of classic Hodgkin lymphoma and therapeutic approaches to counter it. *Int J Mol Sci*. (2019) 20:2416. doi: 10.3390/ijms20102416

4. Mottok A, Steidl C. Biology of classical Hodgkin lymphoma: implications for prognosis and novel therapies. *Blood*. (2018) 131:1654–65. doi: 10.1182/blood-2017-09-772632

5. Cellini A, Scarmozzino F, Angotzi F, Ruggeri E, Dei Tos AP, Trentin L, et al. Tackling the dysregulated immune-checkpoints in classical Hodgkin lymphoma: bidirectional regulations between the microenvironment and Hodgkin/Reed-Sternberg cells. *Front Oncol*. (2023) 13:1203470. doi: 10.3389/fonc.2023.1203470

6. Matsuki E, Younes A. Lymphomagenesis in Hodgkin lymphoma. *Semin Cancer Biol*. (2015) 34:14–21. doi: 10.1016/j.semcancer.2015.02.002

7. Visentin A, Frezzato F, Severin F, Imbergamo S, Pravato S, Romano Gargarella L, et al. Lights and shade of next-generation Pi3k inhibitors in chronic lymphocytic leukemia. *OncoTargets Ther*. (2020) 13:9679–88. doi: 10.2147/OTT.S268899

8. Van Den Neste E, André M, Gastinne T, Stamatoullas A, Haioun C, Belhabri A, et al. A phase II study of the oral JAK1/JAK2 inhibitor ruxolitinib in advanced relapsed/refractory Hodgkin lymphoma. *Haematologica*. (2018) 103:840–8. doi: 10.3324/haematol.2017.180554

9. Fernández S, Solórzano JL, Díaz E, Menéndez V, Maestre L, Palacios S, et al. JAK/STAT blockade reverses the Malignant phenotype of Hodgkin and Reed-Sternberg cells. *Blood Adv*. (2023) 7:4135–47. doi: 10.1182/bloodadvances.2021006336

10. Mascarenhas J, Hoffman R. Ruxolitinib: the first FDA approved therapy for the treatment of myelofibrosis. *Clin Cancer Res*. (2012) 18:3008–14. doi: 10.1158/1078-0432.CCR-11-3145

11. Borgo C, D'Amore C, Sarno S, Salvi M, Ruzzene M. Protein kinase CK2: a potential therapeutic target for diverse human diseases. *Signal Transduct Target Ther*. (2021) 6:183. doi: 10.1038/s41392-021-00567-7

12. Trembley JH, Wang G, Unger G, Slaton J, Ahmed K. Protein Kinase CK2 in Health and Disease: CK2: A key player in cancer biology. *Cell Mol Life Sci*. (2009) 66:1858–67. doi: 10.1007/s00018-009-9154-y

13. Piazza F, Manni S, Ruzzene M, Pinna LA, Gurrieri C, Semenzato G. Protein kinase CK2 in hematologic Malignancies: reliance on a pivotal cell survival regulator by oncogenic signaling pathways. *Leukemia*. (2012) 26:1174–9. doi: 10.1038/leu.2011.385

14. Nuñez de Villavicencio-Diaz T, Rabalski A, Litchfield D. Protein kinase CK2: intricate relationships within regulatory cellular networks. *Pharmaceuticals*. (2017) 10:27. doi: 10.3390/ph10010027

15. Spinello Z, Fregnani A, Quotti Tubi L, Trentin L, Piazza F, Manni S. Targeting protein kinases in blood cancer: focusing on CK1α and CK2. *Int J Mol Sci*. (2021) 22:3716. doi: 10.3390/ijms22073716

16. Quotti Tubi L, Mandato E, Canovas Nunes S, Arjomand A, Zaffino F, Manni S, et al. CK2β-regulated signaling controls B cell differentiation and function. *Front Immunol*. (2023) 13:959138. doi: 10.3389/fimmu.2022.959138

17. Wei H, Yang W, Hong H, Yan Z, Qin H, Benveniste EN. Protein kinase CK2 regulates B cell development and differentiation. *J Immunol*. (2021) 207:799–808. doi: 10.4049/jimmunol.2100059

18. Manni S, Pesavento M, Spinello Z, Saggin L, Arjomand A, Fregnani A, et al. Protein Kinase CK2 represents a new target to boost Ibrutinib and Venetoclax induced cytotoxicity in mantle cell lymphoma. *Front Cell Dev Biol*. (2022) 10:935023. doi: 10.3389/fcell.2022.935023

19. Mandato E, Manni S, Zaffino F, Semenzato G, Piazza F. Targeting CK2-driven non-oncogene addiction in B-cell tumors. *Oncogene*. (2016) 35:6045–52. doi: 10.1038/onc.2016.86

20. Buckel L, Savariar EN, Crisp JL, Jones KA, Hicks AM, Scanderbeg DJ, et al. Tumor radiosensitization by monomethyl auristatin E: mechanism of action and targeted delivery. *Cancer Res*. (2015) 75:1376–87. doi: 10.1158/0008-5472.CAN-14-1931

21. Frezzato F, Trimarco V, Martini V, et al. Leukaemic cells from chronic lymphocytic leukaemia patients undergo apoptosis following microtubule depolymerization and L yn inhibition by nocodazole. *Br J Haematol*. (2014) 165:659–72. doi: 10.1111/bjh.12815

22. Chou TC. Theoretical basis, experimental design, and computerized simulation of synergism and antagonism in drug combination studies. *Pharmacol Rev*. (2006) 58:621–81. doi: 10.1124/pr.58.3.10

23. Pagano MA, Tibaldi E, Molino P, Frezzato F, Trimarco V, Facco M, et al. Mitochondrial apoptosis is induced by Alkoxy phenyl-1-propanone derivatives through PP2A-mediated dephosphorylation of Bad and Foxo3A in CLL. *Leukemia*. (2019) 33:1148–60. doi: 10.1038/s41375-018-0288-5

24. Martini V, Gattazzo C, Frezzato F, Trimarco V, Pizzi M, Chiodin G, et al. Cortactin, a Lyn substrate, is a checkpoint molecule at the intersection of BCR and CXCR4 signalling pathway in chronic lymphocytic leukaemia cells. *Br J Haematol*. (2017) 178:81–93. doi: 10.1111/bjh.14642

25. Pizzi M, Piazza F, Agostinelli C, Fuligni F, Benvenuti P, Mandato E, et al. Protein kinase CK2 is widely expressed in follicular, Burkitt and diffuse large B-cell lymphomas and propels Malignant B-cell growth. *Oncotarget*. (2015) 6:6544–52. doi: 10.18632/oncotarget.3446

26. Quotti Tubi L, Canovas Nunes S, Brancalion A, Breatta Doriguzzi AE, Manni S, Mandato E, et al. Protein kinase CK2 regulates AKT, NF-κB and STAT3 activation, stem cell viability and proliferation in acute myeloid leukemia. *Leukemia*. (2017) 31:292–300. doi: 10.1038/leu.2016.209

27. Olsen BB, Svenstrup TH, Guerra B. Downregulation of protein kinase CK2 induces autophagic cell death through modulation of the mTOR and MAPK signaling pathways in human glioblastoma cells. *Int J Oncol*. (2012) 41:1967–76. doi: 10.3892/ijo.2012.1635

28. Pianko MJ, Goldberg AD, Lesokhin AM. Clinical development of PD-1 blockade in hematologic Malignancies. *Cancer J*. (2018) 24:31–5. doi: 10.1097/PPO.0000000000000297

29. Yi M, Niu M, Xu L, Luo S, Wu K. Regulation of PD-L1 expression in the tumor microenvironment. *J Hematol OncolJ Hematol Oncol*. (2021) 14:10. doi: 10.1186/s13045-020-01027-5

30. Manni S, Toscani D, Mandato E, Brancalion A, Quotti Tubi L, Macaccaro P, et al. Bone marrow stromal cell-fueled multiple myeloma growth and osteoclastogenesis are sustained by protein kinase CK2. *Leukemia*. (2014) 28:2094–7. doi: 10.1038/leu.2014.178

31. St-Denis NA, Litchfield DW. Protein Kinase CK2 in Health and Disease: From birth to death: The role of protein kinase CK2 in the regulation of cell proliferation and survival. *Cell Mol Life Sci*. (2009) 66:1817–29. doi: 10.1007/s00018-009-9150-2

32. Borgo C, Franchin C, Cesaro L, Zaramella S, Arrigoni G, Salvi M, et al. A proteomics analysis of CK2β(−/−) C2C12 cells provides novel insights into the biological functions of the non-catalytic β subunit. *FEBS J*. (2019) 286:1561–75. doi: 10.1111/febs.14799

33. Alcaraz E, Vilardell J, Borgo C, Sarró E, Plana M, Marin O, et al. Effects of CK2β subunit down-regulation on Akt signalling in HK-2 renal cells. *PloS One*. (2020) 15:e0227340. doi: 10.1371/journal.pone.0227340

34. Rodriguez FA, Contreras C, Bolanos-Garcia V, Allende JE. Protein kinase CK2 as an ectokinase: The role of the regulatory CK2β subunit. *Proc Natl Acad Sci*. (2008) 105:5693–8. doi: 10.1073/pnas.0802065105

35. Pinna LA. Protein kinase CK2: a challenge to canons. *J Cell Sci*. (2002) 115:3873–8. doi: 10.1242/jcs.00074

36. Manni S, Brancalion A, Mandato E, Quotti Tubi L, Colpo A, Pizzi M, et al. Protein kinase CK2 inhibition down modulates the NF-κB and STAT3 survival pathways, enhances the cellular proteotoxic stress and synergistically boosts the cytotoxic effect of bortezomib on multiple myeloma and mantle cell lymphoma cells. *PloS One*. (2013) 8:e75280. doi: 10.1371/journal.pone.0075280

37. Küppers R, Engert A, Hansmann ML. Hodgkin lymphoma. *J Clin Invest*. (2012) 122:3439–47. doi: 10.1172/JCI61245

38. Phillips TJ, Forero-Torres A, Sher T, Diefenbach CS, Johnston P, Talpaz M, et al. Phase 1 study of the PI3Kδ inhibitor INCB040093 ± JAK1 inhibitor itacitinib in relapsed/refractory B-cell lymphoma. *Blood*. (2018) 132:293–306. doi: 10.1182/blood-2017-10-812701

39. Siddiqui-Jain A, Drygin D, Streiner N, Chua P, Pierre F, O'Brien SE, et al. CX-4945, an orally bioavailable selective inhibitor of protein kinase CK2, inhibits prosurvival and angiogenic signaling and exhibits antitumor efficacy. *Cancer Res*. (2010) 70:10288–98. doi: 10.1158/0008-5472.CAN-10-1893

40. Chua M, Ortega C, Sheikh A, Lee M, Abdul-Rassoul H, Hartshorn KL, et al. CK2 in cancer: cellular and biochemical mechanisms and potential therapeutic target. *Pharmaceuticals*. (2017) 10:18. doi: 10.3390/ph10010018

41. Martins LR, Lúcio P, Melão A, Antunes I, Cardoso BA, Stansfield R, et al. Activity of the clinical-stage CK2-specific inhibitor CX-4945 against chronic lymphocytic leukemia. *Leukemia*. (2014) 28:179–82. doi: 10.1038/leu.2013.232

42. Strum SW, Gyenis L, Litchfield DW. CSNK2 in cancer: pathophysiology and translational applications. *Br J Cancer*. (2022) 126:994–1003. doi: 10.1038/s41416-021-01616-2

frontiers | Frontiers in Immunology

TYPE Original Research
PUBLISHED 25 June 2024
DOI 10.3389/fimmu.2024.1410638

OPEN ACCESS

EDITED BY
Michael John Robertson,
Indiana University Bloomington, United States

REVIEWED BY
Luis Alberto De Pádua Covas Lage,
University of São Paulo, Brazil
Veenu Tripathi,
National Cancer Institute (NIH), United States
Zoufang Huang,
First Affiliated Hospital of Gannan Medical University, China

*CORRESPONDENCE
Paul Coppo
paul.coppo@aphp.fr

RECEIVED 01 April 2024
ACCEPTED 03 June 2024
PUBLISHED 25 June 2024

CITATION
Ricard L, Cervera P, Stocker N, Corre E, Van de Wyngaert Z, Banet A, Marjanovic Z, Dulery R, Bravetti C, Joly A-C, Baylatry MT and Coppo P (2024) A combination of 5-azacytidine and nivolumab is a potentially effective rescue therapy in relapsed/refractory AITL.
Front. Immunol. 15:1410638.
doi: 10.3389/fimmu.2024.1410638

A combination of 5-azacytidine and nivolumab is a potentially effective rescue therapy in relapsed/refractory AITL

Laure Ricard[1,2], Pascale Cervera[3], Nicolas Stocker[1,2], Elise Corre[2,4], Zoé Van de Wyngaert[2], Anne Banet[2], Zora Marjanovic[2], Rémy Dulery[1,2], Clotilde Bravetti[5], Anne-Christine Joly[6], Minh Tam Baylatry[6] and Paul Coppo[2,4]*

[1]Sorbonne Université, Institut National de la Santé Et de la Recherche Médicale (INSERM), Centre de Recherche Saint-Antoine (CRSA), Paris, France, [2]Service d'Hématologie, Hôpital Saint-Antoine, Assistance Publique - Hôpitaux de Paris (AP-HP)- Sorbonne Université, Paris, France, [3]Service d'Anatomopathologie, Assistance Publique - Hôpitaux de Paris (AP-HP) - Sorbonne Université, Paris, France, [4]Centre de Référence des Microangiopathies Thrombotiques (CNR-MAT), Hôpital Saint-Antoine, Assistance Publique - Hôpitaux de Paris (AP-HP) - Sorbonne Université, Paris, France, [5]Service d'hématologie biologique, Assistance Publique - Hôpitaux de Paris (AP-HP) - Sorbonne Université, Paris, France, [6]Hôpital Saint-Antoine, Pharmacie, Assistance Publique - Hôpitaux de Paris (AP-HP) - Sorbonne Université, Paris, France

Introduction: Angioimmunoblastic T-cell lymphoma (AITL) is a peripheral T-cell lymphoma characterized by a T follicular helper cell phenotype expressing PD-1 (programmed cell death-1). AITL exhibits a poor response to conventional chemotherapy, with a median 5-year overall survival of 44% and a progression-free survival of 32%. Relapse is common, resulting in a median overall survival of 6 months. Recurrent mutations are detected in genes regulating DNA methylation, including TET2, DNMT3A, and IDH2 variants, along with the prevalent RHOA G17V mutation. In this context, patients treated with the hypomethylating agent 5-azacytidine achieved overall response and complete response rates of 75% and 41%, respectively. We hypothesized that targeted therapies combining anti-PD-1 checkpoint blockers with hypomethylating agents could be efficient in AITL patients and less toxic than standard chemotherapy.

Methods: Here, we report the efficacy of a regimen combining 5-azacytidine and nivolumab in nine relapsed or refractory AITL patients.

Results: This regimen was well-tolerated, especially in elderly patients. The overall response rate was 78%, including four partial responses (44%) and three complete responses (33%). Allogeneic hematopoietic stem cell transplantation was performed in two patients who reached complete response.

Discussion: These preliminary favorable results may serve as a basis for further investigation in prospective studies.

KEYWORDS

angioimmunoblastic T cell lymphoma, 5-azacytidine, nivolumab, T follicular helper cell, TET2, RhoA

Introduction

Angioimmunoblastic T-cell lymphoma (AITL) is a subtype of peripheral T-cell lymphoma (PTCL) characterized by a T follicular helper cell phenotype. AITL predominantly affects older individuals, with a median age of 65 years (1). The prognosis is bleak, with a 44% median 5-year overall survival and an 32% progression-free survival (PFS) rate. One of the standard first-line therapeutic approach remains Cyclophosphamide-Doxorubicin-Vincristine-Prednisone (CHOP) therapy. Unfortunately, relapse is frequent, with a median post relapse overall survival of only 6 months (2).

AITL originates from CD4+ T follicular helper cells (Tfh) and is characterized by an exacerbated inflammatory response and immune dysregulation. Molecular studies have identified pathogenic variants in genes regulating DNA methylation and a dysregulation in T-cell signaling. Specifically, *TET2*, *DNMT3A*, and *IDH2* variants are present in 80%, 25%, and 25% of patients with Tfh-derived PTCL, respectively (3, 4). Notably, these mutations alone are insufficient for lymphomagenesis, and 70% of AITL patients also carry a recurrent *RHOA* G17V mutation. Mouse models support the notion that a combination of *RHOA* G17V mutations with *TET2* mutations is necessary to induce lymphomagenesis with a Tfh phenotype (5). First initiator mutations involve epigenetic regulators (TET2 or DNMT3A); secondly, driver-mutations such as RHOA G17V and IDH2 R172K/S promote the expansion of clonal Tfh cells (6).

CD4+ Tfh cells are crucial for germinal center T- and B-cell development, and express the checkpoint inhibitor PD-1 (programmed cell death-1). In AITL lymph nodes, malignant Tfh cells represent a minority of cellular components, coexisting with various immune cells such as immunoblasts, eosinophils, and plasma cells. Most immunoblasts are Epstein-Barr virus (EBV)-infected (1), contributing to increased PDL-1 expression and creating a tolerogenic milieu favoring malignant cell survival while suppressing neighboring macrophages and effector T cells (7, 8). PD-1 expression is detected in 80% of AITL cases, correlating with a poor prognosis (9). Of note, the highly recurrent activating mutation (p.Gly17Val) in the RhoA small GTPase promotes CD4+ T cell polarization in Tfh cells with expression of CXCR5 and PD-1 (10).

Building upon these findings, targeted therapies combining anti-PD-1 checkpoint blockers with hypomethylating agents may offer enhanced efficiency in AITL treatment, while potentially reducing toxicity compared to standard chemotherapy. A retrospective study of 12 AITL patients treated with the single hypomethylating agent 5-azacytidine reported an overall response rate of 75% and a complete response rate of 41% (11). Furthermore, a phase 1 study demonstrated the efficacy of a combination of romidepsin with 5-azacytidine in eight of 11 PTCL patients, including three with complete responses in AITL cases (12) A phase 2 study confirmed the efficacy of 5-azacitidine and romidepsin in 25 treatment-naïve PTCL patients, particularly in those with a Tfh phenotype (13). A phase 3 study comparing 5-azacytidine to romidepsin, gemcitabine, or bendamustine in relapsed or refractory AITL patients showed a median PFS of 5.6 months (95%CI, 2.66–8.11) in the 5-azacytidine arm versus 2.8 months in the standard treatment group (95%CI, 1.87–4.83). In the ORACLE trial, 5-azacytidine exhibited a better safety profile and an overall response rate of 33%, with 11% of patients achieving a complete response (14). A phase 1 study reported an overall response rate of 40% using the PD-1 checkpoint blocker nivolumab in five refractory or relapsed PTCL patients (15). A phase 2 study reported modest activity of the single agent tislelizumab, a programmed cell death protein 1 inhibitor, in 44 patients with refractory PTCL including 11 AITL patients with an ORR of 20.5% and a CR rate of 9.1% (16). We provide here our experience of a therapy combining 5-azacytidine and nivolumab (5-Aza/Nivo) through a compassionate use in nine relapsed or refractory AITL patients when no other therapeutic options were available.

Methods

In this monocentric and retrospective study, patients received 5-azacytidine at 75 mg/m^2 subcutaneously for 7 consecutive days every 28 days and nivolumab at a dose of 3mg/kg every 14 days (5-Aza/Nivo) until progression or until achieving a complete response before undergoing allogeneic hematopoietic stem cell transplantation (allo-HSCT), if deemed eligible. Response to treatment was assessed clinically and using positron emission tomography-computed tomography scans (PET-scanner) every two cycles, according to standardized recommendations (17). Expert pathologists from the national program "Lymphopath" confirmed the AITL diagnosis based on the World Health Organization 2016 classification (18). DNA sequencing was performed using deep next-generation sequencing (NGS) with a 47-gene capture panel (Supplementary Method).

This study was conducted in compliance with the Good Clinical Practice protocol and the principles of the Declaration of Helsinki.

Results

Nine patients underwent treatment with the 5-Aza/Nivo regimen (Table 1). The median age was 69 (interquartile range [IQR] 56–82). None of the patients had a concurrent myelodysplastic/myeloproliferative neoplasm. All individuals presented with advanced disease (stage III-IV), with six patients exhibiting cutaneous lesions and one patient having bone marrow involvement. Two patients had a poor performance status (PS>2), and the median international prognostic index (IPI) was 3 at the time of diagnosis. Eight patients had elevated C-reactive protein (CRP), and five patients had elevated ß2-microglobulin. One patient experienced hypercalcemia >3.0 mmol/L, one had severe autoimmune hemolytic anemia and thrombocytopenia, and another had hypereosinophilia. All patients had relapsed or refractory AITL following a median of one (IQR 1–2) therapies before initiating the 5-Aza/Nivo regimen. First-line therapies included CHOP (n=6), reduced dose CHOP (mini-CHOP) (n=2), or CHOEP (n=1). The median time before relapse/progression

TABLE 1 Patient's characteristics at baseline.

ID	Age at diagnosis	Sex	IPI	stage	LDH>ULN	ECOG	Extranodal sites	B2M>ULN	CRP>ULN	B symptoms	NGS Gene (VAF%)	Status at last Follow up	Number of previous therapy	Number of 5-Aza/ Nivo cycles	Best response	Relapse/ progression	Allo-HSCT	PFS (months)
AITL1	82	M	3	3	no	2	1	NA	yes	yes	*TET2* p.Ser385*,(13%) *TET2* p.Leu532*, (11%)	Dead	1	4	PR	yes	no	4
AITL2	62	F	3	4	yes	1	1	yes	no	yes	*DNMT3*(31%) *RHOA* (6%) *TET2* Exon 03 c.3341del (8%) *TET 2Exon 04 c.3467del* (32%)	Alive	2	5	CR	no	yes	>24
AITL3	81	M	4	3	no	2	1	yes	yes	yes	*TP53 (84%) DNMT3 (74%) TET2 (50%)*	Dead	2	7	PR	yes	no	7
AITL 4	56	M	2	4	yes	1	1	NA	yes	no	No mutation	Dead	2	6	PR	yes	no	6
AITL 5	69	M	3	3	yes	3	0	NA	yes	yes	*TET2* Exon 11 c.4636C>T (11%) *TET2* Exon 3 c.3320C>G (11%) *PLCG1* (2%) *RHOA* (2%) *IDH2* (2%)	Dead	1	3	CR	no	yes	15
AITL 6	56	M	3	4	yes	2	1	yes	yes	yes	*TET2 Exon 3 c.2255_2261delATAAAGA* (8%) *TET2 Exon3 c.2428C>T* (8%) *PLCG1* (6%) *IDH2* (6%)	Dead	1	4	PR	yes	no	3
AITL 7	71	F	4	3	yes	3	1	yes	yes	yes	*DNMT3A (40%) TET 2 Exon 3 c.2739delA (39%) TET2 Exon 10 c.4184T>A (37%) CD28 (7%) RHOA (5%)*	Dead	1	1	PD	yes	no	0
AITL 8	52	M	2	4	yes		2	yes	yes	yes	No NGS analysis	Alive	1	4	CR	yes	no	3
AITL 9	74	M	2	3	no	1	0	NA	yes	yes	*TET2 (12%) RHOA (3%)*	Alive	1	4	PD	yes	no	2

M, male; F, female; IPI, international prognostic index; LDH, lactate dehydrogenase; ECOG/PS, Eastern Cooperative Oncology Group/Performance status; B2M, ß2-microglobulin; NA, not applicable; NGS, next generation sequencing; VAF, variant allele frequency; CRP, C-reactive protein; ULN, upper limit of normal value; PR, partial response; CR, complete response, PD, progression; PFS, progression-free survival.

10.3389/fimmu.2024.1410638

counted from start/end of treatment was 6.1 months (IQR 0.8–14.2). Three patients received a second-line therapy consisting of brentuximab vedotin, ifosfamide, carboplatin, and etoposide (BrICE) (19). The median time before the second relapse was 2.8 months (IQR 2.7–6.2).

Treatment with the 5-Aza/Nivo regimen took place between May 2020 and February 2023. Patients received a median of 4 courses (IQR 1–7) (Figure 1). Rituximab was added for two patients due to EBV-induced B-cell proliferation associated with polyarthralgia in one and steroid-refractory autoimmune hemolytic anemia with thrombocytopenia in the other. Lymph node biopsies revealed EBV-positive immunoblasts in all patients, along with circulating EBV DNA (median PCR 4.2 log IQR (3,95–4,56)). Tfh tumor cells expressed PD-1 and PDL-1, indicating immune tolerance against tumor proliferation and potential immune checkpoint inhibitors response markers (Figure 2). NGS was performed in 8 patients; seven harbored *TET2* mutations alone (1 case) or in association with *DNMT3A* (3 cases), or with *RHOA* mutations (4 cases), or with *IDH2* mutations (1 case), *TP53* (1 cases), and *CD28* mutation (1 case). In one patient, no mutation was found, possibly due to too few tumor cells (Table 1).

The tolerance of the treatment was acceptable. All patients experienced grade 1 to 4 adverse events (AEs), but these were mostly transient and readily manageable. Most grade >2 events were sepsis and cytopenias, especially anemia. Infectious events were a picc-related *Klebsiella pneumoniae* bacteremia, a grade 2 prostatitis and a *Clostridium difficile* infection (one case each), all of favorable outcome. One patient experienced a colitis with grade 4 diarrhea related to anti-PD-1 treatment, which responded favorably to corticosteroids while nivolumab was continued. One additional patient had hypothyroidism with no detectable anti-thyroid antibodies. No treatment-related deaths were reported (details in Table 2).

The overall response rate was 78%, including four partial responses (44%) and three complete responses (33%). Notably, one patient with progressive disease after CHOP and BrICE regimens achieved a complete response after 5 courses of 5-azacytidine and 4 courses of nivolumab, followed by an allo-HSCT (Figure 1). The patient remains in persistent complete remission 24 months after allo-HSCT. Another patient with progressive disease following six courses of CHOP achieved a complete response after two courses of 5-Aza/Nivo; subsequently, an allo-HSCT was performed. This patient was still in complete remission but succumbed to COVID-19 pneumonia 9 months after allo-HSCT. One patient refractory to CHOEP, achieved complete remission after two 5-Aza/Nivo courses but experienced progression after the fourth cycle, precluding the planned allo-HSCT. He was then treated with BrICE (Br ICE, 3 cycles) and an autologous stem cell transplantation was performed. The 5-Aza/Nivo regimen was discontinued in the remaining 6 patients due to progressive disease, after a progression-free survival of 3 months (IQR 0.7–7). Six patients died 0 to 7 months later from progressive disease. Nivolumab can induce autoimmune adverse events. None of the patients developed autoimmune complications, including the patient who presented with autoimmune cytopenia at diagnosis. We did not detect a correlation between response to treatment and the number of *TET2* mutations, or the presence of *RHOA, DNMT3A* or *IDH2* mutations.

Discussion

We present here the first AITL patients treated with a regimen combining 5-azacytidine and nivolumab after standard treatment failed to control the disease. We hypothesized here that nivolumab and azacytidine could act synergistically to confer more response

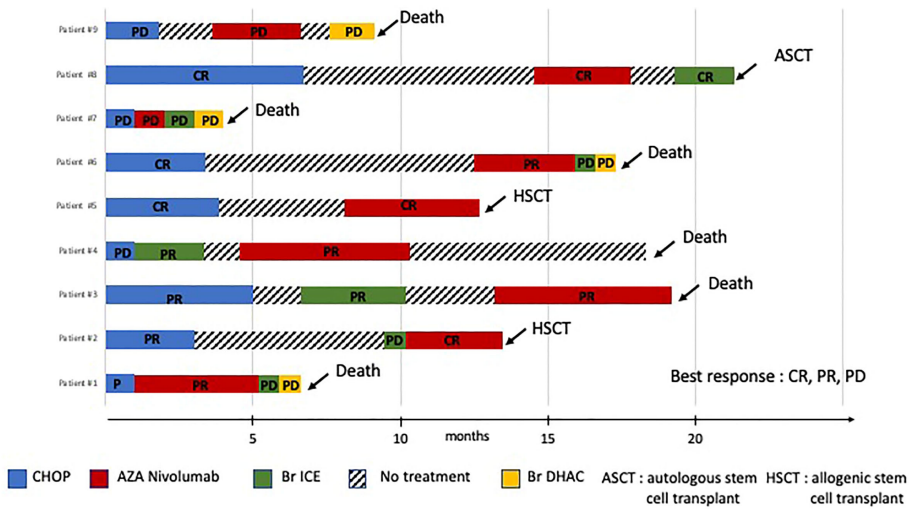

FIGURE 1
Time course of patients from first-line treatment to latest follow-up. The best response and duration of response during the different treatments are shown on the plots. CR, complete response, PR, partial response, PD, progressive disease. HSCT, hematopoietic stem cell transplantation.

10.3389/fimmu.2024.1410638

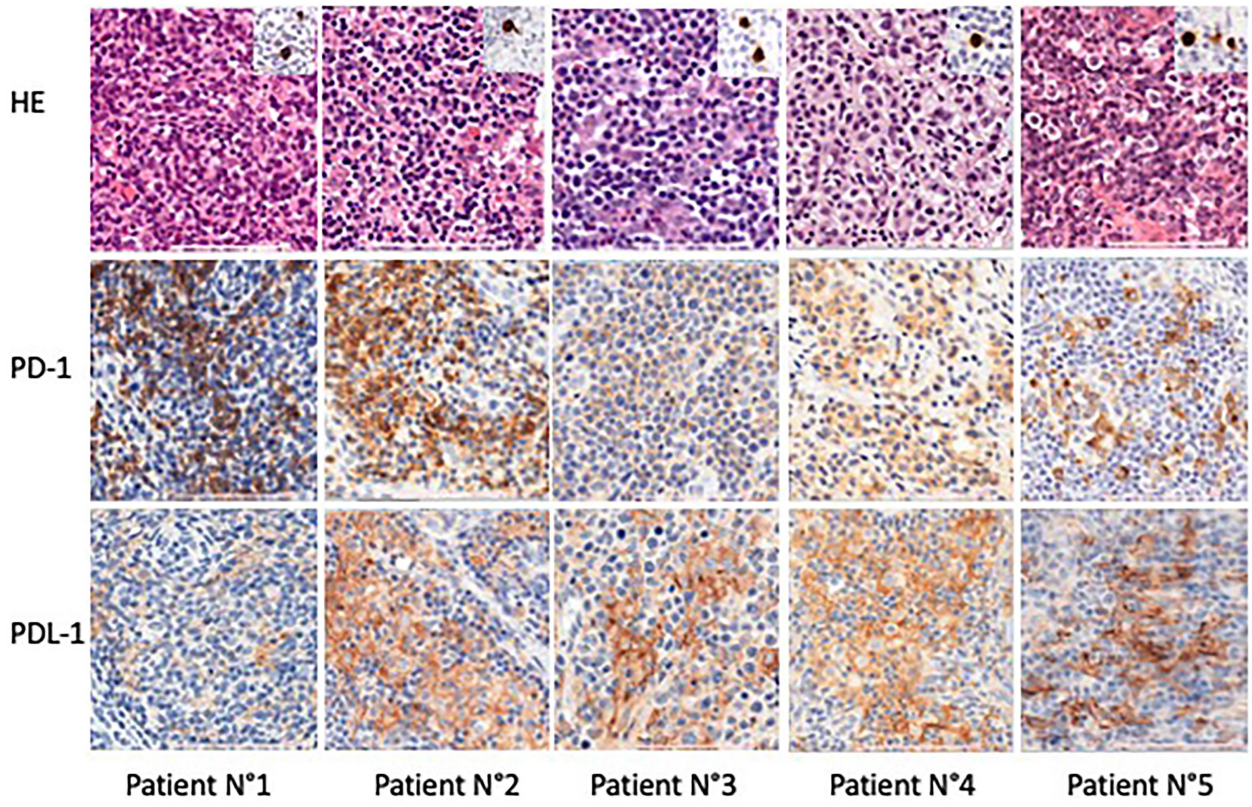

FIGURE 2
Examples of PD-1 and PD-L1 expression in angioimmunoblastic T-cell lymphoma in some patients. x40 Hematoxylin-eosin staining showing typical histopathological features of angioimmunoblastic T-cell lymphoma. Immunostaining with PD-1 and PD-L1 highlighting tumoral T cells. Immunostaining is performed with anti-PD-1 (prediluted, clone NAT105; Roche) and anti-PDL-1 (1/100, Clone QR1; Diagomics) antibodies. The Leica Bond III automated platform (LEICA, Nanterre, France), is used, according to the protocols included in the instructions for antibodies use, applying Bond epitope retrieval solution 1 and 2, respectively for each antibody, 1 (10mn) and 2 (20mn). Tonsil tissue is included on each slide, as positive control.

opportunities in these patients with a dismal prognosis. In line with this view, the majority of patients responded to our regimen, with three cases of complete response. Tolerance was acceptable, supporting the feasibility of this combination, even in elderly and frail patients. Interestingly, this combination could represent an acceptable bridging therapy in patients suitable for an allo-HSCT. A prospective phase 2 study analyzed the effect of single agent nivolumab in refractory peripheral T-cell lymphoma. The study was held because of short-duration response and cases of hyper-progression, particularly in AITL patients (20). Interestingly, we did not observe any case of hyper-progression here, possibly thanks to the combined use of 5-azacytidine. Adding PDL-1 blockers to other

TABLE 2 Patients' complications on vidaza nivolumab regimen.

	Infection	Cytopenia	Other drug-related events
Patient #1	2 grade 3 Picc-related bloodstream infections (*Staphylococus epidermidis*, *Klebsiella pneumoniae*)	Anemia grade 1	no
Patient #2	no	no	Fever related to Nivolumab infusion grade 1
Patient #3	Prostatitis grade 2	Anemia grade 1	Colitis grade 4
Patient #4	*Clostridium difficile* colitis grade 2	Anemia grade 1	no
Patient #5	no	no	Nausea grade 2
Patient #6	no	Neutropenia grade 4	no
Patient #7	no	Anemia grade 2	no
Patient #8	no	no	Hypothyroidism grade 2
Patient #9	no	Anemia grade 3	no

conventional agents showed benefit in non-Hodgkin B cell lymphoma compared to the limited response when given as a single agent (21). In that regard, PDL-1 blockers and PD-1 blockade have been reported to be effective in patients with an aggressive NK/T-cell lymphoma at relapse, as tumor cells harboring EBV genome upregulate PDL-1 (22).

We observed here an encouraging overall response rate of 75% with our regimen. Other doublet regimens for R/R PTCL have also allowed achieving achieved responses in 60% to 80% of patients. Like in our report, the majority of these studies were small phase 1 or phase 2 studies including highly selected patients (12, 13, 23, 24). As opposed to other studies, we included frail patients over 80 years old. Although our results cannot formally demonstrate that nivolumab and 5-azacytidine act synergistically in patients with AITL, we provide evidence that this combination therapy seems at least reasonable in R/R AITL with acceptable side effects. Similarly to other studies, because of the small number of patients and the limited number of patients with wild type *TET2*, we could not provide a correlation between *TET2* mutations and response to 5-azacytidine with anti PDL-1 therapy; interestingly however, two of the three patients who achieved a complete response harbored two *TET2* mutations with *RHOA* mutation (11, 13). Although stemming from a limited number of cases, this observation further supports the rationale of a strategy combining a differentiating agent targeting epigenetic alterations with a checkpoint inhibitor in AITL patients.

Taken together, our preliminary results support 5-azacytidine and nivolumab as a potentially effective rescue combination in relapsed/refractory AITL, and the need for further evaluation of this regimen through formal clinical trials.

Data availability statement

The original contributions presented in the study are included in the article/Supplementary Material. Further inquiries can be directed to the corresponding author.

Ethics statement

Ethical approval was obtained as necessary from local ethical committee. The studies were conducted in accordance with the local legislation and institutional requirements. Written informed consent for participation was not required from the participants or the participants' legal guardians/next of kin in accordance with the national legislation and institutional requirements.

Author contributions

LR: Writing – original draft, Writing – review & editing. PCe: Writing – review & editing. NS: Writing – review & editing. EC: Writing – review & editing. ZV: Writing – review & editing. AB: Writing – review & editing. ZM: Writing – review & editing. RD: Writing – review & editing. CB: Formal analysis, Writing – original draft. A-CJ: Writing – review & editing. MB: Writing – review & editing. PCo: Writing – original draft.

Funding

The author(s) declare that no financial support was received for the research, authorship, and/or publication of this article.

Conflict of interest

The authors declare that the research was conducted in the absence of any commercial or financial relationships that could be construed as a potential conflict of interest.

Publisher's note

Supplementary material

The Supplementary Material for this article can be found online at: https://www.frontiersin.org/articles/10.3389/fimmu.2024.1410638/full#supplementary-material

References

1. Lunning MA, Vose JM. Angioimmunoblastic T-cell lymphoma: the many-faced lymphoma. *Blood*. (2017) 129:1095–102. doi: 10.1182/blood-2016-09-692541

2. Advani RH, Skrypets T, Civallero M, Spinner MA, Manni M, Kim WS, et al. Outcomes and prognostic factors in angioimmunoblastic T-cell lymphoma: final report from the international T-cell Project. *Blood*. (2021) 138:213–20. doi: 10.1182/blood.2020010387

3. Cairns RA, Iqbal J, Lemonnier F, Kucuk C, de Leval L, Jais JP, et al. IDH2 mutations are frequent in angioimmunoblastic T-cell lymphoma. *Blood*. (2012) 119:1901–3. doi: 10.1182/blood-2011-11-391748

4. Couronné L, Bastard C, Bernard OA. TET2 and DNMT3A mutations in human T-cell lymphoma. *N Engl J Med*. (2012) 366:95–6. doi: 10.1056/NEJMc1111708

5. Tari G, Lemonnier F, Morschhauser F. Epigenetic focus on angioimmunoblastic T-cell lymphoma: pathogenesis and treatment. *Curr Opin Oncol*. (2021) 33:400–5. doi: 10.1097/CCO.0000000000000773

6. Lage LA de PC, Culler HF, Reichert CO, da Siqueira SAC, Pereira J. Angioimmunoblastic T-cell lymphoma and correlated neoplasms with T-cell follicular helper phenotype: from molecular mechanisms to therapeutic advances. *Front Oncol*. (2023) 13:1177590/full. doi: 10.3389/fonc.2023.1177590/full

7. Kim S, Kwon D, Koh J, Nam SJ, Kim YA, Kim TM, et al. Clinicopathological features of programmed cell death-1 and programmed cell death-ligand-1 expression in the tumor cells and tumor microenvironment of angioimmunoblastic T cell lymphoma and peripheral T cell lymphoma not otherwise specified. *Virchows Arch Int J Pathol*. (2020) 477:131–42. doi: 10.1007/s00428-020-02790-z

8. Diskin B, Adam S, Cassini MF, Sanchez G, Liria M, Aykut B, et al. PD-L1 engagement on T cells promotes self-tolerance and suppression of neighboring macrophages and effector T cells in cancer. *Nat Immunol*. (2020) 21:442–54. doi: 10.1038/s41590-020-0620-x

9. Qian J, Meng H, Lv B, Wang J, Lu Y, Su L, et al. High expression levels of TLR9 and PD-L1 indicates a poor prognosis in patients with angioimmunoblastic T-cell lymphoma: a retrospective study of 88 cases in a single center. *J Cancer*. (2020) 11:57–68. doi: 10.7150/jca.37033

10. Cortes JR, Ambesi-Impiombato A, Couronné L, Quinn SA, Kim CS, Almeida AC da S, et al. RHOA G17V induces T follicular helper cell specification and promotes lymphomagenesis. *Cancer Cell 12 fèvr*. (2018) 33:259–273.e7. doi: 10.1016/j.ccell.2018.01.001

11. Lemonnier F, Dupuis J, Sujobert P, Tournillhac O, Cheminant M, Sarkozy C, et al. Treatment with 5-azacytidine induces a sustained response in patients with angioimmunoblastic T-cell lymphoma. *Blood*. (2018) 132:2305–9. doi: 10.1182/blood-2018-04-840538

12. O'Connor OA, Falchi L, Lue JK, Marchi E, Kinahan C, Sawas A, et al. Oral 5-azacytidine and romidepsin exhibit marked activity in patients with PTCL: a multicenter phase 1 study. *Blood*. (2019) 134:1395–405. doi: 10.1182/blood.2019001285

13. Falchi L, Ma H, Klein S, Lue JK, Montanari F, Marchi E, et al. Combined oral 5-azacytidine and romidepsin are highly effective in patients with PTCL: a multicenter phase 2 study. *Blood*. (2021) 137:2161–70. doi: 10.1182/blood.2020009004

14. Dupuis J, Tsukasaki K, Bachy E, Morschhauser F, Cartron G, Fukuhara N, et al. Oral azacytidine in patients with relapsed/refractory angioimmunoblastic T-cell lymphoma: final analysis of the oracle phase III study. *Blood*. (2022) 140:2310–2. doi: 10.1182/blood-2022-156789

15. Lesokhin AM, Ansell SM, Armand P, Scott EC, Halwani A, Gutierrez M, et al. Nivolumab in patients with relapsed or refractory hematologic Malignancy: preliminary results of a phase ib study. *J Clin Oncol Off J Am Soc Clin Oncol*. (2016) 34:2698–704. doi: 10.1200/JCO.2015.65.9789

16. Bachy E, Savage KJ, Huang H, Kwong YL, Gritti G, Zhang Q, et al. Treating relapsed/refractory mature T- and NK-cell neoplasms with tislelizumab: a multicenter open-label phase 2 study. *Blood Adv*. (2023) 7:4435–47. doi: 10.1182/bloodadvances.2022009575

17. Cottereau AS, El-Galaly TC, Becker S, Broussais F, Petersen LJ, Bonnet C, et al. Predictive value of PET response combined with baseline metabolic tumor volume in peripheral T-cell lymphoma patients. *J Nucl Med Off Publ Soc Nucl Med*. (2018) 59:589–95. doi: 10.2967/jnumed.117.193946

18. Swerdlow SH, Campo E, Pileri SA, Harris NL, Stein H, Siebert R, et al. The 2016 revision of the World Health Organization classification of lymphoid neoplasms. *Blood*. (2016) 127:2375–90. doi: 10.1182/blood-2016-01-643569

19. Van de Wyngaert Z, Coppo P, Cervera P, Fabiani B, Lemonnier MP, Corre E, et al. Combination of brentuximab-vedotin and ifosfamide, carboplatin, etoposide in relapsed/refractory peripheral T-cell lymphoma. *Eur J Haematol*. (2021) 106:467–72. doi: 10.1111/ejh.13568

20. Bennani NN, Kim HJ, Pederson LD, Atherton PJ, Micallef IN, Thanarajasingam G, et al. Nivolumab in patients with relapsed or refractory peripheral T-cell lymphoma: modest activity and cases of hyperprogression. *J Immunother Cancer. juin*. (2022) 10:e004984. doi: 10.1136/jitc-2022-004984

21. Merryman RW, Armand P, Wright KT, Rodig SJ. Checkpoint blockade in Hodgkin and non-Hodgkin lymphoma. *Blood Adv*. (2017) 1:2643–54. doi: 10.1182/bloodadvances.2017012534

22. Chan TSY, Li J, Loong F, Khong PL, Tse E, Kwong YL. PD-1 blockade with low-dose nivolumab in NK/T cell lymphoma failing L-asparaginase: efficacy and safety. *Ann Hematol*. (2018) 97:193–6. doi: 10.1007/s00277-017-3127-2

23. Amengual JE, Lichtenstein R, Lue J, Sawas A, Deng C, Lichtenstein E, et al. A phase 1 study of romidepsin and pralatrexate reveals marked activity in relapsed and refractory T-cell lymphoma. *Blood*. (2018) 131:397–407. doi: 10.1182/blood-2017-09-806737

24. Moskowitz A, Koch R, Mehta-Shah N, Myskowski P, Kheterpal M, Dogan A, et al. *In vitro*, *in vivo*, and parallel phase I evidence support the safety and activity of duvelisib, a PI3K-δ,γ Inhibitor, in combination with romidepsin or bortezomib in relapsed/refractory T-cell lymphoma. *Blood*. (2017) 130:819–819. doi: 10.1182/blood.V130.Suppl_1.819.819

frontiers | Frontiers in Immunology

TYPE Original Research
PUBLISHED 13 August 2024
DOI 10.3389/fimmu.2024.1415328

OPEN ACCESS

EDITED BY
Michael John Robertson,
Indiana University Bloomington, United States

REVIEWED BY
Eytan Breman,
Celyad SA, Belgium
Erden Atilla,
Fred Hutchinson Cancer Center,
United States
Diogo Gomes Silva,
Universidade de Lisboa, Portugal

*CORRESPONDENCE
Pavel Otáhal
otahal@uhkt.cz

RECEIVED 10 April 2024
ACCEPTED 18 July 2024
PUBLISHED 13 August 2024

CITATION
Mucha M, Štach M, Kaštánková I, Rychlá J, Vydra J, Lesný P and Otáhal P (2024) Good manufacturing practice-grade generation of CD19 and CD123-specific CAR-T cells using piggyBac transposon and allogeneic feeder cells in patients diagnosed with B-cell non-Hodgkin lymphoma and acute myeloid leukemia.
Front. Immunol. 15:1415328.
doi: 10.3389/fimmu.2024.1415328

Good manufacturing practice-grade generation of CD19 and CD123-specific CAR-T cells using piggyBac transposon and allogeneic feeder cells in patients diagnosed with B-cell non-Hodgkin lymphoma and acute myeloid leukemia

Martin Mucha[1,2], Martin Štach[1,2], Iva Kaštánková[1], Jana Rychlá[1], Jan Vydra[1], Petr Lesný[1] and Pavel Otáhal[1*]

[1]Institute of Hematology and Blood Transfusion, Prague, Czechia, [2]Faculty of Science, Charles University, Prague, Czechia

Background: The non-viral production of CAR-T cells through electroporation of transposon DNA plasmids is an alternative approach to lentiviral/retroviral methods. This method is particularly suitable for early-phase clinical trials involving novel types of CAR-T cells. The primary disadvantage of non-viral methods is the lower production efficiency compared to viral-based methods, which becomes a limiting factor for CAR-T production, especially in chemotherapy-pretreated lymphopenic patients.

Methods: We describe a good manufacturing practice (GMP)-compliant protocol for producing CD19 and CD123-specific CAR-T cells based on the electroporation of transposon vectors. The lymphocytes were purified from the blood of patients undergoing chemotherapy for B-NHL or AML and were electroporated with piggyBac transposon encoding CAR19 or CAR123, respectively. Electroporated cells were then polyclonally activated by anti-CD3/CD28 antibodies and a combination of cytokines (IL-4, IL-7, IL-21). The expansion was carried out in the presence of irradiated allogeneic blood-derived mononuclear cells (i.e., the feeder) for up to 21 days.

Results: Expansion in the presence of the feeder enhanced CAR-T production yield (4.5-fold in CAR19 and 9.3-fold in CAR123). Detailed flow-cytometric analysis revealed the persistence of early-memory CAR-T cells and a low vector-copy number after production in the presence of the feeder, with no negative impact on the cytotoxicity of feeder-produced CAR19 and CAR123 T cells. Furthermore, large-scale manufacturing of CAR19 carried out under GMP conditions using PBMCs obtained from B-NHL patients (starting

Abbreviations: CAR, chimeric antigenic receptor; GMP, good manufacturing practice; PBMCs, peripheral blood mononuclear cells; ELP, electroporation.

10.3389/fimmu.2024.1415328

number=200x10e6 cells) enabled the production of >50x10e6 CAR19 in 7 out of 8 cases in the presence of the feeder while only in 2 out of 8 cases without the feeder.

Conclusions: The described approach enables GMP-compatible production of sufficient numbers of CAR19 and CAR123 T cells for clinical application and provides the basis for non-viral manufacturing of novel experimental CAR-T cells that can be tested in early-phase clinical trials. This manufacturing approach can complement and advance novel experimental immunotherapeutic strategies against human hematologic malignancies.

KEYWORDS

CAR-T cells, leukemia, lymphoma, electroporation, PiggyBac PB transposon

Introduction

The efficiency of CAR-T cell production hinges on the quality of the source material obtained from patients. Intensive chemotherapy-induced lymphopenia escalates the likelihood of CAR-T manufacturing failure and diminishes the therapy's effectiveness (1). These factors are critical, particularly for CAR-T production based on less efficient non-viral approaches that employ electroporation of transposable DNA elements like Sleeping Beauty or PiggyBac transposons (2–4). These alternative approaches offer rapid and cost-effective manufacturing, making them suitable for early-phase clinical trials involving novel genetically engineered tumor-reactive T cells. However, effectively utilizing the non-virally-produced CAR-T necessitates novel and improved production processes.

The viral vectors face significant hurdles in their clinical application, such as large-scale vector production and complex biosafety characterization, which impact the availability of clinical-grade vector production. The standard clinical-grade manufacturing of novel types of CAR-T utilizing viral vectors is thus primarily limited by the complexity of the production of viral vectors. In contrast, transposons provide significant advantages compared to viral vectors, such as decreased production costs, increased biosafety, and low immunogenicity. Furthermore, both lentiviruses (LV) and retroviruses (RV) have lower integration capacity, and they often cannot fit more than 8–9 kb (5) compared to transposons, which additionally limits LV/RVs use for complex multi-gene modifications.

However, the use of transposons for large-scale CAR-T manufacturing faces several critical manufacturing issues. The delivery of the transposon vectors by electroporation is far more toxic to T cells than transduction with LV/RVs and requires a specific device - an electroporator. Electroporation cannot be easily performed in a large volume, i.e., this method significantly reduces the starting numbers of T cells in the manufacturing process and, therefore, yields a much lower number of CAR-T cells compared to LV/RVs (6). This low-efficiency production, unfortunately, becomes a critical factor during CAR-T manufacturing for heavily pretreated patients involved in clinical trials who have undergone intensive chemotherapies and are commonly lymphopenic.

In this study, we aimed to improve the non-viral CAR-T production based on the electroporation of transposon vectors (7), and we present a GMP-compliant production process of CD19-specific (CAR19) and CD123-specific (CAR123) CAR-T cells utilizing lethally irradiated allogeneic PBMCs obtained from healthy blood donors (referred to as the "feeder"). Our results demonstrate that the electroporation approach is highly efficient when producing CAR-T cells from T lymphocytes derived from healthy donors compared to patient-derived T lymphocytes. Previous chemotherapies induced lymphopenia in the blood of the B-NHL and AML patients (B-NHL, n=8, median 0.63x10e6 CD3+/µl, AML, n=10, median 1.3x10e6 CD3+/µl) and reduced the percentage of Tscm-like lymphocytes (CD45RA+CD62L+) which critically reduced the outcome of CAR-T manufacturing. Adding the feeder improved the expansion process and increased the CAR-T yield (4.5-fold in CAR19, n=8, p=0.007 and 9.3-fold in CAR123, n=10, p=0.012). The majority of generated CAR-T cells maintained an early memory (CD45RA+CD62L+/-) phenotype (87% of CD4+CAR19, 93% of CD8+CAR19 cells, n=8, 64% of CD4+CAR123 cells, 80% of CD8+CAR123 cells, n=10). Notably, the large-scale manufacturing of CAR19 carried out under GMP conditions using PBMCs (200x10e6 starting number) obtained from B-NHL patients enabled production of >50x10e6 CAR19 in 7 out of 8 cases in the presence of the feeder while only in 2 out of 8 cases without the feeder and this increased production efficiency made it possible to include these patients into a clinical trial (NCT05054257).

In summary, non-viral/electroporation methods for CAR-T production exhibit low production efficiency in lymphopenic patients undergoing chemotherapy compared to healthy donors. This negative factor can be partially mitigated by adding the feeder, which enhances CAR-T production output, reduces manufacturing

10.3389/fimmu.2024.1415328

failure, and is GMP-compatible. The observed improved expansion of CAR19 and CAR123 T cells in the presence of the feeder widens the range of potential clinical applications for this non-viral manufacturing technique, particularly for novel experimental CAR-T cell products in heavily pretreated patients.

Results

Although the allogeneic feeder cells are lethally irradiated by 30Gy, we confirmed their inability to expand and persist during CAR-T production. The feeder cells were initially labeled with blue fluorescent TIV (Tag-It-Violet) dye. Subsequently, PBMCs were electroporated with a transposon plasmid encoding CAR19 and a second transposon plasmid encoding GFP to fluorescently label generated CAR-T cells. The TIV-labeled feeder was mixed with electroporated cells at ratios of 1:1, 1:3, 1:5, and 1:10 or not added. Flow cytometry analysis at days 1, 7, and 14 post-electroporation quantified the remaining live feeder cells. Results showed that feeder cells do not proliferate and are effectively eliminated, even at the highest 1:1 ratio during cultivation with CAR-T cells (Figures 1A, B, D). Additionally, the viability of electroporated cells one day post-electroporation was similar regardless of the feeder being added or not added (Figure 1C), suggesting additional mechanisms of the feeder's effects.

Next, we aimed to identify the feeder's minimal amount leading to improved CAR-T expansion in chemotherapy-pretreated patients (and who were indicated for tisa-cel therapy). Isolated PBMCs were electroporated with CAR19 transposon and mixed with increasing amounts of feeder. Cells were then expanded in 24-well G-Rex plates in a low-scale protocol for 14 days; our results suggested that the CAR19 expansion correlated with the increasing number of feeder cells per well, peaking at a feeder: PBMC ratio of 1:3 (Figure 2A).

The genotoxicity of the transposition event significantly impacts the quality of produced CAR-T cells. This parameter can be indirectly assessed by quantifying the vector copy number (VCN) per CAR-T cell. Electroporation can be optimized to control the VCN by titrating the concentration of the DNA vector during electroporation (Figure 2B). However, lowering the DNA concentration reduces the percentage of T cells expressing CAR (Figure 2C). Therefore, efficient T cell expansion is a critical parameter for providing an effective CAR-T yield. VCN determined by ddPCR method in CD19 and CD123 CAR-T cells (Figure 2E) showed that both CD19 and CD123 CAR-T cells produced without the feeder had significantly higher VCN than cells produced in the presence of the feeder (CAR19: median 7.3 vs. 3.8, n=4; CAR123: median 8.3 vs. 3.7, n=4). Although these values were not significant (paired t test), all feeder-produced CAR19 and CAR123 had VCN within approved limit (≤5) which is considered a critical parameter in the quality control tests of the CAR-T. Based on these findings, the optimal concentration of transposon DNA in the electroporation solution enabling effective transfection and sufficiently low VCN was determined to be 10 µg/ml. To further

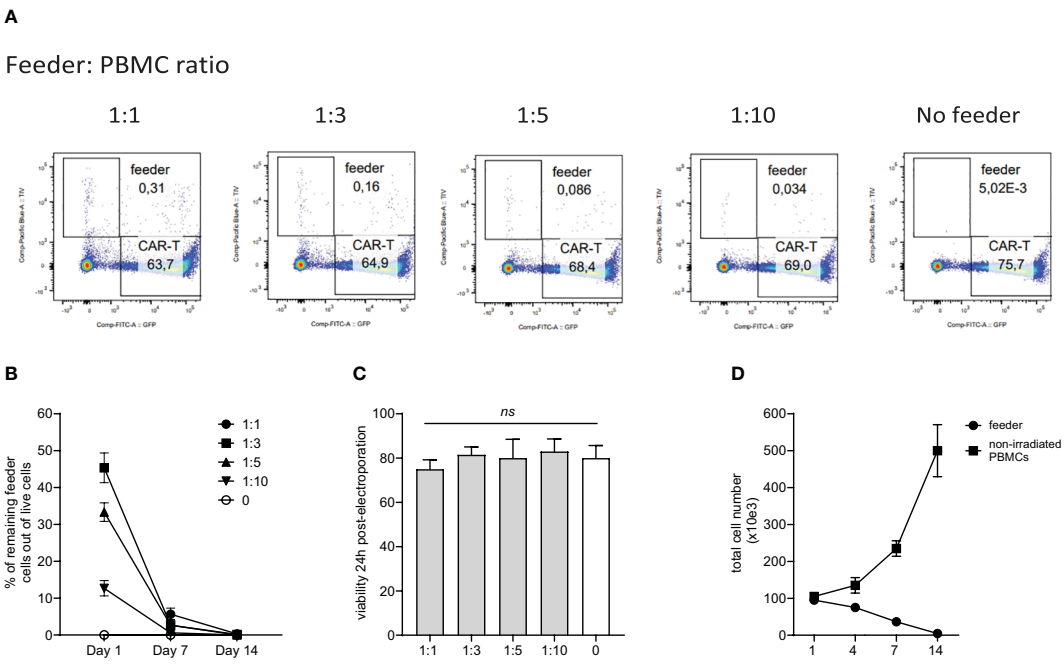

FIGURE 1
Persistence of the feeder cells during *in vitro* expansion of CAR-T cells. PBMCs from healthy donors were electroporated with CAR19 and GFP expressing transposons and mixed with decreasing feeder cells labeled with a blue fluorescent dye (TagItViolet – TIV). The percentage of feeder cells was determined on days 1, 7, and 14 - the representative dot-plot in **(A)** shows the remaining number of feeder cells at day 14 after electroporation, and the kinetics of the feeder persistence is shown in **(B)** (n=3, +/- SD). Next, the effect of the feeder on the viability of electroporated cells was evaluated - the results shown in **(C)** demonstrate that the viability post-electroporation was not significantly influenced by the presence of the feeder (n=3, ns, not significant, +/- SD, one-way ANOVA test). **(D)** Furthermore, we determined the ability of the feeder cell to proliferate *in vitro*. Feeder cells or control non-irradiated PBMCs from the same donors were polyclonally activated with anti-CD3/CD28 antibodies and expanded *in vitro* (n=3, +/- SD). The presented data confirm the inability of feeder cells to proliferate and persist.

10.3389/fimmu.2024.1415328

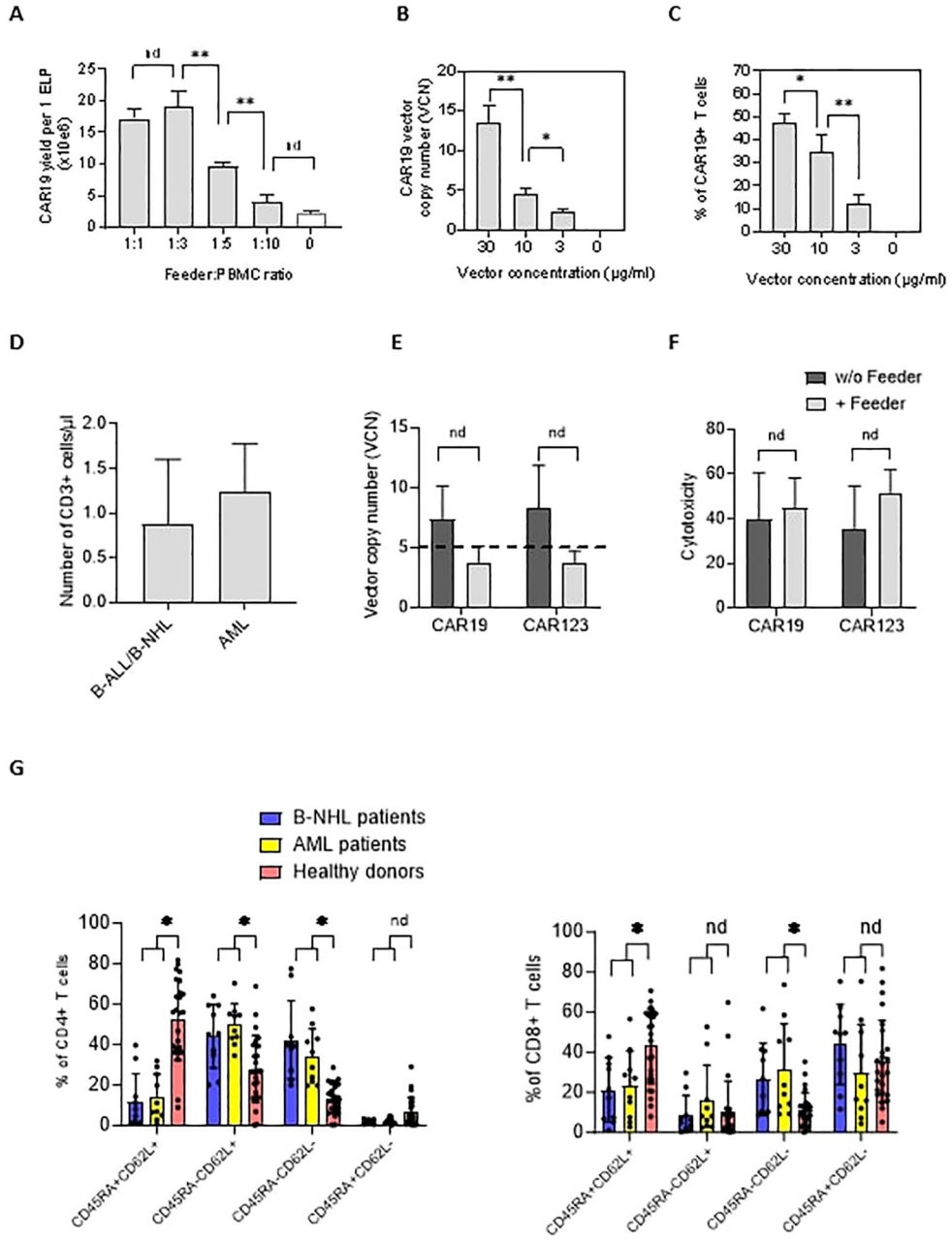

FIGURE 2
The effects of the feeder on the quality of the produced CAR19 and CAR123 T cells. **(A)** The PBMCs from B-NHL patients (n=3) were electroporated with CAR19 transposon and mixed with decreasing amounts of the feeder. The number of CAR+ T cells was determined after 14 days of expansion as a yield per one ELP. The optimal adequate amount of the feeder improving the CAR-T production was estimated to be at a 1:3 feeder: PBMCs ratio. **(B, C)** The concentration of the transposon DNA during electroporation influences the vector copy number (VCN) and the percentage of transfected T cells. The optimal concentration of the transposon vector to meet the VCN limits=5 and to enable effective transfection was determined to be 10 µg/ml (n=3). **(D)** The graph presents the median number and range of CD3+ T lymphocytes in blood samples used for low-scale production of CAR-T cells obtained from B-NHL and AML patients (n=10). Both groups of patients were lymphopenic as a result of previous chemotherapies. **(E)** To evaluate the effects of the feeder on the transposition efficiency, we measured the vector copy number (VCN) per one CAR19+ and CAR123+ T cell in the presence or absence of the feeder (vector concentration =10 µg/ml, PBMCs were obtained from B-NHL and AML patients (n=4)). The differences in VCN were insignificant due to the high variability of the VCN in CAR-T expanded without the feeder. However, all products expanded in the presence of the feeder had acceptable VCN (≤5). **(F)** The biological activity of produced CAR-T in the presence or absence of the feeder was determined by cytotoxic assay against RAMOS cells (CAR19) or THP-1 cells (CAR123) at 1:1 effector: target ratio after 24 hours of co-culture - no significant differences in the cytotoxicity between feeder/no-feeder produced CAR19, and CAR123 T cells were observed (n=4, nd = no difference, unpaired t test). **(G)** The T cell memory phenotype was determined to evaluate the effects of chemotherapies on the quality of T cells by staining for antigens CD45RA and CD62L on CD4+ or CD8+ T cells. Patient-derived samples contained significantly fewer CD45RA+CD62L+ T cells and significantly more T cells having more differentiated phenotype CD45RA-CD62L- in both CD4+ and CD8+ subsets, reflecting the patients' conditions. B-NHL n=8, AML n=10, **P < 0.01, *P < 0.05, nd = no difference, +/- SD, unpaired t test.

evaluate the quality of the produced CAR-T cells, their biological activity was determined by a cytotoxic assay—both CAR19 and CAR123 T cells produced in the presence or absence of the feeder (Figure 2F) effectively killed target cells. In further experiments we used PBMCs obtained from B-NHL and AML patients – all patients received intensive chemotherapies in less than two months before providing the blood samples and both groups were lymphopenic (B-NHL, n=8, median 0.63x10e6 CD3+/µl; AML, n=10, median 1.3x10e6 CD3+/µl, Figure 2D). We determined the T-cell memory phenotype in these samples - significantly less stem-cell memory (Tscm) and significantly more effector memory (Tem) CD4+ and CD8+ T cells were detected (Figure 2G) in comparison to samples obtained from healthy donors.

Improved protocol for the expansion of CD19-specific and CD123-specific CAR-T cells

The effects of the feeder on the production of CAR19 and CAR123 T cells were evaluated using a low-scale/14-day production process utilizing 24-well G-rex plates. At the end of the CAR-T expansion, we determined main parameters reflecting the efficiency of production, such as the percentage of CAR+ T cells, total number of living cells, and the yield of CAR-T per one electroporation of 1x10e7 PBMCs (Figure 3). In the CAR19 expansion model, a significant increase in CAR19 yield (4.5-fold) and total cell number (3.3-fold) in the presence vs. absence of the feeder was observed, while no differences in the percentage of transfected T cells were detected (Figure 3 upper panel). In the case of CAR123, similar effects were also observed: 9.3-fold increase of the CAR123 yield and 15.4-fold increase of total cell numbers in the presence vs. absence of the feeder while minimal effects of the feeder on the percentage of transfected cells were observed (Figure 3 lower panel).

In summary, adding the feeder increases total T-cell expansion and reduces the manufacturing failure rate. Production in the presence of the feeder has no significant negative impacts on the biological activity or the vector copy number.

Large-scale production of CAR T cells

The effects of the feeder on CAR-T production were further evaluated in a large-scale GMP-certified protocol (Figure 4A) in patients with B-NHL involved in a clinical trial (NCT05054257). In this process, a fixed amount of the feeder cells (50x10e6) is added to

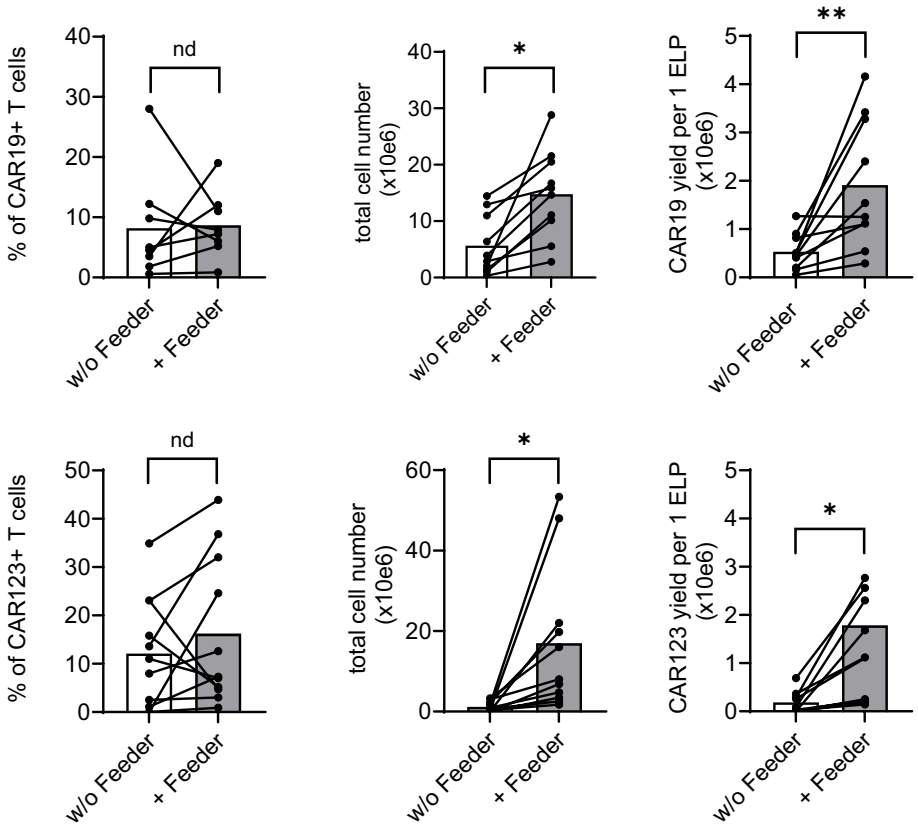

FIGURE 3
Feeder enhances the efficacy of CD19 and CD123 CAR T cell production. PBMCs obtained from B-NHL and AML patients were electroporated with CD19 CAR construct (B-NHL, top panels, N=8) and CD123 CAR construct (AML, lower panels, N=10). Cells were then polyclonally activated with TransAct and expanded in the presence or absence of the feeder for 14 days using a low-scale expansion protocol. The expansion outcome is presented as a percentage of CAR+ T cells, the total live cell numbers, and CAR-T yield per one electroporation. Adding the feeder improved total cell expansion, increasing the production yield of both CAR19 and CAR123 T cells. **P < 0.01, *P < 0.05, nd, no difference, paired t test.

10.3389/fimmu.2024.1415328

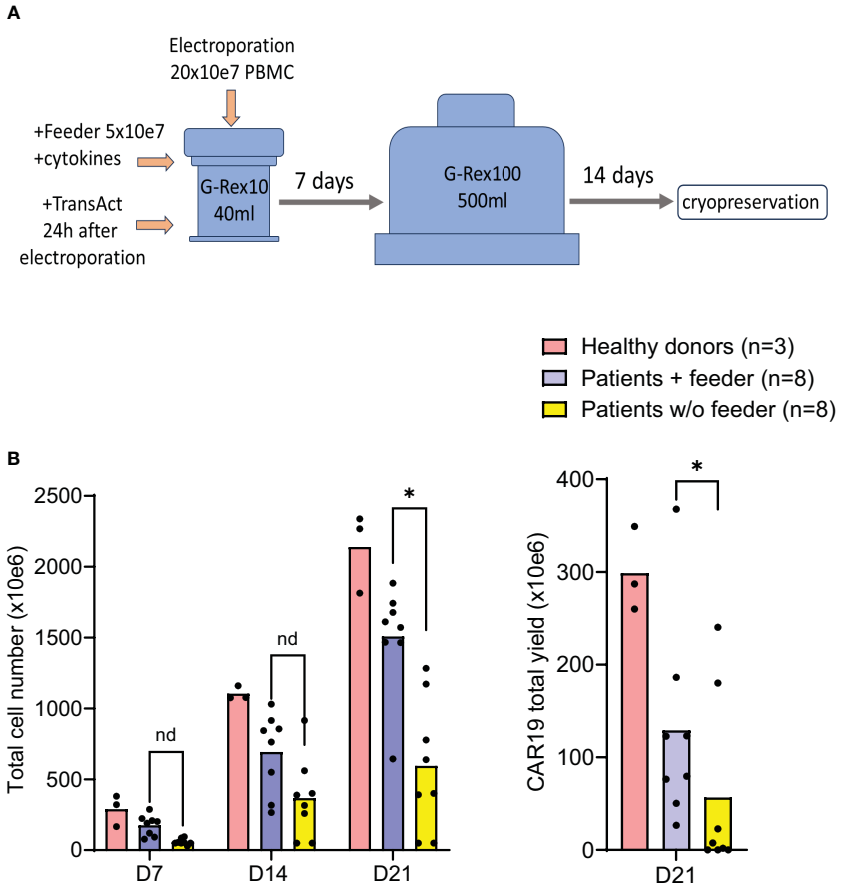

FIGURE 4
Good Manufacturing Practice-grade large-scale production of CAR19 T cells. The production efficacy of CAR19 T cells was validated by a large-scale production protocol under GMP settings. The scheme of the expansion process is shown in **(A)**. Patient-derived PBMCs (n=8) and healthy donors PBMCs (n=3) were transfected with CAR19 transposon (200 million PBMCs electroporated in 20 reactions) and expanded in G-Rex bottles in the presence of cytokines preserving the stem-cell memory phenotype (IL-4, IL-7, IL-21) for up to 21 days. The outcome is presented as a CAR19 total yield [**(A)**, right panel] and the total cell number of viable cells [**(B)** left panel]. *P < 0.05, nd, no difference, unpaired t test.

G-Rex10 bottle and then is mixed with CD19 CAR transposon-electroporated PBMCs. The PBMCs were isolated from a fixed volume of peripheral blood obtained from heavily chemotherapy-pretreated patients suffering from severe T-cell lymphopenia, and based on the obtained amount of PBMCs, the feeder: PBMCs ratio in this large-scale expansion process was within the range of 1:3–1:4, i.e., 150–200 x10e6 PBMCs were electroporated. The following day, T cells were polyclonally activated and further expanded in the presence of cytokines IL-4, IL-7, and IL-21 to preserve the stem-cell memory phenotype of expanding CAR19 T cells. After seven days, the expanding cells were transferred to G-Rex100 bottles and further cultivated until Day 21, when the cells were harvested and cryopreserved. To obtain such high numbers of PBMCs these B-NHL patients underwent leukapheresis as a part of approved clinical trial with CD19 CAR-T cells and all of them had relapsed/refractory B-cell acute leukemia or B-cell lymphoma with more than 3 lines of therapies.

The outcomes of CAR19 T cell production in these patients (n=8) are presented (Figure 4B). These results indicate that the addition of the feeder enables the production of >50x10e6 CAR19 in 7 out of 8 cases in the presence of the feeder while only in 2 out of 8 cases without the feeder. The effective CAR19 expansion without the feeder in these two patients was associated with the presence of high numbers of CD19+ ALL blasts in the blood, which hypothetically might have activated CAR19 during *in vitro* expansion, and no effects of the feeder were observed in these two cases. The remaining patients had minimal numbers of CD19+ B cells in the blood due to previous therapy with anti-CD20 antibody rituximab. The kinetics of T cell expansion (Figure 4B) suggest that the main effect of the feeder is based on the enhancement of total cell expansion rather than primarily increasing the percentage of transfected cells. As previously demonstrated, the combination of cytokines IL-4, IL-7, and IL-21 facilitates the persistence of stem-cell memory CAR-T cells during prolonged *in vitro* expansion (8). A similar analysis was performed to assess the effects of the feeder on the CD19 CAR-T differentiation pattern. Analogically, we analyzed the CAR123 T cells produced by the low-scale method, and the results are presented altogether (Figure 5). The CAR19 and CAR123 produced from healthy donor's PBMCs were expanded without adding the feeder. By multicolor flow cytometry, we identified the expression of antigens CD3, CD4, CD8, CD62L,

10.3389/fimmu.2024.1415328

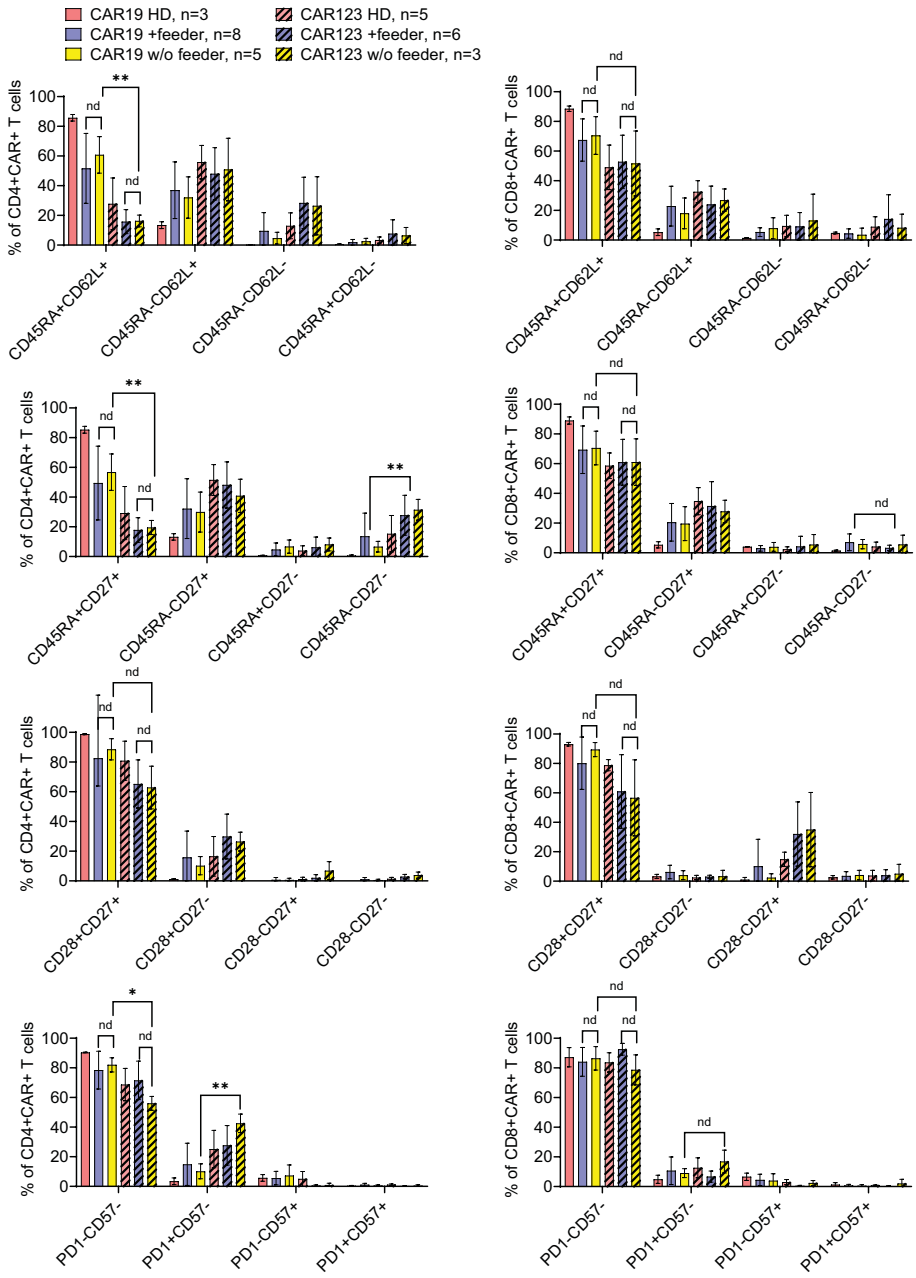

FIGURE 5
The effects of the feeder on the immunophenotype of the produced CAR T cells. CAR19, generated by the large-scale production protocol, and CAR123, generated by the low-scale production protocol, were analyzed by flow cytometry to identify the effects of the feeder on their immunophenotype. PBMCs obtained from healthy donors (HD) were used as control samples. The quantification of individual memory subsets among CAR+ T cells is presented by staining for antigens CD45RA and CD62L, CD27, CD28, PD-1, and CD57 among CD4+ or CD8+ CAR+ T cells. No significant differences in the immunophenotypes were identified between feeder/no-feeder-produced CAR19 and CAR123 T cells. However, CD4+ CAR123 T cells displayed more differentiated/exhausted phenotype in comparison to CD4+ CAR19 T cells (patient-derived/+ feeder groups). **P < 0.01, *P < 0.05, nd, no difference, unpaired t test.

CD45RA, CD27, CD28, PD1, and CD57 to quantify T cell memory subtypes and their exhaustion patterns. No significant differences in CAR-T immunophenotypes after expansion in the presence or absence of the feeder were observed. The majority of CAR19 displayed a less-differentiated (CD45RA+CD27+CD28+PD1-) memory phenotype. However, CAR123 T cells showed more differentiated memory patterns than CAR19 cells, mainly in the CD4+ subtype (Figure 5). A possible explanation is that CD19 antigen is expressed by normal B cells and CD123 antigen is expressed by normal basophils – the recognition of these natural target cells by.

CAR-T during the expansion might influence the differentiation pattern (both CAR19 and CAR123 have identical 4–1BB-zeta signaling domains).

In conclusion, the large-scale expansion of CAR19 T cells in the presence of the feeder results in a more effective production process and generates cells with an optimal immunophenotype. This large-

scale expansion was carried out under GMP conditions, and some of the produced CAR19 were later used in the ongoing clinical trial (NCT05054257).

Materials and methods

Cell source, DNA vectors, feeder production

Peripheral blood mononuclear cells (PBMCs) were isolated from buffy coats obtained from blood donors or from blood samples obtained from AML and B-ALL/B-NHL patients. All human materials used were approved by institutional review boards, and donors and patients signed informed consent for the use of their biological materials. The THP-1 and RAMOS cell lines were acquired from DFMZ, DE. The CAR19 transposon was described previously (9), the CAR123 was created by gene-synthesis using the published sequence as a source (10). The CAR sequences were assembled into parental piggyBac (PB) transposon vectors containing the UBC promoter using standard restriction endonuclease-based cloning techniques. The transposase-expressing vector contained the hyperactive piggyBac transposase driven by the CMV promoter (11, 12). Plasmids were purified using EndoFree kits (Qiagen, Germany). To produce the feeder, buffy coats were lethally irradiated (30 Gy) and processed by Ficoll gradient centrifugation. Isolated PBMCs from five healthy blood donors were mixed and cryopreserved for further use. All cells were grown in CellGenix GMP DC Media supplemented with 10% fetal calf serum and penicillin (100 I.U./mL), streptomycin 100 (µg/mL) antibiotics; the GMP-grade cultivation was without antibiotics.

Production of CAR T cells

PBMCs were transfected with transposon vectors using the Neon electroporator (Thermo Fisher Scientific, USA), following previously established procedures (9). Briefly, 1x10e7 cells were resuspended in 100 µl buffer T containing 1 µg of CAR vector DNA and 1 µg of transposase-expressing vector DNA, then electroporated (20 reactions) using a 1x 20ms/2300V pulse setting per reaction. Subsequently, cells were cultured in G-Rex 10 bottles (Wilson Wolf, USA) in media supplemented with cytokines IL-4 (20 ng/ml), IL-7 (10 ng/ml), and IL-21 (40 ng/ml) in the presence or absence of the feeder (50 mil per G-Rex 10). The next day, cells were activated with TransAct (Miltenyi Biotec, Germany). At day 7, cells were transferred to G-Rex 100 bottles (Wilson Wolf, USA) and continually supplemented with complete media. Small-scale production involved one electroporation reaction of PBMCs obtained from approximately 5–10 ml of blood, followed by cultivation in G-Rex 24 plates (Wilson Wolf, USA) in the presence (5x10e6 cells per well) or, absence of the feeder.

Antibodies and FACS

CAR-T cells were detected with FITC-labeled goat anti-mouse Ab (CAR19) or FITC-labeled anti-FLAG Ab (CAR123). The antigens CD4, CD8, CD45RA, CD62L, CD27, CD28, CD57, and PD1 were used to identify T cell differentiation patterns. The fluorescently labelled antibodies are listed in Table 1. FACS samples were analyzed with a BD Fortessa cytometer, and FlowJo software was used to process FACS data. Statistical analysis was performed using GraphPad Prism software with indicated tests.

TABLE 1 Antibody panel.

Antigen	Fluorochrome	Clone	Manufacturer	Cat. No.
CD3	BV786	UCHT1	BD	565491
CD62L	BV650	DREG-56	BD	563808
CD27	BV480	M-T271	BD	746296
CD4	Pacific Blue	RPA-T4	BD	558116
CD45RA	BUV737	HI100	BD	612846
CD28	PECy7	CD28.2	BioLegend	302926
CD14	Alexa Fluor 594	HCD14	BioLegend	325630
PD-1	PE	EH12.2H7	BioLegend	329906
CD57	APC-Vio770	REA769	Miltenyi Biotec	130–111-813
CD8	Alexa Fluor 700	MEM-31	Exbio	A7–207-T100
Anti-DYKDDDDK Tag	Alexa Fluor 488	L5	BioLegend	637318
F(ab')2 Fragment Goat Anti-Mouse IgG (H+L)	Alexa Fluor 488		Jackson IR	115–546-003
LIVE/DEAD Fixable Blue Dead Cell Stain			Invitrogen	L34962

In vitro assays

Cytotoxic tests of CAR-T cells were performed against AML cell line THP-1 (CAR123) or B-cell line RAMOS (CAR19). Target cells were labeled with CFSE dye at a concentration of 5 µM for 5 min at 37°C (Thermo Fisher, USA) and cultivated with CAR-T cells at a 1:1 effector: target ratio for 24 hours in 1 ml media in 24-w plate. The percentage of dead/live target cells was determined by FACS using DAPI live dye. The cell numbers were determined by using a common counting chamber.

Vector copy number

A droplet digital PCR (ddPCR)-based approach was developed to measure the vector copy number (VCN) of both CAR19 and CAR123 transposons. Genomic DNA was isolated with QIAamp DNA Mini Kit (Qiagen, Germany). Duplex PCR reactions contained ddPCR Supermix for Probes (no dUTP) (cat. n. 186–3024, Bio-Rad Laboratories, USA), 900 nM of each primer pair, 250 nM of each FAM- and HEX-labeled probe, and 40 ng of genomic DNA. ddPCR equipment from Bio-Rad Laboratories (USA) was used in all tests. The reaction mix was split into around 20,000 droplets using a QX200 droplet. The PCR was performed on a C1000 Touch thermal cycler using the following amplification conditions: 10 min at 95°C, 45 cycles of 30s at 94°C and 60s at 54°C, and ending with 10 min at 98°C for droplet stabilization and cooling to 4°C. Droplets were analyzed by QX200 droplet reader based on their fluorescence amplitude into positive or negative. Data were processed with Quanta-Soft Analysis Pro software. The vector copy number (VCN) was determined as the ratio of (CAR copies/albumin copies) x2/% of CAR+ T cells in the sample.

Discussion

In this study, we present a Good Manufacturing Practice-grade method of production of CD19 and CD123-specific CAR-T cells. Non-viral CAR-T production is facing low production efficiency - here, we show that the addition of lethally irradiated allogeneic mixed PBMCs effectively increased the production yield of both CD19 CAR-T and CD123 CAR-T in patients with low T-cell counts/quality due to previous chemotherapies and reduced the manufacturing failure rate. Importantly, no negative effects of the feeder, such as alterations in CAR-T memory phenotype, an increase in vector copy number, or reduction in CAR-T cytotoxicity, were observed. The feeder-based protocol was implemented for the production of GMP-grade therapeutic CAR19 which are currently used in a clinical trial NCT05054257.

Electroporation, a key step in the discussed CAR-T cell manufacturing process, is inherently damaging to T cells (13). Reducing this toxicity is crucial for the successful development of an efficient manufacturing process. When cells are exposed to an electric field in the presence of DNA, a DNA-membrane complex is formed on the membrane facing the cathode. This complex then enters the cells through endocytosis or macropinocytosis (14–16). The presence of DNA in the cytoplasm mitigates viral infection and triggers cell defensive pathways by activating cytosolic DNA sensors (17). These sensors, a subgroup of pattern recognition receptors (PRRs), not only induce an inflammatory immune response in damaged cells but may also lead to cell death, primarily through apoptosis (13). These effects are cell type-specific and dependent on the concentration of DNA. In addition to the mechanisms triggered by PRRs, the physical parameters of electroporation, such as the strong electric field, can cause membrane damage, resulting in electrolyte imbalance, influx of water, osmotic swelling of the cells, and, consequently, cell death by necrosis (18). The physical parameters are defined by the electroporator device's design, such as the electroporation chamber's width. Several instruments, such as Amaxa®Nucleofector®, MaxCyte®, Neon™ transfection system, and Xenon™ electroporation system, are currently available and are used to produce therapeutical CAR-T in various clinical trials. After testing these instruments, we observed that Neon can effectively electroporate non-activated T cells at low DNA concentration (10 µg/ml), resulting in a vector copy number less than 5. We have also tested the electroporation of pre-activated T cells using all of these instruments. However, the outcome was not superior to the presented protocol due to the high toxicity of this type of electroporation, which additionally required a much higher concentration of the plasmids. For these reasons, the Neon device was selected for GMP-grade CAR-T cell production.

The importance of the microenvironment is essential for ELP-based production. For example, CAR-T expansion might be supported by antigenic stimulation via CD19-positive B cells (in the case of CAR19) and CD123-positive basophils (in the cease of CAR123) which are physiologically present in the feeder and also by polyclonal T-cell stimulation by HLA-mismatch between the feeder and electroporated PBMCs. In the past, various engineered cell lines have been developed as feeders - however, the usage of such cell lines poses challenges for Good Manufacturing Practice (GMP) production. For instance, Nakamura et al. compared autologous PBMCs with a modified K562 cell line expressing costimulatory molecules CD80, CD86, CD83, and 4–1BB ligand (19). Both types of feeder cells were highly effective in supporting CD19 CAR-T expansion. Similarly, Numbenjapon et al. described artificial antigen-presenting cells (APCs) derived from K562 cells expressing CD19 antigen and two T-cell costimulatory molecules (4–1BB ligand and major histocompatibility class I–related chains A) (20). The use of this APCs led to enhanced expansion of CD19 CAR-T cells during non-viral/electroporation-based production. Morita et al. used irradiated activated autologous T cells to enhance the production of piggyBac-generated CD19-specific CAR-T cells, resulting in an increased percentage of CAR+ T cells and improved *in vitro* expansion (21). Nakamura et al. demonstrated the importance of autologous APCs in the efficiency of expanding electroporation/piggyBac transposon-generated HER2-specific CAR-T cells (19). Positive effects included an enhanced percentage of CAR-T cells with an early memory phenotype and the avoidance of early T cell exhaustion. Saito et al. described an improved piggyBac-transposons-based protocol for the production of CD19 CAR-T in the presence of autologous feeder cells (20). Additionally, similarly to our report, Ramanayake et al. developed an efficient protocol for

selective antigen-specific CAR19 expansion by stimulation with an allogeneic feeder without polyclonal anti-CD3/CD28 stimulation (22). Our protocol, however, uses different combination of cytokines (i.e. IL-4, IL-7, IL-21) plus polyclonal stimulation with TransAct that leads in our experience to expansion of CAR-T with enhanced early-memory phenotype and is more efficient than expansion in the presence of IL-7 and IL-15 (data not shown) (8, 23).

In summary, we described an improved cultivation technique based on the addition of irradiated, mixed allogeneic PBMCs that improves the efficiency of CAR-T manufacturing by transposon/electroporation based methods especially in lymphopenic patients who recently underwent intensive chemotherapies for B-cell lymphomas and acute myeloid leukemia, respectively. The effect of the allogeneic feeder was based mainly on the enhancement of overall T cell expansion after electroporation. The allogeneic mixed feeder cells can be easily produced from healthy blood-donors using the buffy coats and this method is technically feasible and acceptable for the regulatory authorities.

Data availability statement

The raw data supporting the conclusions of this article will be made available by the authors, without undue reservation.

Ethics statement

The studies involving humans were approved by The Ethics Committee of the Institute of Hematology and Blood Transfusion. The studies were conducted in accordance with the local legislation and institutional requirements. The participants provided their written informed consent to participate in this study.

Author contributions

MM: Writing – original draft, Writing – review & editing. MŠ: Writing – original draft, Writing – review & editing. IK: Writing – original draft, Writing – review & editing. JR: Writing – original draft, Writing – review & editing. PL: Writing – original draft, Writing – review & editing. PO: Writing – original draft, Writing – review & editing. JV: Supervision, Writing – review & editing.

Funding

The author(s) declare financial support was received for the research, authorship, and/or publication of this article. This work was supported by grant AZV NU22–05-00374 to PO and by grant OPVVV CZ.02.1.01/0.0/0.0/16_025/0007428.

Conflict of interest

The authors declare that the research was conducted in the absence of any commercial or financial relationships that could be construed as a potential conflict of interest.

Publisher's note

References

1. Jo T, Yoshihara S, Okuyama Y, Fujii K, Henzan T, Kahata K, et al. Risk factors for CAR-T cell manufacturing failure among DLBCL patients: A nationwide survey in Japan. *Br J Haematol*. (2023) 202:256–66. doi: 10.1111/bjh.18831

2. Huang X, Guo H, Tammana S, Jung Y, Mellgren E, Bassi P, et al. Gene transfer efficiency and genome-wide integration profiling of sleeping beauty, tol2, and piggyBac transposons in human primary T cells. *Mol Ther*. (2009) 18:1803–13. doi: 10.1038/mt.2010.141

3. Galvan DL, Nakazawa Y, Kaja A, Kettlun C, Cooper LJN, Rooney CM, et al. Genome-wide mapping of Piggybac transposon integrations in primary human T cells. *J Immunother*. (2009) 32:837–44. doi: 10.1097/CJI.0b013e3181b2914c

4. Manuri PVR, Wilson MH, Maiti SN, Mi T, Singh H, Olivares S, et al. PiggyBac transposon/transposase system to generate CD19-specific T cells for the treatment of B-lineage Malignancies. *Hum Gene Ther*. (2010) 21:427–37. doi: 10.1089/hum.2009.114

5. Bulcha JT, Wang Y, Ma H, Tai PWL, Gao G. Viral vector platforms within the gene therapy landscape. *Signal Transduct Target Ther*. (2021) 6:53. doi: 10.1038/s41392-021-00487-6

6. Moretti A, Ponzo M, Nicolette CA, Tcherepanova IY, Biondi A, Magnani CF. The past, present, and future of non-viral CAR T cells. *Front Immunol*. (2022) 13:867013. doi: 10.3389/fimmu.2022.867013

7. Kaštánková I, Štach M, Žižková H, Ptáčková P, Šmilauerová K, Mucha M, et al. Enzymatically produced piggyBac transposon vectors for efficient non-viral manufacturing of CD19-specific CAR T cells. *Mol Ther Methods Clin Dev*. (2021) 23:119–27. doi: 10.1016/j.omtm.2021.08.006

8. Štach M, Ptáčková P, Mucha M, Musil J, Klener P, Otáhal P. Inducible secretion of IL-21 augments anti-tumor activity of piggyBac-manufactured chimeric antigen receptor T cells. *Cytotherapy*. (2020) 22:744–54. doi: 10.1016/j.jcyt.2020.08.005

9. Ptáčková P, Musil J, Štach M, Lesný P, Němečková Š, Král V, et al. A new approach to CAR T-cell gene engineering and cultivation using piggyBac transposon in the presence of IL-4, IL-7 and IL-21. *Cytotherapy*. (2018) 20:507–20. doi: 10.1016/j.jcyt.2017.10.001

10. Riberdy JM, Zhou S, Zheng F, Kim YI, Moore J, Vaidya A, et al. The art and science of selecting a CD123-specific chimeric antigen receptor for clinical testing. *Mol Ther Methods Clin Dev*. (2020) 18:571–81. doi: 10.1016/j.omtm.2020.06.024

11. Li X, Burnight ER, Cooney AL, Malani N, Brady T, Sander JD, et al. piggyBac transposase tools for genome engineering. *Proc Natl Acad Sci U S A*. (2013) 110:2279–87. doi: 10.1073/pnas.1305987110

12. Yusa K, Zhou L, Li MA, Bradley A, Craig NL. A hyperactive piggyBac transposase for mammalian applications. *Proc Natl Acad Sci U.S.A*. (2011) 108:1531–6. doi: 10.1073/pnas.1008322108

13. Beebe SJ, Fox PM, Rec LJ, Willis ELK, Schoenbach KH. Nanosecond, high-intensity pulsed electric fields induce apoptosis in human cells. *FASEB Journal: Off Publ Fed Am Societies Exp Biol*. (2003) 17:1–23. doi: 10.1096/fj.02-0859fje

14. Escoffre JM, Portet T, Favard C, Teissié J, Dean DS, Rols MP. Electromediated formation of DNA complexes with cell membranes and its consequences for gene delivery. *Biochim Biophys Acta Biomembr*. (2011) 1808:1538–43. doi: 10.1016/j.bbamem.2010.10.009

15. Rosazza C, Deschout H, Buntz A, Braeckmans K, Rols MP, Zumbusch A. Endocytosis and endosomal trafficking of DNA after gene electrotransfer *in* vitro. *Mol Ther Nucleic Acids*. (2016) 5:e286. doi: 10.1038/mtna.2015.59

16. Lambricht L, Lopes A, Kos S, Sersa G, Préat V, Vandermeulen G. Clinical potential of electroporation for gene therapy and DNA vaccine delivery. *Expert Opin Drug Deliv*. (2016) 13:295–310. doi: 10.1517/17425247.2016.1121990

17. Mao M, Wang L, Chang CC, Rothenberg KE, Huang J, Wang Y, et al. Involvement of a rac1-dependent macropinocytosis pathway in plasmid DNA delivery by electrotransfection. *Mol Ther*. (2017) 25:803–15. doi: 10.1016/j.ymthe.2016.12.009

18. Golzio M, Escoffre J-M, Portet T, Mauroy C, Teissie J, S. Dean D, et al. Observations of the mechanisms of electromediated DNA uptake - from vesicles to tissues. *Curr Gene Ther*. (2010) 10:256–66. doi: 10.2174/156652310791823461

19. Nakamura K, Yagyu S, Hirota S, Tomida A, Kondo M, Shigeura T, et al. Autologous antigen-presenting cells efficiently expand piggyBac transposon CAR-T cells with predominant memory phenotype. *Mol Ther Methods Clin Dev*. (2021) 21:315–24. doi: 10.1016/j.omtm.2021.03.011

20. Numbenjapon T, Serrano LM, Chang WC, Forman SJ, Jensen MC, Cooper LJN. Antigen-independent and antigen-dependent methods to numerically expand CD19-specific CD8+ T cells. *Exp Hematol*. (2007) 35:1083–90. doi: 10.1016/j.exphem.2007.04.007

21. Morita D, Nishio N, Saito S, Tanaka M, Kawashima N, Okuno Y, et al. Enhanced expression of anti-CD19 chimeric antigen receptor in piggyBac transposon-engineered T cells. *Mol Ther Methods Clin Dev*. (2018) 8:131–40. doi: 10.1016/j.omtm.2017.12.003

22. Saito S, Nakazawa Y, Sueki A, Matsuda K, Tanaka M, Yanagisawa R, et al. Anti-leukemic potency of piggyBac-mediated CD19-specific T cells against refractory Philadelphia chromosome-positive acute lymphoblastic leukemia. *Cytother*. (2014) 16:1257–69. doi: 10.1016/j.jcyt.2014.05.022

23. Ramanayake S, Bilmon IAN, Bishop D, Dubosq M, Blyth E, Clancy L, et al. Low-cost generation of Good Manufacturing Practice-grade CD19-specific chimeric antigen receptor-expressing T cells using piggyBac gene transfer and patient-derived materials. *J Cytother*. (2015) 17:1251–67. doi: 10.1016/j.jcyt.2015.05.013

frontiers | Frontiers in Immunology

TYPE Correction
PUBLISHED 09 September 2024
DOI 10.3389/fimmu.2024.1483043

OPEN ACCESS

APPROVED BY
Frontiers Editorial Office,
Frontiers Media SA, Switzerland

*CORRESPONDENCE
Pavel Otáhal
otahal@uhkt.cz

RECEIVED 19 August 2024
ACCEPTED 21 August 2024
PUBLISHED 09 September 2024

CITATION
Mucha M, Štach M, Kaštánková I, Rychlá J, Vydra J, Lesný P and Otáhal P (2024) Corrigendum: Good manufacturing practice-grade generation of CD19 and CD123-specific CAR-T cells using piggyBac transposon and allogeneic feeder cells in patients diagnosed with B-cell non-Hodgkin lymphoma and acute myeloid leukemia. *Front. Immunol.* 15:1483043. doi: 10.3389/fimmu.2024.1483043

Corrigendum: Good manufacturing practice-grade generation of CD19 and CD123-specific CAR-T cells using piggyBac transposon and allogeneic feeder cells in patients diagnosed with B-cell non-Hodgkin lymphoma and acute myeloid leukemia

Martin Mucha[1,2], Martin Štach[1,2], Iva Kaštánková[1], Jana Rychlá[1], Jan Vydra[1], Petr Lesný[1] and Pavel Otáhal[1]*

[1]Institute of Hematology and Blood Transfusion, Prague, Czechia, [2]Faculty of Science, Charles University, Prague, Czechia

KEYWORDS

CAR-T cells, leukemia, lymphoma, electroporation, PiggyBac PB transposon

A Corrigendum on

Good manufacturing practice-grade generation of CD19 and CD123-specific CAR-T cells using piggyBac transposon and allogeneic feeder cells in patients diagnosed with B-cell non-Hodgkin lymphoma and acute myeloid leukemia

By Mucha M, Štach M, Kaštánková I, Rychlá J, Vydra J, Lesný P and Otáhal P (2024). *Front. Immunol.* 15:1415328. doi: 10.3389/fimmu.2024.1415328

In the published article, there was an error in Figure 2 as published. The description under Figure 2A was displayed as "PBMC:feeder ratio".

Correct description is "Feeder: PBMC ratio".

The authors apologize for this error and state that this does not change the scientific conclusions of the article in any way. The original article has been updated.

Publisher's note

All claims expressed in this article are solely those of the authors and do not necessarily represent those of their affiliated organizations, or those of the publisher, the editors and the reviewers. Any product that may be evaluated in this article, or claim that may be made by its manufacturer, is not guaranteed or endorsed by the publisher.

10.3389/fimmu.2024.1483043

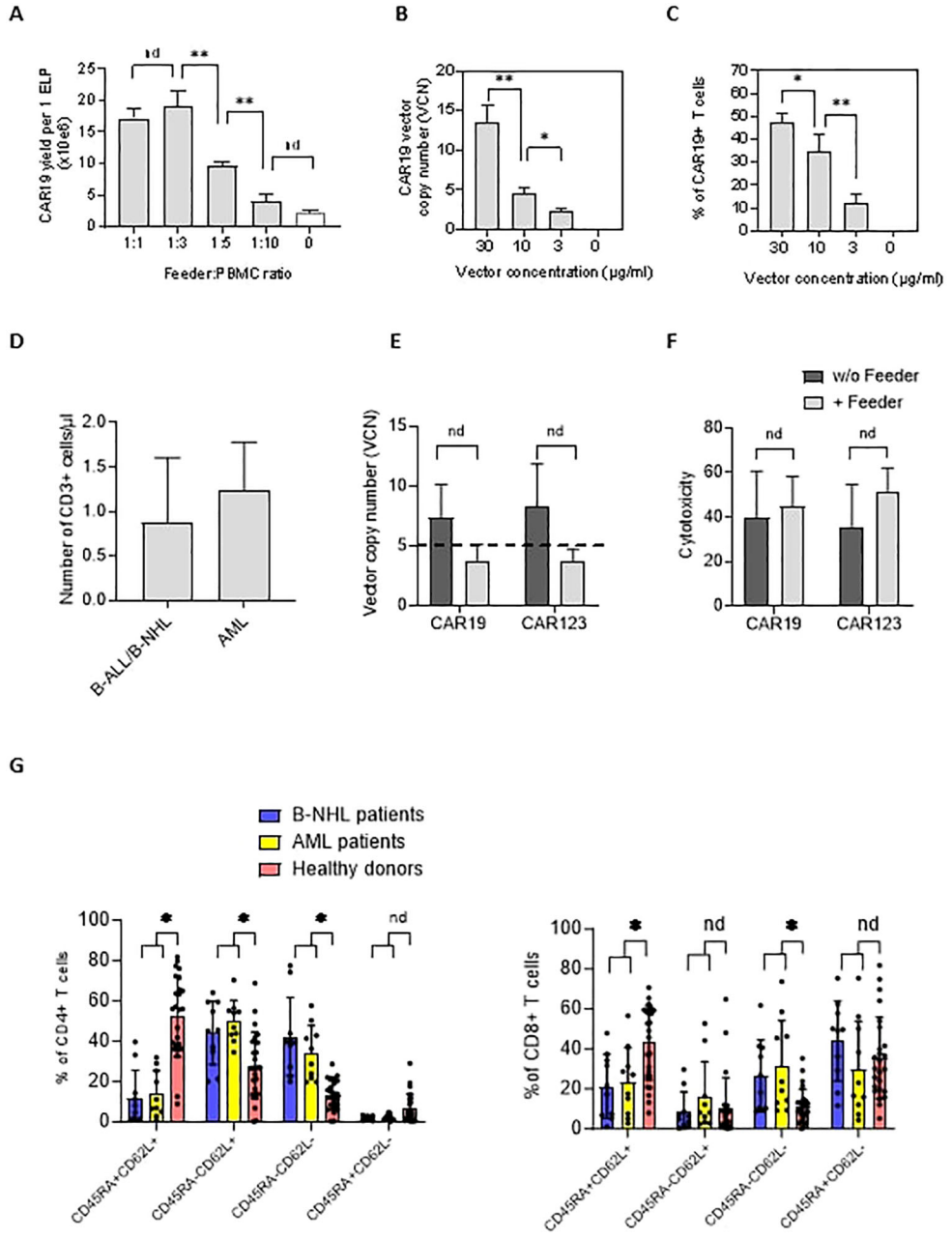

FIGURE 2
The effects of the feeder on the quality of the produced CAR19 and CAR123 T cells. **(A)** The PBMCs from B-NHL patients (n=3) were electroporated with CAR19 transposon and mixed with decreasing amounts of the feeder. The number of CAR+ T cells was determined after 14 days of expansion as a yield per one ELP. The optimal adequate amount of the feeder improving the CAR-T production was estimated to be at a 1:3 feeder: PBMCs ratio. **(B, C)** The concentration of the transposon DNA during electroporation influences the vector copy number (VCN) and the percentage of transfected T cells. The optimal concentration of the transposon vector to meet the VCN limits=5 and to enable effective transfection was determined to be 10 µg/ml (n=3). **(D)** The graph presents the median number and range of CD3+ T lymphocytes in blood samples used for low-scale production of CAR-T cells obtained from B-NHL and AML patients (n=10). Both groups of patients were lymphopenic as a result of previous chemotherapies. **(E)** To evaluate the effects of the feeder on the transposition efficiency, we measured the vector copy number (VCN) per one CAR19+ and CAR123+ T cell in the presence or absence of the feeder (vector concentration =10 µg/ml, PBMCs were obtained from B-NHL and AML patients (n=4)). The differences in VCN were insignificant due to the high variability of the VCN in CAR-T expanded without the feeder. However, all products expanded in the presence of the feeder had acceptable VCN (≤5). **(F)** The biological activity of produced CAR-T in the presence or absence of the feeder was determined by cytotoxic assay against RAMOS cells (CAR19) or THP-1 cells (CAR123) at 1:1 effector: target ratio after 24 hours of co-culture - no significant differences in the cytotoxicity between feeder/no-feeder produced CAR19, and CAR123 T cells were observed (n=4, nd = no difference, unpaired t test). **(G)** The T cell memory phenotype was determined to evaluate the effects of chemotherapies on the quality of T cells by staining for antigens CD45RA and CD62L on CD4+ or CD8+ T cells. Patient-derived samples contained significantly fewer CD45RA+CD62L+ T cells and significantly more T cells having more differentiated phenotype CD45RA-CD62L- in both CD4+ and CD8+ subsets, reflecting the patients' conditions. B-NHL n=8, AML n=10, **P < 0.01, *P < 0.05, nd = no difference, +/- SD, unpaired t test.

frontiers | Frontiers in Immunology

TYPE Original Research
PUBLISHED 23 September 2024
DOI 10.3389/fimmu.2024.1466859

OPEN ACCESS

EDITED BY
Michael John Robertson,
Indiana University Bloomington, United States

REVIEWED BY
Tao Yang,
Guizhou University of Traditional Chinese Medicine, China
Varun Mittal,
Indiana University Bloomington, United States

*CORRESPONDENCE
Ou Bai
baiou@jlu.edu.cn

†These authors have contributed equally to this work

RECEIVED 18 July 2024
ACCEPTED 05 September 2024
PUBLISHED 23 September 2024

CITATION
Wang H, Zhang Y, Li Z and Bai O (2024) Characteristics, efficacy, and prognosis analysis of newly diagnosed marginal zone lymphoma.
Front. Immunol. 15:1466859.
doi: 10.3389/fimmu.2024.1466859

Characteristics, efficacy, and prognosis analysis of newly diagnosed marginal zone lymphoma

Haotian Wang†, Ying Zhang†, Zhaoxia Li and Ou Bai*

Department of Hematology, The First Hospital of Jilin University, ChangChun, Jilin, China

Objective: To retrospectively analyze the characteristics of newly diagnosed marginal zone lymphoma (MZL) patients, evaluate the efficacy of different treatment regimens, and explore prognostic factors in the era of immunotherapy.

Methods: We reviewed the clinical data of newly diagnosed MZL patients treated at the Department of Hematology, The First Hospital of Jilin University, from October 2013 to October 2023. Survival differences between groups were analyzed using the log-rank test, and prognostic factors were identified.

Results: A total of 265 newly diagnosed MZL patients were included, with a median age of 59 years (range 22-90). The most common pathological type was mucosa-associated lymphoid tissue (MALT) lymphoma, accounting for 66.0% of cases. Among the 147 MZL patients included in the efficacy analysis, the median follow-up was 43.4 months. Both the median progression-free survival (PFS) and overall survival (OS) were not reached. The 5-year PFS and OS rates were 76.0% and 86.6%, respectively. Patients who achieved complete response (CR) after induction therapy had significantly better PFS (P=0.0045), OS (P<0.001), and time to next treatment (TTNT) (P=0.0045) compared to those who did not achieve CR. A subgroup analysis was conducted on 51 MZL patients with high tumor burden who received ≥4 cycles of treatment. It was found that the CR rate (CRR) in patients receiving obinutuzumab (G) ± chemotherapy was significantly higher than in those receiving rituximab (R) ± chemotherapy (93.8% *vs*. 48.6%, P=0.002). Multivariate analysis revealed that disease progression or death within 24 months of initial treatment (POD24) was an independent risk factor affecting OS (P<0.001). Patients who experienced POD24 had a median survival of only 19.7 months, with a 3-year OS rate of just 37.6%, whereas those without POD24 had a 3-year OS rate of 97.3%.

Conclusion: MZL is predominantly seen in middle-aged and elderly patients and is a specific indolent B-cell lymphoma, with MALT lymphoma being the most common subtype. Achieving CR after induction therapy significantly prolongs survival in MZL patients. Compared to R ± chemotherapy, G ± chemotherapy achieves a higher CRR in high tumor burden MZL patients. In the era of immunotherapy, POD24 is an independent prognostic factor for MZL.

KEYWORDS

lymphoma, marginal zone lymphoma, rituximab, obinutuzumab, survival analysis

1 Introduction

Marginal zone lymphoma (MZL) is a group of B-cell lymphomas originating from the marginal zone of lymphoid follicles, accounting for 5-15% of all non-Hodgkin lymphomas (NHL) (1, 2). MZL is considered an indolent NHL (iNHL). The World Health Organization (WHO) classifies MZL into three subtypes: extranodal MZL of mucosa-associated lymphoid tissue (MALT), splenic MZL (SMZL), and nodal MZL (NMZL) (3). In the United States, MALT lymphoma is the most common subtype, comprising 61% of all MZL cases, followed by NMZL (30%) and SMZL (9%) (4). The median survival for MZL exceeds 10 years, with varied prognoses across different pathological subtypes. MALT lymphoma has the best prognosis, with a 5-year relative survival rate of 93.8%, compared to 85.3% for SMZL and 82.8% for NMZL (4). The treatment strategies for MZL are tailored to the individual patient and include watchful waiting, anti-infective therapy, surgical resection, radiotherapy, chemotherapy, and immunochemotherapy (5, 6). Currently, there is no international consensus on the preferred first-line treatment for MZL. However, the use of anti-CD20 monoclonal antibody rituximab (R) ± chemotherapy has become widely accepted in clinical practice. Common regimens include R combined with chlorambucil, R-CHOP (rituximab, cyclophosphamide, doxorubicin, vincristine, prednisone), R-CVP (rituximab, cyclophosphamide, vincristine, prednisone), and BR (rituximab, bendamustine) (6–11). These R ± chemotherapy regimens achieve an overall response rate (ORR) of 81%, with 4-year PFS and OS rates of 64.1% and 78.1%, respectively. Nevertheless, some patients exhibit resistance, either not responding to R treatment or experiencing rapid disease progression post-treatment (12, 13). Encouragingly, the advent of obinutuzumab (GA101; G) offers new possibilities for improving MZL treatment outcomes. G is a next-generation, humanized, glycoengineered type II anti-CD20 monoclonal antibody, characterized by enhanced antibody stability, superior antibody-dependent cellular cytotoxicity (ADCC), direct cell death induction, and faster target binding kinetics (14, 15). G has demonstrated efficacy in various B-cell NHL types, such as follicular lymphoma (FL) and chronic lymphocytic leukemia/small lymphocytic lymphoma (CLL/SLL) (16, 17). Notably, the GALLIUM study, which included 1202 patients, aimed to compare the efficacy of G-chemotherapy versus R-chemotherapy as first-line treatment for FL (16). With a median follow-up of 41 months, the G-chemotherapy group showed a 46.0% reduction in the risk of disease progression or death within 24 months of initial treatment (POD24) compared to the R-chemotherapy group (18, 19). Consequently, in June 2021, the National Medical Products Administration (NMPA) of China approved G for adult FL patients. Given the similarities between MZL and FL, both being highly heterogeneous and currently incurable iNHLs, G, with its remarkable mechanism of action and pharmacological profile, has the potential to become a novel therapeutic option for MZL patients.

To explore real-world efficacy, this study aims to retrospectively analyze 265 newly diagnosed MZL cases treated at the Department of Hematology, The First Hospital of Jilin University, from October 2013 to October 2023. The study will summarize the characteristics of MZL, evaluate the effectiveness of different treatment regimens, and investigate prognostic factors in the era of immunotherapy.

2 Materials and methods

2.1 Study subjects

This study included newly diagnosed MZL patients treated at the Department of Hematology, The First Hospital of Jilin University, from October 2013 to October 2023. The diagnostic criteria were based on the 2016 WHO classification of lymphoid neoplasms (20). Inclusion Criteria: Patients of any gender, aged 18 years or older. Pathologically confirmed diagnosis of MZL. No prior treatment history. Exclusion Criteria: Patients with no clear indication for treatment. Patients who received only anti-infective therapy, surgery, or radiotherapy. Patients who received only chemotherapy. Patients who underwent fewer than two treatment cycles. Patients with a history of malignancies. Patients lost to follow-up. This study was conducted in accordance with the guidelines of the Declaration of Helsinki and was approved by the Ethics Committee of The First Hospital of Jilin University.

2.2 Study data

2.2.1 Relevant data

The study collected various types of data, including: General Information: Name, gender, age, etc. Clinical Data: B symptoms, ECOG performance status, marginal zone lymphoma international prognostic index (MZL-IPI), etc. Pathological Results: Pathological subtype, immunohistochemistry, etc. Laboratory Tests: Complete blood count, blood biochemistry, lactate dehydrogenase (LDH), β2-microglobulin (β2-MG), bone marrow biopsy, etc. Imaging Studies: CT, PET-CT, etc. Treatment Regimens: Rituximab (R) ± chemotherapy, obinutuzumab (G) ± chemotherapy. Treatment Efficacy: Complete response (CR), partial response (PR), overall response rate (ORR), progression-free survival (PFS), overall survival (OS), time to next treatment (TTNT) etc.

2.2.2 Disease-related concepts

2.2.2.1 Treatment indications for MZL patients (referencing FL)

Availability of suitable clinical trials. Presence of any discomfort affecting normal work and life. End-organ function impairment. Lymphoma-induced cytopenias due to bone marrow involvement. Bulky disease (referencing GELF criteria). Persistent or rapidly progressing disease.

2.2.2.2 GELF high tumor burden criteria

Involvement of ≥3 lymph node regions with diameters ≥3 cm. Any lymph node or extranodal tumor mass with a diameter ≥7 cm. B symptoms. Splenomegaly. Presence of pleural effusion or ascites.

White blood cell count <1.0×10^9/L or platelet count <100×10^9/L. Malignant cell count >5.0×10^9/L.

2.2.2.3 MZL-IPI

LDH, hemoglobin levels, platelet count, absolute lymphocyte count, MZL subtype.

2.3 Efficacy evaluation

Efficacy was assessed using the revised Lugano classification criteria from the 2014 Lugano Conference, categorizing responses into CR, PR, stable disease (SD), progressive disease (PD), and ORR (21).

2.4 Statistical methods

This study utilized SPSS Statistics 27.0 and R version 4.4.1 for data analysis. Continuous variables following a normal distribution were described using mean ± standard deviation and compared between groups using independent sample t-tests. Categorical variables were described using frequencies and percentages, and differences between groups were assessed using the chi-square test or Fisher's exact test. Survival curves were plotted using GraphPad Prism 10, and differences in survival between groups were analyzed using the log-rank test. Univariate and multivariate prognostic analyses were performed using the Cox proportional hazards model. A $P < 0.05$ was considered statistically significant. Factors with a $P < 0.05$ were used to construct a nomogram using R.

3 Results

3.1 Characteristic analysis

From October 2013 to October 2023, a total of 265 newly diagnosed MZL patients were treated at our center. The median age at diagnosis was 59 years (range: 22-90 years), with a male-to-female ratio of 1.10:1. The most common pathological subtype was MALT lymphoma, accounting for 66.0% (n=175) of cases, followed by NMZL (n=42, 15.8%) and SMZL (n=40, 15.1%). Among the 191 MALT lymphoma cases, the most frequently involved extranodal site was the stomach (n=63, 36.0%), followed by ocular adnexa (n=29, 16.6%), lungs (n=19, 10.9%), intestines (n=15, 8.6%), and bone marrow (13, 7.4%) (Figure 1).

At initial diagnosis, nearly half of the patients (44.9%) were in the early stages (Stage I-II). The majority of patients did not present with B symptoms (n=208, 79.1%), and most were classified into the low-to-intermediate risk group based on the MZL-IPI score (n=234, 88.3%). Laboratory findings indicated that 216 patients (81.5%) had normal LDH levels, and 189 patients (71.3%) had no bone marrow involvement. Among the 40 SMZL patients, 39 underwent bone marrow biopsy, with 92.3% (n=36) showing bone marrow involvement, which was significantly higher than the rates in MALT lymphoma and NMZL (7.4% and 43.9%, respectively) ($P < 0.001$). Helicobacter pylori infection was detected in 29 patients (10.9%), with 96.6% (28/29) of these cases being MALT lymphoma, and 60.7% (17/28) involving the gastrointestinal tract. Additionally, 29 patients (10.9%) had hepatitis B virus infection/carrier status, and 16 patients (6.0%) had Epstein-Barr virus infection (Table 1).

3.2 Efficacy analysis

Based on the inclusion and exclusion criteria (Figure 2), a total of 147 MZL patients were included in the final efficacy analysis. Following induction therapy, 83 patients (56.5%) achieved CR, with an ORR of 92.5%. No significant difference in CR rates (CRR) was observed between patients receiving R or G induction therapy (55.8% *vs.* 58.3%, P=0.8483). Additionally, there was no significant difference in CRR between the same chemotherapy regimens combined with R or G (R-CVP/CHOP *vs.* G-CVP/CHOP: 56.4% *vs.* 66.7%, P>0.999; BR *vs.* GB: 61.5% *vs.* 66.7%, P>0.999) (Figure 3, Table 2). With a median follow-up of 43.4 months, neither the median PFS nor the OS was reached. In the overall analysis, the 3-year and 5-year PFS rates were 83.8% and 76.3%, respectively, while the 3-year and 5-year OS rates were 89.5% and 86.6%, respectively (Figure 4).

Seventeen MZL patients (11.6%) experienced POD24. Survival analysis was performed based on whether patients experienced POD24. The results showed that the median OS for patients with POD24 was only 19.7 months. In contrast, the median OS for patients without POD24 was not reached (P<0.001) (Figure 5), with a 5-year OS rate of 94.0%.

A total of 83 patients (56.7%) achieved CR following induction therapy. A subgroup analysis was conducted based on whether patients achieved CR after induction therapy. The results indicated that the median PFS, OS, and TTNT were not reached in either group. In the CR group, the 3-year and 5-year PFS rates were 91.8% and 83.6%, respectively; the 3-year and 5-year OS rates were 98.6% and 95.9%, respectively; and the 3-year and 5-year TTNT rates were 91.7% and 82.5%, respectively. In contrast, the non-CR group had 3-year and 5-year PFS rates of 73.2% and 66.2%, respectively; 3-year and 5-year OS rates of 77.7% and 74.5%, respectively; and 3-year and 5-year TTNT rates of 71.2% and 63.8%, respectively. Patients who achieved CR after induction therapy had significantly longer PFS (P=0.0045), OS (P<0.001), and TTNT (P=0.0045) compared to those who did not achieve CR (Figure 6).

A subgroup analysis was conducted comparing G ± chemotherapy and R ± chemotherapy. There was a significant difference in baseline characteristics between the two groups, particularly in the presence of high tumor burden (P=0.003) (Table 3). Among the 63 MZL patients with high tumor burden, 51 patients (35 in the R ± chemotherapy group and 16 in the G ± chemotherapy group) received four or more treatment cycles. A short-term efficacy analysis was performed based on the different treatment regimens for these patients. The results showed that after four treatment cycles, 15 patients (93.8%) in the G ± chemotherapy group achieved CR, compared to 17 patients (48.6%) in the R ± chemotherapy group, with a significant difference between the two groups (P=0.002). However, among MZL patients without high

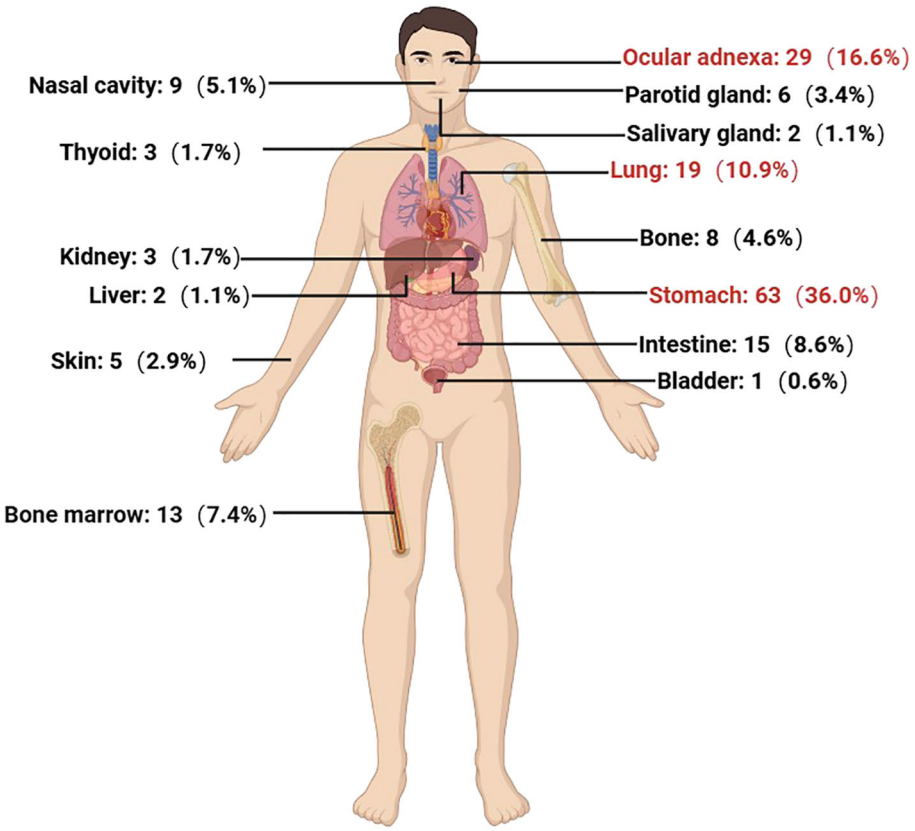

FIGURE 1
Distribution of extranodal involvement in 175 cases of MALT lymphoma.

tumor burden, there was no significant difference in the CRR between the G ± chemotherapy and R ± chemotherapy groups (54.5% *vs.* 63.4%, P=0.740).

2.3 Prognostic analysis

After conducting univariate and multivariate analyses on 147 MZL patients, the results indicated that failure to achieve CR following induction therapy (HR: 3.250, 95% CI=1.409-7.500, P=0.006) was an independent factor affecting PFS. Additionally, failure to achieve CR after induction therapy (HR: 5.1766, 95% CI=1.075-24.934, P=0.040) and the occurrence of POD24 (HR: 22.544, 95% CI=6.390-79.541, P<0.001) were independent factors influencing OS (Supplementary Data, Supplementary Tables S1, S2). Based on these results, we assigned values to factors with P<0.05 and summed the scores of each parameter to obtain a total score. This total score was then converted to OS using a conversion relationship, leading to the construction of a nomogram related to OS. The results demonstrated that the occurrence of POD24 had the greatest impact on prognosis (Figure 7). Furthermore, the effectiveness of the model was evaluated using ROC curve analysis. The results showed that the AUC for the OS prediction model was 0.938 at 3 years and 0.843 at 5 years, indicating that the nomogram had good discriminative ability (Supplementary Data, Supplementary Figure S1). The calibration curve showed slight bias (Supplementary Data, Supplementary Figures S2, S3).

Based on the MZL-IPI score, patients were classified into low-risk, intermediate-risk, and high-risk groups. The low-risk group included 52 patients (35.4%), the intermediate-risk group included 81 patients (55.1%), and the high-risk group included 14 patients (9.5%). The 5-year PFS rates for the low-risk, intermediate-risk, and high-risk groups were 85.5%, 73.6%, and 55.0%, respectively. Similarly, the 5-year OS rates were 95.1%, 82.8%, and 69.6%, respectively. Statistical analysis revealed that, compared to the low-risk group, the high-risk group had significantly shorter PFS (P=0.025) and OS (P=0.040) (Figure 8, Table 4).

3.4 Safety analysis

In this retrospective study, we observed a relatively low number of adverse events (AEs) across the treatment groups. Due to the limited sample size and the infrequency of AEs, the study did not achieve sufficient statistical power to conduct a comprehensive analysis of safety differences. Therefore, we did not perform a significance comparison of AE incidence rates between the different treatment groups.

Despite a higher proportion of infusion reactions in the G± chemotherapy group (41.7%) compared to the R± chemotherapy group (16.2%), no patients discontinued treatment as a result (Table 5). In the R± chemotherapy group, 31.5% of patients experienced grade 3-4 adverse events, with the most common

10.3389/fimmu.2024.1466859

TABLE 1 Baseline characteristics of 265 MZL patients.

Characteristics		n (%)
Age	<60 years	134 (50.6)
	≥60 years	131 (49.4)
Sex	Male	139 (52.5)
	Female	126 (47.5)
Pathological subtype	MALT	175(66.0)
	SMZL	40 (15.1)
	NMZL	42 (15.8)
	MZL (unclassified)	8 (3.0)
Ann Arbor stage	I-II	119 (44.9)
	III-IV	135 (50.9)
	Missing	11 (4.2)
B symptoms	No	208 (79.1)
	Yes	55 (20.9)
MZL-IPI	0	106 (40.0)
	1-2	128 (48.3)
	3-5	25 (9.4)
	Missing	6 (2.3)
ECOG	<2	224 (84.5)
	≥2	41 (15.5)
LDH	Normal	216 (81.5)
	Raise	43 (16.2)
	Missing	6 (2.3)
β2-MG	Normal	48 (18.1)
	Raise	255 (78.1)
	Missing	10 (3.8)
Bone marrow involvement	No	189 (71.3)
	Yes	71 (26.8)
	Missing	5 (1.9)
Infection	Helicobacter pylori	29 (10.9)
	Hepatitis B virus	29 (10.9)
	Epstein-Barr virus	16 (6.0)

MALT, mucosa-associated lymphoma tissue; SMZL, splenic marginal zone lymphoma; NMZL, nodal marginal zone lymphoma; MZL, marginal zone lymphoma; IPI, international prognostic index; ECOG, Eastern Cooperative Oncology Group; LDH, lactate dehydrogenase; β2-MG, β2-microglobulin.

hematologic AEs being leukopenia and neutropenia (both occurring in 17 patients, 15.3%). The most common non-hematologic AE was pneumonia (9 patients, 8.1%). In contrast, 52.8% of patients in the G± chemotherapy group experienced grade 3-4 AEs, with leukopenia being the most common hematologic AE (16 patients, 44.4%) and pneumonia being the most common non-hematologic AE (8 patients, 22.2%). Additionally, two patients in the G± chemotherapy group died from COVID-19 infections within 1-6 months after completing treatment.

4 Discussion

4.1 Characteristic analysis

MZL is the second most common iHNL after FL, accounting for 5-15% of all NHL cases (1). MZL originates from the marginal zone of lymphoid follicles and can occur in mucosa-associated lymphoid tissue, the spleen, and lymph nodes. MZL is highly heterogeneous, and the WHO classifies it into three subtypes: MALT lymphoma, SMZL, and NMZL (3). According to epidemiological studies in the United States, MALT lymphoma is the most common subtype of MZL, comprising 61% of cases, followed by NMZL (30%) and SMZL (9%) (4). In this retrospective study, the median age at diagnosis for 265 newly diagnosed MZL patients was 59 years (range: 22-90 years). Among these patients, 66.0% had MALT lymphoma, 15.8% had NMZL, 15.1% had SMZL, and 3.0% had unclassified MZL. Unlike previous studies, the incidence of SMZL in our study was notably higher. This discrepancy may be attributed to the following reasons: historically, the diagnosis of SMZL relied on splenic biopsy. Currently, for patients who cannot undergo splenic biopsy, diagnosis can be made based on the characteristic cytomorphology in peripheral blood or bone marrow, combined with immunophenotyping and the presence of CD20-positive sinusoidal infiltration in bone marrow pathology (22).

Most patients had low to intermediate-risk prognostic scores (88.3%), normal LDH levels (81.5%), an ECOG performance status of less than 2 (84.5%), and no B symptoms (79.1%). These factors collectively suggest that MZL is an indolent lymphoma characterized by a prolonged disease course and slow progression. In the absence of clear treatment indications, a strategy of watchful waiting is feasible (23). The extranodal involvement of MZL exhibits specificity. Current studies confirm that the most common site of extranodal involvement in MALT lymphoma is the stomach, followed by ocular adnexa and lungs, which is consistent with our findings (1, 24). In our cohort of 265 MZL patients, 71 (26.8%) had bone marrow involvement. Among these, 36 cases were SMZL, accounting for 90.0% of all SMZL cases in this study, which is significantly higher than NMZL and MALT lymphoma (43.9% and 7.4%, respectively; $P < 0.001$). This aligns with previous research (25, 26), indicating that SMZL is more prone to bone marrow involvement compared to MALT lymphoma and NMZL.

In summary, at our center, MZL predominantly affects middle-aged and elderly patients, with MALT lymphoma being the most common pathological subtype. Most patients fall into the low to intermediate-risk prognostic group, with the stomach being the most frequent site of extranodal involvement. SMZL shows a higher propensity for bone marrow involvement compared to other MZL subtypes.

4.2 Efficacy analysis

This study included 147 patients for efficacy analysis. After induction therapy, the ORR reached 92.5%, and the CRR exceeded 50%. Specifically, the ORR and CRR in the G± chemotherapy group were 100% and 58.3%, respectively, which are higher than the results

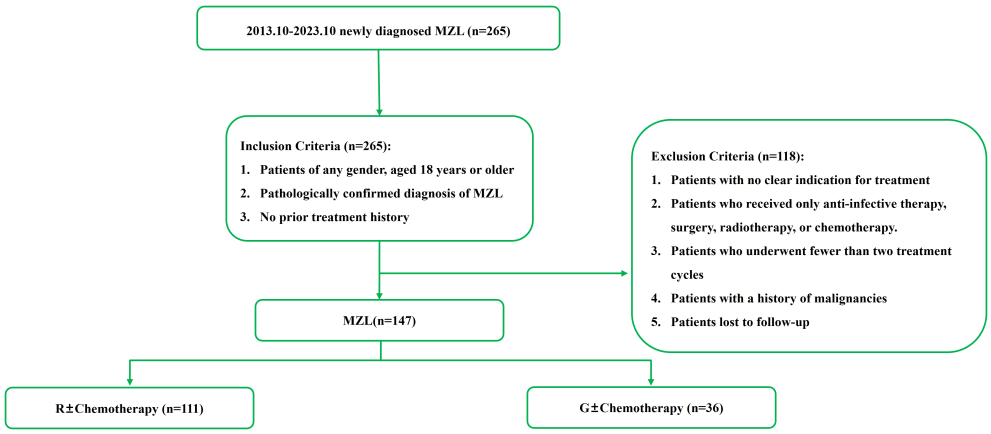

FIGURE 2
Inclusion of cases for efficacy and prognosis analysis in this study.

reported in the GALLIUM study for the G-chemotherapy group (ORR of 81.8% and CRR of 17.2%) (12). These differences may be attributed to factors such as baseline patient characteristics and treatment protocols, and they may also reflect variations in the efficacy of G in different study settings. These findings highlight the potential advantages and prospects of G in the frontline treatment of MZL.

In the study by Kang et al. (8), 40 treatment-naïve MZL patients received R-CVP as first-line therapy. With a median follow-up of 38.2 months, neither median PFS nor OS was reached, with estimated 3-year PFS and OS rates of 59% and 95%, respectively. In the GALLIUM study (12), the R-chemotherapy group included 96 patients with a median follow-up of 59.3 months, reporting 4-year PFS and OS rates of 64.1% and 78.1%, respectively. The G-chemotherapy group, comprising 99 patients, demonstrated 4-year PFS and OS rates of 72.6% and 81.8%, respectively. Our study included 147 treatment-naïve MZL patients who received anti-CD20 monoclonal antibody therapy with or without chemotherapy. The median follow-up was 43.4 months, and neither median PFS nor OS was reached. The 5-year PFS and OS rates were 76.3% and 86.6%, respectively. In the R ± chemotherapy subgroup (111 patients), the 5-year PFS and OS were 76.0% and 86.9%, respectively. Compared to other studies, our R ± chemotherapy group had a larger patient cohort and a longer median follow-up than Kang et al.'s study, showing a slight advantage in PFS and OS.

It remains unclear whether the degree of disease remission influences prognosis. In this study, we performed a survival analysis on patients who achieved CR after induction therapy and found that CR significantly prolonged the survival of patients with MZL. These findings hold significant implications for clinical practice. Firstly, patients who achieved CR after induction therapy showed marked improvements in PFS, OS, and TTNT. This indicates that patients achieving CR have a clear advantage in terms of long-term survival and quality of life. However, it is important to note that while achieving CR is associated with better survival rates, this observation should not be simply interpreted as a direct causal relationship. Patients achieving CR may have inherently favorable disease biological characteristics, which contribute to their

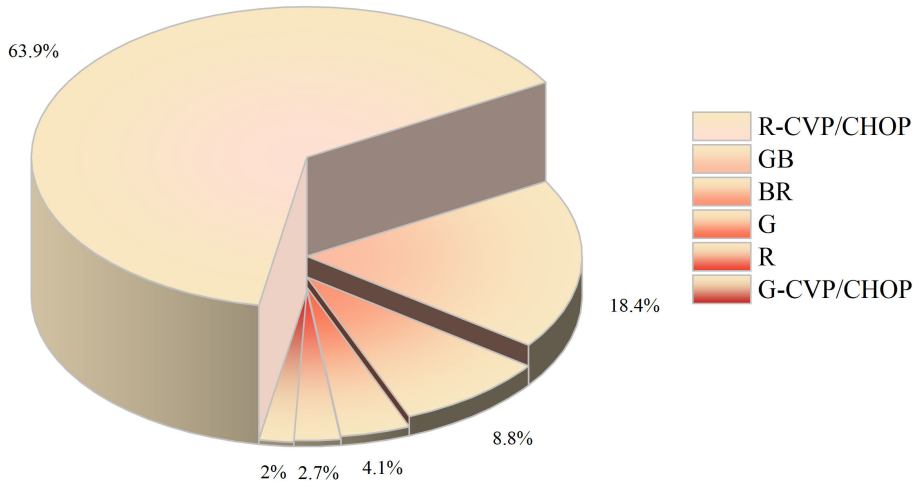

FIGURE 3
Different induction therapy regimens for first-line treatment of MZL.

TABLE 2 Short-term efficacy of different induction therapy regimens.

n (%)	G-CVP/ CHOP (n=3)	GB (n=27)	G (n=6)	G±chemo (n=36)	R-CVP/ CHOP (n=94)	BR (n=13)	R (n=4)	R±chemo (n=111)
CR	2 (66.7)	18 (66.7)	1 (16.7)	21 (58.3)	53 (56.4)	8 (61.5)	1 (25.0)	62 (55.8)
PR	1 (33.3)	9 (33.3)	5 (83.3)	15 (41.7)	31 (33.0)	5 (38.5)	2 (50.0)	38 (34.2)
SD/PD	0 (0)	0 (0)	0 (0)	0 (0)	10 (10.6)	0 (0)	1 (25.0)	11 (9.9)

G, obinutuzumab; R, rituximab; CVP, cyclophosphamide, vincristine, prednisone; CHOP, cyclophosphamide, doxorubicin, vincristine, prednisone; B, bendamustine; chemo, chemotherapy; CR, complete response; PR, partial response; SD, stable disease; PD, progressive disease.

improved outcomes, rather than solely the effect of the treatment itself. Secondly, these results underscore the importance of early assessment of treatment efficacy. By adjusting treatment plans based on early assessment results, clinicians can maximize patient benefits. Early assessment not only helps identify patients who are not responding well to the current treatment regimen but also allows for the development of more individualized treatment strategies for these patients, thereby enhancing the effectiveness and safety of the treatment. Additionally, we must consider the individual differences among patients. Patients who achieve CR may possess more favorable disease characteristics, such as lower tumor burden and better biomarker status. Therefore, in clinical practice, physicians should comprehensively consider the individual characteristics and biological features of the disease in

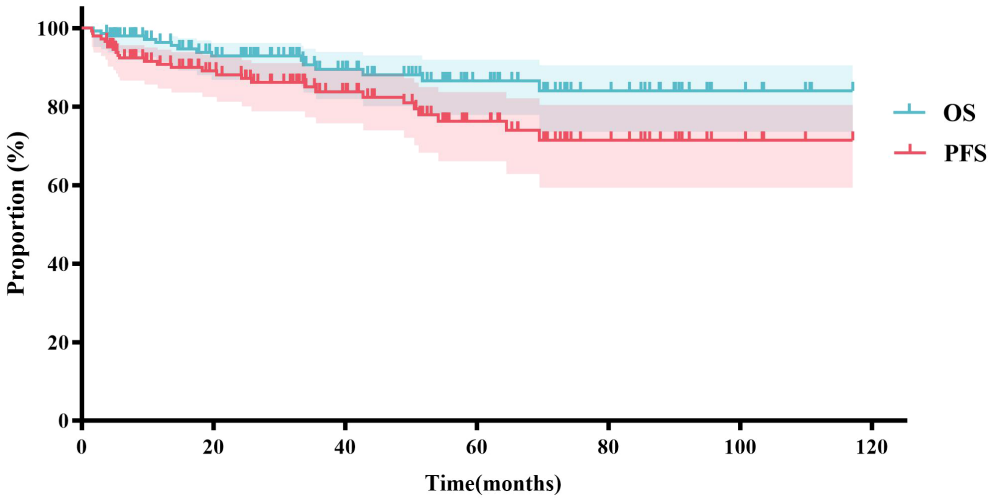

FIGURE 4
Efficacy analysis of 147 MZL cases.

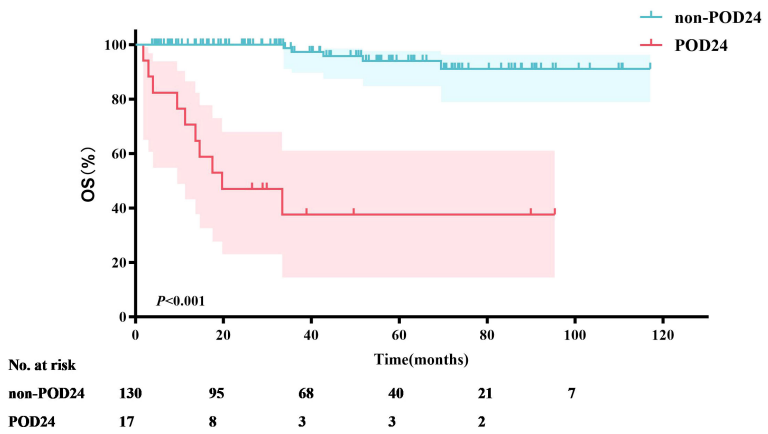

FIGURE 5
Survival analysis of POD24 *vs.* non-POD24 (OS).

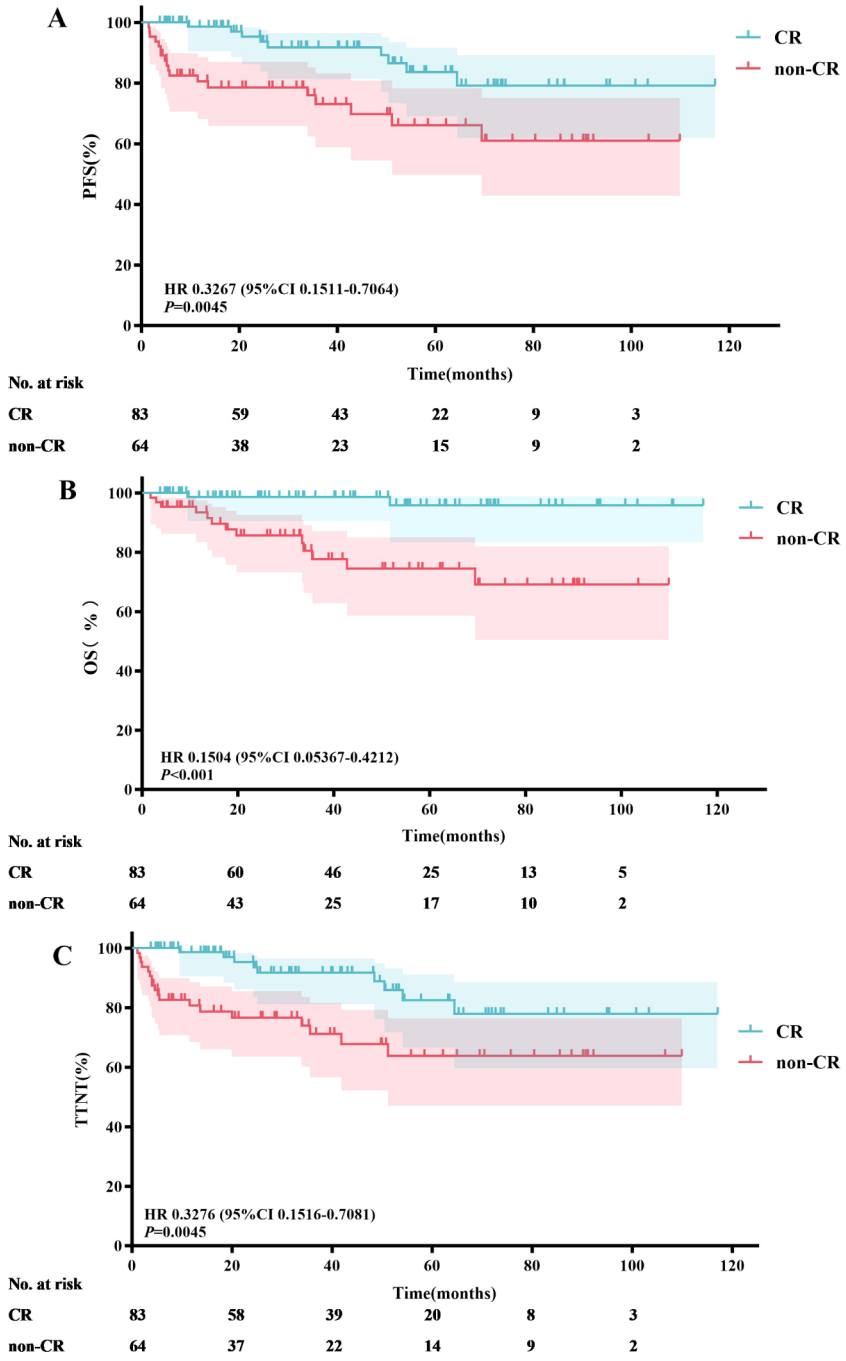

FIGURE 6
Efficacy analysis of patients achieving CR *vs.* not achieving CR after induction therapy: PFS **(A)**, OS **(B)** and TTNT **(C)**.

TABLE 3 Baseline characteristics of MZL patients treated with different anti-CD20 monoclonal antibodies.

Characteristics		R±chemotherapy (n=111)	G±chemotherapy (n=36)	χ^2	*P*
Sex				0.055	0.814
	Male	58 (52.3%)	18 (50.0%)		
	Female	53 (47.7%)	18 (50.0%)		

(Continued)

10.3389/fimmu.2024.1466859

TABLE 3 Continued

Characteristics		R±chemotherapy (n=111)	G±chemotherapy (n=36)	χ^2	*P*
Age				0.055	0.814
	<60 years	58 (52.3%)	18 (50.0%)		
	≥60 years	53 (47.7%)	18 (50.0%)		
Ann Arbor stage				0.625	0.429
	I-II	42 (37.8%)	11 (30.6%)		
	III-IV	69 (62.2%)	25 (69.4%)		
MZL-IPI				0.634	0.811
	0	41 (36.9%)	11 (30.6%)		
	1-2	60 (54.1%)	21 (58.3%)		
	3-5	10 (9.0%)	4 (11.1%)		
B symptoms				3.244	0.072
	no	90 (81.1%)	24 (66.7%)		
	yes	21 (18.9%)	12 (33.3%)		
ECOG				0.006	0.940
	0-1	87 (78.4%)	28 (77.8%)		
	≥2	24 (21.6%)	8 (22.2%)		
High tumor burden				8.611	0.003
	no	71 (64.0%)	13 (36.1%)		
	yes	40 (36.0%)	23 (63.9%)		
INV-assessed response				4.195	0.128
	CR	62 (55.9%)	21 (58.3%)		
	PR	38 (34.2%)	15 (41.7%)		
	SD/PD	11 (9.9%)	0 (0)		

MZL, marginal zone lymphoma; MZL-IPI, MZL-international prognostic index; ECOG, Eastern Cooperative Oncology Group; G, obinutuzumab; R, rituximab; INV, investigator; CR, complete response; PR, partial response; SD, stable disease; PD, progressive disease.

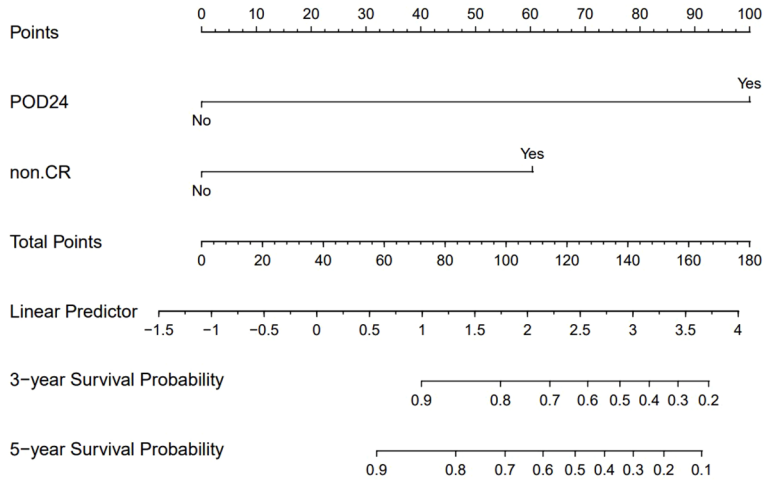

FIGURE 7
OS nomogram prognostic model.

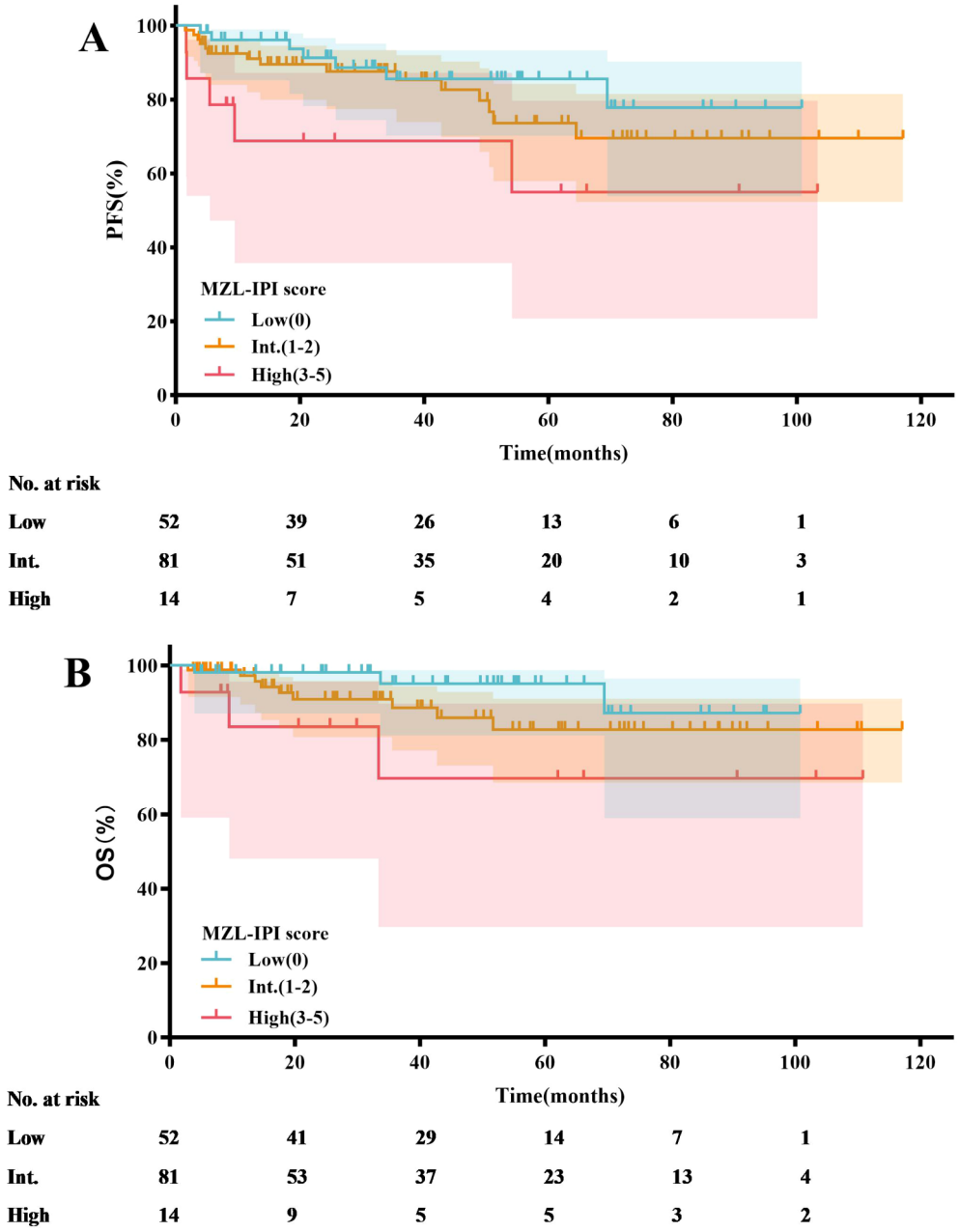

FIGURE 8
MZL-IPI risk stratification analysis: PFS **(A)**, OS **(B)**.

each patient to formulate the most appropriate treatment plan. In conclusion, although this study indicates that achieving CR is associated with better prognosis in MZL patients, we should interpret this result with caution and avoid simply viewing it as a causal relationship. Clinicians should strive to evaluate and optimize treatment plans throughout the treatment process to achieve the best possible long-term survival and quality of life for suitable patients. Future research should further explore the relationship between CR and prognosis and investigate additional factors influencing prognosis to guide clinical practice.

Drawing from previous research, G has shown efficacy in treating high tumor burden FL (27). In this study, we analyzed 63 patients who had a high tumor burden, of which 51 patients received at least four cycles of treatment. We compared the short-term efficacy (ORR and CRR) between patients receiving G ± chemotherapy and those receiving R ± chemotherapy. The results showed that G ± chemotherapy significantly improved the CRR in patients with a high tumor burden (P=0.002). Notably, the GALLIUM study did not specifically investigate the subgroup effects of different treatment regimens in high tumor burden MZL patients (12). Our study preliminarily reveals the potential advantage of G in treating high tumor burden MZL, suggesting superior efficacy. This finding has important implications for clinical practice. For patients with high tumor burden MZL, G combined with chemotherapy may offer a

10.3389/fimmu.2024.1466859

TABLE 4 MZL-IPI risk stratification analysis.

(A) PFS				
Group	n (%)	5-yr PFS%	HR (95%CI)	*P*
Low (0)	52 (35.4)	85.5		
Int. (1-2)	81 (55.1)	73.6	1.520 (0.6511-3.546)	0.333
High (3-5)	14 (9.5)	55	5.529 (1.234-24.76)	0.025
High *vs.* Int.			2.610 (0.728-9.358)	0.141
(B) OS				
Group	n (%)	5-yr OS%	HR (95%CI)	*P*
Low (0)	52 (35.4)	95.1		
Int. (1-2)	81 (55.1)	82.8	2.031 (0.6451-6.396)	0.226
High (3-5)	14 (9.5)	69.6	8.940 (1.104-72.39)	0.04
High *vs.* Int.			2.835 (0.5304-15.16)	0.223

MZL-IPI, marginal zone lymphoma-international prognostic index; PFS, progression-free survival; OS, overall survival; Int., Intermediate.

higher CRR and should be considered by clinicians when devising treatment plans. In contrast, for patients with low tumor burden, the efficacy of the two monoclonal antibodies appears similar, allowing for a balanced choice based on the patient's specific condition and the side effect profiles of the drugs. However, it is undeniable that the small sample size of our study limits the generalizability of the results. In the future, we aim to expand the sample size and extend the follow-up period to more accurately assess the efficacy of G in this specific patient population.

4.3 Prognostic analysis

Previous studies have established POD24 as a critical prognostic factor for MZL patients (28). Conconi et al. (29) analyzed patients from the IELSG-19 study who received immunochemotherapy and found that 18% (69/386) experienced a POD24 event. These patients had a 10-year OS of 64%, compared to 85% in the control group who did not experience POD24. Similarly, in the NF10 observational study (30), 18% (59/321) of MZL patients experienced POD24, leading to a 3-year OS of 53%, whereas patients without POD24 had a 3-year OS of 95%. In our study, 11.6% (17/147) of patients experienced POD24, a lower incidence than reported in the aforementioned studies. However, the median survival for patients with POD24 in our cohort was only 19.7 months, with a 3-year OS of just 37.6%. In contrast, patients who did not experience POD24 had a 3-year OS of 97.3%. This finding underscores the severe impact of POD24 on the survival of MZL patients. This study utilized nomogram analysis to identify key factors influencing OS, with a particular emphasis on the significant impact of POD24. However, due to the insufficient sample size, the calibration curve exhibited some bias. This finding suggests that future research should focus on increasing the sample size and further validating the predictive performance of the model to enhance its clinical applicability.

In recent studies, the MZL-IPI has been established as the first prognostic index for all subtypes of newly diagnosed symptomatic MZL (31). An external validation cohort from the United States included 353 MZL patients, with 94 (27%) classified as low-risk, 192 (54%) as intermediate-risk, and 67 (19%) as high-risk. After a median follow-up of 77.8 months, the 5-year PFS rates for these groups were 69%, 57%, and 45%, respectively (P=0.0018), while the 5-year OS rates were 93%, 84%, and 69%, respectively (P<0.001). In contrast to the aforementioned study, our research found that only the low-risk group had significantly better PFS (P=0.025) and OS (P=0.040) compared to the high-risk group according to the MZL-IPI. Potential reasons for this discrepancy include our relatively smaller sample size. We plan to address this by increasing the sample size and extending the follow-up period in future studies to more accurately validate the clinical utility of the MZL-IPI. Additionally, unlike the U.S. study, all patients in our research received anti-CD20 monoclonal antibody therapy, whereas some patients in the U.S. study did not. Consequently, the 5-year PFS and OS rates in our study were numerically higher. Nonetheless, the MZL-IPI, as the first prognostic index encompassing all MZL subtypes, provides critical guidance for clinicians in developing treatment strategies. Effective risk stratification based on the MZL-IPI allows clinicians to tailor individualized treatment plans, potentially improving long-term survival outcomes. Future research should further explore the application of MZL-IPI in different therapeutic contexts, including novel targeted therapies and immunotherapies. Additionally, studies could investigate integrated prognostic models that combine MZL-IPI with other biomarkers to enhance the predictive accuracy for MZL patient outcomes.

TABLE 5 AEs by chemotherapy arm.

n (%)		G-CVP/ CHOP (n=3)	GB (n=27)	G (n=6)	G±chemo (n=36)	R-CVP/ CHOP (n=94)	BR (n=13)	R (n=4)	R±chemo (n=111)
Infusion reactions		2 (66.7)	11 (40.7)	2 (33.3)	15 (41.7)	15 (16.0)	2 (15.4)	1 (25.0)	18 (16.2)
Grade 3-4AEs		3 (100)	14 (51.9)	2 (33.3)	19 (52.8)	29 (30.9)	6 (46.2)	0 (0)	35 (31.5)
	Hematological	3 (100)	12 (44.4)	1 (16.7)	13 (36.1)	20 (21.3)	6 (46.2)	0 (0)	26 (23.4)
	Non-hematological	0 (0)	6 (22.2)	2 (33.3)	8 (22.2)	11 (11.7)	3 (23.1)	0 (0)	14 (12.6)

AEs, adverse events; G, obinutuzumab; R, rituximab; CVP, cyclophosphamide, vincristine, prednisone; CHOP, cyclophosphamide, doxorubicin, vincristine, prednisone; B, bendamustine; chemo, chemotherapy.

4.4 Safety analysis

The results of the GALLIUM study indicate that the proportion of patients experiencing Grade 3-5 AEs was higher in the group receiving G-chemotherapy compared to those receiving R-chemotherapy (86.1% vs. 77.4%), suggesting that G-chemotherapy has lower tolerability than R-chemotherapy (12). In our study, the incidence of Grade 3-4 AEs was also higher in the G ± chemotherapy group compared to the R ± chemotherapy group (52.8% vs. 31.5%). Additionally, two patients in the G ± chemotherapy group died from COVID-19 infection within 1-6 months after completing treatment. According to the AEs assessment criteria in the GALLIUM study, these were classified as Grade 5 serious AEs. This phenomenon may be related to the stronger ADCC effect associated with G-chemotherapy, which can lead to more significant immunosuppressive effects (32). Therefore, we need to pay closer attention to the severe immunosuppressive consequences that may arise from G ± chemotherapy regimens. In summary, although G-chemotherapy demonstrates better efficacy in certain aspects, the risk of immunosuppression it induces requires significant clinical attention. By optimizing treatment strategies and enhancing monitoring, we can improve efficacy while maximizing patient safety.

5 Limitations

This study has several limitations: (1) As a retrospective study, it inherently suffers from limitations such as selection bias, ambiguous temporal relationships, and restricted generalizability; (2) The wide time span of sample collection poses challenges in data retrieval for certain cases; (3) Regarding the use of novel anti-CD20 monoclonal antibody, the limited application duration and small sample size necessitate future studies to expand the sample size and extend the follow-up period.

6 Conclusion

MZL, commonly seen in middle-aged and elderly individuals, is a specific indolent B-cell lymphoma, with MALT lymphoma being the most prevalent pathological type. Achieving CR after induction therapy significantly prolongs the survival of MZL patients. Compared to R ± chemotherapy, G ± chemotherapy has achieved higher CRR in high tumor burden MZL, particularly in patients with a high tumor burden. In the era of immunotherapy, POD24 remains an independent prognostic factor for MZL.

Data availability statement

The raw data supporting the conclusions of this article will be made available by the authors, without undue reservation.

Ethics statement

The studies involving humans were approved by Ethics Committee of the First Hospital of Jilin University. The studies were conducted in accordance with the local legislation and institutional requirements. The ethics committee/institutional review board waived the requirement of written informed consent for participation from the participants or the participants' legal guardians/next of kin because this was a retrospective study and written informed consent could not be obtained. Written informed consent was not obtained from the individual(s) for the publication of any potentially identifiable images or data included in this article because this was a retrospective study and written informed consent could not be obtained.

Author contributions

HW: Data curation, Methodology, Writing – original draft. YZ: Writing – review & editing. ZL: Writing – review & editing. OB: Funding acquisition, Writing – review & editing.

Funding

The author(s) declare financial support was received for the research, authorship, and/or publication of this article. This study was funded by the Department of Finance of Jilin Province (JLSWSRCZX2023-8).

Acknowledgments

We thank all participants for their contributions.

Conflict of interest

The authors declare that the research was conducted in the absence of any commercial or financial relationships that could be construed as a potential conflict of interest.

Publisher's note

Supplementary material

The Supplementary Material for this article can be found online at: https://www.frontiersin.org/articles/10.3389/fimmu.2024.1466859/full#supplementary-material

References

1. Zucca E, Arcaini L, Buske C, Johnson PW, Ponzoni M, Raderer M, et al. Marginal zone lymphomas: ESMO Clinical Practice Guidelines for diagnosis, treatment and follow-up. *Ann Oncol*. (2020) 31:17–29. doi: 10.1016/j.annonc.2019.10.010

2. Silkenstedt E, Salles G, Campo E, Dreyling M. B-cell non-Hodgkin lymphomas. *Lancet*. (2024) 403:1791–807. doi: 10.1016/s0140-6736(23)02705-8

3. Alaggio R, Amador C, Anagnostopoulos I, Attygalle AD, Araujo IBDO, Berti E, et al. The 5th edition of the world health organization classification of haematolymphoid tumours: lymphoid neoplasms. *Leukemia*. (2022) 36:1720–48. doi: 10.1038/s41375-022-01620-2

4. Cerhan JR, Habermann TM. Epidemiology of marginal zone lymphoma. *Ann Lymphoma*. (2021) 5. doi: 10.21037/aol-20-28

5. Cheah CY, Seymour JF. Marginal zone lymphoma: 2023 update on diagnosis and management. *Am J Hematol*. (2023) 98:1645–57. doi: 10.1002/ajh.27058

6. Sindel A, Al-Juhaishi T, Yazbeck V. Marginal zone lymphoma: state-of-the-art treatment. *Curr Treat Options Oncol*. (2019) 20:90. doi: 10.1007/s11864-019-0687-5

7. Zucca E, Conconi A, Martinelli G, Bouabdallah R, Tucci A, Vitolo U, et al. Final results of the IELSG-19 randomized trial of mucosa-associated lymphoid tissue lymphoma: improved event-free and progression-free survival with rituximab plus chlorambucil versus either chlorambucil or rituximab monotherapy. *J Clin Oncol*. (2017) 35:1905–12. doi: 10.1200/jco.2016.70.6994

8. Kang HJ, Kim WS, Kim SJ, Lee JJ, Yang DH, Kim JS, et al. Phase II trial of rituximab plus CVP combination chemotherapy for advanced stage marginal zone lymphoma as a first-line therapy: Consortium for Improving Survival of Lymphoma (CISL) study. *Ann Hematol*. (2012) 91:543–51. doi: 10.1007/s00277-011-1337-6

9. Alderuccio JP, Arcaini L, Watkins MP, Beaven AW, Shouse G, Epperla N, et al. An international analysis evaluating frontline bendamustine with rituximab in extranodal marginal zone lymphoma. *Blood Adv*. (2022) 6:2035–44. doi: 10.1182/bloodadvances.2021006844

10. Salar A, Domingo-Domenech E, Panizo C, Nicolás C, Bargay J, Muntañola A, et al. Long-term results of a phase 2 study of rituximab and bendamustine for mucosa-associated lymphoid tissue lymphoma. *Blood*. (2017) 130:1772–4. doi: 10.1182/blood-2017-07-795302

11. Salar A, Domingo-Domenech E, Panizo C, Nicolás C, Bargay J, Muntañola A, et al. First-line response-adapted treatment with the combination of bendamustine and rituximab in patients with mucosa-associated lymphoid tissue lymphoma (MALT2008-01): a multicentre, single-arm, phase 2 trial. *Lancet Haematol*. (2014) 1:e104–11. doi: 10.1016/s2352-3026(14)00021-0

12. Herold M, Hoster E, Janssens A, McCarthy H, Tedeschi A, Pocock C, et al. Immunochemotherapy and maintenance with obinutuzumab or rituximab in patients with previously untreated marginal zone lymphoma in the randomized GALLIUM trial. *Hemasphere*. (2022) 6:e699. doi: 10.1097/hs9.0000000000000699

13. Rossi D, Bertoni F, Zucca E. Marginal-zone lymphomas. *N Engl J Med*. (2022) 386:568–81. doi: 10.1056/NEJMra2102568

14. Mössner E, Brünker P, Moser S, Püntener U, Schmidt C, Herter S, et al. Increasing the efficacy of CD20 antibody therapy through the engineering of a new type II anti-CD20 antibody with enhanced direct and immune effector cell-mediated B-cell cytotoxicity. *Blood*. (2010) 115:4393–402. doi: 10.1182/blood-2009-06-225979

15. Goede V, Klein C, Stilgenbauer S. Obinutuzumab (GA101) for the treatment of chronic lymphocytic leukemia and other B-cell non-hodgkin's lymphomas: a glycoengineered type II CD20 antibody. *Oncol Res Treat*. (2015) 38:185–92. doi: 10.1159/000381524

16. Marcus R, Davies A, Ando K, Klapper W, Opat S, Owen C, et al. Obinutuzumab for the first-line treatment of follicular lymphoma. *N Engl J Med*. (2017) 377:1331–44. doi: 10.1056/NEJMoa1614598

17. Goede V, Fischer K, Busch R, Engelke A, Eichhorst B, Wendtner CM, et al. Obinutuzumab plus chlorambucil in patients with CLL and coexisting conditions. *N Engl J Med*. (2014) 370:1101–10. doi: 10.1056/NEJMoa1313984

18. Seymour JF, Marcus R, Davies A, Gallop-Evans E, Grigg A, Haynes A, et al. Association of early disease progression and very poor survival in the GALLIUM study in follicular lymphoma: benefit of obinutuzumab in reducing the rate of early progression. *Haematologica*. (2019) 104:1202–8. doi: 10.3324/haematol.2018.209015

19. Seymour JF, Marcus R, Davies A, Gallop-Evans E, Grigg A, Haynes A, et al. Association of early disease progression and very poor survival in the GALLIUM study in follicular lymphoma: benefit of obinutuzumab in reducing the rate of early progression. *Haematologica*. (2020) 105:1465. doi: 10.3324/haematol.2020.246991

20. Swerdlow SH, Campo E, Pileri SA, Harris NL, Stein H, Siebert R, et al. The 2016 revision of the World Health Organization classification of lymphoid neoplasms. *Blood*. (2016) 127:2375–90. doi: 10.1182/blood-2016-01-643569

21. Cheson BD, Fisher RI, Barrington SF, Cavalli F, Schwartz LH, Zucca E, et al. Recommendations for initial evaluation, staging, and response assessment of Hodgkin and non-Hodgkin lymphoma: the Lugano classification. *J Clin Oncol*. (2014) 32:3059–68. doi: 10.1200/jco.2013.54.8800

22. Walewska R, Eyre TA, Barrington S, Brady J, Fields P, Iyengar S, et al. Guideline for the diagnosis and management of marginal zone lymphomas: A British Society of Haematology Guideline. *Br J Haematol*. (2024) 204:86–107. doi: 10.1111/bjh.19064

23. Zelenetz AD, Gordon LI, Abramson JS, Advani RH, Andreadis B, Bartlett NL, et al. NCCN guidelines® Insights: B-cell lymphomas, version 6.2023. *J Natl Compr Canc Netw*. (2023) 21:1118–31. doi: 10.6004/jnccn.2023.0057

24. Khalil MO, Morton LM, Devesa SS, Check DP, Curtis RE, Weisenburger DD, et al. Incidence of marginal zone lymphoma in the United States, 2001-2009 with a focus on primary anatomic site. *Br J Haematol*. (2014) 165:67–77. doi: 10.1111/bjh.12730

25. Raderer M, Kiesewetter B, Ferreri AJ. Clinicopathologic characteristics and treatment of marginal zone lymphoma of mucosa-associated lymphoid tissue (MALT lymphoma). *CA Cancer J Clin*. (2016) 66:153–71. doi: 10.3322/caac.21330

26. Nakamura S, Ponzoni M. Marginal zone B-cell lymphoma: lessons from Western and Eastern diagnostic approaches. *Pathology*. (2020) 52:15–29. doi: 10.1016/j.pathol.2019.08.012

27. Bachy E, Houot R, Feugier P, Bouabdallah K, Bouabdallah R, Virelizier EN, et al. Obinutuzumab plus lenalidomide in advanced, previously untreated follicular lymphoma in need of systemic therapy: a LYSA study. *Blood*. (2022) 139:2338–46. doi: 10.1182/blood.2021013526

28. Epperla N, Welkie RL, Torka P, Shouse G, Karmali R, Shea L, et al. Impact of early relapse within 24 months after first-line systemic therapy (POD24) on outcomes in patients with marginal zone lymphoma: A US multisite study. *J Hematol Oncol*. (2023) 16:49. doi: 10.1186/s13045-023-01448-y

29. Conconi A, Thieblemont C, Cascione L, Torri V, Kiesewetter B, Margiotta Casaluci G, et al. Early progression of disease predicts shorter survival in MALT lymphoma patients receiving systemic treatment. *Haematologica*. (2020) 105:2592–7. doi: 10.3324/haematol.2019.237990

30. Luminari S, Merli M, Rattotti S, Tarantino V, Marcheselli L, Cavallo F, et al. Early progression as a predictor of survival in marginal zone lymphomas: an analysis from the FIL-NF10 study. *Blood*. (2019) 134:798–801. doi: 10.1182/blood.2019001088

31. Arcaini L, Bommier C, Alderuccio JP, Merli M, Fabbri N, Nizzoli ME, et al. Marginal zone lymphoma international prognostic index: a unifying prognostic index for marginal zone lymphomas requiring systemic treatment. *EClinicalMedicine*. (2024) 72:102592. doi: 10.1016/j.eclinm.2024.102592

32. Klein C, Jamois C, Nielsen T. Anti-CD20 treatment for B-cell Malignancies: current status and future directions. *Expert Opin Biol Ther*. (2021) 21:161–81. doi: 10.1080/14712598.2020.1822318

frontiers | Frontiers in Immunology

TYPE Original Research
PUBLISHED 25 September 2024
DOI 10.3389/fimmu.2024.1431261

OPEN ACCESS

EDITED BY
Rebecca A Baillie,
Independent researcher, Sacramento, CA, United States

REVIEWED BY
Shashi Anand,
University of Mississippi Medical Center, United States
Dao Wang,
First Affiliated Hospital of Zhengzhou University, China

*CORRESPONDENCE
Lixiang Yan
ylx0415@126.com
Zhexin Shi
shzhx0604@163.com

RECEIVED 11 May 2024
ACCEPTED 09 September 2024
PUBLISHED 25 September 2024

CITATION
Fan C, Yuan P, Yang X, Zhang W, Wang X, Xie J, He J, Chen H, Yan L and Shi Z (2024) Metabolite, immunocyte phenotype, and lymphoma: a Mendelian randomization study. *Front. Immunol.* 15:1431261.
doi: 10.3389/fimmu.2024.1431261

Metabolite, immunocyte phenotype, and lymphoma: a Mendelian randomization study

Chenyang Fan[1], Pengying Yuan[2], Xiangdong Yang[1], Weifeng Zhang[1], Xingli Wang[1], Juan Xie[1], Jing He[1], Haijing Chen[1], Lixiang Yan[1]* and Zhexin Shi[1]*

[1]First Teaching Hospital of Tianjin University of Traditional Chinese Medicine, National Clinical Research Center for Chinese Medicine Acupuncture and Moxibustion, Tianjin, China, [2]Hospital of University of International Business and Economics, Beijing, China

Background: Recent studies have confirmed that metabolites and immunocyte phenotype may be associated with the risk of lymphoma. However, the bidirectional causality between metabolites, immunocyte phenotype, disease risk, and whether immunity is an intermediate mediator between metabolism and lymphoma causality is still unclear.

Objective: To elucidate the causal relationship between metabolites, immune cell phenotypes, and lymphomas, we used two-sample Mendelian randomization (MR) and two-step MR analysis.

Methods: Applying large-scale genome-wide association studies (GWAS) pooled data, we selected 1400 metabolites and 731 immunocyte phenotypes with eight lymphoma subtypes for two-sample bi-directional MR analysis. In addition, we used two-step MR to quantify the proportion of metabolite effects on lymphomas mediated by immunocyte phenotype.

Results: This study yielded a bidirectional causal relationship between 17 metabolites and lymphoma and a bidirectional causal relationship between 12 immunocyte phenotypes and lymphoma. In addition, we found causal associations between metabolites and lymphomas, three groups of which were mediated by immunocyte phenotypes. Among them, CD27 on plasmablast/plasma cell (PB/PC) was a mediator of the positive association of arginine to glutamate ratio with chronic lymphocytic leukemia, with a mediator ratio of 14.60% (95% CI=1.29-28.00%, P=3.17 × 10-2). Natural killer (NK) cells as a percentage of all lymphocytes(NK %lymphocyte) was a mediator of the negative association of X-18922(unknown metabolite) levels with diffuse large B-cell lymphoma, with a mediation proportion of -8.940% (95% CI=-0.063-(-17.800) %, P=4.84 × 10-2). CD25 on IgD- CD24- B cell was the mediator of the positive association between X-24531(unknown metabolite) levels and diffuse large B-cell lymphoma, with a mediation proportion of 13.200% (95% CI=-0.156-26.200%, P=4.73 × 10-2).

Conclusion: In the present study, we identified a causal relationship between metabolites and lymphoma, in which immunocyte phenotypes as mediators are involved in only a minor part. The mediators by which most metabolites affect the risk of lymphoma development remain unclear and require further exploration in the future.

KEYWORDS

immunocyte phenotype, Mendelian randomization, lymphoma, metabolite, intermediation factor

Introduction

Lymphoma is a group of highly heterogeneous malignant tumors originating in the lymphohematopoietic system (1). It is mainly divided into two categories, Hodgkin's lymphoma (HL) and non-Hodgkin's lymphoma (NHL), of which about 85-90% are derived from B cells, while the rest of NHL is derived from T cells or natural killer (NK) cells. B-cell NHL is further classified according to its histology, phenotype, and genetics into diffuse large B-cell lymphoma (DLBCL), follicular lymphoma (FL), mantle cell lymphoma (MCL), marginal zone B-cell lymphoma (MZL), chronic lymphocytic leukemia (CLL), Waldenstrom macroglobulinemia (WM) and others (2). Lymphoma is a malignant tumor characterized by disease at multiple sites throughout the body. Its etiology is complex and difficult to map out. Overall, lymphoma treatment is based on systemic chemotherapy. Despite the proliferation of therapeutic options for lymphoma patients in recent years, the prognosis for lymphoma patients remains worrisome.

Metabolites are intermediate or final products of metabolic reactions, including lipids, amino acids, nucleotides, cofactors, vitamins, carbohydrates, peptides, energy, and several unnamed small molecule metabolites (3). Their levels are influenced by various factors such as genetics, diet, and gut microbes, as well as being associated with disease risk, and are potential therapeutic targets for disease interventions (4). In addition to currently identified blood metabolites, intermetabolite ratios are strongly associated with disease risk (5).

Immunodeficiency has become a recognized risk factor for developing lymphoma (6, 7). However, immunotherapy has demonstrated variable therapeutic efficacy for different types of lymphoma (1). For example, DLBCL responds poorly to immune checkpoint inhibition compared to HL. Therefore, immune targets for various lymphoma types need to be further explored.

Metabolites and immune characteristics appear to be strongly associated with the risk of lymphoma. Recent studies have overturned the previously held belief that "metabolic disorders caused by immune abnormalities lead to cancer" (8–10). "Metabolites influence tumor development by modulating immunity" has become the mainstream view on the relationship between metabolism, immunity, and tumor (11, 12). This conclusion is not only applicable to solid tumors but also to hematological tumors (13).

We can verify the causal relationship between metabolites, immune characteristics, and the risk of developing lymphoma through randomized controlled trials (RCT). However, because metabolite and immunocyte phenotypes are affected by real-world confounding factors, it is difficult to distinguish the sequential causality of the two in the human body. At this point, we can conduct the study through Mendelian randomization (MR). MR refers to Mendel's second law, which states that alleles segregate independently during reproduction, combine randomly during hybridization, and are passed on to offspring with equal probability (14). Therefore, it is generally assumed that this genetic variation is randomly distributed in the population and is independent of environmental or lifestyle factors (15). Genetic variation can thus be used as an instrumental variable (IV) to mimic the process of randomly assigning treatment factors to experimental and control groups in RCT studies, thereby reducing the influence of confounding factors in the results of these studies and avoiding the difficulty of determining the temporal order of antecedents and consequences in traditional observational studies (16).

In the present study, we verified the association between metabolites, immunocyte phenotypes, and lymphomas (including HL, DLBCL, FL, MCL, MZL, WM, CLL, and Mature T/NK-cell lymphomas) using MR. We also verified whether immunity mediates metabolic abnormalities leading to lymphomas. Finally, we also reverse-validated the trends of metabolites and immunocyte phenotypes that accompanied the development of lymphomas.

Methods

Study design

As shown in Figure 1, this study consists of three parts. First, the first two parts verified the bidirectional causal relationship between

Abbreviations: AC, Absolute Count; DC, Dendritic cells; DNA, Deoxyribonucleic acid; RNA, Ribonucleic acid.

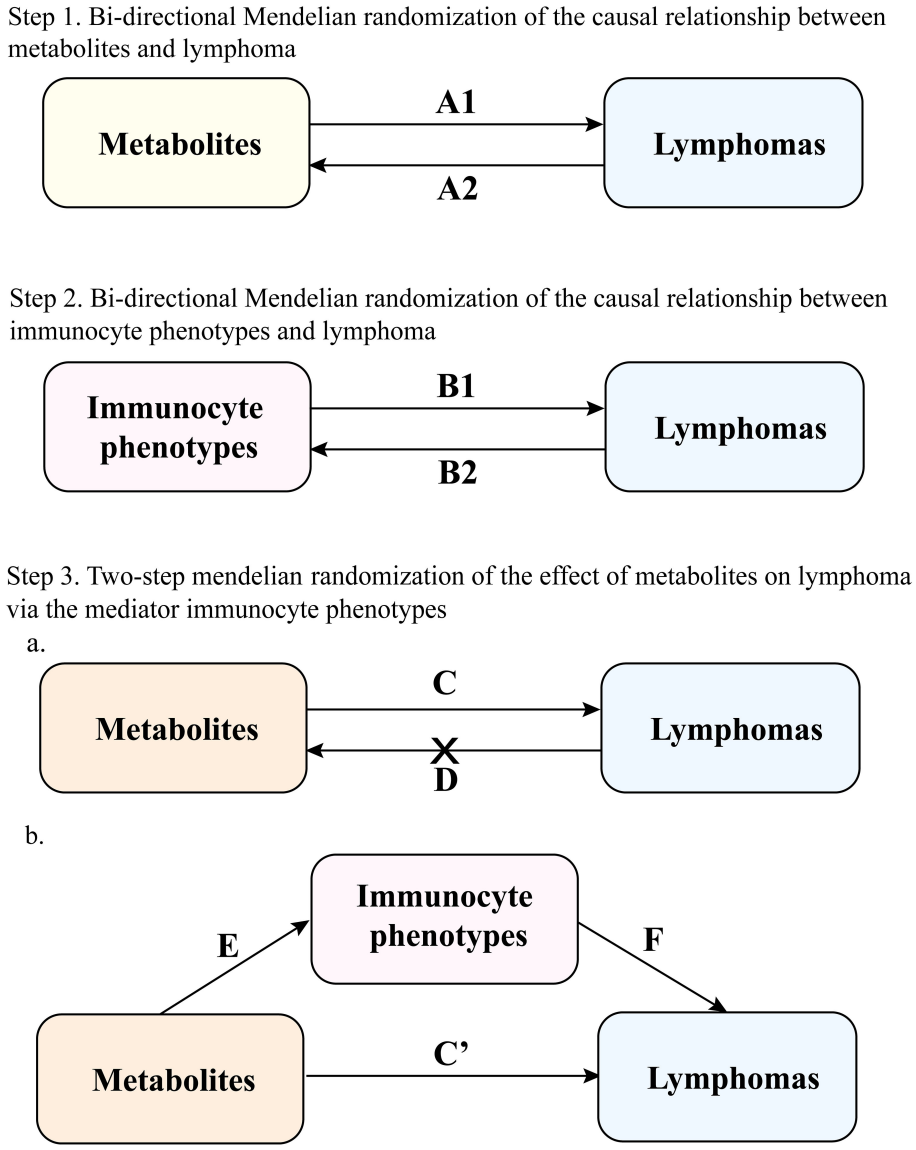

FIGURE 1
Study overview. A1 represents the positive effect of metabolites on lymphoma; A2 represents the reverse effect of lymphoma on metabolites; B1 represents the positive effect of immunocyte phenotypes on lymphoma; B2 represents the reverse effect of lymphoma on immunocyte phenotypes; C represents the total effect of metabolites on lymphoma; D represents the reverse total effect of lymphoma on metabolites, and screened for metabolites with negative reverse MR; in Step 3 the mediating effect (E represents the effect of the metabolite on the immunocyte phenotypes and F represents the effect of the immunocyte phenotypes on the lymphoma) was calculated as (E × F). The direct effect C' was calculated as (total effect C - mediating effect E × F).

metabolites, immunocyte phenotypes, and lymphomas using bi-directional MR, respectively. The third part verified the mediating effect of immunocyte phenotypes between metabolites and lymphoma using two-step MR.

Data source

The GWAS data for metabolites are derived from the most recent summary of genetic data for the European population. The GWAS data include 1091 plasma metabolites and 309 metabolite ratios. The 1091 plasma metabolites include 850 metabolic constituents already confirmed in the eight super pathways (i.e., lipids, amino acids, probiotics, nucleotides, cofactors and vitamins, carbohydrates, peptides, and energy), with the remaining 241 classified as unknown molecules (3).

We downloaded all single nucleotide polymorphisms (SNPs) associated with human immunocyte phenotypes as IVs in the IEU Open GWAS project (https://gwas.mrcieu.ac.uk/). It is a 22 million variant pair of RNA gene sequencing and genotyping data on immunocyte phenotypes from 3757 European participants. to explore the complex genetic regulation of immune cells in autoimmune diseases. The total of 731 immunocyte phenotypes included absolute cell counts (n=118), relative counts (n=192), median fluorescence intensities (MFIs) of surface antigens (n=389), and morphological parameters (n=32) (17).

We obtained all GWAS pooled data (controls excluding all cancers) with the eight lymphoma subtypes from the FinnGen Consortium database (version R10). All data are of European origin. Detailed information on participants, genotype platforms, and statistical analysis protocols is available on the FinnGen website (https://www.FinnGen.fi/en/). Detailed information is available in an Additional File (Supplementary Table S1).

Selecting genetic instruments

The genetic instruments employed had to fulfill three assumptions (15): 1) the genetic variants should be strongly associated with the exposure, 2) the genetic variants should not be associated with any potential confounding factors, and 3) the genetic variants should not affect the outcome independently of exposure. We excluded variants with minor allele frequencies <0.01 in the GWAS dataset. We used a strict r^2 <0.001 threshold, a 10,000 kb window, and a clustering method with P <1 × 10^{-5}. Notably, because of the limited number of SNPs in WM, P was chosen as a threshold of 5 × 10^{-5} when WM was used as an exposure factor. To ensure consistency, we harmonized the effects of SNPs on both exposure and outcome by aligning the beta values to the identical alleles. F statistics were calculated to evaluate the strength of instrumental variables, with F > 10 indicating no weak instrumental variable bias, and instrumental variables with F < 10 were excluded.

MR analysis

Primary analysis

First, we used two-sample bidirectional MR (corresponding to A1 and B1 in Figure 1) to demonstrate the causal associations between metabolites, immunocyte phenotypes, and eight lymphoma subtypes. The inverse variance weighted (IVW) was used as the primary method to analyze the causal association between exposure factors and outcome variables (16). We validate the results using MR-Egger and Weighted median. In contrast to IVW, the MR-Egger method accounts for the presence of an intercept term (18). The weighted median provides consistent estimates if at least 50% of the valid instrumental variables are present in the analysis (19). According to the third hypothesis of MR analysis, instrumental variables must be associated with outcomes only through exposure. Therefore, this study used the MR-Egger regression method to assess potential horizontal pleiotropy through intercept term. Additionally, this study utilized Simple mode versus Weighted mode analysis.

Bi–directional causality analysis

We performed to verify the reverse causality of lymphoma with metabolites and immunocyte phenotypes. We chose lymphoma as an exposure factor and metabolites and immunocyte phenotypes as outcome factors (corresponding to A2 and B2 in Figure 1).

Mediation analysis

We designed a two-step MR for mediation analysis to verify whether immunocyte phenotypes are intermediate mediators of the causal relationship between metabolites and lymphoma. This study yielded a positive MR total effect for metabolites and lymphoma (corresponding to C in Figure 1). Reverse MR analysis was then performed to derive metabolites with negative MR correlations as exposure data in the following analyses (corresponding to D in Figure 1). Next, this study yielded two overall effects, an indirect effect through mediators and a direct effect without mediators (20). The total effect of metabolites on lymphomas was divided into (1) the direct effect of metabolites on lymphomas (corresponding to C' in Figure 1) and (2) the mediated effect of metabolites mediated through a mediator (corresponding to E×F in Figure 1). The mediated effect divided by the total effect is the mediated proportion (corresponding to (E × F)/C in Figure 1). We applied the delta method to calculate 95% confidence intervals (18).

Sensitivity analysis

The direction of MR was verified using MR Steiger to exclude the effect of reverse causality. The results were tested for heterogeneity using Cochran's Q test, with P<0.05 indicating the presence of heterogeneity and P>0.05 indicating the absence of heterogeneity (20). Horizontal pleiotropy was analyzed using the MR-Egger intercept method. The leave-one-out analysis was used to analyze whether a single SNP affected the MR results. Possible horizontal pleiotropy was examined by looking at the symmetry of the funnel plot to gauge the reliability of the current MR analysis. Outliers were analyzed with the Radial package, and the MR-PRESSO method was used to test the effect of outliers on the results (21).

Results

Bi-directional association of metabolites with lymphoma

We validated bi-directional MR between 1400 metabolite metrics and eight lymphomas (Figure 2). IVW results showed that two metabolites were bi-directionally associated with DLBCL: X-11632(unknown metabolite) level and Phosphate to the 2'-deoxyuridine ratio (Supplementary Table S1). Four metabolites were bi-directionally associated with FL in this study: kynurenine levels, 1-methylxanthine levels, Dihydroferulate levels, and 2'-o-methylcytidine levels (Supplementary Table S2). Four metabolites were bi-directionally associated with MCL in this study: octanoylcarnitine (c8) levels, linoleate (18:2n6) levels, X-15728 (unknown metabolite) levels, and Arachidonate (20:4n6) to linoleate (18:2n6) ratio (Supplementary Table S3). In this study, three metabolites were bi-directionally associated with CLL: Palmitate (16:0) to myristate (14:0) ratio, Glucose to maltose ratio, and Adenosine 5'-diphosphate (ADP) to glycerol 3-phosphate ratio (Supplementary Table S5). There was one

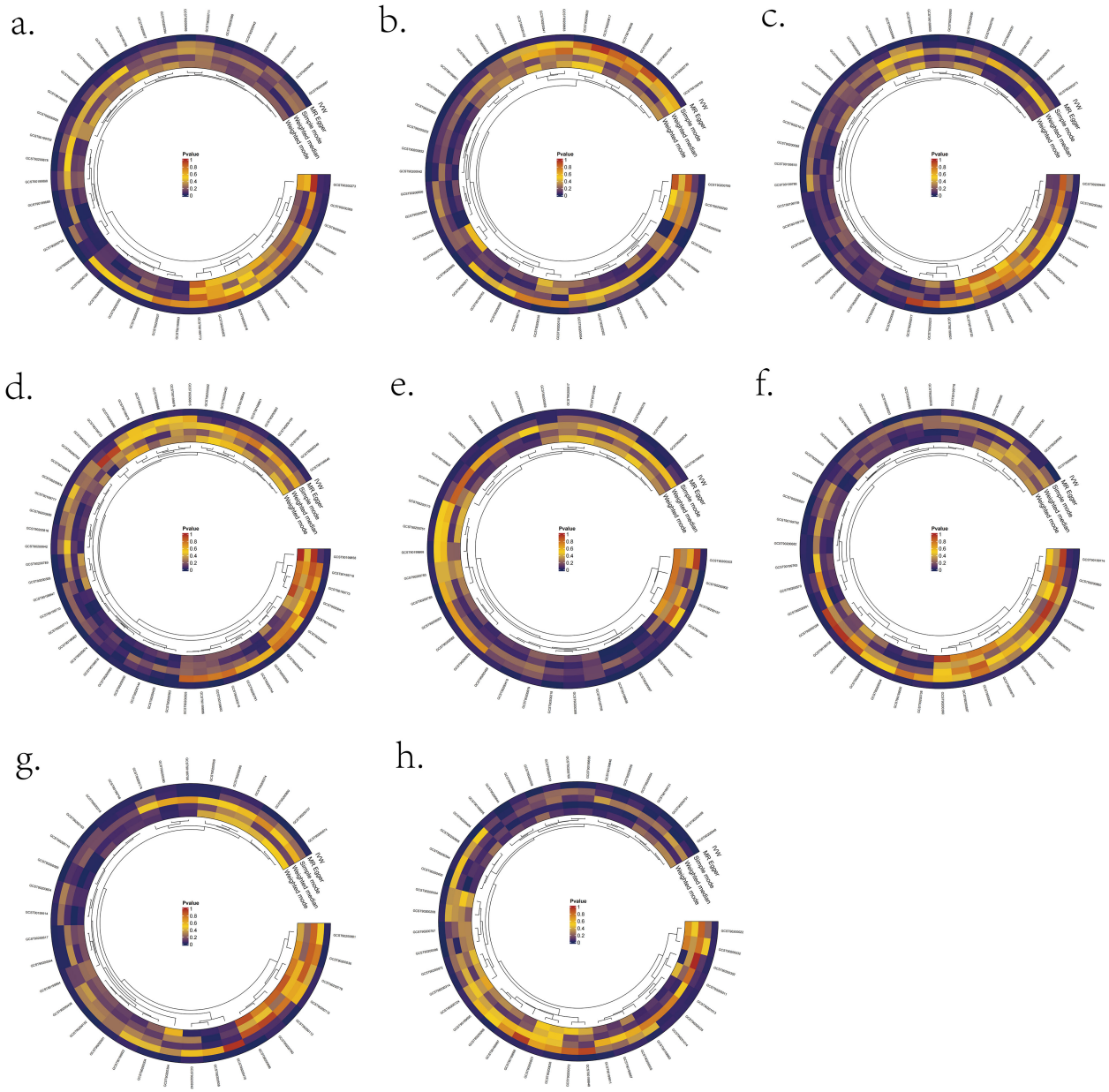

FIGURE 2
Significant MR results for the relationship between 1400 metabolites and eight types of Lymphomas. **(A)** MR analysis results between metabolites and DLBCL. **(B)** MR analysis results between metabolites and FL. **(C)** MR analysis results between metabolites and MCL. **(D)** MR analysis results between metabolites and CLL. **(E)** MR analysis results between metabolites and MTCL. **(F)** MR analysis results between metabolites and HL. **(G)** MR analysis results between metabolites and WM. **(H)** MR analysis results between metabolites and MZL.

metabolite that was bi-directionally associated with Mature T/NK-cell lymphomas (MTCL) in this study: the mannose to N-acetylglucosamine to N-acetylgalactosamine ratio (Supplementary Table S6). Three metabolites were bi-directionally associated with HL in this study: propionylglycine levels, X-21258(unknown metabolite) levels, and Adenosine 5'-monophosphate (AMP) to inosine 5'-monophosphate (IMP) ratio (Supplementary Table S7). There was no bi-directional correlation between WM, MZL, and metabolites (Supplementary Tables S4/S8).

Bi-directional association of immunocyte phenotypes with lymphoma

We validated bidirectional MR between 731 immunocyte phenotypes and eight lymphomas (Figure 3). The most prominent IVW results showed that six immunocyte phenotypes were bi-directionally associated with DLBCL: T cell as a percentage of all lymphocytes (T cell %lymphocyte), CD8br as a percentage of all leukocytes (CD8br %leukocyte), B cell as a percentage of CD3-

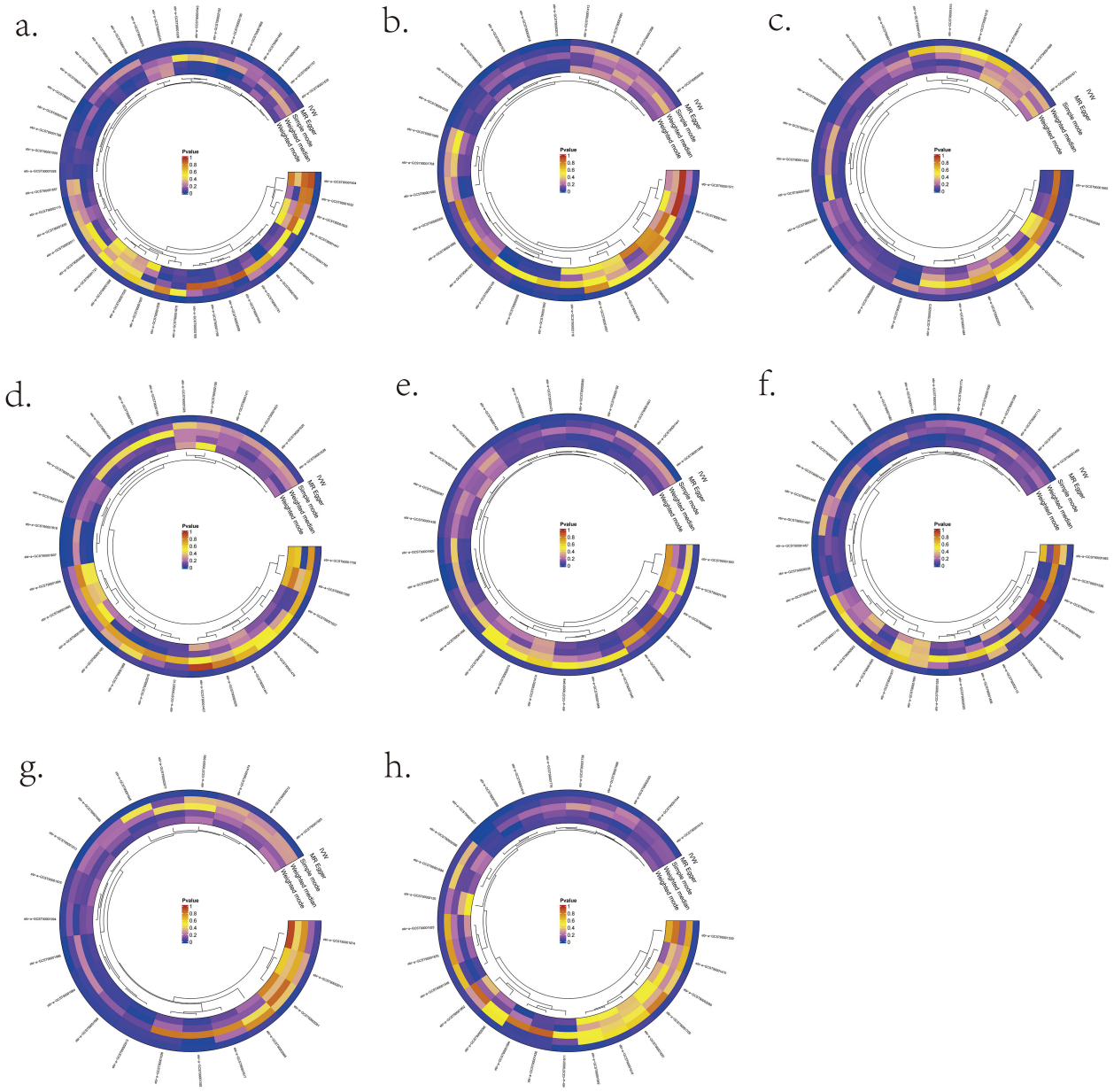

FIGURE 3
Significant MR results for the relationship between 731 immunocyte phenotypes and eight types of Lymphomas. **(A)** MR analysis results between immunocyte phenotypes and DLBCL. **(B)** MR analysis results between immunocyte phenotypes and FL. **(C)** MR analysis results between immunocyte phenotypes and MCL. **(D)** MR analysis results between immunocyte phenotypes and CLL. **(E)** MR analysis results between immunocyte phenotypes and MTCL. **(F)** MR analysis results between immunocyte phenotypes and HL. **(G)** MR analysis results between immunocyte phenotypes and WM. **(H)** MR analysis results between immunocyte phenotypes and MZL.

lymphocytes (B cell %CD3- lymphocyte), NK cells as a percentage of CD3- lymphocytes (NK %CD3- lymphocyte), NK cells as a percentage of all lymphocytes (NK %lymphocyte), and CD19 on CD20- (Supplementary Table S1). Two immunocyte phenotypes were bi-directionally associated with FL in the present study: the CD28 on CD39+ secreting Treg and the CC chemokine receptor 2 (CCR2) on CD14+ CD16+ monocyte (Supplementary Table S2). In the present study, one immunocyte phenotype was bi-directionally associated with MCL: CD25 on transitional (Supplementary Table S3). Two immunocyte phenotypes were bi-directionally associated with WM from this study: the CX3CR1 on CD14- CD16- and CD45 on basophil (Supplementary Table S4). In the present study, three immunocyte phenotypes were bi-directionally associated with CLL: Unswitched memory B cell Absolute Count (Unsw mem AC), CD86 + plasmacytoid Dendritic Cell Absolute Count (DC AC) and CD127 on CD28+ CD45RA- CD8br (Supplementary Table S5). In this study, one immunocyte phenotype was bi-directionally correlated with MTCL: CD4 Treg %CD4 (Supplementary Table S6). There was no bi-directional correlation between HL, MZL, and immune cell phenotypes (Supplementary Table S7/S8).

Role of immunocyte phenotypes in mediating the effect of metabolites on lymphomas

We analyzed whether 731 immunocyte phenotypes were causal mediators between 1400 metabolites and eight phenotypic lymphomas. The results revealed three significant groups of mediating correlations between metabolites, immunocyte phenotypes, and lymphomas (Table 1) (Figure 4). Among them, CD27 on Plasma Blast-Plasma Cells (CD27 on PB/PC) can mediate the causal relationship between arginine to glutamate ratio and CLL (Figure 5). Arginine to glutamate ratio was negatively associated with CD27 on PB/PC (β=0.226,95% CI=0.086-0.336, P=1.56 × 10^{-3}), which subsequently led to an increased risk of CLL with a mediation ratio of 14.60% (95% CI=1.29- 28.00%, P=3.17 × 10^{-2}) (Supplementary Table S9).

NK %lymphocyte mediated the causal relationship between X-18922 (unknown metabolite) levels and DLBCL (Figure 6). X-18922 levels were negatively correlated with NK %lymphocyte (β=-0.126, 95%CI=-0.225-(-0.029) %, P=1.14 ×10^{-2}), which subsequently led to an increased risk of DLBCL with a mediation ratio of -8.940% (95% CI=-0.063-(-17.800) %, P=4.84 × 10^{-2}) (Supplementary Table S9).

CD25 on IgD- CD24- B mediated the causal relationship between X-24531 (unknown metabolite) levels and DLBCL (Figure 7). X-24531 levels were negatively correlated with CD25 on IgD- CD24- B cell (β=-0.176,95%CI=-0.295-(- 0.058), P=3.55 × 10^{-3}), which subsequently led to an increased risk of DLBCL with a mediation ratio of 13.200% (95% CI=-0.156-26.200%, P=4.73 × 10^{-2}) (Supplementary Table S9).

Sensitivity analyses

According to the MR-Egger regression intercept approach, genetic pleiotropy did not bias the results.MR-PRESSO analysis revealed that two immunocyte phenotypes (T cell %lymphocyte and CD8br %leukocyte) were horizontally pleiotropic for DLBCL (P < 0.05), and one immunocyte phenotype (CCR2 on CD14+ CD16+ monocyte) was horizontally pleiotropic for FL (P < 0.05, (Supplementary Table S10), and therefore the above results were excluded. MR-PRESSO analysis demonstrated no horizontal pleiotropy in the other parts of the MR study (P > 0.05, (Supplementary Table S10). Cochran's Q test showed significant heterogeneity of four immunocyte phenotypes (T cell %lymphocyte, CD8br %leukocyte, B cell % CD3- lymphocyte, and NK %CD3- lymphocyte) for DLBCL (P < 0.05) and one immunocyte phenotype (CCR2 on CD14+ CD16+ monocyte) for FL (P > 0.05, (Supplementary Table S10). The other sections did not show significant heterogeneity in Cochran's Q test (P > 0.05, (Supplementary Table S10).

The "leave-one-out" analysis proved that the MR results were reliable (Supplementary Figures S11, S1-6). The scatter plot shows the overall effect of metabolites on lymphoma (Supplementary Figures S11, S7-12). Finally, the forest plot shows the causal relationship between metabolites and lymphoma (Supplementary Figures S11, S13-18).

Discussion

Metabolites are small molecular compounds into which metabolism converts nutrients. It is also essential for all types of cells in the body to maintain their functions (22). It has been known that the metabolic pathways of tumor cells are different from those of other cells. According to the "Warburg effect," glycolysis is preferred over oxidative phosphorylation in tumor cells (23). Glycolysis will supply adenosine triphosphate to tumor cells more rapidly, providing a faster energy supply for unlimited proliferation of tumor cells (24). Of course, the metabolism of lymphoma cells also follows the "Warburg effect," and this unique metabolism inevitably makes metabolites a risk factor for lymphoma progression.

Immunity has always been a critical challenge in cancer risk research (25). Several immunologic drugs have been approved for clinical use, including various immunosuppressants and chimeric antigen receptor-T cell therapies (6). Among them, lymphomas are malignant tumors originating from the cells of the immune system (26). It is even more inextricably linked to immunization. However,

TABLE 1 Mendelian randomization probes the mediating role of immunocyte phenotype in the association between metabolites and lymphoma.

Metabolite	Immunity trait	Outcome	Total Effect	Direct Effect A	Direct Effect B	Mediated effect		Mediated proportion
			β (95% CI)	β (95% CI)	β (95% CI)	β (95% CI)	*P*-value	
Arginine to glutamate ratio	CD27 on PB/PC	Chronic lymphocytic leukaemia	0.3345 (0.0258, 0.6432)	0.2261 (0.0860, 0.3662)	0.2167 (0.0712, 0.3622)	0.0490 (0.0043, 0.0937)	0.0317	14.600% (1.290%, 28.000%)
X-18922 levels	NK %lymphocyte	Diffuse large B-cell lymphoma	-0.2035 (-0.3811, -0.0258)	-0.1266 (-0.2247, -0.0285)	-0.1437 (-0.2351, -0.0524)	0.0182 (0.0001, 0.0363)	0.0484	-8.940% (-0.063%, -17.800%)
X-24531 levels	CD25 on IgD- CD24-		-0.2431 (-0.4630, -0.0234)	-0.1764 (-0.2949, -0.0578)	0.1816 (0.0508, 0.3125)	-0.0320 (-0.0637, -0.0004)	0.0473	13.200% (0.156%, 26.200%)

Total effect: indicates the effect of metabolite on lymphoma; direct effect A: the effect of metabolite on immunocyte phenotype; direct effect B: the effect of immunocyte phenotype on lymphoma; mediation effect: the effect of metabolite on lymphoma through affecting immunocyte phenotype. The total effect, direct effect A, and direct effect B were derived using the inverse-variance weighted method; the mediation effect was derived using the delta method. All statistical tests were 2-sided. P<0.05 was considered significant.

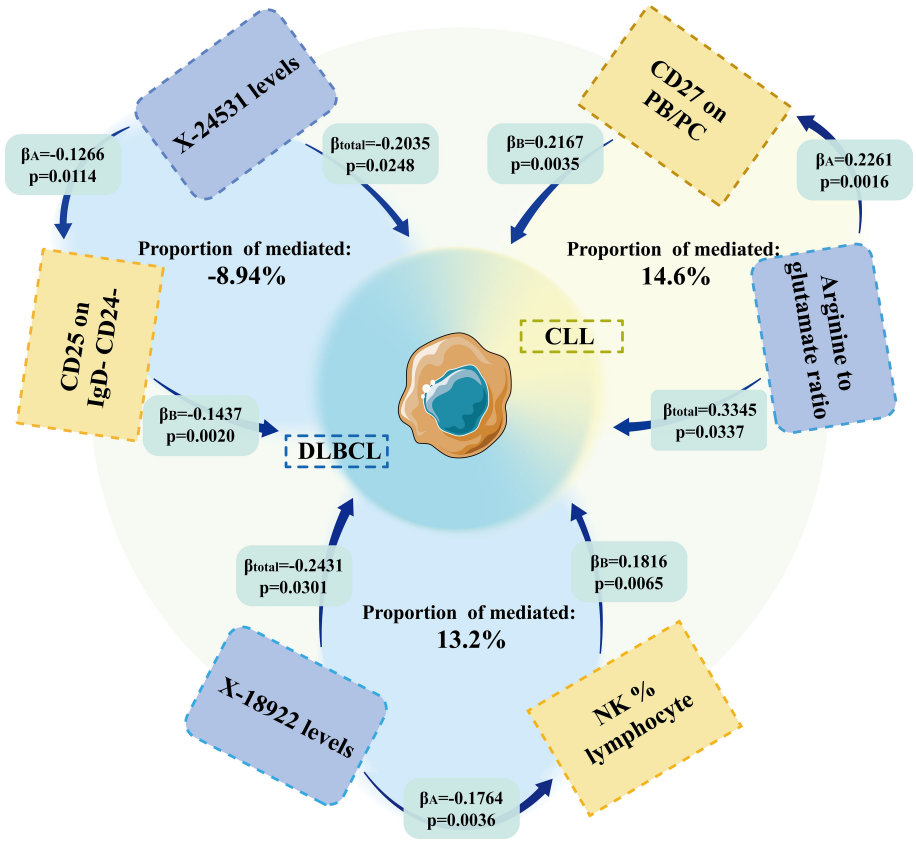

FIGURE 4
MR results showed that immune cell phenotype was an essential mediator of the causal relationship between metabolites and lymphoma.

we still do not know which immune phenotype is involved in the disease process of lymphoma.

Notably, according to recent studies, tumor cells compete for metabolic energy through a unique metabolic approach, which affects immune cell metabolism and inhibits the anti-tumor activity of immune cells (11). Lymphoma is closely related to both. Exploring the cascade effect between metabolites, immunophenotypes, and lymphomas would provide a new basis for new drug development and clinical therapeutic direction. The treatment effect will be twice as favorable with half the effort. Therefore, in this study, we applied MR analysis to verify the causal relationship between 1400 metabolites, 731 immunocyte phenotypes, and eight types of lymphomas (DLBCL, FL, MCL, MZL, CLL, WM, MTCL, and HL). And whether immunocyte phenotypes mediate the causal relationship between metabolites and the risk of lymphoma development.

exposureTrait	outcomeTrait	nsnp	method	pval	OR(95% CI)
CD27 on PB/PC	Chronic lymphocytic leukaemia	19	MR Egger	**0.008**	1.321 (1.101 to 1.585)
		19	Weighted median	**0.016**	1.331 (1.054 to 1.681)
		19	Inverse variance weighted	**0.004**	1.242 (1.074 to 1.437)
		19	Simple mode	0.242	1.336 (0.835 to 2.137)
		19	Weighted mode	**0.009**	1.362 (1.108 to 1.675)
Arginine to glutamate ratio	CD27 on PB/PC	25	MR Egger	0.125	1.304 (0.941 to 1.807)
		25	Weighted median	**0.043**	1.220 (1.006 to 1.479)
		25	Inverse variance weighted	**0.002**	1.254 (1.090 to 1.442)
		25	Simple mode	0.218	1.243 (0.887 to 1.743)
		25	Weighted mode	0.329	1.172 (0.858 to 1.601)
Arginine to glutamate ratio	Chronic lymphocytic leukaemia	25	MR Egger	0.594	1.209 (0.607 to 2.406)
		25	Weighted median	**0.032**	1.570 (1.041 to 2.370)
		25	Inverse variance weighted	**0.034**	1.397 (1.026 to 1.902)
		25	Simple mode	0.177	1.637 (0.817 to 3.279)
		25	Weighted mode	0.170	1.675 (0.820 to 3.422)

FIGURE 5
Forest plot to visualize the causal effects of CD27 on PB/PC with arginine to glutamate ratio and chronic lymphocytic leukaemia.

10.3389/fimmu.2024.1431261

exposureTrait	outcomeTrait	nsnp	method	pval	OR(95% CI)
NK %lymphocyte	Diffuse large B−cell lymphoma	27	MR Egger	**0.011**	0.840 (0.741 to 0.951)
		27	Weighted median	**0.014**	0.862 (0.766 to 0.970)
		27	Inverse variance weighted	**0.002**	0.866 (0.791 to 0.949)
		27	Simple mode	0.160	0.881 (0.742 to 1.046)
		27	Weighted mode	**0.024**	0.869 (0.775 to 0.974)
X−18922 levels	NK %lymphocyte	29	MR Egger	0.137	0.849 (0.688 to 1.047)
		29	Weighted median	**0.028**	0.862 (0.755 to 0.984)
		29	Inverse variance weighted	**0.011**	0.881 (0.799 to 0.972)
		29	Simple mode	0.310	0.888 (0.709 to 1.112)
		29	Weighted mode	0.063	0.849 (0.719 to 1.002)
X−18922 levels	Diffuse large B−cell lymphoma	29	MR Egger	0.513	0.879 (0.599 to 1.289)
		29	Weighted median	0.516	0.919 (0.712 to 1.187)
		29	Inverse variance weighted	**0.025**	0.816 (0.683 to 0.975)
		29	Simple mode	0.302	0.791 (0.511 to 1.225)
		29	Weighted mode	0.428	0.895 (0.682 to 1.174)

FIGURE 6
Forest plot to visualize the causal effects of NK %lymphocyte with X-18922 levels and diffuse large B-cell lymphoma.

Unknown metabolite X-11632 levels and a high phosphate to 2'-deoxyuridine ratio decreased the risk of DLBCL. High values of immunocyte phenotype B cell % CD3- lymphocyte increased the risk of DLBCL, and high values of NK %CD3- lymphocyte, NK % lymphocyte, and CD19 on CD20- decreased the risk of DLBCL. NK cells are derived from bone marrow hematopoietic stem cells and are essential components of the intrinsic immune system (27). NK cells not only act as killer cells to inhibit tumors, but NK cells can also use interferon gamma (IFNγ) to directly act on T cells to engage them in generating, shaping, and maintaining adaptive immune response (28). The present study found that an increase in the proportion of NK cells inhibited the progression of DLBCL. It has even been found that the development of resistance to rituximab, the first-line drug used to treat DLBCL, is also inextricably linked to abnormal NK cell counts (29). This finding is consistent with the current study (30).

Increases in the metabolites Kynurenine levels and 2'-o-methylcytidine levels increased the risk of FL, and increases in 1-methylxanthine levels and dihydroferulate levels decreased the risk of FL. It has been found that kynurenine is associated with high levels of inflammation and is involved in the abnormal regulation of endocrine, metabolic, and hormonal systems (31). All of the above provide theoretical hypotheses that kynurenine levels increase the risk of FL. An increase in the ratio of the immunocyte phenotype CD28 on CD39+ secreting Treg increases the risk of FL.

Increases in Octanoylcarnitine (c8) levels, Linoleate (18:2n6) levels, and levels of the unknown metabolite X-15728 decreased the risk of MCL and increases in Arachidonate (20:4n6) to linoleate (18:2n6) increased the risk of MCL. It has been established that obesity is associated with the risk of developing multiple subtypes of NHL (32). L-octanoylcarnitine is an independent predictor of atherosclerosis in adults (33). Thus octanoylcarnitine (c8) levels might be a potential factor in the increased risk of HNL due to obesity. The immunocyte phenotype CD25 on transitional was positively associated with the risk of developing MCL.

Immunocyte phenotypes of CX3CR1 on CD14- CD16- and CD45 on basophil increase the risk of WM. This study did not find a significant causal relationship between metabolites and WM. Considering that the original data on WM are only available for 88 cases, the risk factors for WM need to be further explored.

exposureTrait	outcomeTrait	nsnp	method	pval	OR(95% CI)
CD25 on IgD− CD24−	Diffuse large B−cell lymphoma	26	MR Egger	0.272	1.149 (0.902 to 1.462)
		26	Weighted median	**0.022**	1.245 (1.032 to 1.502)
		26	Inverse variance weighted	**0.007**	1.199 (1.052 to 1.367)
		26	Simple mode	0.099	1.319 (0.961 to 1.810)
		26	Weighted mode	0.053	1.272 (1.008 to 1.606)
X−24531 levels	CD25 on IgD− CD24−	23	MR Egger	0.682	0.952 (0.754 to 1.201)
		23	Weighted median	0.151	0.891 (0.761 to 1.043)
		23	Inverse variance weighted	**0.004**	0.838 (0.745 to 0.944)
		23	Simple mode	0.193	0.856 (0.682 to 1.074)
		23	Weighted mode	0.189	0.889 (0.750 to 1.054)
X−24531 levels	Diffuse large B−cell lymphoma	23	MR Egger	0.761	0.924 (0.560 to 1.524)
		23	Weighted median	0.100	0.770 (0.564 to 1.051)
		23	Inverse variance weighted	**0.030**	0.784 (0.629 to 0.977)
		23	Simple mode	0.080	0.630 (0.384 to 1.032)
		23	Weighted mode	0.079	0.701 (0.481 to 1.023)

FIGURE 7
Forest plot to visualize the causal effects of CD25 on IgD- CD24- B cell with X-24531 levels and diffuse large B-cell lymphoma.

Increases in Palmitate (16:0) to myristate (14:0) ratio, Glucose to maltose ratio, and ADP to glycerol 3-phosphate ratio reduced the risk of CLL. It was found that Palmitate could activate mitogen-activated protein kinases (MAPK) and then contribute to DNA damage in CLL cells (34, 35), ultimately leading to CLL cell apoptosis. The increased ADP rate reduces the risk of CLL is also consistent with previous studies (36). Unsw mem AC was positively associated with the risk of developing MCL. Increased CD86+ plasmacytoid DC AC and CD127 on CD28+ CD45RA- CD8br decreased the risk of developing CLL.

Mannose to N-acetylglucosamine to N-acetylgalactosamine ratio was negatively correlated with the risk of developing MTCL.CD4 Treg %CD4 was positively correlated with the risk of developing MTCL, a result that is consistent with the findings of conventional studies. A high Treg ratio will inhibit T cells from exerting immune activity, leading to an increased risk of MTCL, which is characterized by abnormalities in the T cell system (37).

Increases in the unnamed metabolites X-21258 levels and Propionylglycine levels decreased the risk of HL, and increases in the AMP to IMP ratio increased the risk of HL. No significant correlation between immunocyte phenotypes and HL was found in this study. This study did not find a significant bidirectional causal relationship between metabolites or immunocyte phenotypes and MZL.

In summary, we have found a strong link between metabolites and lymphoma. However, there is no established mechanism by which metabolites affect lymphomas. Follow-up studies have shown that CD27 on PB/PC may be an intermediate mediator of the positive correlation between Arginine to glutamate ratio and CLL risk. NK % lymphocyte is an intermediate mediator of the negative correlation of the unknown metabolite X-18922 levels with DLBCL. CD25 on IgD-CD24- is an intermediate mediator of the negative association of unknown metabolite X-24531 levels with DLBCL. Kara IO et al. found that sCD27 was an independent prognostic factor in the assessment of CLL (38), consistent with the findings of this study. NK cells are derived from bone marrow hematopoietic stem cells and represent an essential component of the intrinsic immune system (27). NK cells not only act as killer cells to suppress tumors, but NK cells can also use IFNγ to act directly on T cells to engage them in generating, shaping, and maintaining adaptive immune responses (28). Thus the percentage of NK cells to lymphocytes can represent a mediator of metabolite-negative regulation of lymphomas.

So far, we are the first to explore the causal relationship between metabolites, immunocyte phenotypes, and lymphoma risk by MR, and demonstrated that some immunocyte phenotypes are mediators between metabolites and lymphoma. However, there are still some flaws in this study: (1) Three immunocyte phenotypes were horizontally pleiotropic when analyzed with lymphoma MR, requiring replacement of the database for further research. (2) Possibly due to differences in the study population and investigators, five immunocyte phenotypes were heterogeneous when analyzed with lymphoma MR. (3) We screened for IVs using a p-value of P less than 1×10^{-5}, so the IVs were not strongly correlated enough, although they did allow for a more comprehensive assessment of the association between metabolites, immune cell phenotypes, and lymphoma. (4) Insufficient SNP data on WM. When WM is used as an exposure factor, the thresholds for the selected P-values are different from those for other subtypes of lymphoma. The above may lead to the conclusion that WM is not equivalent compared to other subtypes of lymphoma. (5) Although the GWAS for metabolite data selected for this study focused more on individuals of European ancestry, the cases selected were Canadian. In addition, SNPs associated with human immune cell phenotypes were referenced from the Sardinian population, an isolated, homogeneous island population. The GWAS pooled data for eight types of lymphomas from Finngen (https://www.FinnGen.fi/en/) which has a population with multiple known population bottlenecks and was isolated from the general European population. In addition, the two-sample Mendelian randomization analysis method has limitations when dealing with multiple exposures. Therefore, there is a need to explore suitable analytical methods. Finally, to draw clinical conclusions, we also need to conduct comprehensive clinical trials for validation; therefore, a more comprehensive GWAS database and further analytical methods or experimental validation are required to elucidate the relationship between individual metabolites, immune cell phenotypes, and lymphomas as well as their impact mechanisms.

Conclusion

Here in this study, we comprehensively explored the causal relationship between metabolites, immunocyte phenotypes, and lymphoma. We found that 17 metabolites were causally associated with lymphoma in both directions, and 12 immunocyte phenotypes were causally associated with lymphoma in both directions. We also identified causal relationships between metabolites and lymphomas, with three groups mediated by immunocyte phenotypes. In addition, we identified a causal relationship between metabolites and lymphomas, with three groups mediated by immunocyte phenotypes. We could inhibit disease progression by interfering with the expression of CD25, NK cells, and CD27 in future studies of DLBCL and CLL, respectively, with a multiplier effect. These are potential research opportunities.

Data availability statement

The original contributions presented in the study are included in the article/Supplementary Material. Further inquiries can be directed to the corresponding author/s.

Author contributions

CF: Conceptualization, Funding acquisition, Methodology, Supervision, Validation, Writing – original draft, Writing – review & editing. PY: Investigation, Resources, Validation, Visualization, Writing – review & editing. XY: Investigation, Methodology, Supervision, Writing – review & editing. WZ: Data curation, Formal analysis, Investigation, Writing – review & editing. XW: Investigation, Methodology, Software, Writing – review & editing. JX:

Formal analysis, Investigation, Writing – review & editing. JH: Software, Writing – review & editing. HC: Data curation, Writing – review & editing. LY: Project administration, Validation, Writing – original draft, Writing – review & editing. ZS: Project administration, Validation, Writing – original draft, Writing – review & editing.

Funding

The author(s) declare financial support was received for the research, authorship, and/or publication of this article. The present study was supported by Tianjin Municipal Education Commission, General Program of Natural Science Research (grant number 2021KJ145), Tianjin Science and Technology Program (grant number 21JCQNJC01210), Tianjin Municipal Education Commission, Tianjin Municipal Health Commission of Chinese Medicine, Integrative Medicine and Western Medicine Scientific Research Project (grant number 2023130), General Program of Natural Science Research (grant number 2023KJ157), Tianjin Municipal Health Commission (grant number 2023018).

Acknowledgments

The authors would like to thank all the participants in the GWAS cohort in this study, and the researchers at the IEU Open GWAS project and FINNGEN for sharing the GWAS summary statistics.

Conflict of interest

The authors declare that the research was conducted in the absence of any commercial or financial relationships that could be construed as a potential conflict of interest.

Publisher's note

Supplementary material

The Supplementary Material for this article can be found online at: https://www.frontiersin.org/articles/10.3389/fimmu.2024.1431261/full#supplementary-material

References

1. Lewis WD, Lilly S, Jones KL. Lymphoma: diagnosis and treatment. *Am Fam Physician*. (2020) 101:34–41.

2. Armitage JO, Gascoyne RD, Lunning MA, Cavalli F. Non-Hodgkin lymphoma. *Lancet*. (2017) 390:298–310. doi: 10.1016/S0140-6736(16)32407-2

3. Chen Y, Lu T, Pettersson-Kymmer U, Stewart ID, Butler-Laporte G, Nakanishi T, et al. Genomic atlas of the plasma metabolome prioritizes metabolites implicated in human diseases. *Nat Genet*. (2023) 55:44–53. doi: 10.1038/s41588-022-01270-1

4. Pietzner M, Stewart ID, Raffler J, Khaw K-T, Michelotti GA, Kastenmüller G, et al. Plasma metabolites to profile pathways in noncommunicable disease multimorbidity. *Nat Med*. (2021) 27:471–9. doi: 10.1038/s41591-021-01266-0

5. Lotta LA, Pietzner M, Stewart ID, Wittemans LBL, Li C, Bonelli R, et al. A cross-platform approach identifies genetic regulators of human metabolism and health. *Nat Genet*. (2021) 53:54–64. doi: 10.1038/s41588-020-00751-5

6. Csizmar CM, Ansell SM. Engaging the innate and adaptive antitumor immune response in lymphoma. *Int J Mol Sci*. (2021) 22:3302. doi: 10.3390/ijms22073302

7. Mancuso S, Mattana M, Carlisi M, Santoro M, Siragusa S. Effects of B-cell lymphoma on the immune system and immune recovery after treatment: the paradigm of targeted therapy. *Int J Mol Sci*. (2022) 23:3368. doi: 10.3390/ijms23063368

8. Cronin SJF, Seehus C, Weidinger A, Talbot S, Reissig S, Seifert M, et al. The metabolite BH4 controls T cell proliferation in autoimmunity and cancer. *Nature*. (2018) 563:564–8. doi: 10.1038/s41586-018-0701-2

9. Moon J-Y, Zolnik CP, Wang Z, Qiu Y, Usyk M, Wang T, et al. Gut microbiota and plasma metabolites associated with diabetes in women with, or at high risk for, HIV infection. *EBioMedicine*. (2018) 37:392–400. doi: 10.1016/j.ebiom.2018.10.037

10. Oliveira L de M, Teixeira FME, Sato MN. Impact of retinoic acid on immune cells and inflammatory diseases. *Mediators Inflamm*. (2018) 2018:3067126. doi: 10.1155/2018/3067126

11. Xia L, Oyang L, Lin J, Tan S, Han Y, Wu N, et al. The cancer metabolic reprogramming and immune response. *Mol Cancer*. (2021) 20:28. doi: 10.1186/s12943-021-01316-8

12. Yuan X, Ouedraogo SY, Trawally M, Tan Y, Bajinka O. Cancer energy reprogramming and the immune responses. *Cytokine*. (2024) 177:156561. doi: 10.1016/j.cyto.2024.156561

13. Chen K-C, Hsiao I-H, Huang Y-N, Chou Y-T, Lin Y-C, Hsieh J-Y, et al. Targeting human mitochondrial NAD(P)+-dependent Malic enzyme (ME2) impairs energy metabolism and redox state and exhibits antileukemic activity in acute myeloid leukemia. *Cell Oncol (Dordr)*. (2023) 46:1301–16. doi: 10.1007/s13402-023-00812-x

14. Li J, Li C, Huang Y, Guan P, Huang D, Yu H, et al. Mendelian randomization analyses in ocular disease: a powerful approach to causal inference with human genetic data. *J Transl Med*. (2022) 20:621. doi: 10.1186/s12967-022-03822-9

15. Gupta V, Walia GK, Sachdeva MP. Mendelian randomization": an approach for exploring causal relations in epidemiology. *Public Health*. (2017) 145:113–9. doi: 10.1016/j.puhe.2016.12.033

16. Davies NM, Holmes MV, Davey Smith G. Reading Mendelian randomisation studies: a guide, glossary, and checklist for clinicians. *BMJ*. (2018) 362:k601. doi: 10.1136/bmj.k601

17. Orrù V, Steri M, Sidore C, Marongiu M, Serra V, Olla S, et al. Complex genetic signatures in immune cells underlie autoimmunity and inform therapy. *Nat Genet*. (2020) 52:1036–45. doi: 10.1038/s41588-020-0684-4

18. Burgess S, Thompson SG. Interpreting findings from Mendelian randomization using the MR-Egger method. *Eur J Epidemiol*. (2017) 32:377–89. doi: 10.1007/s10654-017-0255-x

19. Bowden J, Davey Smith G, Haycock PC, Burgess S. Consistent estimation in Mendelian randomization with some invalid instruments using a weighted median estimator. *Genet Epidemiol*. (2016) 40:304–14. doi: 10.1002/gepi.21965

20. Higgins JPT, Thompson SG, Deeks JJ, Altman DG. Measuring inconsistency in meta-analyses. *BMJ*. (2003) 327:557–60. doi: 10.1136/bmj.327.7414.557

21. Yavorska OO, Burgess S. MendelianRandomization: an R package for performing Mendelian randomization analyses using summarized data. *Int J Epidemiol*. (2017) 46:1734–9. doi: 10.1093/ije/dyx034

22. Rodríguez C, Puente-Moncada N, Reiter RJ, Sánchez-Sánchez AM, Herrera F, Rodríguez-Blanco J, et al. Regulation of cancer cell glucose metabolism is determinant for cancer cell fate after melatonin administration. *J Cell Physiol*. (2021) 236:27–40. doi: 10.1002/jcp.29886

23. Callao V, Montoya E. Toxohormone-like factor from microorganisms with impaired respiration. *Science*. (1961) 134:2041–2. doi: 10.1126/science.134.3495.2041

24. Zhang J, Yang J, Lin C, Liu W, Huo Y, Yang M, et al. Endoplasmic Reticulum stress-dependent expression of ERO1L promotes aerobic glycolysis in Pancreatic Cancer. *Theranostics*. (2020) 10:8400–14. doi: 10.7150/thno.45124

25. Rui R, Zhou L, He S. Cancer immunotherapies: advances and bottlenecks. *Front Immunol*. (2023) 14:1212476. doi: 10.3389/fimmu.2023.1212476

26. Scott DW, Gascoyne RD. The tumour microenvironment in B cell lymphomas. *Nat Rev Cancer*. (2014) 14:517–34. doi: 10.1038/nrc3774

27. O'Brien KL, Finlay DK. Immunometabolism and natural killer cell responses. *Nat Rev Immunol*. (2019) 19:282–90. doi: 10.1038/s41577-019-0139-2

28. Vivier E, Rebuffet L, Narni-Mancinelli E, Cornen S, Igarashi RY, Fantin VR. Natural killer cell therapies. *Nature*. (2024) 626:727–36. doi: 10.1038/s41586-023-06945-1

29. Cox MC, Battella S, La Scaleia R, Pelliccia S, Di Napoli A, Porzia A, et al. Tumor-associated and immunochemotherapy-dependent long-term alterations of the peripheral blood NK cell compartment in DLBCL patients. *Oncoimmunology*. (2015) 4:e990773. doi: 10.4161/2162402X.2014.990773

30. de Jonge AV, Duetz C, Bruins WSC, Korst CLBM, Rentenaar R, Cosovic M, et al. Distinct peripheral T-cell and NK-cell profiles in HGBL-MYC/BCL2 vs patients with DLBCL NOS. *Blood Adv*. (2024) 8:1094–104. doi: 10.1182/bloodadvances.2023011687

31. Savitz J. The kynurenine pathway: a finger in every pie. *Mol Psychiatry*. (2020) 25:131–47. doi: 10.1038/s41380-019-0414-4

32. Maskarinec G, Brown SM, Lee J, Bogumil D, Walsh C, Haiman CA, et al. Association of obesity and type 2 diabetes with non-Hodgkin lymphoma: the multiethnic cohort. *Cancer Epidemiol Biomarkers Prev*. (2023) 32:1348–55. doi: 10.1158/1055-9965.EPI-23-0565

33. Kim M, Jung S, Lee S-H, Lee JH. Association between arterial stiffness and serum L-octanoylcarnitine and lactosylceramide in overweight middle-aged subjects: 3-year follow-up study. *PloS One*. (2015) 10:e0119519. doi: 10.1371/journal.pone.0119519

34. Wang S, Gu J, Xu Z, Zhang Z, Bai T, Xu J, et al. Zinc rescues obesity-induced cardiac hypertrophy *via* stimulating metallothionein to suppress oxidative stress-activated BCL10/CARD9/p38 MAPK pathway. *J Cell Mol Med*. (2017) 21:1182–92. doi: 10.1111/jcmm.13050

35. Ecker V, Brandmeier L, Stumpf M, Giansanti P, Moreira AV, Pfeuffer L, et al. Negative feedback regulation of MAPK signaling is an important driver of chronic lymphocytic leukemia progression. *Cell Rep*. (2023) 42:113017. doi: 10.1016/j.celrep.2023.113017

36. Bellosillo B, Piqué M, Barragán M, Castaño E, Villamor N, Colomer D, et al. Aspirin and salicylate induce apoptosis and activation of caspases in B-cell chronic lymphocytic leukemia cells. *Blood*. (1998) 92:1406–14. doi: 10.1182/blood.V92.4.1406

37. Bittner S, Hehlgans T, Feuerer M. Engineered Treg cells as putative therapeutics against inflammatory diseases and beyond. *Trends Immunol*. (2023) 44:468–83. doi: 10.1016/j.it.2023.04.005

38. Kara IO, Sahin B, Gunesacar R. Expression of soluble CD27 and interleukins-8 and -10 in B-cell chronic lymphocytic leukemia: correlation with disease stage and prognosis. *Adv Ther*. (2007) 24:29–40. doi: 10.1007/BF02849990

frontiers | Frontiers in Immunology

TYPE Original Research
PUBLISHED 02 December 2024
DOI 10.3389/fimmu.2024.1481080

OPEN ACCESS

EDITED BY
Michael John Robertson,
Indiana University Bloomington, United States

REVIEWED BY
Hazim Ababneh,
Massachusetts General Hospital and Harvard Medical School, United States
Gabriele Casirati,
Dana–Farber Cancer Institute, United States

*CORRESPONDENCE
Xiaorong Hou
houxr@pumch.cn
Wei Zhang
vv1223@vip.sina.com

RECEIVED 15 August 2024
ACCEPTED 13 November 2024
PUBLISHED 02 December 2024

CITATION
Ruan J, Zhou D, Zhang Y, Zhao D, Wei C, Hu K, Zhang F, Hou X and Zhang W (2024) Hyper-fractionated radiotherapy as a bridging strategy to enhance CAR-T efficacy by regulating T-cell co-stimulatory molecules in relapsed/refractory diffuse large B-cell lymphoma. *Front. Immunol.* 15:1481080. doi: 10.3389/fimmu.2024.1481080

Hyper-fractionated radiotherapy as a bridging strategy to enhance CAR-T efficacy by regulating T-cell co-stimulatory molecules in relapsed/refractory diffuse large B-cell lymphoma

Jing Ruan[1], Daobin Zhou[1], Yan Zhang[1], Danqing Zhao[1], Chong Wei[1], Ke Hu[2], Fuquan Zhang[2], Xiaorong Hou[2]* and Wei Zhang[1]*

[1]Department of Hematology, Peking Union Medical College Hospital, Beijing, China, [2]Department of Radiotherapy, Peking Union Medical College Hospital, Beijing, China

Background: Bridging therapy can prevent patients from disease progression while waiting for CAR-T cell preparation. Hyper-fractionated radiotherapy can achieve an effective target dose within a short period, minimize radiation damage, and may modify immune environment compared to conventional radiotherapy.

Aims: This study aims to investigate the efficacy and safety of bridging hyper-fractionated radiotherapy in combination with CAR-T therapy for relapsed/refractory diffuse large B-cell lymphoma. The potential mechanisms were explored.

Methods: This is a prospective pilot study. After T-cell collection, the patients underwent hyper-fractionated radiotherapy at lesion sites with 1.5 Gy twice daily for 10 days before CAR-T cell infusion. Peripheral blood immune cell subsets and quantitative serum proteomics were assessed before radiotherapy and after radiotherapy before CAR-T cell infusion.

Results: A total of 13 patients have been enrolled. The median follow-up time was 6 (3–24) months after CAR-T infusion. At 3-month follow-up, 9/13(69%) patients had CR, 1/13(8%) patient had PR, 1/13(8%) patient remained SD, and 2/13(15%) patients died of disease progression. The local recurrence rate was 1/13(8%). Seven patients have been followed up for more than 6 months, and they remain in CR. The median PFS and OS were not reached. No grade 3–4 CRS or ICANS were reported. After hyper-fractionated radiotherapy, peripheral PD1+CD8+T/T ratio significantly decreased while quantitative serum proteomics profiling showed a decrease in sCD28.

Conclusion: Hyper-fractionated radiotherapy can rapidly control tumor progression sites without delaying the infusion time. This approach can improve the ORR and does not increase the incidence of CRS and ICANS. The mechanism may be related to the regulation of T-cell co-stimulatory molecules, which demands further exploration.

KEYWORDS

hyper-fractionated radiotherapy, DLBCL, CAR-T, bridging therapy, T-cell co-stimulatory molecules

Highlights

- Hyper-fractionated radiotherapy can rapidly control tumor, potentially improve the outcome of CAR T therapy, and does not appear to increase the incidence of CRS and ICANS.
- T-cell co-stimulatory molecules were modified by hyper-fractionated radiotherapy to enhance CAR-T efficacy.

Background

Patients with relapsed/refractory diffuse large B-cell lymphoma have poor overall survival with few treatment options. CAR-T therapy is a breakthrough in helping these patients to achieve long-term remission.

However, the preparation of CAR-T cell usually takes approximately 4 weeks. To prevent disease progression that would affect CAR-T cell infusion, bridging therapy is needed in most patients (1). The current approach for bridging therapy mainly involves conventional chemotherapy, while patients with relapsed/refractory diffuse large B-cell lymphoma often develop resistance. Some patients may even have progressively large mass that compress important organs, resulting in liver and kidney dysfunction, pain, and even paralysis.

Local radiotherapy can effectively and significantly reduce tumors and improve symptoms in these patients. Cases have reported the effectiveness and safety of radiotherapy bridging CAR-T therapy in refractory relapsed lymphoma (2, 3). Recently, several retrospective studies have confirmed that radiotherapy bridging can be safely and effectively used even in advanced stage and high-risk disease, while whether it brings superior outcome than systematic treatment remains controversial (4–7). Furthermore, patients who received radiotherapy before CAR-T seemed to have lower incidence of life-threatening toxicities including cytokine release syndrome (CRS) and immune effector cell-associated neurotoxicity syndrome (ICANS) (8). The previously reported cases in the literature mostly employ conventional fractionation as bridging treatment. In fact, hyper-fractionated radiotherapy can achieve an effective target dose within a shorter period and minimize radiation damage compared to conventional radiotherapy. In addition, studies in mice models proved that low-dose radiotherapy may promote the recruitment of CAR-T cells to tumors and enhance CAR-T cell cytotoxicity. The tumor microenvironment may also be modified to improve immune escape (9, 10).

Therefore, in this pilot study, we aimed to prospectively investigate the efficacy and safety of bridging hyper-fractionated radiotherapy in combination with CAR-T therapy for relapsed/refractory diffuse large B-cell lymphoma. The potential mechanisms would also be explored (NCT05514327).

Methods

Patient population

This is a pilot study. We prospectively enrolled relapsed/refractory diffuse large B-cell lymphoma patients with measurable lesions in Peking Union Medical College Hospital between 2022 and 2024. Written informed consent was signed by the patients. The study was approved by the ethics committee of Peking Union Medical College Hospital and was conducted in accordance with the Declaration of Helsinki.

Treatment and follow-up

After T-cell collection, the patients underwent hyper-fractionated radiotherapy at the sites of maximum lesion size (or highest SUV), rapidly progressing sites, and sites with compressive symptoms (total radiation sites ≤3). The radiotherapy regimen consisted of 1.5 Gy twice daily for 10 days. CAR-T cell infusion was performed 1–2 weeks after the completion of radiotherapy. Adverse reactions at different time points after radiotherapy and CAR-T cell infusion were monitored and analyzed. CRS and ICANS were documented by primary care physicians based on consensus guidelines from the

American Society of Transplantation and Cellular Therapy for Cytokine Release Syndrome and Neurologic Toxicity Associated with Immune Effector Cells (11). Radiation-related adverse events were graded using Common Terminology Criteria for Adverse Events version 5.0. PET/CT was scheduled at 1 month, 3 months, 6 months, 1 year, and 2 years to evaluate the disease according to the Lugano criteria. Peripheral blood immune cell subsets were assessed by flow cytometry before and after radiotherapy (12, 13). Plasma was also obtained and analyzed using an Olink proteomics Target-96 immuno-oncology-panel that included multiple markers of angiogenesis and proliferation (14, 15).

Statistical analysis

Descriptive variables were displayed as percent of all patients with available data, while continuous variables were expressed as mean ± SEM. Quantitative data were compared by two-sample (unpaired Student's) two-tailed t-test assuming equal variance, while categorical data were compared using the Chi-square test. Comparisons among groups were calculated by paired-samples t-test. Progression-free survival (PFS) and overall survival (OS) were analyzed using Kaplan–Meier survival analysis. A two-sided p-value of <0.05 was considered statistically significant. All the statistical tests were performed using SPSS 21.0 statistical software.

Results

Patient characteristics

From 2022 to 2024, 13 relapsed/refractory diffuse large B-cell lymphoma (DLBCL) patients have been prospectively enrolled in our study. Baseline clinicopathological features are listed in Table 1. The median age was 52 years old (27–66 years), and 69% of them were men. Four (31%) were GCB type, five (38%) were double expressor, one (8%) was double hit, and one (8%) was transformed from marginal zone B-cell lymphoma. Seven (54%) patients were stage IV at diagnosis according to Ann Arbor stages, and the international prognostic index (IPI) scores at diagnosis were commonly 2–3 (54%). Four (31%) patients had bulky disease before radiotherapy, which was defined by one or more lesions ≥7.5 cm in greatest dimension. Six (46%) patients were primary refractory. The median lines of therapy prior to CAR-T were three (two to six lines), and two (15%) of them had undergone previous autologous stem cell transplantation.

Bridging therapy characteristics

Four (31%) patients received whole brain radiotherapy, among whom one was primary central nervous system lymphoma (PCNSL) and three patients were systemic DLBCL. The other radiotherapy treated anatomic sites including the neck (n=2), mediastinum (n=2), breast (n=1), abdomen (n=3), and pelvis (n=1). Hyper-fractionated radiotherapy was prescribed for all patients; in detail, the total dose was 30 Gy for all patients, and the regimen was 1.5 Gy twice a day in continuous 10 days. Prescription coverage of 100% of 95% of the planned gross tumor volume (PGTV) was performed. Intensity-modulated radiation therapy (IMRT) was performed for all patients. As for the radiotherapy field, three (23%) patients had comprehensive radiotherapy, which was defined as treating all active sites of disease seen on PET/CT; six (46%) patients had focal radiotherapy, which was defined in cases where not all disease was treated; and four (31%) patients received whole brain radiotherapy (WBRT) (Supplementary Table S1).

Five (38%) patients also received systemic therapy during the bridging period. Two patients received orelabrutinib continuously to CAR-T cell infusion, while the dosage was reduced during

TABLE 1 Basic characteristics of the patients enrolled in our study.

Basic characteristics	Value
Age at BRT, year, median (range)	52 (27–66)
Sex, n(%)	
Male	9 (69%)
Female	4(31%)
Pathology at diagnosis, n(%)	
DLBCL	12 (92%)
Transformed marginal zone B-cell lymphoma	1 (8%)
Germinal center type	4 (31%)
Double expressor	5 (38%)
Double/triple hit	1 (8%)
Ann Arbor stage at diagnosis, n(%)	
IEA	2 (15%)
II	4 (31%)
IV	7 (54%)
International prognostic index score at diagnosis, n(%)	
Low (0–1)	5 (38%)
Intermediate (2–3)	7 (54%)
High (4–5)	1 (8%)
Bulky disease (≥7.5 cm in greatest dimension)	4 (31%)
Primary refractory disease, n (%)	6 (46%)
Lines of therapy prior to CAR-T, n median (range)	3 (2–6)
Prior autologous stem cell transplantation, n (%)	2 (15%)
Radiotherapy field	
Comprehensive	3 (23%)
Focal	6 (46%)
WBRT	4 (31%)
CAR-T cell product	
Relmacabtagene autoleucel	8 (62%)
Axicabtagene ciloleucel	5 (38%)

radiotherapy. The other three patients were treated with VP16 and dexamethasone, oxaliplatin and dexamethasone, brentuximab vedotin, and tislelizumab, separately.

The time interval between the completion of radiotherapy and CAR-T cell infusion was 7–25 days (median, 12 days). All patients received fludarabine and cyclophosphamide lymphodepletion before CAR-T cell infusion. The CAR-T cell products were relmacabtagene autoleucel in eight (62%) patients and axicabtagene ciloleucel in five (38%) patients.

Clinical outcomes

Clinical response and survival outcomes

All of them achieved partial response (PR) after the completion of hyper-fractionated radiotherapy (Figure 1) and successfully completed CAR-T cell infusion later. The detailed information is shown in Supplementary Table S1.

Till submission, the median follow-up time was 6 (3–24) months after CAR-T infusion. At 1-month follow-up, 7/13 (54%) patients achieved CR, 2/13 (15%) achieved PR, 1/13 (8%) achieved SD, and 3/13 (23%) achieved PD; the ORR was 69%. At 3-month follow-up, 9/13(69%) patients had CR and 1/13 (8%) patient had PR, 1/13 (8%) patient remained SD, and 2/13 (15%) patients died of disease progression; the ORR was 77%. Seven patients have been followed up for more than 6 months, and they remain in CR. The median PFS and OS were not reached (Figure 2).

The local recurrence rate defined by disease progression inside the irradiated field was 1/13 (8%), and this patient was PCNSL who received WBRT. Two patients with PR at 1-month follow-up had residual lesions at the site of prior radiotherapy and received salvage radiotherapy at the same site; both achieved CR at 3-month follow-up. One patient had partial response in in-field radiotherapy site (abdominal disease), while bone lesions outside the radiotherapy field were progressed at 1-month follow-up after CAR-T cell infusion. He achieved PR at 3-month follow-up with salvage therapy of four cycles of tislelizumab and ibrutinib; CR was reached at 6-month follow-up with ibrutinib maintenance.

Adverse effects

The adverse effects after radiotherapy and before CAR-T cell infusion were limited. One patient experienced cerebral edema and relieved after dexamethasone. One patient had aspiration pneumonia and recovered from antibiotics. Two patients had grade 4 neutropenia; one of them received orelabrutinib during radiotherapy, and the other one had systemic chemotherapy therapy before radiotherapy during the bridging period.

Following CAR-T cell infusion, CRS was observed in 10/13 (77%) patients, and 5/13 (38%) were grade 1, 5/13 (38%) were grade 2. No grade 3–4 CRS or ICANS were reported. Grade 3 neutropenia was reported in 2/13 (15%) patients, and grade 4 neutropenia was reported in 10/13 (77%) patients after CAR-T cell infusion. The median time from infusion to neutropenia was 3.5 days (−1 to 14 days), the median time for neutropenia recovery was 5.5 days (1–29 days), and 10/12 (83%) recovered within 1 week. One patient had bloodstream infection, and two patients had COVID-19 infection. Grade 1–3 thrombocytopenia was observed in 6/13 (46%) patients.

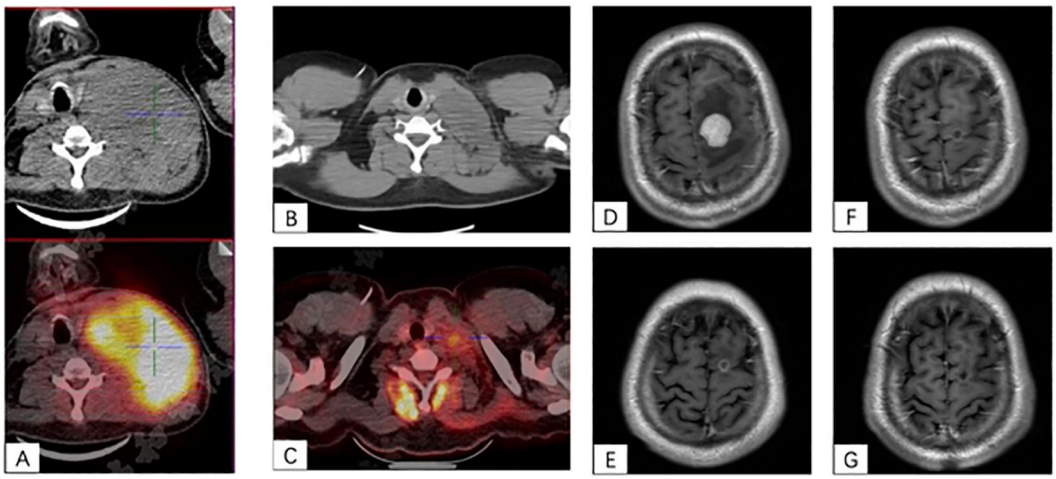

FIGURE 1
(A–C) A case of bulky left cervical disease. **(A)** Baseline PET/CT scan showed a 13.1 cm × 8.4 cm × 10.5 cm mass with SUVmax to be 20.5 at the left side of the neck and pushing the trachea to the right. **(B)** The mass quickly shrank to 6×2.6 cm after hyper-fractionated radiotherapy. **(C)** After CAR-T cell infusion at 1 month, PET/CT scan showed a 3.2 cm × 1.9 cm mass with SUVmax of 3.2. **(D–F)** A case of CNS lesion. **(D)** Baseline contrast-enhanced MRI showed a 2.5-cm enhanced nodule with peripheral edema in the left frontal lobe. **(E)** After radiotherapy, the lesion shrank to 0.75 cm with ring-like enhancement. **(F)** After CAR-T cell infusion at 1 month, the lesion was 0.5 cm with ring-like enhancement. **(G)** The lesion had no enhancement on the contrast-enhanced MRI at 3-month after CAR-T cell infusion.

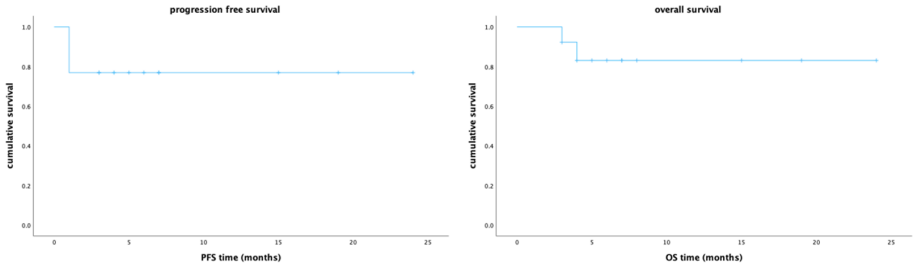

FIGURE 2
The Kaplan–Meier survival curves for progression free survival and overall survival of the 13 patients in our study.

Peripheral blood immune cell subsets and quantitative serum proteomics before and after hyper-fractionated radiotherapy

The percentage and absolute number of peripheral blood immune cell subsets before and after hyper-fractionated radiotherapy were compared (Supplementary Tables S2, S3). Preliminary analysis showed that after hyper-fractionated radiotherapy, peripheral PD1+CD8+T/T ratio significantly decreased (15% vs. 8%, p=0.017) (Figure 3), while the absolute number of PD1+CD8+T tended to be decreased (120×10^6/L vs. 46×10^6/L, p=0.09). Peripheral monocyte/WBC ratio also increased (9% vs. 13%, p=0.029) and granulocyte/WBC ratio decreased (73% vs. 58%, p=0.049). There were no differences between percentage of naïve T cell, memory T cell, effector T cell, Treg cell, TEMRA cell, Tim3+ T cell, NK cell, and dendritic cell. Furthermore, the absolute numbers of total Treg (15.7×10^6/L vs. 10.9×10^6/L, p=0.027) and CD45 RA-Treg (11.5×10^6/L vs. 8.2×10^6/L, p=0.025) subsets were significantly decreased, while the percentage of these subsets remained unchanged after radiotherapy. Quantitative serum proteomics profiling showed a decrease in sCD28 (p=0.016). CXCL12 (p=0.013), NOS3 (p=0.003), and PTN (p=0.034) also significantly decreased and Gal1 (p=0.009) (Figure 4) increased after hyper-fractionated radiotherapy. GO enrichment analysis showed that the differentially expressed proteins were mainly involved in immune cell chemotaxis and signal transduction.

Discussion

Here, we reported the first prospective study about the efficacy and safety of bridging CAR-T with hyper-fractionated radiotherapy in relapsed/refractory diffuse large B-cell lymphoma.

The integration of radiotherapy as a bridging strategy prior to CAR-T cell therapy is an emerging approach being explored in the management of lymphoma. Importantly, the radiotherapy did not appear to significantly impair CAR-T expansion or persistence. Within the limits of the small cohorts retrieved, radiotherapy seems a superior option compared with systemic treatment as a "bridge" to CAR-T and could as well reduce severe complications rates (4, 16). In the largest multi-center retrospective cohort from the UK, 169/717(24%) patients received bridging radiotherapy before CAR-T cell infusion. The best ORR/CR rates by single-modality radiotherapy, combined modality treatment (CMT), and systemic

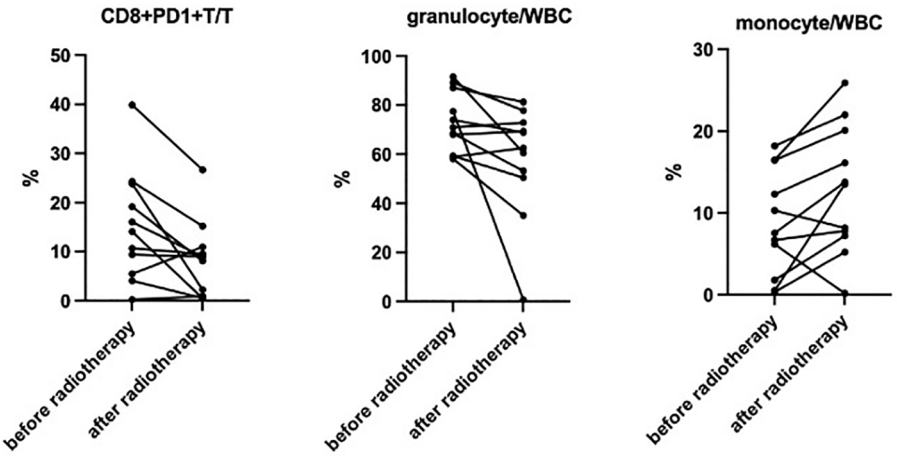

FIGURE 3
Significantly decreased CD8+PD1+T/T (15% vs. 8%, p=0.017), decreased granulocyte/WBC (73% vs. 58%, p=0.049), and increased monocyte/WBC (9% vs. 13%, p=0.029) ratio were observed after hyper-fractionated radiotherapy.

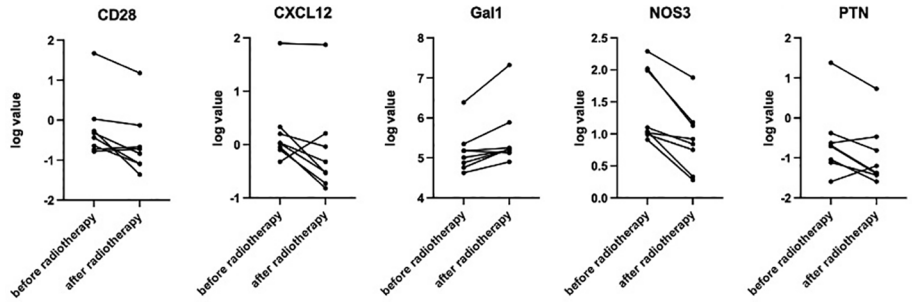

FIGURE 4
Paired t-test showed significantly decreased sCD28 (p=0.016), CXCL12 (p=0.013), NOS3 (p=0.003), and PTN (p=0.034) and increased Gal1 (p=0.009) after hyper-fractionated radiotherapy.

bridging were 82.1%/62.5%, 81.8%/63.6%, and 74%/55.9%, respectively. Furthermore, radiotherapy-bridged patients had favorable outcomes with 1-year PFS of 56% for single modality and 47% for CMT, while 1-year PFS for systemic bridging was 43%. In a study from China, 29/60 patients received radiotherapy before CAR T-cell infusion. Compared to the 31/60 patients with only bridging chemotherapy, the radiotherapy bridging group achieved a higher ORR at day 30 (82.8% vs. 45.2%), better 1-year PFS (46.9% vs. 22.6%) while reduced CRS of grade≥3; patients with bulky disease even had better 1-year OS (17). However, another multi-institutional study showed that the patients with radiotherapy bridging had lower median OS compared to the CMT and systemic bridging group despite comparable baseline characteristics (5). In our prospectively pilot study, CR at 1 month and at 3 months was 54% and 69%, respectively, while the ORR was 60% and 77%, respectively. A total of 54% patients who have been followed up for more than 6 months remained CR. The ORR tended to be higher than in patients without bridging therapy and was comparable to patients who received conventional radiotherapy, while the rate of CR at more than 3 months tended to be higher compared to historical records (1, 18). The median PFS and OS have not been reached with the median follow-up time of 6 (3–24) months in our report.

Debulking tumor burden before infusion is important to improve CAR-T therapy outcome and reduce side effects. Bridging radiation therapy could effectively cytoreduce high-risk relapsed/refractory aggressive B-cell lymphoma after multi-lines therapy including tumor diameter, SUV, and serum LDH, all predictors of poor post-CAR-T therapy outcomes (18). Currently, no consensus exists for dose/fractionation for the purposes of bridging RT, and an interesting pilot trial by Ababneh is ongoing (5). Our study innovatively utilized hyper-fractionated radiotherapy where the total radiation dose is delivered in more frequency and lower single doses compared to conventional fractionation. Therefore, an effective target dose could be achieved within a shorter period to rapidly effectively shrink the tumor load without delay or affect CAR-T cell infusion and could minimize radiation damage.

In addition, low-lose radiation may have a better synergistic effect with CAR-T therapy due to its potential role in tumor recruiting and immune modulating. According to DeSelm, low-dose radiation conditioning enables CAR-T cells to mitigate antigen escape in a TRAIL-dependent manner (19). Furthermore, radiation-induced IFN-gamma production within the tumor microenvironment may help CAR-T cell infiltration and tumor cell target recognition in glioblastoma mice model (20, 21). In our study, we found that peripheral PD1+CD8+T and sCD28 decreased after hyper-fractionated radiotherapy. CD28 and PD-1 are two important co-stimulatory molecules that play a critical role in T-cell activation and regulation of immune responses. CD28 binds to the B7 molecules (including CD80 and CD86) on the surface of antigen-presenting cells, providing the second signal to promote T-cell activation and proliferation. PD-1, on the other hand, is a negative regulatory molecule mainly expressed on activated immune cells such as T cells, and its binding to PD-L1 suppresses T-cell activation and function. After hyper-fractionated radiotherapy, the level of serum soluble CD28 (sCD28) decreased, and since previous studies have shown a negative correlation between serum sCD28 and the level of CD28 on the T-cell membrane surface (22), we speculate that hyper-fractionated radiotherapy can increase the level of CD28 on the surface of T cells in DLBCL patients, thereby enhancing the anti-tumor effect. However, it is a pity that we did not prospectively perform flow cytometry to assess CD28 expression on T cells. On the other hand, PD1+CD8+T cells play an exhaustive role in the tumor microenvironment. Studies have proved that decreased peripheral PD1+CD8+ T cells after immunotherapy may indicate better outcome (23), and a higher proportion of PD1+CD8+T in the serum corresponded to shortened PFS in lung cancer (24). Therefore, we hypothesize that hyper-fractionated radiotherapy also helps improve the tumor immune microenvironment by reducing the percentage of PD1+CD8+ T cells. Further direct studies should be conducted to explore the potential mechanisms. Notably, three patients evaluated to be PR/PD at 1 month finally reached CR at 3 months or 6 months after salvage therapy including complementary radiotherapy or PD-1 blockade. According to Ababneh and Saifi, patients with limited post-CART disease who received salvage comprehensive RT had better overall survival and freedom from subsequent progression (25, 26). Radiotherapy or PD-1 may help priming the tumor microenvironment and enhance tumor antigen presentation (25, 27, 28) even after CAR-T cell infusion, and several related clinical trials have been ongoing. Another interesting finding is the decreased number of Treg cells after hyper-fractionated radiotherapy, especially the CD45RA– Treg cells. CD45RA– Treg

cells are mainly effector Treg and effector memory Treg cells (29). Studies have shown that CD45RA− Treg cell subsets have immunosuppressive properties, and the accumulation of CD45RA− Treg in tumor microenvironment correlated with tumor progression and poor prognosis in solid tumors (30–32). Furthermore, the infiltration of CD4+ Treg cells could decrease the efficacy of CAR-T therapy by CTLA-4 expression and IL-2 production. Therefore, hyper-fractionated radiotherapy may help enhance the efficacy of CAR-T by decreasing CD45RA− Treg cells.

There are some important safety considerations that need to be carefully monitored when combining radiotherapy and CAR-T cell therapy. First of all, since both radiotherapy and CAR-T cell therapy can cause myelosuppression, cytopenia, and infections, it has drawn attention. In our study, although grade 3–4 neutropenia was common, the duration of neutropenia was less than 7 days for most patients, and no fatal infection was recorded. Still, a close monitoring of blood counts and infection prevention are suggested especially for patients with combined bridging therapy other than radiotherapy or for special anatomy radiation field including whole brain radiotherapy. Furthermore, CAR-T cell therapy can trigger severe irAEs, such as CRS and ICANS; the addition of hyper-fractionated radiotherapy may potentially enhance immune response. However, no grade 3–4 CRS or ICANS were reported in this study. The addition of radiotherapy or even hyper-fractionated radiotherapy in turn reduces the incidence or severity of CRS and ICANS, which may be due to reduced tumor burden (33). In addition, the combination of radiotherapy and CAR-T cell therapy may theoretically increase the risk of developing secondary cancers, especially given the potential for radiotherapy-induced genomic instability. Long-term follow-up and surveillance will be crucial to monitor for this potential complication.

This study has several limitations. Most notably, the sample size is relatively small, which also limits subgroup analyses, and the follow-up duration was relatively short to have long-term efficacy and survival data. We would continue to enroll more patients and update the data with longer follow-up time. In addition, 38% patients also received other systemic therapy in addition to hyper-fractionated radiotherapy during the bridging period, which may affect both outcomes and toxicity, although it may reflect real-world practice patterns. Moreover, we did not perform a PET/CT evaluation before CAR-T cell infusion to evaluate the effect of hyper-fractionated radiotherapy to help provide more interesting information.

Conclusion

In conclusion, bridging hyper-fractionated radiotherapy with CAR-T therapy is safe and effective for patients with relapsed/refractory diffuse large B-cell lymphoma. Ultra-hyper-fractionated radiotherapy can rapidly control tumor progression sites without delaying the infusion time. This approach can improve the outcome and does not increase the incidence of CRS and ICANS. Further follow-up is needed to assess long-term efficacy and survival. The mechanism may be related to the regulation of T-cell co-stimulatory molecules by hyper-fractionated radiotherapy, which demands further exploration.

Data availability statement

The original contributions presented in the study are included in the article/Supplementary Material. Further inquiries can be directed to the corresponding authors.

Ethics statement

The studies involving humans were approved by The Ethics Committee of Peking Union Medical College Hospital. The studies were conducted in accordance with the local legislation and institutional requirements. The participants provided their written informed consent to participate in this study. Written informed consent was obtained from the individual(s) for the publication of any potentially identifiable images or data included in this article.

Author contributions

JR: Data curation, Formal analysis, Funding acquisition, Investigation, Methodology, Software, Writing – original draft, Writing – review & editing. DBZ: Conceptualization, Methodology, Supervision, Visualization, Writing – original draft, Writing – review & editing. YZ: Data curation, Investigation, Writing – original draft, Writing – review & editing. DQZ: Data curation, Investigation, Writing – original draft, Writing – review & editing. CW: Data curation, Investigation, Writing – original draft, Writing – review & editing. KH: Data curation, Methodology, Supervision, Writing – original draft, Writing – review & editing. FZ: Conceptualization, Data curation, Methodology, Supervision, Writing – original draft, Writing – review & editing. XH: Conceptualization, Data curation, Investigation, Methodology, Supervision, Writing – original draft, Writing – review & editing. WZ: Conceptualization, Data curation, Investigation, Methodology, Supervision, Validation, Visualization, Writing – original draft, Writing – review & editing.

Funding

The author(s) declare financial support was received for the research, authorship, and/or publication of this article. This study was supported by the National High Level Hospital Clinical Research Funding 2022-PUMCH-A-250, National High Level Hospital Clinical Research Funding 2022-PUMCH-C-056, and Beijing Xisike Clinical Oncology Research Foundation Y-2022YMJN/MS-0044.

Conflict of interest

The authors declare that the research was conducted in the absence of any commercial or financial relationships that could be construed as a potential conflict of interest.

Publisher's note

All claims expressed in this article are solely those of the authors and do not necessarily represent those of their affiliated organizations, or those of the publisher, the editors and the reviewers. Any product that may be evaluated in this article, or claim that may be made by its manufacturer, is not guaranteed or endorsed by the publisher.

Supplementary material

The Supplementary Material for this article can be found online at: https://www.frontiersin.org/articles/10.3389/fimmu.2024.1481080/full#supplementary-material

References

1. Roddie C, Neill L, Osborne W, Iyengar S, Tholouli E, Irvine D, et al. Effective bridging therapy can improve CD19 CAR-T outcomes while maintaining safety in patients with large B-cell lymphoma. *Blood Adv*. (2023) 7:2872-83. doi: 10.1182/bloodadvances.2022009019

2. Deshpande A, Rule W, Rosenthal A. Radiation and chimeric antigen receptor T-cell therapy in B-cell non-hodgkin lymphomas. *Curr Treat Options Oncol*. (2022) 23:89–98. doi: 10.1007/s11864-021-00935-z

3. Sim AJ, Jain MD, Figura NB, Chavez JC, Shah BD, Khimani F, et al. Radiation therapy as a bridging strategy for CAR T cell therapy with axicabtagene ciloleucel in diffuse large B-cell lymphoma. *Int J Radiat Oncol Biol Phys*. (2019) 105:1012–21. doi: 10.1016/j.ijrobp.2019.05.065

4. Pinnix CC, Gunther JR, Dabaja BS, Strati P, Fang P, Hawkins MC, et al. Bridging therapy prior to axicabtagene ciloleucel for relapsed/refractory large B-cell lymphoma. *Blood Adv*. (2020) 4:2871–83. doi: 10.1182/bloodadvances.2020001837

5. Ababneh HS, Ng AK, Frigault MJ, Jacobson CA, Patel CG. Radiotherapy as a bridging strategy for patients with relapsed or refractory large B-cell lymphoma undergoing CAR T-cell therapy. *Am J Hematol*. (2024) 99:1837–40. doi: 10.1002/ajh.27409

6. Kuhnl A, Roddie C, Kirkwood AA, Chaganti S, Norman J, Lugthart S, et al. Outcome and feasibility of radiotherapy bridging in large B-cell lymphoma patients receiving CD19 CAR T in the UK. *Br J Haematol*. (2024) 205:483–94. doi: 10.1111/bjh.v205.2

7. Ababneh HS, Abramson JS, Johnson PC, Patel CG. Assessing the role of radiotherapy in patients with refractory or relapsed high-grade B-cell lymphomas treated with CAR T-cell therapy. *Radiother Oncol*. (2022) 175:65–72. doi: 10.1016/j.radonc.2022.08.007

8. Qu C, Ping N, Kang L, Liu H, Qin S, Wu Q, et al. Radiation priming chimeric antigen receptor T-cell therapy in relapsed/refractory diffuse large B-cell lymphoma with high tumor burden. *J Immunother*. (2020) 43:32–7. doi: 10.1097/CJI.0000000000000284

9. Flynn JP, O'Hara MH, Gandhi SJ. Preclinical rationale for combining radiation therapy and immunotherapy beyond checkpoint inhibitors (i.e., CART). *Transl Lung Cancer Res*. (2017) 6:159–68. doi: 10.21037/tlcr.2017.03.07

10. Hauth F, Ho AY, Ferrone S, Duda DG. Radiotherapy to enhance chimeric antigen receptor T-cell therapeutic efficacy in solid tumors: A narrative review. *JAMA Oncol*. (2021) 7:1051–9. doi: 10.1001/jamaoncol.2021.0168

11. Lee DW, Santomasso BD, Locke FL, Ghobadi A, Turtle CJ, Brudno JN, et al. ASTCT consensus grading for cytokine release syndrome and neurologic toxicity associated with immune effector cells. *Biol Blood Marrow Transplant*. (2019) 25:625–38. doi: 10.1016/j.bbmt.2018.12.758

12. Ferrer-Font L, Small SJ, Lewer B, Pilkington KR, Johnston LK, Park LM, et al. Panel optimization for high-dimensional immunophenotyping assays using full-spectrum flow cytometry. *Curr Protoc*. (2021) 1:e222. doi: 10.1002/cpz1.222

13. Park LM, Lannigan J, Jaimes MC. OMIP-069: forty-color full spectrum flow cytometry panel for deep immunophenotyping of major cell subsets in human peripheral blood. *Cytom A*. (2020) 97:1044–51. doi: 10.1002/cyto.a.v97.10

14. Christensen TD, Maag E, Theile S, Madsen K, Lindgaard SC, Hasselby JP, et al. Circulating immune-related proteins associated with immune checkpoint inhibitor efficacy in patients with pancreatic ductal adenocarcinoma. *ESMO Open*. (2024) 9:103489. doi: 10.1016/j.esmoop.2024.103489

15. Gunnarsdottir FB, Bendahl PO, Johansson A, Benfeitas R, Rydén L, Bergenfelz C, et al. Serum immuno-oncology markers carry independent prognostic information in patients with newly diagnosed metastatic breast cancer, from a prospective observational study. *Breast Cancer Res*. (2023) 25:29. doi: 10.1186/s13058-023-01631-6

16. Guerini AE, Filippi AR, Tucci A, Simontacchi G, Re A, Guaineri A, et al. [amp]] lsquo;Le Roi est mort, vive le Roi': New Roles of Radiotherapy in the Treatment of Lymphomas in Combination With Immunotherapy. *Clin Lymph Myeloma Leuk*. (2022) 22:e135–e48. doi: 10.1016/j.clml.2021.09.005

17. Yu Q, Zhang X, Wang N, Li C, Zhang Y, Zhou J, et al. Radiation prior to chimeric antigen receptor T-cell therapy is an optimizing bridging strategy in relapsed/refractory aggressive B-cell lymphoma. *Radiother Oncol*. (2022) 177:53–60. doi: 10.1016/j.radonc.2022.10.018

18. Hubbeling H, Silverman EA, Michaud L, Tomas AA, Shouval R, Flynn J, et al. Bridging radiation rapidly and effectively cytoreduces high-risk relapsed/refractory aggressive B cell lymphomas prior to chimeric antigen receptor T cell therapy. *Transplant Cell Ther*. (2023) 29:259.e1–.e10. doi: 10.1016/j.jtct.2022.12.021

19. DeSelm C, Palomba ML, Yahalom J, Hamieh M, Eyquem J, Rajasekhar VK, et al. Low-dose radiation conditioning enables CAR T cells to mitigate antigen escape. *Mol Ther*. (2018) 26:2542–52. doi: 10.1016/j.ymthe.2018.09.008

20. Lugade AA, Sorensen EW, Gerber SA, Moran JP, Frelinger JG, Lord EM. Radiation-induced IFN-gamma production within the tumor microenvironment influences antitumor immunity. *J Immunol*. (2008) 180:3132–9. doi: 10.4049/jimmunol.180.5.3132

21. Weiss T, Weller M, Guckenberger M, Sentman CL, Roth P. NKG2D-based CAR T cells and radiotherapy exert synergistic efficacy in glioblastoma. *Cancer Res*. (2018) 78:1031–43. doi: 10.1158/0008-5472.CAN-17-1788

22. Aprilia A, Handono K, Sujuti H, Sabarudin A, Winaris N. sCD163, sCD28, sCD80, and sCTLA-4 as soluble marker candidates for detecting immunosenescence. *Immun Ageing*. (2024) 21:9. doi: 10.1186/s12979-023-00405-0

23. Kim CG, Hong MH, Kim KH, Seo IH, Ahn BC, Pyo KH, et al. Dynamic changes in circulating PD-1(+)CD8(+) T lymphocytes for predicting treatment response to PD-1 blockade in patients with non-small-cell lung cancer. *Eur J Cancer*. (2021) 143:113–26. doi: 10.1016/j.ejca.2020.10.028

24. Kotsakis A, Kallergi G, Aggouraki D, Lyristi Z, Koinis F, Lagoudaki E, et al. CD8(+) PD-1(+) T-cells and PD-L1(+) circulating tumor cells in chemotherapy-naïve non-small cell lung cancer: towards their clinical relevance? *Ther Adv Med Oncol*. (2019) 11:1758835919853193. doi: 10.1177/1758835919853193

25. Saifi O, Breen WG, Lester SC, Rule WG, Stish BJ, Rosenthal A, et al. Don't put the CART before the horse: the role of radiation therapy in peri-CAR T-cell therapy for aggressive B-cell non-hodgkin lymphoma. *Int J Radiat Oncol Biol Phys*. (2023) 116:999–1007. doi: 10.1016/j.ijrobp.2022.12.017

26. Ababneh HS, Ng AK, Frigault MJ, Abramson JS, Johnson PC, Jacobson CA, et al. Salvage radiotherapy in relapsed/refractory large B-cell lymphoma after failure of CAR T-cell therapy. *Haematologica*. (2023) 108:2972–81. doi: 10.3324/haematol.2023.282804

27. Twyman-Saint Victor C, Rech AJ, Maity A, Rengan R, Pauken KE, Stelekati E, et al. Radiation and dual checkpoint blockade activate non-redundant immune mechanisms in cancer. *Nature*. (2015) 520:373–7. doi: 10.1038/nature14292

28. Qin VM, Haynes NM, D'Souza C, Neeson PJ, Zhu JJ. CAR-T plus radiotherapy: A promising combination for immunosuppressive tumors. *Front Immunol*. (2021) 12:813832. doi: 10.3389/fimmu.2021.813832

29. Golubovskaya V, Wu L. Different subsets of T cells, memory, effector functions, and CAR-T immunotherapy. *Cancers (Basel)*. (2016) 8:36. doi: 10.3390/cancers8030036

30. Lin YC, Mahalingam J, Chiang JM, Su PJ, Chu YY, Lai HY, et al. Activated but not resting regulatory T cells accumulated in tumor microenvironment and correlated with tumor progression in patients with colorectal cancer. *Int J cancer*. (2013) 132:1341–50. doi: 10.1002/ijc.v132.6

31. Mao FY, Kong H, Zhao YL, Peng LS, Chen W, Zhang JY, et al. Increased tumor-infiltrating CD45RA(-)CCR7(-) regulatory T-cell subset with immunosuppressive properties foster gastric cancer progress. *Cell Death Dis*. (2017) 8:e3002. doi: 10.1038/cddis.2017.388

32. Suto A, Minaguchi T, Qi N, Fujieda K, Itagaki H, Tenjimbayashi Y, et al. CD25(+)FOXP3(+)CD45RA(-) regulatory T-cell infiltration as a prognostic biomarker for endometrial carcinoma. *BMC Cancer*. (2024) 24:1100. doi: 10.1186/s12885-024-12851-0

33. Fan J, Adams A, Sieg N, Heger JM, Gödel P, Kutsch N, et al. Potential synergy between radiotherapy and CAR T-cells - a multicentric analysis of the role of radiotherapy in the combination of CAR T cell therapy. *Radiother Oncol*. (2023) 183:109580. doi: 10.1016/j.radonc.2023.109580

frontiers | Frontiers in Immunology

TYPE Original Research
PUBLISHED 06 December 2024
DOI 10.3389/fimmu.2024.1483617

OPEN ACCESS

EDITED BY
Penny Fang,
University of Texas MD Anderson Cancer Center, United States

REVIEWED BY
Eden Kleiman,
JSR Life Sciences, United States
Zhenyu Dai,
Stanford University, United States

*CORRESPONDENCE
Sandra Kleinau
sandra.kleinau@icm.uu.se

RECEIVED 20 August 2024
ACCEPTED 14 November 2024
PUBLISHED 06 December 2024

CITATION
Nguyen OTP, Lara S, Ferro G, Peipp M and Kleinau S (2024) Rituximab-IgG2 is a phagocytic enhancer in antibody-based immunotherapy of B-cell lymphoma by altering CD47 expression.
Front. Immunol. 15:1483617.
doi: 10.3389/fimmu.2024.1483617

Rituximab-IgG2 is a phagocytic enhancer in antibody-based immunotherapy of B-cell lymphoma by altering CD47 expression

Oanh T. P. Nguyen[1], Sandra Lara[1], Giovanni Ferro[1], Matthias Peipp[2] and Sandra Kleinau[1]*

[1]Department of Cell and Molecular Biology, Uppsala University, Uppsala, Sweden, [2]Division of Antibody-Based Immunotherapy, University Hospital Schleswig-Holstein, Kiel, Germany

Antibody-dependent cellular phagocytosis (ADCP) by monocytes and macrophages contributes significantly to the efficacy of many therapeutic monoclonal antibodies (mAbs), including anti-CD20 rituximab (RTX) targeting $CD20^+$ B-cell non-Hodgkin lymphomas (NHL). However, ADCP is constrained by various immune checkpoints, notably the anti-phagocytic CD47 molecule, necessitating strategies to overcome this resistance. We have previously shown that the IgG2 isotype of RTX induces CD20-mediated apoptosis in B-cell lymphoma cells and, when combined with RTX-IgG1 or RTX-IgG3 mAbs, can significantly enhance Fc receptor-mediated phagocytosis. Here, we report that the apoptotic effect of RTX-IgG2 on lymphoma cells contributes to changes in the tumor cell's CD47 profile by reducing its overall expression and altering its surface distribution. Furthermore, when RTX-IgG2 is combined with other lymphoma-targeting mAbs, such as anti-CD59 or anti-PD-L1, it significantly enhances the ADCP of lymphoma cells compared to single mAb treatment. In summary, RTX-IgG2 acts as a potent phagocytic enhancer by promoting Fc-receptor mediated phagocytosis through apoptosis and reduction of CD47 in $CD20^+$ malignant B-cells. RTX-IgG2 represents a valuable therapeutic component in enhancing the effectiveness of different mAbs targeting B-cell NHL.

KEYWORDS

anti-CD20 antibody, apoptosis, CD47, cancer immunotherapy, monocyte, phagocytosis, rituximab

1 Introduction

Among various hematological malignancies classified under non-Hodgkin lymphoma (NHL), B-cell lymphoma is the most prevalent subtype (1). In the past decades, the survival rate of B-cell lymphoma patients has been significantly improved thanks to advancements in therapeutic monoclonal antibodies (mAbs). Nevertheless, predicting the treatment responses of most B-cell lymphomas remains challenging due to their significant heterogeneity, highlighting the critical need for ongoing research to improve treatment efficacy and address these complexities (2).

Since its initial approval in 1997, the chimeric CD20-targeting IgG1 mAb rituximab (RTX) has remained a cornerstone in cancer immunotherapy (3). Despite its widespread use, the precise *in vivo* mechanisms of RTX's action remain uncertain (4). Preclinical and clinical data have associated RTX's efficacy in eliminating $CD20^+$ lymphoma cells with various immune responses such as antibody-dependent cellular phagocytosis (ADCP), complement-dependent cytotoxicity (CDC), and to a lesser extent, apoptosis (5–7). Increasing evidence now suggests that the efficacy of RTX monotherapy is primarily mediated through Fc receptor (FcR)-dependent phagocytosis by monocytes and macrophages (6, 8–13). However, opsonization with RTX alone often fails to induce a complete eradication of the target cells, indicating the presence of resistance mechanisms (3).

In recent years, a number of important insights into the regulation of phagocytosis have been established. CD47, a transmembrane protein, has been identified as a crucial regulator of phagocytosis by providing an anti-phagocytic (or "don't-eat-me") signal (14). CD47 achieves its anti-phagocytic effect by binding to its cognate receptor – the signal regulatory protein-α (SIRP-α) – which is highly expressed on macrophages (15, 16). CD47 is ubiquitously expressed in the body and acts as a "marker-of-self", protecting healthy cells from being phagocytosed, thus maintaining immune homeostasis and preventing autoimmunity (15). Senescent or damaged cells, for example, erythrocytes, and apoptotic cells have been shown to have reduced CD47 expression or express CD47 with altered conformation. These alterations consequently render the anti-phagocytic CD47/SIRP-α signal ineffective and allow for the removal of these cells (17–20). Interestingly, recent studies have shown that various malignancies overexpress CD47 as a part of their immune evasion, dampening ADCP induced by therapeutic mAbs (15, 16). This suggests that disrupting CD47-SIRP-α interaction may be pro-phagocytotic, thus potentially improving the therapeutic efficacy of anti-tumor mAbs. Indeed, Métayer et al. showed that blocking CD47 greatly increased phagocytosis of B-cell lymphoma cells by macrophages (21). Along the same lines, Chao et al. reported a synergistic ADCP-mediated anti-tumor activity when combining a CD47-blocking mAb with RTX (13). Despite these promising findings, clinical trials have revealed significant toxicity associated with CD47-blocking mAbs, including anemia, neutropenia, and thrombocytopenia (15, 22). Nonetheless, CD47 remains a potential therapeutic target for improving the efficacy of anti-tumor Abs, provided that the therapy of choice selectively targets only CD47 on the target tumor cells.

We have previously demonstrated that the IgG2 isotype of RTX (RTX-IgG2) is capable of inducing CD20-mediated apoptosis in B-cell lymphoma cells (9). When combining RTX-IgG2 with the phagocytosis-efficient RTX-IgG1 or RTX-IgG3, it significantly enhances phagocytosis of B-cell lymphoma cells. In contrast, a combination of RTX-IgG1 and RTX-IgG3 does not enhance ADCP of B-cell lymphoma cells (9). This suggests that RTX-IgG2 is specific in enhancing the efficacy of other RTX isotypes without contributing to adverse effects.

Here, we aim to investigate the mechanisms underlying the enhancing effect of RTX-IgG2 on phagocytosis when combined with other RTX isotypes and further explore its potential when combined with mAbs targeting other lymphoma antigens (CD59 and PD-L1). Our findings reveal, for the first time, that RTX-IgG2-mediated apoptosis is associated with a reduced and altered CD47 expression on $CD20^+$ B-cell lymphoma cells, enhancing FcR-mediated phagocytosis by tumor-specific mAbs.

2 Materials and methods

2.1 Cell cultures

The human acute monocytic leukemia cell line MonoMac-6, kindly provided by Dr. Helena Jernberg Wiklund (Department of Immunology, Genetics and Pathology (IGP), Uppsala University, Uppsala, Sweden) and authenticated by STR-profiling (Microsynth AG, Balgach, Switzerland), was used as monocytic effector cells in the ADCP assay. MonoMac-6 cells express the phagocytosis-regulating receptor FcγRII (CD32) (Supplementary Figure S1A) as well as FcγRI (CD64) (9) and display SIRP-α (Supplementary Figure S1B). MonoMac-6 cells were cultured in complete Roswell Park Memorial Institute medium (cRPMI) that contained RPMI 1640 (21875034, Thermo Fisher Scientific), 10% heat-inactivated (h.i.) fetal bovine serum (FBS) (11550356, Thermo Fisher Scientific), and 1% Penicillin-Streptomycin (PenStrep) (P4333, Merck, Darmstadt, Germany).

The CD20-expressing B-cell lymphoma cell lines Granta-519 and Raji – originating from human mantle cell lymphoma and Burkitt lymphoma, respectively – were used as tumor target cells. Granta-519 cell line was purchased from the German Collection of Microorganisms and Cell Culture (ACC 342, DMSZ, Braunschweig, Germany) and was cultured in Dulbecco's Modified Eagle Medium (DMEM) (11965092, Thermo Fisher Scientific, Waltham, MA, USA) with addition of 10% h.i. FBS and 1% PenStrep (complete DMEM; cDMEM). Raji cell line was kindly provided by Dr. Fredrik Öberg (IGP, Uppsala University), authenticated by STR-profiling at Microsynth AG, and cultured in cRPMI.

The human B-cell precursor leukemia cell line Reh, lacking expression of CD20 (Supplementary Figure S2A), was used as control cells. Reh cells were kindly provided by Dr. Ola Söderberg (Department of Pharmaceutical Biosciences, Uppsala University) and maintained in cRPMI.

All cells were cultured in suspension cell culture flasks (3910.502, Sarstedt, Nümbrecht, Germany) using a humidified cell culture incubator (InCuSafe, LabRum, Östersund, Sweden) at 37°C under 5% CO_2. The cells were routinely tested for mycoplasma contamination using MycoStrip™ detection kit (rep-mys, *In vivo*Gen, San Diego, CA, USA).

2.2 Antibodies

The human anti-CD20 (RTX) isotype family, including IgG1, IgG2, IgG3, and IgG4 anti-CD20 mAbs, was purchased from *In vivo*Gen (hcd20-mab1, hcd20-mab2, hcd20-mab3, and hcd20-mab4). Human recombinant isotype controls (kappa allotype) IgG1, IgG2, IgG3, and IgG4 were obtained from BioRad (Hercules, CA, USA) (HCA192, HCA193, HCA194, HCA195). Blocking of CD47 was performed with purified mouse anti-human CD47 mAb (αCD47-fuFc) clone CC2C6 (323102, Biolegend, San Diego, CA, USA) and humanized anti-CD47 IgG2σ mAb (αCD47-siFc) – a variant of magrolimab harboring a completely silenced Fc (23).

For cell surface staining, the following mAbs were used: APC-conjugated mouse IgG2a anti-human CD20 (clone LT20, H12155A, EuroBioScience, Friesoythe, Germany), PE-conjugated mouse IgG1 anti-human CD47 (clone CC2C6, 323108, Biolegend), PE-conjugated mouse IgG2a anti-human CD59 (clone p282 (H19), 304707, Biolegend), recombinant human IgG1 anti-human PD-L1 (hpdl1-mab1, *In vivo*Gen), APC-conjugated mouse anti-human IgG secondary Ab (αhIgG-APC) (562025, BD Biosciences, Franklin Lakes, NJ, USA), APC-conjugated mouse IgG2a anti-human SIRP-α Ab (clone 15-414, 372109, Biolegend), and FITC-conjugated mouse IgG2b anti-human CD32 Ab (clone IV.3, 60012Fl.1, StemCell Technologies, Vancouver, BC, Canada). Mouse isotype controls, including APC-conjugated IgG2a, PE-conjugated IgG1, PE-conjugated IgG2a, and FITC-conjugated IgG2b (C12386A, C12385B, C12386P, C12387F), were purchased from EuroBioScience.

2.3 Antibody-dependent cellular phagocytosis

MonoMac-6 effector cells were stained with 10 µM of CellTrace™ Far Red dye (CTFR, C34564, Thermo Fisher Scientific) in PBS (M09-9400-100, Medicago, Quebec City, QC, Canada), at 10^6 cells/mL for 20 min at 37°C. After washing with pre-warmed cRPMI (to remove excessive dye), the cells were adjusted to 7.5×10^5 cells/mL and stimulated with recombinant human interferon γ (IFNγ, PHP050, BioRad) at 0.2 µg/mL for 3 hours at 37°C. Meanwhile, Granta-519 target cells were stained with Vybrant™ CFDA SE dye (CFSE, V12883, Thermo Fisher Scientific) following manufacturer's instruction before seeding for monolayers at a cell density of 7.5×10^4 cells/100 µL per well in a round-bottomed 96-well plate (83.3925, Sarstedt). After 3 hours, MonoMac-6 cells were harvested, resuspended at 7.5×10^4 or 15×10^4 cells/100 µL per well (for an effector to target (E:T) ratio of 1:1 or 2:1, respectively), and added to the target cells for co-culturing. For the co-cultures, both cell types were resuspended in an assay medium ($cDMEM_{low\text{-}Glu}$) which contained low-glucose (1 g/L) DMEM (31885023, Thermo Fisher Scientific), 10% h.i. FBS, and 1% PenStrep. Co-cultures of effectors and target cells were immediately incubated with RTX or isotype control Abs at a concentration of 1.5 µg/mL, and kept at 37°C for 1 hour. Untreated co-cultures were used as negative controls. After 1 hour, the plate was centrifuged at 500 ×g for 3 min at 4°C and the supernatant was removed. Cells were washed twice with 250 µL of cold PBS containing 0.5% h.i. FBS (flow staining buffer). After the last washing step, cells were resuspended in 100-200 µL of cold flow staining buffer, kept on ice, and analyzed immediately using a MACSQuant VYB flow cytometer (Miltenyi Biotec, Bergisch Gladbach, Germany). Before analyzing cell samples, the flow cytometer was calibrated with MACSQuant Calibration Beads (130-093-607, Milteny Biotec) and compensation was performed using unstained and single-stained samples. A minimum of 15'000 events were acquired for each sample. $CTFR^+$ $CFSE^+$ MonoMac-6 cells were considered positive phagocytic cells.

For enhanced phagocytosis assays, target cells (7.5×10^4 cells/100 µL per well) were pre-incubated with RTX-IgG2 (1.5 µg/mL), αCD47-fuFc (1 µg/mL), or αCD47-siFc (10 µg/mL), for 30 min before addition of MonoMac-6 cells and RTX-IgG1 or RTX-IgG3 (1.5 µg/mL). In another set of experiments, the same amount of target cells per well was treated with staurosporine (STR, S1421, Selleck Chemicals, Houston, TX, USA) at 7.5 µM for 6 hours at 37°C prior to incubation with effector cells and RTX-IgG1 or RTX-IgG3 for 1 hour. Dimethyl sulfoxide (DMSO, D8418, Merck) was used to prepare the STR stock solution and thus, was used as vehicle control for these experiments.

2.4 Apoptosis assay and CD47 expression analysis

Granta-519 cells were seeded in monolayers at a cell density of 7.5×10^4 cells/100 µL per well in a round-bottomed 96-well plate prior to treatment. The cells were then incubated with 7.5 µM STR for 6 hours or 1.5 µg/mL of RTX isotypes for 30 min at 37°C. After centrifugation for 5 min at 600 ×g at 4°C, cells were washed with cold flow staining buffer, resuspended in 50 µL of flow staining buffer containing 1× LIVE/DEAD™ Fixable Violet dye (DC-Violet, L34963, Thermo Fisher Scientific) and 1× Human TruStain FcX™ (Fc Receptor Blocking Solution, 422302, Biolegend), and kept at room temperature (RT) for 10 min. Positive controls for DC-Violet were prepared by treating Granta-519 cells with 90% ethanol (20821.310, VWR, Radnor, PA, USA) for 1 min. Subsequently, PE-IgG1 anti-CD47 and PE-IgG1 isotype control Abs were added and the cells were stained for 30 min on ice. Cells were subsequently centrifuged at 600 ×g at 4°C, washed with flow staining buffer, resuspended in 100 µL of FITC-conjugated Annexin V (640906, Biolegend) prepared in 1× Annexin V binding buffer (556454, BD Biosciences), and stained for 15 min at RT. After adding 100 µL of 1× Annexin V binding buffer per well, cells were collected and analyzed using the MACSQuant VYB flow cytometer. Unstained and single-stained samples were used for compensation and gating.

A minimum of 10'000 events were acquired for each sample. DC-Violet$^+$ cells were considered necrotic cells and thus, excluded from further analyses. All DC-Violet$^-$ cells were analyzed for CD47 expression, and Annexin V$^+$ DC-Violet$^-$ Granta-519 cells were considered apoptotic cells.

2.5 Immunofluorescence staining and fluorescence microscopy

For live-cell imaging, Granta-519 and MonoMac-6 cells were prepared according to the ADCP protocol before being loaded into a flat-bottomed 96-well plate (32096, SPL Life Sciences Co., Ltd., Gyeonggi-do, Korea). Live-cell imaging was performed after 1 hour of incubation at 37°C on a fluorescence Nikon Eclipse Ti microscope (Nikon Europe B.V., Amsterdam, Netherlands) using a Plan Apo 10×/0.45 objective.

To analyze the expression of CD47, RTX- or STR-treated Granta-519 cells were washed with cold flow staining buffer and fixed with 50 µL of fixation buffer (88-8824, Thermo Fisher Scientific) for 15 min on ice. The fixed cells were washed twice with cold flow staining buffer and blocked by 1% bovine serum albumin (BSA, Fraction V, 422371X, VWR) in PBS for 1 hour. Next, the cells were incubated overnight at 4°C with 3 µg/mL of CF®640R-conjugated mouse anti-human CD47 Ab (clone B6H12.2, BNC400437-100, Biotium, Fremont, CA, USA) and 1× Hoechst 33342 Ready Flow™ Reagent (R37165, Thermo Fisher Scientific) prepared in 1% BSA in PBS. Stained cells were then washed, centrifuged, re-dispersed in 20 µL of deionized water, and added onto Superfrost plus microscope slides (J1800AMNZ, Thermo Fisher Scientific) for air-drying. Glass coverslips (#1.5, 12323148, Fisher Scientific, Hampton, NH, USA) were mounted on the microscope slides using Epredia™ Immu-Mount™ mounting medium (10662815, Fisher Scientific). Fluorescence images of mounted cells were acquired with a Zeiss LSM 700 confocal microscope (Carl Zeiss AG, Oberkochen, Germany) using a Plan-Apochromat 63×/1.4 Oil DIC M27 objective.

2.6 Data analysis

Microscope images were processed and analyzed by ZEISS ZEN lite (black edition) software (Carl Zeiss AG) or the open-source Java application ImageJ (https://imagej.nih.gov/ij/). Flow cytometry data were analyzed by FlowJo 10.9.0 software (BD Biosciences). Data were statistically analyzed with one-way ANOVA with Tukey-Kramer *post-hoc* test and visualized using GraphPad Prism 10.2.2 software (GraphPad Software, Boston, MA, USA). All results are displayed as mean ± standard error of the mean (SEM) of three independent experiments with a significance of $p<0.05$, unless indicated differently. All data were visualized by Adobe Illustrator (Adobe Inc., San Jose, CA, USA) using input files from the aforementioned software.

3 Results

3.1 ADCP induced by RTX-IgG1 or RTX-IgG3 is enhanced if combined with RTX-IgG2

The capacity of different anti-CD20 RTX isotype variants to stimulate human monocytes to phagocytose CD20$^+$ B-cell lymphoma cells varies significantly, and use of certain isotype combinations can further improve the ADCP function (9, 10). Indeed, *in vitro* ADCP analyses of human FcR-positive monocytic MonoMac-6 cells, in co-cultures with human CD20$^+$ B-cell lymphoma Granta-519 cells opsonized with different IgG isotypes of RTX, demonstrate that RTX-IgG3 is more effective than RTX-IgG1 in inducing phagocytosis (Figure 1A) (Supplementary Figures S3, S4). In contrast, RTX-IgG2 exhibits quite modest phagocytic activity (Figure 1A) (Supplementary Figure S3). However, when RTX-IgG2 is combined with either RTX-IgG1 or RTX-IgG3, it significantly enhances the ADCP response compared with RTX-IgG1 or RTX-IgG3 alone (Figures 1A, B).

As shown in Table 1, RTX-IgG1 achieves an approximately 19% increase in ADCP when combined with RTX-IgG2, while RTX-IgG3 shows an increase of about 12% when combined with RTX-IgG2. This phagocytosis-enhancing effect of RTX-IgG2 has been associated with CD20-mediated apoptosis, but the mechanisms involved remain unclear (9). To address this gap, we have delved deeper into the phagocytic enhancing effect by RTX-IgG2.

3.2 RTX-IgG2 induces significant CD20-mediated apoptosis but minor necrosis

To study the role of apoptosis in ADCP, we first optimized the concentration and treatment duration of RTX-IgG2 in relation with the apoptosis-inducing agent STR in Granta-519 cells, while minimizing necrosis. We identified that RTX-IgG2, at a concentration of 1.5 µg/mL, and STR at 7.5 µM, induced comparable levels of apoptosis (27% ± 1.7 and 26% ± 1.3, respectively), which were significantly higher than apoptosis levels observed in untreated Granta-519 cells (10% ± 1) (Figures 2A, B, Supplementary Figures S5A, D). In contrast, RTX-IgG1 and RTX-IgG3 did not induce apoptosis in the Granta-519 cells (Figures 2A, B). Notably, RTX-IgG2 was able to induce a comparable level of apoptosis as STR, but within a significantly shorter timeframe – 30 min for RTX-IgG2 versus 6 hours for STR. Moreover, RTX-IgG2-induced apoptosis was accompanied by negligible levels of necrosis compared to untreated controls (Figure 2C, Supplementary Figure S5B). Similarly, neither RTX-IgG1 nor RTX-IgG3 induced necrosis. STR induced approximately 20% more necrosis in Granta-519 cells compared to untreated controls (Figure 2C, Supplementary Figure S5E), yet the level of necrosis in STR-treated cells remained relatively low, accounting for less than 12% of the total analyzed cell population.

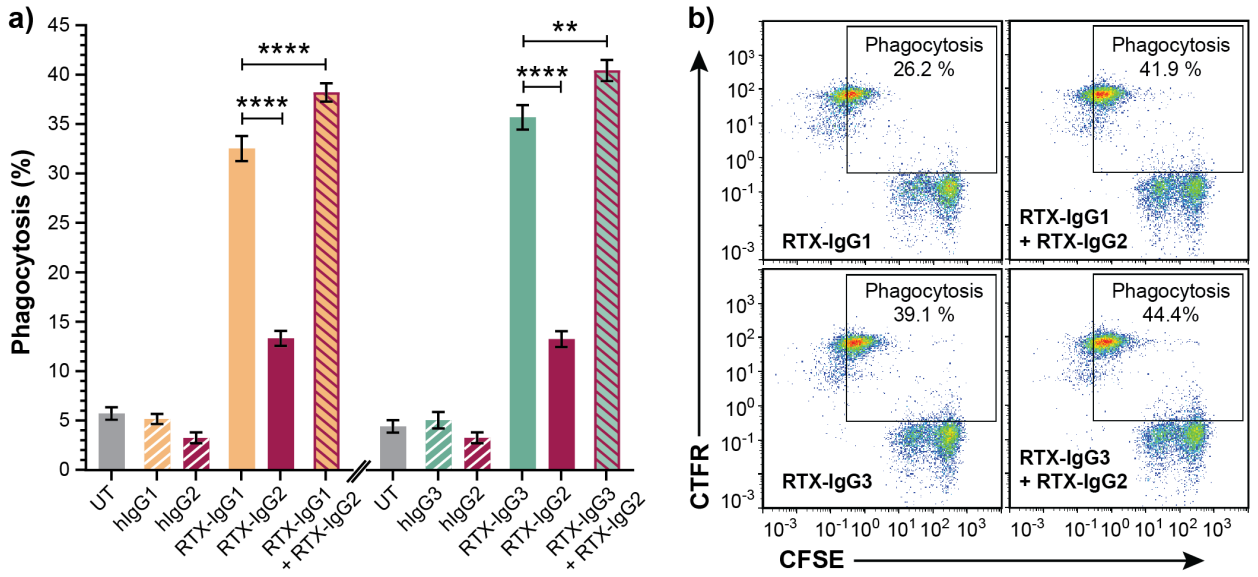

FIGURE 1
RTX-IgG2 enhances phagocytosis of RTX-IgG1- or RTX-IgG3-treated CD20$^+$ B-cell lymphoma cells. Flow cytometry analysis of ADCP of Granta-519 B-cell lymphoma cells, treated with anti-CD20 RTX isotypes or human isotype control Abs (1.5 µg/ml), by MonoMac-6 cells at an E:T ratio of 1:1. **(A)** Percentage phagocytosis of Granta-519 cells induced by single RTX isotypes, or dual combinations of RTX-IgG2 with RTX-IgG1 or RTX-IgG3. Untreated cells (UT), and human Ab isotypes: hIgG1, hIgG2, hIgG3, were used as controls. For dual treatments, Granta-519 cells were pre-opsonized with 1.5 µg/mL of RTX-IgG2 for 30 min followed by 1.5 µg/mL of RTX-IgG1 or RTX-IgG3. Results are shown as mean ± SEM of three independent experiments, each with three biological replicates. Statistical analysis by one-way ANOVA with Tukey-Kramer post-hoc test (****p<0.0001, **p<0.01). **(B)** Representative bivariate plots showing phagocytosis of RTX-treated CFSE-labeled Granta-519 target cells by CTFR-labeled MonoMac-6 effector cells. Phagocytosis was quantified as the percentage of double positive CFSE$^+$ CTFR$^+$ MonoMac-6 cells (square gate). Increased phagocytosis was observed when RTX-IgG2 was combined with RTX-IgG1 or RTX-IgG3.

TABLE 1 Summary of percentage increase in phagocytosis of CD20$^+$ B-cell lymphoma cells (Granta-519) induced by tumor-specific mAb (anti-CD20 RTX, anti-CD59, or anti-PD-L1) in combination with RTX-IgG2 or anti-CD47 mAb (where applicable) in comparison with single use of tumor-specific mAb.

Treatment	RTX-IgG1	RTX-IgG3	αCD59	αPD-L1
+RTX-IgG2	19%*	12%	44%	31%
+αCD47-fuFc	52%	28%	nd	nd
+αCD47-siFc	42%	17%	nd	nd

*Mean (%); fuFc, functional Fc domain; siFc, silenced Fc domain; nd, not determined.

Control experiments with a human CD20-negative B-cell precursor leukemia cell line (Reh) (24) further affirmed that the apoptosis induced by RTX-IgG2 was CD20-dependent as RTX-IgG2 did not induce apoptosis or necrosis in the Reh cells (Supplementary Figures S2B, C).

3.3 Apoptosis enhances FcR-mediated phagocytosis

To verify that apoptosis contributes to enhanced ADCP, we also investigated the effect of CD20-independent apoptosis, induced by STR, on ADCP mediated by RTX isotypes. Indeed, when combined with RTX-IgG1 or RTX-IgG3 treatment on Granta-519 cells, STR significantly enhanced ADCP compared to single RTX treatment (Figure 3). Unaccompanied use of STR resulted in higher ADCP of Granta-519 cells compared to untreated controls, although at inferior levels compared to anti-CD20 mAb single treatment (Figure 3).

3.4 Apoptosis enhances RTX-mediated phagocytosis by impairing "don't-eat-me" CD47 expression

The level of "don't-eat-me" anti-phagocytic CD47 protein varies on the surfaces of different B-cell lymphoma cell lines (Supplementary Figure S6A). Among the tested cell lines, Granta-519 cells expressed the highest level of CD47, implying its high resistance to ADCP (Supplementary Figure S6B). Interestingly, we discovered that apoptosis, induced by either RTX-IgG2 or STR, led to a reduction of CD47 expression in Granta-519 cells (Figures 4A, B). STR – being a very efficient apoptosis inducer – significantly reduced the expression level of CD47 to 0.55-fold of the level detected in untreated cells (Figure 4B) (Supplementary Figure S5F). Similarly, CD20-mediated apoptosis induced by RTX-IgG2 reduced the expression level of CD47 in Granta-519 cells to 0.78-fold of the level detected in untreated cells, corresponding to a 22% reduction in CD47 on the cell surface (Figure 4B, Supplementary Figure S5C).

The expression pattern of CD47 on the cell surface was further examined using confocal microscopy. As shown by Figure 4C (upper panel), CD47 was evenly distributed on the cell membrane of untreated and RTX-IgG1-treated Granta-519 cells. In contrast, RTX-IgG2- or STR-treated Granta-519 cells showed decreased

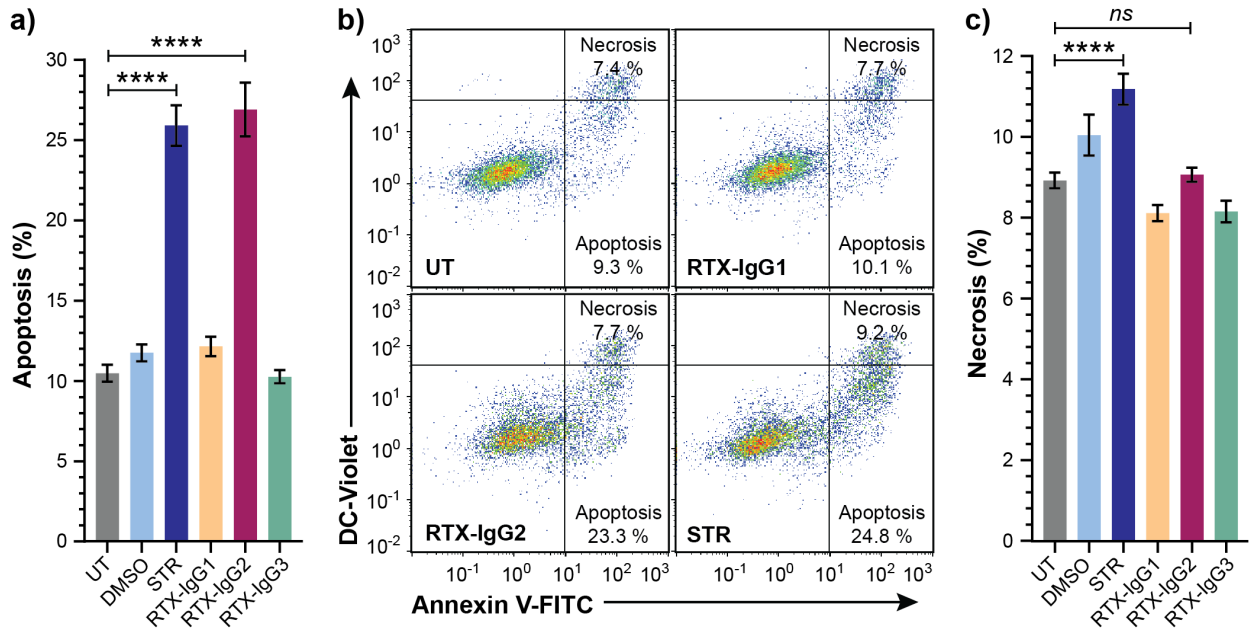

FIGURE 2
Analysis of cell death in CD20$^+$ B-cell lymphoma cells treated with STR or RTX isotypes. Granta-519 cells treated with STR (6 hours) or RTX isotypes (30 min) were analyzed for apoptosis or necrosis compared to untreated cells (UT). Dimethyl sulfoxide (DMSO) was used as vehicle control of STR treatment. **(A)** Percentage apoptosis in UT or treated Granta-519 cells. **(B)** Representative bivariate plots of Granta-519 cells, showing apoptosis and necrosis, in UT and after treatment with RTX isotypes or STR. Apoptotic cells were identified as Annexin V$^+$ DC-Violet$^-$ cells, while double positive (Annexin V$^+$ DC-Violet$^+$) cells were identified as necrotic cells with compromised cell membrane. **(C)** Percentage necrosis in UT or treated Granta-519 cells. Results in **(A, C)** show mean ± SEM of three independent experiments, each with three biological replicates. Statistical analysis by one-way ANOVA with Tukey-Kramer post-hoc test (****p<0.0001; ns, not significant).

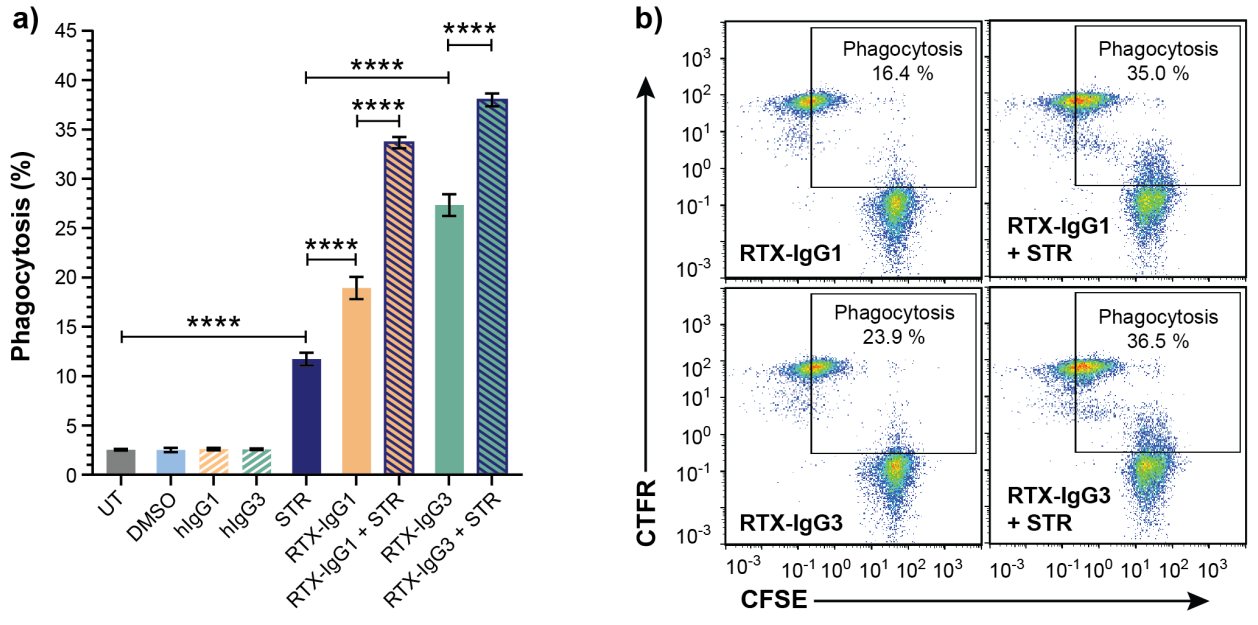

FIGURE 3
Apoptosis induced by STR in CD20$^+$ B-cell lymphoma cells enhances ADCP. Flow cytometry analysis of phagocytosis of Granta-519 cells, untreated (UT) or incubated with STR for 6 hours before addition of RTX isotypes or isotype controls (1.5 µg/mL), by MonoMac-6 cells (E:T ratio = 1:1). **(A)** Percentage phagocytosis of UT Granta-519 cells, treated with STR, RTX-IgG1 or RTX-IgG3 or combinations thereof. Results shows mean ± SEM of three independent experiments, each with three biological replicates. Statistical analysis by one-way ANOVA with Tukey-Kramer post-hoc test (****p<0.0001). **(B)** Representative bivariate plots showing phagocytosis of CFSE-labeled Granta-519 target cells, treated with RTX isotypes alone or in combination with STR. Phagocytosis was quantified as the percentage of double positive CFSE$^+$ CTFR$^+$ MonoMac-6 cells (square gate). Increased phagocytosis was observed when RTX-IgG1 or RTX-IgG3 is combined with STR.

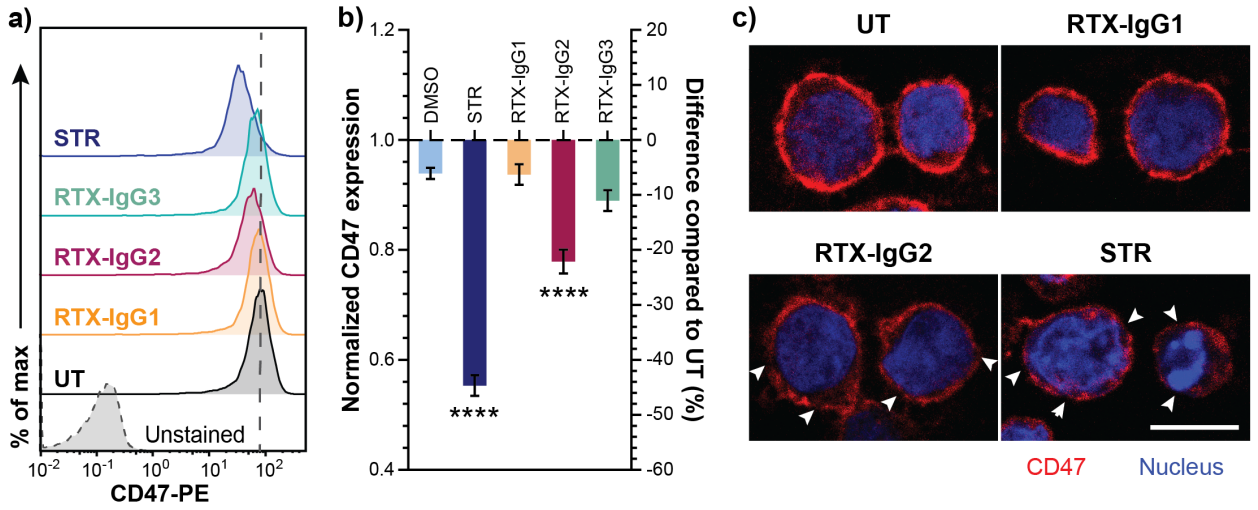

FIGURE 4
Decreased CD47 expression in RTX-IgG2-treated CD20$^+$ B-cell lymphoma cells. CD47 expression was evaluated in Granta-519 cells after incubation with STR (6 hours) or treatment with RTX isotypes (1.5 µg/mL) (30 min). **(A)** Representative histograms of CD47 expression in Granta-519 cells after treatment with RTX-IgG1, RTX-IgG2, RTX-IgG3, or STR. Grey dashed line indicates the level of CD47 on untreated cells (UT). **(B)** Bar graph representation of fold change (left Y-axis) and percentage difference (right Y-axis) in CD47 expression on Granta-519 cells induced by STR or RTX isotypes, normalized to CD47 expression on UT. To obtain the fold change values, mean fluorescence intensity (MFI) of treated samples was first adjusted by subtracting MFI of isotype controls and then normalized to the MFI of UT samples. The percentage difference was calculated by the following formula: $((MFI_{treated\ sample} - MFI_{UT})*100)/MFI_{UT}$. Results show mean fold change ± SEM of three independent experiments, each with three biological replicates. Statistical analysis by one-way ANOVA with Tukey-Kramer post-hoc test (****p<0.0001). **(C)** Confocal microscopy images of CD47 expression in untreated, RTX-IgG1-, RTX-IgG2-, and STR-treated Granta-519 cells. Cells were counterstained with Hoescht 33342 nucleus stain. Disruptions in CD47 cell surface pattern are indicated by white arrows. Scale bar: 10 µm.

CD47 expression, with CD47 redistributed into scattered clusters on the cell membrane (Figure 4C, lower panel). Remarkably, while STR and RTX-IgG2 induced similar levels of apoptosis, STR-treated cells exhibited signs of a later stage of apoptosis, such as nuclear deformation and condensed chromatin (visualized by Hoechst 33342 dye), which were absent in RTX-IgG2-treated cells (Figure 4C, lower panel).

3.5 RTX-IgG2 enhances the efficacy of other tumor-targeting mAbs in inducing ADCP of B-cell lymphoma cells

Since RTX-IgG2 was capable of altering and reducing the expression of CD47 on the target Granta-519 cells (Figure 4), we hypothesized that a pre-treatment of Granta-519 cells with RTX-IgG2 would enhance the efficacy of other tumor-targeting mAbs to induce ADCP. For this experiment, we chose two target molecules with different expression levels on Granta-519 cells – the immune checkpoint PD-L1 and the complement inhibitor CD59. As shown by Figure 5A, Granta-519 cells expressed the CD59 antigen markedly, while PD-L1 was weakly expressed (Figure 5B). When Granta-519 cells were treated with RTX-IgG2 in combination with mAbs targeting CD59 (αCD59) or PD-L1 (αPD-L1) antigens, the level of phagocytosis increased significantly compared to cells treated with αCD59 or αPD-L1 mAb alone (Figures 5C, D). Notably, the mAb targeting the highly expressed CD59 antigen mediated significant phagocytosis alone, in contrast to the mAb reactive to the low-expressing PD-L1 molecule. Correspondingly, RTX-IgG2 enhanced the phagocytic efficacy of αCD59 by 44% and of αPD-L1 by 31% (Table 1).

3.6 Blocking of CD47 enhances RTX-mediated phagocytosis

Our data suggested that the decreased levels of CD47 on the surface of Granta-519 cells, induced by RTX-IgG2 or STR, were associated with an enhancing effect on phagocytic activity by the MonoMac-6 effector cells. Therefore, in the next experiment, we used CD47-blocking mAbs, either with a functional or a silenced Fc domain, together with RTX-IgG1 or RTX-IgG3. As shown in Figure 6, blocking CD47 on the Granta-519 target cells significantly enhanced the phagocytic activity by MonoMac-6 cells. When combined with RTX-IgG1 and RTX-IgG3, the CD47-blocking Ab with a functional Fc domain (αCD47-fuFc) increased ADCP by 52% and 28%, respectively (Table 1). Meanwhile, the CD47-blocking Ab with a silenced Fc domain (αCD47-siFc) showed a modestly lower yet comparable enhancing effect on phagocytosis compared to the αCD47-fuFc, achieving an increase of 42% and 17% when combined with RTX-IgG1 and RTX-IgG3, respectively (Table 1). Notably, αCD47-fuFc alone triggered significant ADCP compared to untreated co-cultures, though at much lower level than when combined with RTX-IgG1 or RTX-IgG3 (Figure 6). The phagocytosis level induced by αCD47-fuFc (20% ± 3) was double that induced by αCD47-siFc alone (10% ± 1), underscoring the FcR-mediated phagocytosis induced by the Fc domain of the αCD47-fuFc.

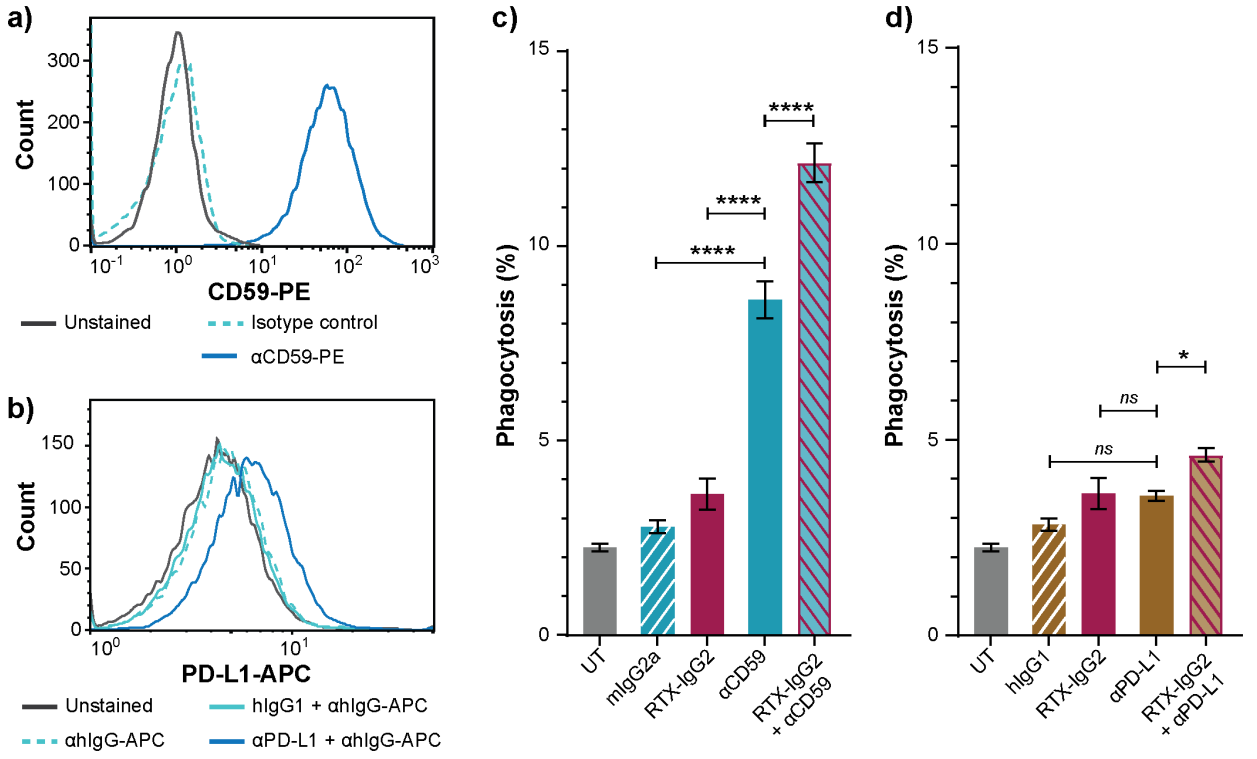

FIGURE 5
RTX-IgG2 enhances phagocytosis of CD20$^+$ B-cell lymphoma cells induced by anti-CD59 or anti-PD-L1 mAb. Representative histograms of **(A)** CD59 and **(B)** PD-L1 expression on Granta-519 cells. **(C, D)** Percentage phagocytosis of Granta-519 cells by MonoMac-6 cells (E:T ratio = 1:1), induced by c) mouse anti-human CD59 mAb (αCD59, 2.5 µg/mL) and d) human anti-PD-L1 mAb (αPD-L1, 1.5 µg/mL) alone, or in combination with a pre-treatment with RTX-IgG2. Data are presented as mean ± SEM of three independent experiments, each with three biological replicates. Statistical analysis by one-way ANOVA with Tukey-Kramer post-hoc test (****p<0.0001, *p<0.05; ns, not significant).

3.7 Lower CD20 and CD47 expression on tumor target cells diminishes the phagocytic-enhancing effect of RTX-IgG2

The effect of RTX-IgG2 was further validated on Raji B-cell lymphoma cells, which express lower levels of CD20, CD47, and CD59 compared to Granta-519 cells (Figure 7A, Supplementary Figure S6A). Notably, Raji cells demonstrated greater resistance to apoptosis, necessitating higher concentrations of STR (30 µM) and RTX-IgG2 (2.5 µg/mL) to achieve comparable levels of apoptosis and CD47 reduction as observed in Granta-519 cells treated with 7.5 µM of STR and 1.5 µg/mL of RTX-IgG2 (Figures 7B, C) (Figure 2A). The phagocytosis-enhancing effect of RTX-IgG2 on Raji cells was not observed when a higher concentration of RTX-IgG2 (2.5µg/mL) was used together with RTX-IgG1 or RTX-IgG3 (Figure 7D). However, when RTX-IgG2 was combined with a mAb targeting a non-CD20 molecule, such as CD59, enhanced phagocytosis of Raji cells was observed compared with anti-CD59 mAb alone (Figure 7E).

4 Discussion

Macrophages are the most abundant tumor-infiltrating immune cells in most human solid tumors, making them appealing therapeutic targets for cancer therapy (25, 26). However, their role as effector cells in cancer therapy remains underappreciated due to their intricate and polarized roles within the tumor microenvironment. A number of studies have associated a high content of tumor-infiltrating macrophages with unfavorable prognoses, especially in patients treated with certain chemotherapeutic agents (27–29). Conversely, macrophages have been shown to contribute significantly to the efficacy of mAb-based cancer immunotherapies through ADCP (8, 9, 30–33). In fact, macrophage infiltration has been shown to improve therapeutic responses in patients receiving a combined regimen of tumor-targeting mAb and chemotherapy (34). Additionally, monocytes – which express activating FcRs such as FcγRI (CD64) and FcγRIIa (CD32a) – have demonstrated the ability to eliminate tumor cells through ADCP as well (9–11). These lines of research necessitate further investigation on monocytes/macrophages-based cancer therapies to unlock their full anti-tumor potential.

Phagocytosis by macrophages/monocytes is mainly governed by the ubiquitously expressed “don’t-eat-me” CD47. Overexpression of CD47 has been shown to be associated with adverse prognosis in mantle cell lymphoma patients and play an important role in the dissemination of B-cell NHL (13) (35). Strategies targeting the interaction between CD47 and its receptor SIRP-α have demonstrated promising results either as monotherapies or in combination with other tumor-targeting therapies (36). However,

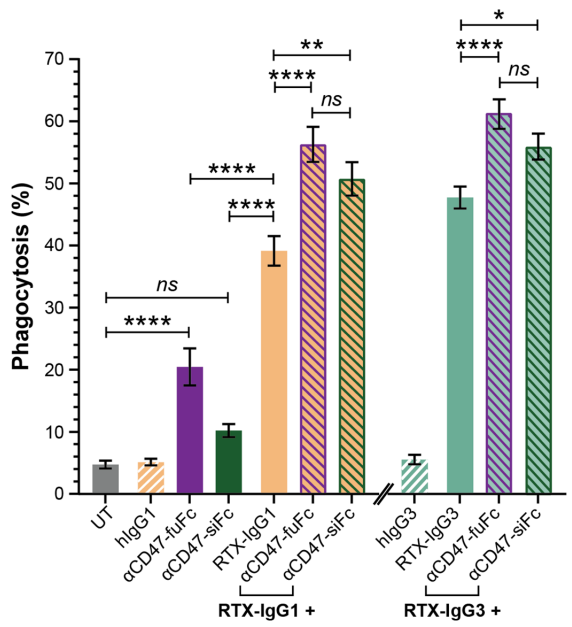

FIGURE 6
Blocking of CD47 on CD20$^+$ B-cell lymphoma cells enhances FcR-mediated ADCP. Percentage phagocytosis of Granta-519 cells treated with RTX-IgG1 or RTX-IgG3, and in combination with blocking of CD47 by mouse anti-human CD47 mAb with a functional Fc domain (αCD47-fuFc, 1 µg/mL) or humanized anti-CD47 mAb with a silenced Fc domain (αCD47-siFc, 10 µg/mL), by MonoMac-6 cells (E:T ratio = 2:1). Data are presented as mean ± SEM of three independent experiments, each with three biological replicates. Statistical analysis by one-way ANOVA with Tukey-Kramer post-hoc test (****p<0.0001, **p<0.01, *p <0.05; ns, not significant).

anti-CD47 therapies still encounter many setbacks in terms of selectivity, efficacy, and safety profile as CD47 is expressed not only on tumor cells but also on non-malignant cells.

In this study, utilizing the CD20$^+$CD47^{high} Granta-519 B-cell lymphoma cell line, we found that CD20-mediated apoptosis induced by RTX-IgG2 resulted in a reduction of CD47 expression on the Granta-519 cells. We also demonstrate that RTX-IgG2-treated lymphoma cells became significantly more susceptible to RTX-IgG1- or RTX-IgG3-mediated phagocytosis, which is consistent with our previous results (9). The apoptosis-inducer STR generated comparable levels of apoptosis as RTX-IgG2 and, similarly to RTX-IgG2, caused a reduction in CD47 expression, confirming the cause-effect relationship between apoptosis and CD47 reduction. STR also exhibited equivalent enhancing effect on phagocytosis when combined with RTX-IgG1 or RTX-IgG3. In support of our data, similar apoptosis associated decreased CD47 expression was reported by Gardai et al. (17). It is important to note that STR-induced effects are unselective and independent of CD20, resulting in high levels of background apoptosis. In contrast, RTX-IgG2 specifically targets only CD20$^+$ cells.

While apoptosis induction by RTX-IgG2 has been previously reported, its exact mechanism remains incompletely understood (9, 37). Compared to RTX-IgG1, RTX-IgG2 induces similar level of homotypic adhesion (Supplementary Figure S4), while exhibiting a substantially reduced ability to induce ADCP and CDC (6, 9, 37). In fact, RTX-IgG2 binds CD20$^+$ B-cell lymphoma cells at only half the density of RTX-IgG1 and RTX-IgG3 (Supplementary Figure S7) (37), but induces significantly more apoptosis in these cells (9, 37). For these reasons, we propose that RTX-IgG2, although binding to the same CD20 epitope as RTX-IgG1, attaches in different binding modes and geometries, in support of the hypothesis by Konitzer et al. (37). Among all IgG isotypes, IgG2 possesses the most rigid hinge region and unique alternative covalent links between its Fab domains and the hinge (38, 39). Given the significant differences in the hinge region of IgG2, it is reasonable to speculate that these distinct structural features may affect its binding geometry to target receptor (37, 40–42). Indeed, recent studies have correlated the rigidity of the IgG2 hinge with agonistic function (40, 43, 44), suggesting that mAbs of the IgG2 isotype can elicit agonistic activity upon target binding by closely crosslinking target receptors, thereby promoting downstream signaling (40–45). Based on these literature, here, we attribute the apoptosis-inducing ability of RTX-IgG2 to its unique hinge structure and the resulted agonistic activity.

To our knowledge, our experiment is the first that associates RTX-IgG2-mediated apoptosis with a reduced CD47 expression and an enhancing effect on phagocytosis. We also reveal with microscopic analysis that the pattern of CD47 expression on the surface of RTX-IgG2-treated cells shifts from a homogeneous distribution to a more clustered arrangement. A similar change in spatial distribution of CD47 has previously been reported in aged mouse erythrocytes and human Jurkat T-cells (17, 20). These studies, together with our observation, suggest that apoptosis trigger major structural alterations of the cell plasma membrane, which may either destabilize lateral molecular interactions needed for the proper CD47 "don't-eat-me" signaling (17, 20) or induce conformation changes of CD47, hindering its interaction with SIRP-α (46).

Based on these findings, we hypothesized that pre-treatment with the agonistic RTX-IgG2 – which reduces the anti-phagocytic CD47 on the surface of target cells – could enhance the phagocytic efficacy of other tumor-targeting mAbs. Indeed, RTX-IgG2 pre-treatment significantly increased the phagocytosis of Granta-519 cells when combined with anti-CD59 or anti-PD-L1 mAbs. Importantly, a higher expression level of the target molecules correlated with a higher level of enhanced phagocytosis, as demonstrated by CD59. Notably, targeting of low-expressing tumor antigens, such as PD-L1 on Granta-519 cells, can still be enhanced by RTX-IgG2. The efficacy of RTX-IgG2 as a phagocytic enhancer improves when it does not need to compete with mAbs targeting the same antigen/epitope (CD20). Indeed, similar CD47-reducing and phagocytosis-enhancing effects by RTX-IgG2 were also evident in CD47^{low} Raji cells when RTX-IgG2 was combined with anti-CD59 mAbs, but not with RTX-IgG1 or RTX-IgG3.

Collectively, our results highlight the role of RTX-IgG2 as an exclusive and target-specific enhancer for FcR-mediated phagocytosis of CD20$^+$ B-cell lymphoma cells, an effect associated with induction of apoptosis and reduction of CD47 on target cells.

Considering that the downregulation of CD47 is essential in driving the ADCP enhancement by RTX-IgG2, we conducted a

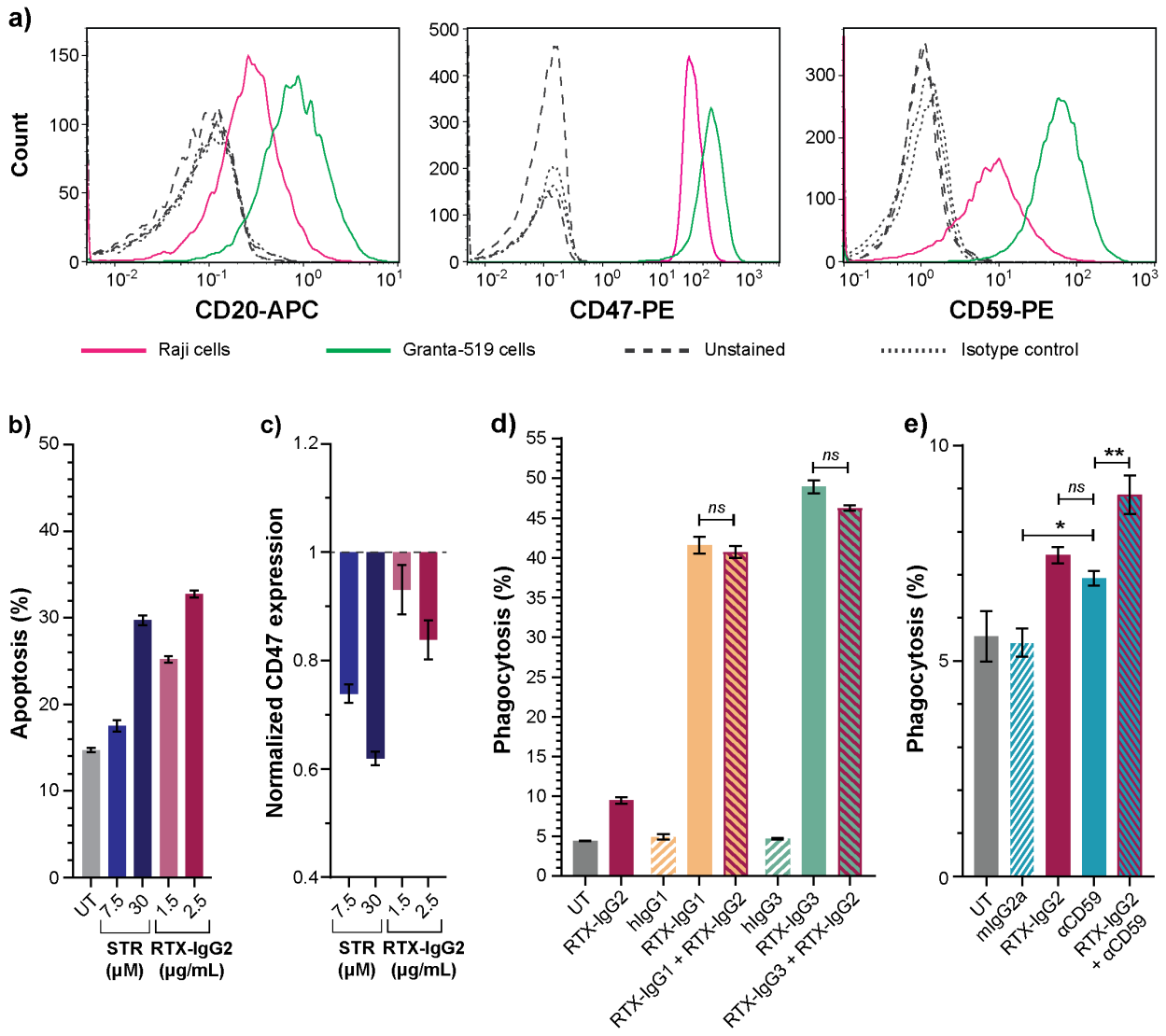

FIGURE 7
Effects of RTX-IgG2 on Raji B-cell lymphoma cells. **(A)** Representative histograms of CD20, CD47, and CD59 expression on Raji and Granta-519 B-cell lymphoma cells. **(B)** Percentage apoptosis in untreated (UT) and STR- or RTX-IgG2-treated Raji cells. **(C)** Fold change in CD47 expression on Raji cells induced by STR or RTX-IgG2, normalized to CD47 expression on untreated cells (UT). **(D)** Percentage phagocytosis of Raji cells by MonoMac-6 cells (E:T ratio = 1:1), induced by single RTX isotypes, or dual combinations of RTX-IgG2 with RTX-IgG1 or RTX-IgG3. Untreated cells (UT), and human Ab isotypes (hIgG1, hIgG2, hIgG3) were used as controls. For dual treatments, Raji cells were pre-opsonized with 2.5 μg/mL of RTX-IgG2 for 30 min followed by 1.5 μg/mL of RTX-IgG1 or RTX-IgG3. **(E)** Percentage phagocytosis of Raji cells by MonoMac-6 cells (E:T ratio = 1:1), induced by mouse anti-human CD59 mAb (αCD59, 2.5 μg/mL) alone, or in combination with a pre-treatment with RTX-IgG2. Results in **(B-E)** are shown as mean ± SEM of three biological replicates from one representative experiment out of two. Statistical analysis by one-way ANOVA with Tukey-Kramer post-hoc test (**p<0.01, *p<0.05; ns, not significant).

CD47-blocking experiment to further validate our findings. For this experiment, we used two different versions of CD47-blocking mAbs: a commercially available mouse IgG2a anti-human CD47 Ab (αCD47-fuFc) and an engineered humanized IgG2 anti-CD47 Ab harboring a completely silenced Fc domain (αCD47-siFc) (23). Both CD47-blocking mAbs effectively enhanced the phagocytic uptake of Granta-519 cells by MonoMac-6 cells when combined with RTX-IgG1 or RTX-IgG3 (Table 1). However, αCD47-fuFc alone exerted notable Fc-mediated phagocytosis, suggesting potential on-target, off-tumor effects. The pronounced phagocytosis induced by αCD47-fuFc was likely mediated by its functional Fc domain, complicating the assessment of whether a synergistic effect between this Ab and RTX-IgG1 and RTX-IgG3 was achieved. In contrast, the αCD47-siFc alone induced negligible phagocytosis, indicating effective abrogation of undesired Fc-mediated engagement. This experiment conclusively confirmed that blocking CD47 can synergistically enhance RTX-mediated phagocytosis, provided that the CD47-blocking mAb is carefully designed to avoid undesired Fc receptor engagement on effectors cells and consequent toxicity. As agonistic activity of IgG2 mAbs

has been demonstrated to occur independently of FcγR engagement (41), further utilization of αCD47-siFc warrants comprehensive analyses of its potential agonistic effects.

In conclusion, our *in vitro* studies show that RTX-IgG2, in combination with tumor-targeting mAbs, enhances ADCP of $CD20^+$ B-cell lymphoma cells via CD20-mediated apoptosis and CD47 reduction. This suggests that RTX-IgG2 could serve as a valuable agonist for B-cell NHL therapy and additionally be used to improve efficacy of RTX treatment of other B-cell disorders. Developing tumor-specific IgG2 mAbs with apoptotic capacity presents a promising approach to enhance antibody-based immunotherapy. To improve clinical relevance, future studies should incorporate three-dimensional human B-cell lymphoma models or xenograft mouse models to better assess therapeutic efficacy.

Data availability statement

The raw data supporting the conclusions of this article will be made available by the authors, without undue reservation.

Ethics statement

Ethical approval was not required for the studies on humans in accordance with the local legislation and institutional requirements because only commercially available established cell lines were used.

Author contributions

ON: Writing – original draft, Writing – review & editing, Data curation, Formal analysis, Investigation, Methodology, Validation, Visualization. SL: Writing – review & editing. GF: Writing – review & editing. MP: Writing – review & editing. SK: Conceptualization, Funding acquisition, Methodology, Project administration, Resources, Supervision, Writing – review & editing.

Funding

The author(s) declare financial support was received for the research, authorship, and/or publication of this article. This work was financially supported by Uppsala University.

Acknowledgments

The authors thank the staff at the BioVis facility, especially Jeremy Adler (Rudbeck Laboratory, Uppsala University, Uppsala, Sweden), and Inkyung Jang (Department of Cell and Molecular Biology, Uppsala University) for technical support.

Conflict of interest

The authors declare that the research was conducted in the absence of any commercial or financial relationships that could be construed as a potential conflict of interest.

Publisher's note

Supplementary material

The Supplementary Material for this article can be found online at: https://www.frontiersin.org/articles/10.3389/fimmu.2024.1483617/full#supplementary-material

References

1. Sun HF, Xue L, Guo YH, Du JQ, Nan KJ, Li M. Global, regional and national burden of non-Hodgkin lymphoma from 1990 to 2017: estimates from global burden of disease study in 2017. *Ann Med.* (2022) 54:633–45. doi: 10.1080/07853890.2022.2039957

2. O'Connor OA, Tobinai K. Putting the clinical and biological heterogeneity of non-Hodgkin lymphoma into context. *Clin Cancer Res.* (2014) 20:5173–81. doi: 10.1158/1078-0432.Ccr-14-0574

3. Smith MR. Rituximab (monoclonal anti-CD20 antibody): mechanisms of action and resistance. *Oncogene.* (2003) 22:7359–68. doi: 10.1038/sj.onc.1206939

4. Pierpont TM, Limper CB, Richards KL. Past, present, and future of rituximab - the world's first oncology monoclonal antibody therapy. *Front Oncol.* (2018) 8:163. doi: 10.3389/fonc.2018.00163

5. Johnson P, Glennie M. The mechanisms of action of rituximab in the elimination of tumor cells. *Semin Oncol.* (2003) 30:3–8. doi: 10.1053/sonc.2003.50025

6. Glennie MJ, French RR, Cragg MS, Taylor RP. Mechanisms of killing by anti-CD20 monoclonal antibodies. *Mol Immunol.* (2007) 44:3823–37. doi: 10.1016/j.molimm.2007.06.151

7. Boross P, Leusen JHW. Mechanisms of action of CD20 antibodies. *Am J Cancer Res.* (2012) 2:676–90.

8. Lefebvre ML, Krause SW, Salcedo M, Nardin A. Ex vivo-activated human macrophages kill chronic lymphocytic leukemia cells in the presence of rituximab: mechanism of antibody-dependent cellular cytotoxicity and impact of human serum. *J Immunother.* (2006) 29:388–97. doi: 10.1097/01.cji.0000203081.43235.d7

9. Lara S, Anania JC, Virtanen A, Stenhammar V, Kleinau S. Importance of antibody isotypes in antitumor immunity by monocytes and complement using human-immune tumor models. *Eur J Immunol.* (2021) 51:1218–33. doi: 10.1002/eji.202048885

10. Kleinau S. Impact of Fc receptors and host characteristics on myeloid phagocytic response to rituximab-treated 3D-cultured B-cell lymphoma. *Immunother Adv.* (2023) 3. doi: 10.1093/immadv/ltad025

11. Uchida JJ, Hamaguchi Y, Oliver JA, Ravetch JV, Poe JC, Haas KM, et al. The innate mononuclear phagocyte network depletes B lymphocytes through Fc receptor-dependent mechanisms during anti-CD20 antibody immunotherapy. *J Exp Med.* (2004) 199:1659–69. doi: 10.1084/jem.20040119

12. Minard-Colin V, Xiu Y, Poe JC, Horikawa M, Magro CM, Hamaguchi Y, et al. Lymphoma depletion during CD20 immunotherapy in mice is mediated by macrophage FcγRI, FcγRIII, and FcγRIV. *Blood.* (2008) 112:1205–13. doi: 10.1182/blood-2008-01-135160

13. Chao MP, Alizadeh AA, Tang C, Myklebust JH, Varghese B, Gill S, et al. Anti-CD47 antibody synergizes with rituximab to promote phagocytosis and eradicate non-Hodgkin lymphoma. *Cell*. (2010) 142:699–713. doi: 10.1016/j.cell.2010.07.044

14. Brown EJ, Frazier WA. Integrin-associated protein (CD47) and its ligands. *Trends Cell Biol*. (2001) 11:130–5. doi: 10.1016/S0962-8924(00)01906-1

15. Bouwstra R, van Meerten T, Bremer E. CD47-SIRPα blocking-based immunotherapy: Current and prospective therapeutic strategies. *Clin Transl Med*. (2022) 12:e943. doi: 10.1002/ctm2.943

16. Russ A, Hua AB, Montfort WR, Rahman B, Bin Riaz I, Khalid MU, et al. Blocking "don't eat me" signal of CD47-SIRPα in hematological Malignancies, an in-depth review. *Blood Rev*. (2018) 32:480–9. doi: 10.1016/j.blre.2018.04.005

17. Gardai SJ, McPhillips KA, Frasch SC, Janssen WJ, Starefeldt A, Murphy-Ullrich JE, et al. Cell-surface calreticulin initiates clearance of viable or apoptotic cells through trans-activation of LRP on the phagocyte. *Cell*. (2005) 123:321–34. doi: 10.1016/j.cell.2005.08.032

18. Lv Z, Bian Z, Shi L, Niu S, Ha B, Tremblay A, et al. Loss of cell surface CD47 clustering formation and binding avidity to SIRPα Facilitate apoptotic cell clearance by macrophages. *J Immunol*. (2015) 195:661–71. doi: 10.4049/jimmunol.1401719

19. Burger P, Hilarius-Stokman P, de Korte D, van den Berg TK, van Bruggen R. CD47 functions as a molecular switch for erythrocyte phagocytosis. *Blood*. (2012) 119:5512–21. doi: 10.1182/blood-2011-10-386805

20. Wang F, Liu YH, Zhang T, Gao J, Xu Y, Xie GY, et al. Aging-associated changes in CD47 arrangement and interaction with thrombospondin-1 on red blood cells visualized by super-resolution imaging. *Aging Cell*. (2020) 19:e13224. doi: 10.1111/acel.13224

21. Métayer LE, Vilalta A, Burke GAA, Brown GC. Anti-CD47 antibodies induce phagocytosis of live, Malignant B cells by macrophages via the Fc domain, resulting in cell death by phagoptosis. *Oncotarget*. (2017) 8:60892–903. doi: 10.18632/oncotarget.18492

22. Abrisqueta P, Sancho JM, Cordoba R, Persky DO, Andreadis C, Huntington SF, et al. Anti-CD47 antibody, CC-90002, in combination with rituximab in subjects with relapsed and/or refractory non-Hodgkin lymphoma (R/R NHL). *Blood*. (2019) 134 (Supplement_1):4089. doi: 10.1182/blood-2019-125310

23. Zeller T, Lutz S, Münnich IA, Windisch R, Hilger P, Herold T, et al. Dual checkpoint blockade of CD47 and LILRB1 enhances CD20 antibody-dependent phagocytosis of lymphoma cells by macrophages. *Front Immunol*. (2022) 13:929339. doi: 10.3389/fimmu.2022.929339

24. Schneider D, Xiong Y, Wu D, Nölle V, Schmitz S, Haso W, et al. A tandem CD19/CD20 CAR lentiviral vector drives on-target and off-target antigen modulation in leukemia cell lines. *J Immunother Cancer*. (2017) 5:42. doi: 10.1186/s40425-017-0246-1

25. Liu Y, Wang YJ, Yang YR, Weng LJ, Wu Q, Zhang J, et al. Emerging phagocytosis checkpoints in cancer immunotherapy. *Signal Transduct Tar*. (2023) 8:104. doi: 10.1038/s41392-023-01365-z

26. Gentles AJ, Newman AM, Liu CL, Bratman SV, Feng WG, Kim D, et al. The prognostic landscape of genes and infiltrating immune cells across human cancers. *Nat Med*. (2015) 21:938–45. doi: 10.1038/nm.3909

27. Farinha P, Masoudi H, Skinnider BF, Shumansky K, Spinelli JJ, Gill K, et al. Analysis of multiple biomarkers, shows that lymphoma-associated macrophage (LAM) content is an independent predictor of survival in follicular lymphoma (FL). *Blood*. (2005) 106:2169–74. doi: 10.1182/blood-2005-04-1565

28. Steidl C, Lee T, Shah SP, Farinha P, Han G, Nayar T, et al. Tumor-associated macrophages and survival in classic Hodgkin's lymphoma. *New Engl J Med*. (2010) 362:875–85. doi: 10.1056/NEJMoa0905680

29. Mantovani A, Allavena P, Marchesi F, Garlanda C. Macrophages as tools and targets in cancer therapy. *Nat Rev Drug Discovery*. (2022) 21:799–820. doi: 10.1038/s41573-022-00520-5

30. Oflazoglu E, Stone IJ, Gordon KA, Grewal IS, van Rooijen N, Law CL, et al. Macrophages contribute to the antitumor activity of the anti-CD30 antibody SGN-30. *Blood*. (2007) 110:4370–2. doi: 10.1182/blood-2007-06-097014

31. Oflazoglu E, Stone IJ, Brown L, Gordon KA, van Rooijen N, Jonas M, et al. Macrophages and Fc-receptor interactions contribute to the antitumour activities of the anti-CD40 antibody SGN-40. *Brit J Cancer*. (2009) 100:113–7. doi: 10.1038/sj.bjc.6604812

32. Watanabe M, Wallace PK, Keler T, Deo YM, Akewanlop C, Hayes DF. Antibody dependent cellular phagocytosis (ADCP) and antibody dependent cellular cytotoxicity (ADCC) of breast cancer cells mediated by bispecific antibody, MDX-210. *Breast Cancer Res Tr*. (1999) 53:199–207. doi: 10.1023/A:1006145507567

33. Weiskopf K, Weissman IL. Macrophages are critical effectors of antibody therapies for cancer. *MAbs*. (2015) 7:303–10. doi: 10.1080/19420862.2015.1011450

34. Taskinen M, Karjalainen-Lindsberg ML, Nyman H, Eerola LM, Leppä S. A high tumor-associated macrophage content predicts favorable outcome in follicular lymphoma patients treated with rituximab and cyclophosphamide-doxorubicin-vincristine-prednisone. *Clin Cancer Res*. (2007) 13:5784–9. doi: 10.1158/1078-0432.Ccr-07-0778

35. Chao MP, Tang C, Pachynski RK, Chin R, Majeti R, Weissman IL. Extranodal dissemination of non-Hodgkin lymphoma requires CD47 and is inhibited by anti-CD47 antibody therapy. *Blood*. (2011) 118:4890–901. doi: 10.1182/blood-2011-02-338020

36. Eladl E, Tremblay-LeMay R, Rastgoo N, Musani R, Chen WM, Liu AJ, et al. Role of CD47 in hematological Malignancies. *J Hematol Oncol*. (2020) 13:96. doi: 10.1186/s13045-020-00930-1

37. Konitzer JD, Sieron A, Wacker A, Enenkel B. Reformatting rituximab into human IgG2 and IgG4 isotypes dramatically improves apoptosis induction *in vitro*. *PloS One*. (2015) 10. doi: 10.1371/journal.pone.0145633

38. Roux KH, Strelets L, Michaelsen TE. Flexibility of human IgG subclasses. *J Immunol*. (1997) 159:3372–82. doi: 10.4049/jimmunol.159.7.3372

39. Wypych J, Li M, Guo A, Zhang ZQ, Martinez T, Allen MJ, et al. Human IgG2 antibodies display disulfide-mediated structural isoforms. *J Biol Chem*. (2008) 283:16194–205. doi: 10.1074/jbc.M709987200

40. Yu XJ, Chan HTC, Fisher H, Penfold CA, Kim J, Inzhelevskaya T, et al. Isotype switching converts anti-CD40 antagonism to agonism to elicit potent antitumor activity. *Cancer Cell*. (2020) 37:850–66. doi: 10.1016/j.ccell.2020.04.013

41. White AL, Chan HTC, French RR, Willoughby J, Mockridge CI, Roghanian A, et al. Conformation of the human immunoglobulin G2 hinge imparts superagonistic properties to immunostimulatory anticancer antibodies. *Cancer Cell*. (2015) 27:138–48. doi: 10.1016/j.ccell.2014.11.001

42. Orr CM, Fisher H, Yu XJ, Chan CHT, Gao YY, Duriez PJ, et al. Hinge disulfides in human IgG2 CD40 antibodies modulate receptor signaling by regulation of conformation and flexibility. *Sci Immunol*. (2022) 7:eabm3723. doi: 10.1126/sciimmunol.abm3723

43. Liu XB, Zhao YJ, Shi H, Zhang Y, Yin XY, Liu MD, et al. Human immunoglobulin G hinge regulates agonistic anti-CD40 immunostimulatory and antitumour activities through biophysical flexibility. *Nat Commun*. (2019) 10:10. doi: 10.1038/s41467-019-12097-6

44. Allen MJ, Guo A, Martinez T, Han M, Flynn GC, Wypych J, et al. Interchain disulfide bonding in human IgG2 antibodies probed by site-directed mutagenesis. *Biochemistry-Us*. (2009) 48:3755–66. doi: 10.1021/bi8022174

45. Yu XJ, James S, Felce JH, Kellermayer B, Johnston DA, Chan HTC, et al. TNF receptor agonists induce distinct receptor clusters to mediate differential agonistic activity. *Commun Biol*. (2021) 4:772. doi: 10.1038/s42003-021-02309-5

46. Dufour S, Tacnet-Delorme P, Kleman JP, Glushonkov O, Thielens N, Bourgeois D, et al. Nanoscale imaging of CD47 informs how plasma membrane modifications shape apoptotic cell recognition. *Commun Biol*. (2023) 6:207. doi: 10.1038/s42003-023-04558-y

frontiers | Frontiers in Immunology

TYPE Case Report
PUBLISHED 09 December 2024
DOI 10.3389/fimmu.2024.1497736

OPEN ACCESS

EDITED BY
Penny Fang,
University of Texas MD Anderson Cancer Center, United States

REVIEWED BY
Jichang Han,
Washington University in St. Louis, United States
Huiting Qu,
Shandong Provincial Hospital, China

*CORRESPONDENCE
Runhui Zheng
zhengrunhui@gzhmu.edu.cn
Peng Li
li_peng@gibh.ac.cn

†These authors have contributed equally to this work

RECEIVED 17 September 2024
ACCEPTED 20 November 2024
PUBLISHED 09 December 2024

CITATION
Luo X, Chen A, Qin L, Weinkove R, Zhao R, Ye T, Chen S, Tang J, Liu J, Huang J, Shi B, Yuan D, Tan H, Qin D, Tang Z, Li P and Zheng R (2024) Case report: A novel third-generation anti-CD19/CD22 CAR T-cells combined with auto-HSCT for relapsed Burkitt lymphoma. *Front. Immunol.* 15:1497736. doi: 10.3389/fimmu.2024.1497736

Case report: A novel third-generation anti-CD19/CD22 CAR T-cells combined with auto-HSCT for relapsed Burkitt lymphoma

Xiaodan Luo[1†], Ao Chen[1†], Le Qin[2], Robert Weinkove[3], Rong Zhao[1], Ting Ye[1], Sihui Chen[1], Jianli Tang[1], Jianbo Liu[1], Jiayu Huang[1], Boyun Shi[1], Danyun Yuan[1], Huo Tan[1], Dajiang Qin[1], Zhaoyang Tang[4], Peng Li[2*] and Runhui Zheng[1*]

[1]The Fifth Affiliated Hospital, Guangzhou Medical University, Guangzhou, China, [2]China-New Zealand Joint Laboratory on Biomedicine and Health, Key Laboratory of Immune Response and Immunotherapy, Guangdong Provincial Key Laboratory of Stem Cell and Regenerative Medicine, GIBH-HKU Guangdong-Hong Kong Stem Cell and Regenerative Medicine Research Centre, GIBH-CUHK Joint Research Laboratory on Stem Cell and Regenerative Medicine, Institute of Drug Discovery, Guangzhou Institutes of Biomedicine and Health, Chinese Academy of Sciences, Guangzhou, China, [3]Cancer Immunotherapy Program, Malaghan Institute of Medical Research, Wellington, New Zealand, [4]Department of Automation, Tsinghua University, Beijing, China

This study explores a novel therapeutic strategy for relapsed/refractory (R/R) Burkitt lymphoma (BL) by integrating autologous hematopoietic stem cell transplantation (ASCT) with tandem anti-CD19/CD22 chimeric antigen receptor (CAR) T cell therapy. A 20-year-old Asian male with refractory BL, whose lymphoma had not responded to multiple chemoimmunotherapy regimens, received myeloablative ASCT followed three days later by infusion of a novel third-generation CAR T cells engineered with CD28 and CD3ζ signaling domains, along with a TLR2 costimulatory domain. This resulted in sustained complete remission at the 306-day follow-up, without experiencing any severe complications. This case suggests that combining myeloablative ASCT with tandem anti-CD19/CD22 CAR T cell therapy could be an effective approach for R/R BL, warranting further clinical validation.

KEYWORDS

relapsed/refractory Burkitt lymphoma, CAR T-cell therapy, autologous hematopoietic stem cell transplantation, CD19/CD22 dual target, immunotherapy

Introduction

Burkitt lymphoma (BL) is a highly aggressive B-cell non-Hodgkin lymphoma. Although responses to first-line therapy are high, relapsed or refractory (R/R) BL, carries a dismal prognosis with a median survival < 3 months, and fewer than 5% of patients surviving longer than two years (1). The few durable remissions reported for relapsed

Burkitt lymphoma employ chemoimmunotherapy followed by autologous or allogeneic stem cell transplantation (2).

Chimeric antigen receptor (CAR) T-cell therapies directed against the B-cell antigen CD19 have been widely used as a salvage approach for R/R CD19$^+$ acute lymphoblastic leukemia. Patients with BL were excluded from key lymphoma CAR T-cell registration trials, however, likely owing to the challenges that very rapid tumor growth presents to successful CAR T-cell manufacture and delivery. A lack of response to, or relapse following, CD19-directed CAR T-cell therapy for large cell lymphoma is common, due in part to downregulation of CD19 on tumor cells (3, 4). While subsequent treatment with CAR-T cells targeting the alternative B-cell antigen CD22 can result in clinical responses, these responses are often brief (5, 6). The disappointing results of single-targeting CAR-T cells in challenging disease settings have paved the way for the development of CAR-T cell therapies with specificity for two or more antigens (7–9). Liu, et al. sequentially infused CAR-T cells targeting CD19, CD22, and CD20 to 23 children with R/R BL, achieving a complete remission (CR) rate of 91% (10). However, this strategy requires manufacture of multiple CAR T-cell products. Another strategy is to combine multiple antigen specificities within a single CAR construct. We developed third-generation tandem anti-CD19/CD22 CAR T-cells employing CD28 and CD3 zeta (CD3ζ) intracellular signaling domains with a novel TLR2 costimulatory domain. Here, we report a case of successful treatment of an adult with R/R BL using myeloablative auto-HSCT followed by this new CAR T-cell therapy.

Case presentation

We developed a novel tandem CAR, termed 192228zT2. This CAR incorporates humanized single-chain variable fragments (scFv) targeting both CD19 and CD22 extracellularly, and intracellularly incorporates a CD28 costimulatory domain, a Toll-like receptor 2 intracellular domain that is known to enhance the antitumor efficacy and migratory capacity of CAR-T cells (11–13), and a CD3ζmotif. The project was approved by the ethics committee of Guangzhou Medical University (GYWY-G2024-02), and the patient gave informed consent. The 192228zT2 cells were manufactured at the Good Manufacturing Practice (GMP) facility of Guangdong Zhaotai Cell Biology Technology Ltd. Briefly, T cells were isolated from peripheral blood mononuclear cells (PBMCs) using CliniMACS CD4 and CD8 reagents (Miltenyi Biotec). These cells were activated with MACS GMP T Cell Transact (Miltenyi Biotec). Subsequently, cells were transduced using a lentiviral vector encoding the 192228zT2 CAR, and the transduction efficiency was measured through protein L staining (Figure 1A). CAR T-cells were expanded in the presence of recombinant human IL-2 and harvested once the cell quantity met dosage requirements. *In vitro* killing assays demonstrated the efficient lysis of CD19-overexpressing K562 cells (K562-CD19GL) and CD22-overexpressing K562 cells (K562-CD22GL) by 192228zT2 T cells (Figures 1B, C), indicating the function of both anti-CD19 and anti-CD22 single-chain variable fragments (scFvs). Furthermore, 192228zT2 T cells exhibited effective killing of the human B-cell acute lymphoblastic leukemia (B-ALL) cell line, NALM6-GL, which expresses both CD19 and CD22 (Figure 1D).

A 20-year-old Asian male had been diagnosed with stage 3B BL, presenting with abdominal and pelvis lymphadenopathy. The patient was HIV-negative at diagnosis, and the tumor tissue was positive for the t (8, 14) IGH/MYC translocation with a proliferation index (Ki67) of 95%. Tumor cells were negative for Epstein-Barr virus-encoded RNA (EBER) and next-generation sequencing (NGS) of lymphoma-related genes indicated a class I mutation of TP53 p.E258fs. A first cycle of R-CODOX-M/R-IVAC (R-CODOX-M: rituximab, cyclophosphamide, vincristine, doxorubicin and methotrexate; R-IVAC: rituximab, ifosfamide, etoposide and cytarabine), resulted in complete metabolic response on (18)F-FDG PET/CT (Deauville 5-point score 2). Following two more cycles, CD34$^+$ cells (10.86 × 10^6/kg) were harvested in preparation for a future auto-HSCT. However, a repeat PET/CT showed disease progression in the ileocecal mesenteric region. Right hemicolectomy was followed by one cycle of R-GDP (rituximab, gemcitabine, cisplatin and dexamethasone) and a cycle of a combination treatment comprising an anti-PD-1 antibody, demethylating agent, histone deacetylase inhibitor and Bruton tyrosine kinase (BTK) inhibitor, but disease continued to

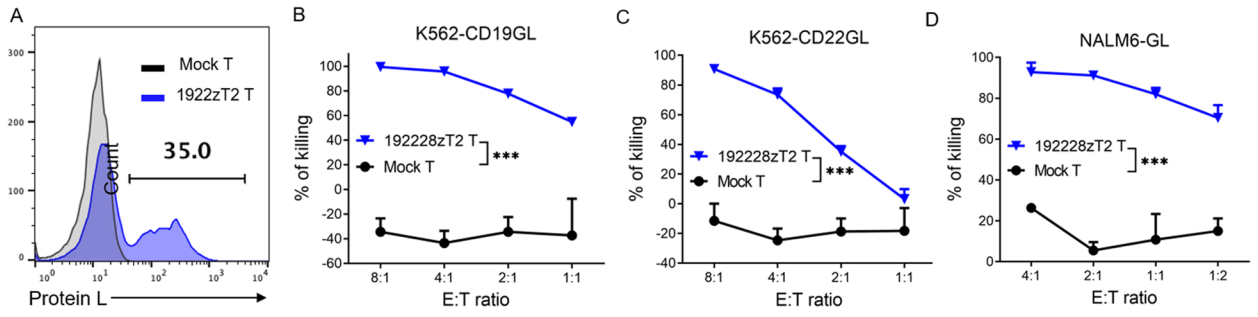

FIGURE 1
(A) The transduction efficiency of 1922zT2 T cells. **(B–D)**. The cytotoxicity activity of 1922zT2 T and mock T cells against CD19+ K562-CD19GL **(B)**, CD22$^+$ K562-CD22GL **(C)** and CD19$^+$CD22$^+$ NALM6-GL **(D)** target cells *in vitro*. ALL target cells expressed GFP and Luciferase (GL). Data are presented as mean ± SD. *p* Values of B, C and D were calculated by two-way ANOVA with Tukey's multiple comparisons test. ***$p < 0.001$.

progress, with multiple new lesions in the mesentery and pelvic peritoneum. Re-biopsy of enlarged pericolic lymph nodes confirmed refractory BL and indicated partial CD19 expression (in 50% of tumor cells) and uniform expression of CD22 (in 100% of tumor cells). A decision was made to treat with 192228zT2 CAR T-cell therapy followed by auto-SCT. Time-line of disease evolution and therapeutic interventions were shown in Figure 2A. PET/CT images at different time points were shown in Figure 2B.

After successful 192228zT2 T manufacture, the patient received a myeloablative R-TEAM (rituximab, thiotepa, etoposide, cytarabine and melphalan) conditioning regimen, which replaced the lymphodepletion (LD) regimen, followed by auto-HSCT. Three days after auto-HSCT, 1.2×10^6 CAR T cells per kilogram 192228zT2 CAR T-cells were administered. Grade 1 cytokine release syndrome (CRS) was diagnosed, and tocilizumab (8 mg/kg, administered every day to every 8 hours) was delivered for persistent fevers, which resolved by day 7. The patient achieved neutrophil engraftment on day 19 and platelet engraftment on day 22, No infectious complications were observed. PET/CT at day 59 revealed complete metabolic remission (Deauville 5-point score 3) (Figure 2B). Following this, the patient continued maintenance monotherapy with Tislelizumab (anti-PD-1 monoclonal antibody, BeiGene) every 28 days. We detected the proportion of 192228zT2 T in peripheral blood after injection. Gating strategy for detecting CAR-T cells is shown in Figure 3A. The result showed that 192228zT cell began to expand on day 7 (3.66%) and persist for an extended period (Figure 3B). Total $CD3^+$ cells and Protein L+ cells per milliliter of blood at all time points (Figure 3C). As at day 306, the patient is in ongoing complete remission.

Discussion

BL disease progression after multi-line chemotherapy is a catastrophic event lacking a defined effective treatment approach. The expected therapeutic efficacy of HSCT is not optimistic, since on one hand, disease progression indicates high chemo-resistance, which diminishes the potential benefits from heavy conditioning regimen before HSCT. On the other hand, HSCT showed poor outcome in BL patients, and it is unclear whether there is a strong graft-versus-lymphoma effect following allo-SCT (14, 15). The Center for International Bone and Marrow Transplantation Research (CIBMTR) reported the outcomes of 241 patients undergoing HSCT for BL, and those with R/R disease had a 5-year PFS and OS of 27% and 31% for auto HSCT, and only 19% and 20% for allogenic HSCT, respectively (14).

While CAR T-cell therapy is a promising modality of treatment, patients with R/R BL are liable to experience disease progression during CAR T-cell manufacture, LD chemotherapy and/or before CAR T-cells can proliferate and exert effector activity *in vivo*. There's an urgent need for new treatment strategies. Here, we describe a novel approach that combines three strategies: (1) the use of myeloablative chemotherapy followed by auto-HSCT to both debulk the BL and provide lymphodepletion; (2) the administration of CAR T-cells shortly after auto-HSCT, before engraftment; (3) use of a new third-generation tandem CD19/CD22 CAR T-cell product to maximize antitumor efficacy, and (4) maintenance anti-PD1 therapy in an effort to prevent CAR T-cell exhaustion.

CAR-T cell treatment failure have been reported for lymphomas compared with ALL patients. The mechanism

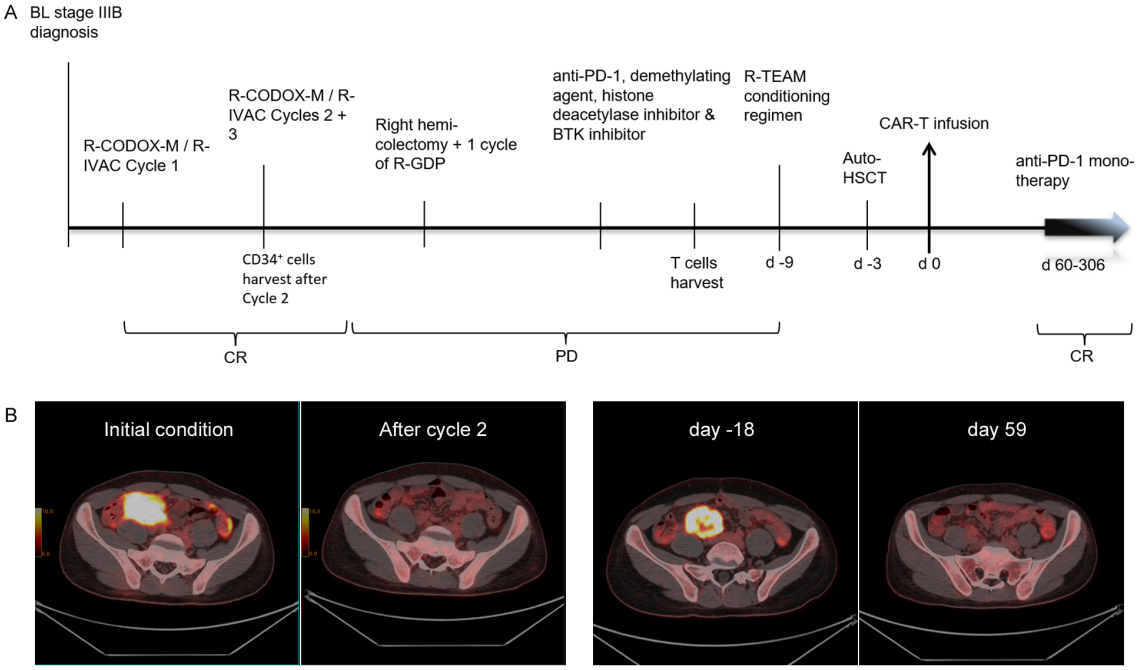

FIGURE 2
(A) Time-line of disease evolution and therapeutic interventions. **(B)**. PET/CT images at different time points: baseline, after 2 cycles of chemotherapy (CR), on day -18, and on day +59 following CAR T-cell therapy.

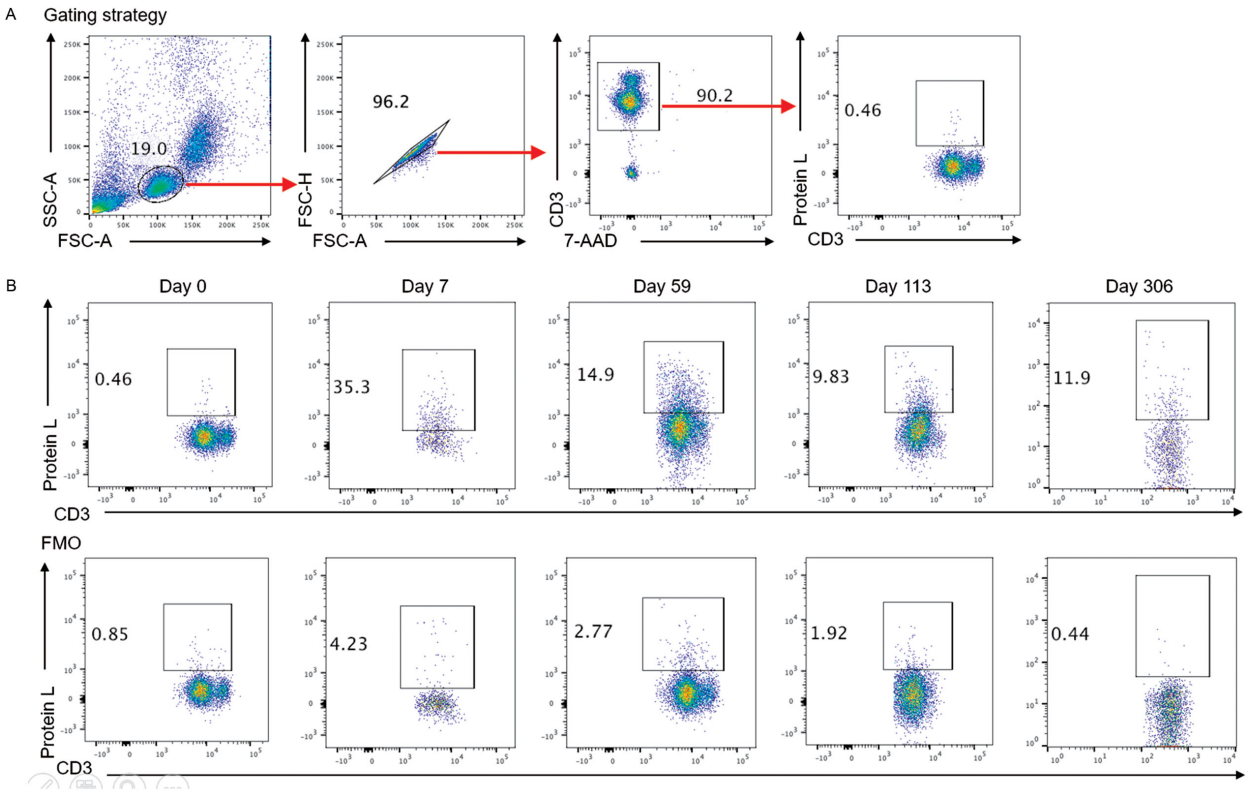

C

	Day 0	Day 7	Day 59	Day 113	Day 306
Total CD3+ T cells per milliliter of blood	8234	936	10169	6550	1485
Protein L+ cells per milliliter of blood	38	329	1511	644	176

FIGURE 3
(A) Gating strategy for detecting CAR-T cells. The flow cytometry staining panel includes CD3-PE-Cy, 7-AAD, Protein L-Biotin, and either APC-streptavidin or PE-streptavidin. **(B)**. Flow Cytometry of Peripheral Blood: Blood samples were collected on day 7, 14, 28, 59, 113 and 306 days, and the presence of CAR T-cells was detected by protein L labeling within the $CD3^+$ T-cell population. Fluorescence Minus One (FMO) control were applied at each time point to validate the threshold and ensure accurate detection. **(C)**. Total $CD3^+$ cells and Protein L+ cells per milliliter of blood at all time points.

may includerapid lymphoma progression, antigen escape, immunosuppressive tumor microenvironment (TME) and CAR-T cell exhaustion (3, 16–18). By combining a myeloablative auto-HSCT with CAR T-cell therapy, the opportunities for rapid lymphoma progression were diminished. Noting the partial CD19 expression on the BL cells at the time of lymphoma progression, 1922zT2 T cells used in this study, incorporating humanized scFvs targeting both CD19 and CD22, may have reduced the risk of antigen escape. Incorporation of a TLR2-derived intracellular domain has the potential to promote specific activation and expansion of T cells, showing improved TME and antitumor efficacy of CARs (11, 12, 19). T-cell exhaustion and an immunosuppressive TME may contribute to CAR T-cell failure, and PD-1 blockade has been reported to improve the antitumor activity of CAR-T cells (20–22). In the phase 1b PORTIA study (NCT03630159), the ORR of patients with R/R DLBCL treated with tisagenlecleucel in combination with pembrolizumab was 50% and the CR rate was 33.3% (23). A phase 1/2a trial (NCT02650999), evaluating pembrolizumab for B-cell lymphomas relapsing after or refractory to CD19-directed CAR T-cell therapy, showed a best ORR of 25%. In this trial, CAR T-cell profiling before and after pembrolizumab treatment was analyzed and high levels of inhibitory receptors such as LAG-3, Tim-3 and CTLA-4 before permbrolizumab were found to be decreased after PD-1 blockade (21). Therefore, the pre-emptive use of anti-PD1 therapy in this case may have improve the CAR T-cell activity.

With auto-HSCT alone, it is difficult for patients to achieve CR, while with CAR T-cell therapy alone, a high tumor burden increases the risk of severe cytokine release syndrome (CRS) and affects hematopoiesis. Combining myeloablative auto-HSCT with CAR T-cell therapy could effectively reduce tumor burden, diminish the immunosuppressive microenvironment, and therefore enhance CAR T-cell function, promote engraftment, and support immune reconstitution (19, 24, 25). Despite the potential risks of CRS or Immune Effector Cell-Associated Neurotoxicity Syndrome (ICANS) caused by an inflammatory environment, we did not observe severe CRS or ICANS, nor was hematopoietic reconstitution delayed in this case.

In conclusion, the combination of auto-HSCT followed by 192228zT2 therapy offers a promising new approach for treating R/R BL.

Data availability statement

The raw data supporting the conclusions of this article will be made available by the authors, without undue reservation.

Ethics statement

The studies involving humans were approved by the ethics committee of Guangzhou Medical University. The studies were conducted in accordance with the local legislation and institutional requirements. The participants provided their written informed consent to participate in this study. Written informed consent was obtained from the individual(s) for the publication of any potentially identifiable images or data included in this article.

Author contributions

XL: Conceptualization, Writing – original draft. AC: Conceptualization, Formal analysis, Writing – review & editing. LQ: Methodology, Writing – review & editing. RW: Data curation, Writing – review & editing. RoZ: Investigation, Writing – review & editing. TY: Investigation, Writing – review & editing. SC: Data curation, Writing – review & editing. JT: Data curation, Writing – review & editing. JL: Data curation, Writing – review & editing. JH: Data curation, Writing – review & editing. BS: Data curation, Writing – review & editing. DY: Data curation, Writing – review & editing. HT: Validation, Writing – review & editing. DQ: Validation, Writing – review & editing. ZT: Supervision, Writing – review & editing. PL: Methodology, Supervision, Writing – review & editing. RuZ: Methodology, Supervision, Writing – review & editing.

Funding

The author(s) declare that no financial support was received for the research, authorship, and/or publication of this article.

Conflict of interest

The authors declare that the research was conducted in the absence of any commercial or financial relationships that could be construed as a potential conflict of interest.

Publisher's note

All claims expressed in this article are solely those of the authors and do not necessarily represent those of their affiliated organizations, or those of the publisher, the editors and the reviewers. Any product that may be evaluated in this article, or claim that may be made by its manufacturer, is not guaranteed or endorsed by the publisher.

References

1. Short NJ, Kantarjian HM, Ko H, Khoury JD, Ravandi F, Thomas DA, et al. Outcomes of adults with relapsed or refractory Burkitt and high-grade B-cell leukemia/lymphoma. *Am J Hematol*. (2017) 92:E114–E7. doi: 10.1002/ajh.24720

2. Gardenswartz A, Mehta B, El-Mallawany NK, van de Ven C, Hochberg J, Flower A, et al. Safety and efficacy of combinatorial therapy utilizing myeloablative conditioning and autologous stem cell transplantation, targeted immunotherapy, and reduced intensity conditioning and allogeneic stem cell transplantation in children, adolescents, and young adults with relapsed/refractory mature B-cell non-Hodgkin lymphoma. *Leuk Lymphoma*. (2023) 64:234–7. doi: 10.1080/10428194.2022.2133542

3. Neelapu SS, Locke FL, Bartlett NL, Lekakis LJ, Miklos DB, Jacobson CA, et al. Axicabtagene ciloleucel CAR T-cell therapy in refractory large B-cell lymphoma. *N Engl J Med*. (2017) 377:2531–44. doi: 10.1056/NEJMoa1707447

4. Schuster SJ, Bishop MR, Tam CS, Waller EK, Borchmann P, McGuirk JP, et al. Tisagenlecleucel in adult relapsed or refractory diffuse large B-cell lymphoma. *N Engl J Med*. (2019) 380:45–56. doi: 10.1056/NEJMoa1804980

5. Fry TJ, Shah NN, Orentas RJ, Stetler-Stevenson M, Yuan CM, Ramakrishna S, et al. CD22-targeted CAR T cells induce remission in B-ALL that is naive or resistant to CD19-targeted CAR immunotherapy. *Nat Med*. (2018) 24:20–8. doi: 10.1038/nm.4441

6. Shah NN, Highfill SL, Shalabi H, Yates B, Jin J, Wolters PL, et al. CD4/CD8 T-cell selection affects chimeric antigen receptor (CAR) T-cell potency and toxicity: updated results from a phase I anti-CD22 CAR T-cell trial. *J Clin Oncol*. (2020) 38:1938–50. doi: 10.1200/JCO.19.03279

7. Furqan F, Shah NN. Bispecific CAR T-cells for B-cell Malignancies. *Expert Opin Biol Ther*. (2022) 22:1005–15. doi: 10.1080/14712598.2022.2086043

8. Roddie C, Lekakis LJ, Marzolini MAV, Ramakrishnan A, Zhang Y, Hu Y, et al. Dual targeting of CD19 and CD22 with bicistronic CAR-T cells in patients with relapsed/refractory large B-cell lymphoma. *Blood*. (2023) 141:2470–82. doi: 10.1182/blood.2022018598

9. Du J, Zhang Y. Sequential anti-CD19, 22, and 20 autologous chimeric antigen receptor T-cell (CAR-T) treatments of a child with relapsed refractory Burkitt lymphoma: a case report and literature review. *J Cancer Res Clin Oncol*. (2020) 146:1575–82. doi: 10.1007/s00432-020-03198-7

10. Liu Y, Deng B, Hu B, Zhang W, Zhu Q, Liu Y, et al. Sequential different B-cell antigen-targeted CAR T-cell therapy for pediatric refractory/relapsed Burkitt lymphoma. *Blood Adv*. (2022) 6:717–30. doi: 10.1182/bloodadvances.2021004557

11. Lai Y, Weng J, Wei X, Qin L, Lai P, Zhao R, et al. Toll-like receptor 2 costimulation potentiates the antitumor efficacy of CAR T Cells. *Leukemia*. (2018) 32:801–8. doi: 10.1038/leu.2017.249

12. Weng J, Lai P, Qin L, Lai Y, Jiang Z, Luo C, et al. A novel generation 1928zT2 CAR T cells induce remission in extramedullary relapse of acute lymphoblastic leukemia. *J Hematol Oncol*. (2018) 11:25. doi: 10.1186/s13045-018-0572-x

13. Qin L, Zhao R, Chen D, Wei X, Wu Q, Long Y, et al. Chimeric antigen receptor T cells targeting PD-L1 suppress tumor growth. *biomark Res*. (2020) 8:19. doi: 10.1186/s40364-020-00198-0

14. Maramattom LV, Hari PN, Burns LJ, Carreras J, Arcese W, Cairo MS, et al. Autologous and allogeneic transplantation for burkitt lymphoma outcomes and changes in utilization: a report from the center for international blood and marrow transplant research. *Biol Blood Marrow Transplant*. (2013) 19:173–9. doi: 10.1016/j.bbmt.2012.11.016

15. Malfona F, Testi AM, Chiaretti S, Moleti ML. Refractory burkitt lymphoma: diagnosis and interventional strategies. *Blood Lymphat Cancer*. (2024) 14:1–15. doi: 10.2147/BLCTT.S407804

16. Chong EA, Ruella M, Schuster SJ. Lymphoma program investigators at the university of P. Five-year outcomes for refractory B-cell lymphomas with CAR T-cell therapy. *N Engl J Med*. (2021) 384:673–4. doi: 10.1056/NEJMc2030164

17. Laetsch TW, Maude SL, Rives S, Hiramatsu H, Bittencourt H, Bader P, et al. Three-year update of tisagenlecleucel in pediatric and young adult patients with relapsed/refractory acute lymphoblastic leukemia in the ELIANA trial. *J Clin Oncol*. (2023) 41:1664–9. doi: 10.1200/JCO.22.00642

18. Shah BD, Ghobadi A, Oluwole OO, Logan AC, Boissel N, Cassaday RD, et al. KTE-X19 for relapsed or refractory adult B-cell acute lymphoblastic leukaemia: phase 2 results of the single-arm, open-label, multicentre ZUMA-3 study. *Lancet*. (2021) 398:491–502. doi: 10.1016/S0140-6736(21)01222-8

19. Lin H, Deng T, Jiang L, Meng F, Cao Y, Zhang Y, et al. Adverse reactions in relapsed/refractory B-cell lymphoma administered with chimeric antigen receptor T cell alone or in combination with autologous stem cell transplantation. *Cancers (Basel)*. (2024) 16(9):1722. doi: 10.3390/cancers16091722

20. Xin X, Zhu X, Yang Y, Wang N, Wang J, Xu J, et al. Efficacy of programmed cell death 1 inhibitor maintenance after chimeric antigen receptor T cells in patients with relapsed/refractory B-cell non-Hodgkin-lymphoma. *Cell Oncol (Dordr)*. (2024) 47 (4):1425–40. doi: 10.1007/s13402-024-00940-y

21. Chong EA, Alanio C, Svoboda J, Nasta SD, Landsburg DJ, Lacey SF, et al. Pembrolizumab for B-cell lymphomas relapsing after or refractory to CD19-directed CAR T-cell therapy. *Blood*. (2022) 139:1026–38. doi: 10.1182/blood.2021012634

22. Lee YH, Lee HJ, Kim HC, Lee Y, Nam SK, Hupperetz C, et al. PD-1 and TIGIT downregulation distinctly affect the effector and early memory phenotypes of CD19-targeting CAR T cells. *Mol Ther*. (2022) 30:579–92. doi: 10.1016/j.ymthe.2021.10.004

23. Jaeger U, Worel N, McGuirk JP, Riedell PA, Fleury I, Du Y, et al. Safety and efficacy of tisagenlecleucel plus pembrolizumab in patients with r/r DLBCL: phase 1b PORTIA study results. *Blood Adv*. (2023) 7:2283–6. doi: 10.1182/bloodadvances.2022007779

24. Liu W, Liu W, Zou H, Chen L, Huang W, Lv R, et al. Combinational therapy of CAR T-cell and HDT/ASCT demonstrates impressive clinical efficacy and improved CAR T-cell behavior in relapsed/refractory large B-cell lymphoma. *J Immunother Cancer*. (2024) 12(4):e008857. doi: 10.1136/jitc-2024-008857

25. Jain T, Knezevic A, Pennisi M, Chen Y, Ruiz JD, Purdon TJ, et al. Hematopoietic recovery in patients receiving chimeric antigen receptor T-cell therapy for hematologic Malignancies. *Blood Adv*. (2020) 4:3776–87. doi: 10.1182/bloodadvances.2020002509

frontiers | Frontiers in Immunology

TYPE Review
PUBLISHED 26 February 2025
DOI 10.3389/fimmu.2025.1533444

OPEN ACCESS

EDITED BY
Penny Fang,
University of Texas MD Anderson Cancer Center, United States

REVIEWED BY
Ken Young,
Duke University, United States
Xin Meng,
Fudan University, China

*CORRESPONDENCE
Shuling Hou
csxtyhsl@126.com

†These authors have contributed equally to this work

RECEIVED 24 November 2024
ACCEPTED 07 February 2025
PUBLISHED 26 February 2025

CITATION
Wang L, Guo M and Hou S (2025) Advances in primary large B-cell lymphoma of immune-privileged sites. *Front. Immunol.* 16:1533444. doi: 10.3389/fimmu.2025.1533444

Advances in primary large B-cell lymphoma of immune-privileged sites

Liao Wang[1,2†], Meiru Guo[3†] and Shuling Hou[1,2,3*]

[1]Shanxi Bethune Hospital Cancer Center Lymphoma Department, Shanxi Academy of Medical Sciences, Tongji Shanxi Hospital, Third Hospital of Shanxi Medical University, Taiyuan, China, [2]Tongji Hospital, Tongji Medical College, Huazhong University of Science and Technology, Wuhan, China, [3]Third Hospital of Shanxi Medical University, Shanxi Bethune Hospital, Shanxi Academy of Medical Sciences, Tongji Shanxi Hospital, Taiyuan, China

Primary large B-cell lymphoma of immune-privileged sites (IP-LBCL) encompasses a spectrum of relatively rare aggressive B-cell lymphomas, such as primary central nervous system lymphoma (PCNSL), primary testicular large B-cell lymphoma (PTL), and primary vitreoretinal large B-cell lymphoma (PVRL). Macroscopically, the development of IPI-LBCL may be associated with the dysfunction of meningeal lymphatic vessels (mLVs) and the perivascular channel system formed by astrocytes. Microscopically, mutation in MYD88 and CD79B genes plays a pivotal role in the pathogenesis of IP-LBCL. Pathological examination remains the cornerstone for establishing a diagnosis of IP-LBCL. Moreover, traditional imaging is now supplemented by a suite of advanced diagnostic methods, including cytological, genetic, immunological, multiple omics, and molecular biological, which collectively enhance the diagnostic accuracy of IP-LBCL. Despite these advancements, the high recurrence rates and attendant high mortality rates pose significant challenges to achieving long-term survival in IP-LBCL patients. However, the emergence of novel therapeutic agents, such as Bruton's tyrosine kinase inhibitors (BTKi), immune checkpoint inhibitors, immunomodulators, and anti-CD19 chimeric antigen receptor T (CAR-T) cell therapy, has offered promising new avenues for the treatment of IP-LBCL, demonstrating remarkable anti-tumor efficacy in recent years. This review delves into the epidemiology, pathogenesis mechanisms, diagnosis approaches, therapeutic strategies, and prognosis factors associated with IP-LBCL. It meticulously examines the parallels and divergences between the National Comprehensive Cancer Network (NCCN) and European Society for Medical Oncology (ESMO) guidelines, enhancing the professional comprehension of the complexities inherent to IP-LBCL.

KEYWORDS

primary large B-cell lymphoma of immune-privileged sites, pathology, diagnosis, treatment, prognosis

1 Introduction

Primary large B-cell lymphoma of immune-privileged sites (IP-LBCL) was introduced in the 5th edition of the World Health Organization Classification of Lymphoid Neoplasms in 2022. This classification delineates IP-LBCL as a distinct group of aggressive B-cell lymphomas that primarily manifest in the central nervous system, vitreous retina, or testes. This group encompasses primary central nervous system lymphoma (PCNSL), primary testicular large B-cell lymphoma (PTL), and primary vitreoretinal large B-cell lymphoma (PVRL). Given the significant biological similarities and shared intravascular microenvironment between intravascular large B-cell lymphoma (IVLBCL) and IP-LBCL, which may also be considered a site of immune privilege, IVLBCL has been incorporated into the IP-LBCL category (1). Furthermore, primary cutaneous diffuse large B-cell lymphoma (DLBCL) leg-type and primary breast or adrenal DLBCL are also posited to be variants of IP-LBCL. The pathogenesis of IP-LBCL is intricate due to physiological barriers such as the blood-brain barrier (BBB), blood-retina barrier, and blood-testis barrier, leading to poor treatment responses, high recurrence rates, and unfavorable prognoses. Accurate diagnosis and effective treatment protocols are essential for managing IP-LBCL patients. This review aims to synthesize the current research on IP-LBCL, offering a robust foundation for clinical practice to provide a reliable reference for clinical work.

2 Epidemiology

IP-LBCL represents a rare and highly aggressive subset of extranodal non-Hodgkin lymphomas (NHLs) from non-germinal centers. The annual incidence rate of PCNSL is 0.4/100,000 (2), constituting 4% to 6% of all extranodal lymphomas. While PCNSL can manifest at any age, its incidence escalates with increasing age, peaking at a median age of approximately 67. Among those over 70, the condition affects approximately 4 cases per 100,000 individuals (3). PTL comprises 1-2% of all NHLs and accounts for 4% of extranodal NHLs (4). It is more prevalent in the elderly male population, with a median age at diagnosis ranging from 66 to 68 years (5). PVRL usually occurs in immunocompetent adults in their 50s, with a slight female predominance but no racial predilection. PVRL incidence is estimated to be 50 cases annually in the United States. PVRL represents ~5% of the patients registered in the French database for oculocerebral lymphomas and accounts for 10 new cases annually (6). There is a lack of incidence statistics for PVRL in other regions. Apart from immunosuppression related to the human immunodeficiency virus (HIV), there is a lack of information regarding the incidence, geographic or racial disparities, and potential risk factors for the broader category of IP-LBCL.

3 Pathology

From a macro perspective, immune-privileged sites typically lack lymphatic tissue. Whether lymphomas originate in these organs or develop outside and subsequently home to them is a contentious and ongoing area of research. Currently, there is a paucity of research on the pathogenesis of PTL. Regarding the mechanisms of PCNSL and PVRL, some studies suggest that PCNSL and PVRL may originate outside the CNS and then migrate to the CNS or the eye, proliferating in the immunologically permissive microenvironment (6).

Identifying meningeal lymphatic vessels (mLVs) in the dura mater challenges this traditional view. These anatomical structures serve as potential drainage pathways for molecular clearance and as conduits for immune cells to access the peripheral lymphatic system from the cerebrospinal fluid. Dysfunction of mLVs has been correlated with impaired brain waste clearance, potentially contributing to the development of PCNSL (7). Moreover, the glial lymphatic system, implicated in waste removal, fluid/ion homeostasis, inflammatory response, and immune surveillance in the CNS, appears to play a significant role in the proliferation and spread of lymphomas (8). This system includes perivascular channels formed by astrocytes, such as the Virchow-Robin perivascular hiatus, facilitating the flow of cerebrospinal fluid from the subarachnoid space and interstitial fluid into the dural sinuses. Additionally, a growing body of research indicates that in IP-LBCL, inhibitory microenvironmental factors, including T cell depletion and macrophage immune function downregulation, substantially influence tumor cell proliferation, immune escape, and drug resistance.

Microscopically, IP-LBCL is characterized by genomic instability affecting multiple signaling pathways and cellular processes (Figure 1), including nuclear factor-κB (NF-κB), B-cell receptor (BCR), Toll-like receptor (TLR), JAK-STAT signaling pathway, mitogen-activated protein kinase signaling pathway, DNA damage response, apoptosis, cell-cycle regulation as well as tumor immune microenvironment (TME) dysfunction, notably including the signature mutations MYD88 L265P (67%), CD79B (63%), and CDKN2A deletions (83%) (9).

Mutations in the myeloid differentiation primary response gene 88 (MYD88) and the B-cell receptor beta chain (CD79B) are pivotal in the pathogenesis of IP-LBCL. Staudt's team has proposed the 'gene heptad' that classifies DLBCL with co-mutations in MYD88 L265P and CD79B as the MCD type, while Shipp's team 'gene quintet' suggests that C5 corresponds to the MCD type, hence IP-LBCL is also referred to as MCD/C5 subtype lymphomas. These mutations in MYD88 and CD79B enhance B-cell survival and proliferation by activating TLR and BCR signaling, leading to constitutive activation of the NF-κB pathway downstream (10). It should be noted that Roschewski et al. identified the "My-T-BCR" supercomplex in PCNSL. This supercomplex, named for its co-localization of MYD88 with TLR9 and BCR, serves as a site for NF-κB activation. Receptor tyrosine kinase-like orphan receptor 1 (ROR1), typically absent or minimally expressed in normal tissues, and over-expressed in R/R DLBCL, interacts with Wnt-related proteins, promoting tumor cell proliferation, activation, and epithelial-to-mesenchymal transformation through the Wnt/β classical pathway and PI3Kδ/AKT/mTOR non-classical Wnt pathway (11). The role of ROR1 in the development of IP-LBCL warrants further investigation. Deletions of the cell cycle-dependent kinase inhibitor 2A (CDKN2A) gene and the human leukocyte antigen (HLA) locus also contribute to developing IP-LBCL.

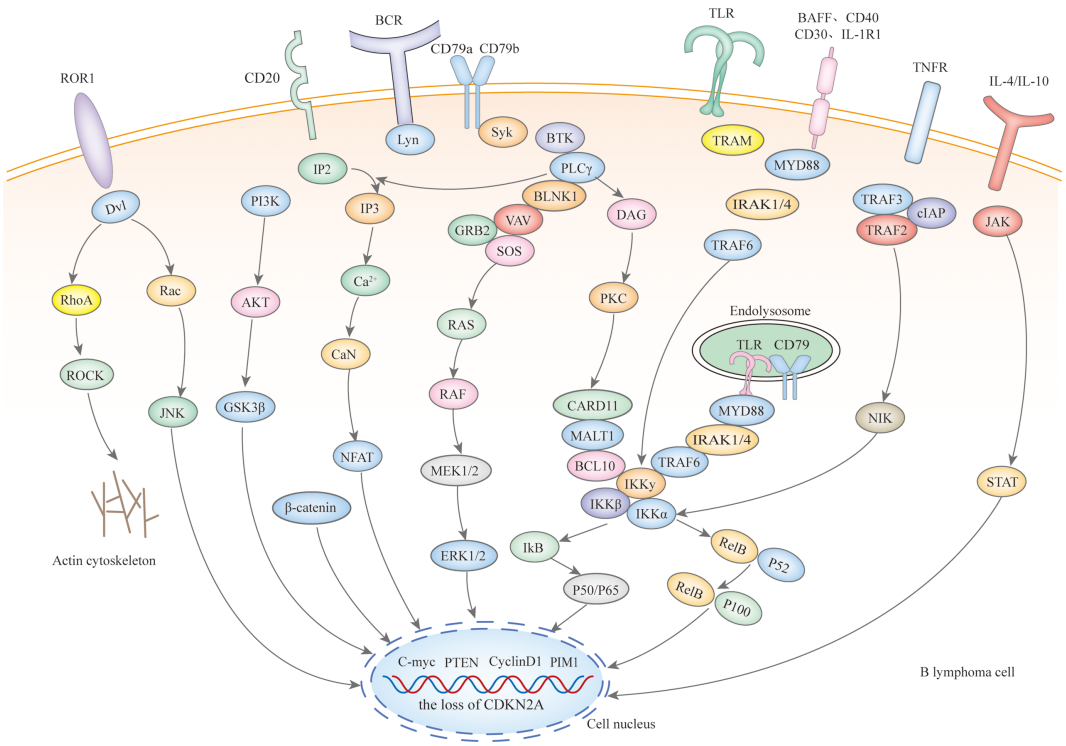

FIGURE 1
The signaling mechanisms within IP-LBCL.

CDKN2A, a critical tumor suppressor gene located in the 9p21 region of the human chromosome, when deleted, leads to loss of cell cycle regulation and an increased risk of cancer development. Although TP53 mutations are rare in IP-LBCL, they can disrupt the p53 pathway through upstream CDKN2A loss, which is often near-uniform and involves a double allele.

Copy number alterations(CNAs) at 9p24.1/PD-L1, along with translocations with concomitant protein overexpression, the loss of HLA class I and II expression, and the loss of HLA loci, form the basis of immune escape in PCNSL and PTL (Figure 2), with the latter playing a significant role (12). PCNSL notably demonstrates a higher frequency of focal deletions in the HLA-D (6p21) locus, suggesting a potential mechanism of immune evasion (9). Immune escape and sustained signaling are hallmark features of PTL, encompassing structural rearrangements of the core components of antigen presentation, including CIITA, B2M, and HLA loci, as well as programmed death ligands 1 (CD274) and 2 (PDCD1LG2). Somatic mutation enrichment within NF-κB pathway genes - namely MYD88, CD79B, NFKBIZ, BCL10, and MALT1- is also a prominent feature of PTL (4). These genetic alterations within the NF-κB pathway underscore the significance of immune evasion and sustained signaling in the pathogenesis of PTL (13). PVRL's mutational spectrum, which includes activation of the toll-like receptor and B-cell receptor pathway alongside the loss of CDKN2A, substantiates its close affiliation with other IP-LBCL (14). Similarly, analogous genetic alterations in IVLBCL, primary cutaneous DLBCL leg-type, and primary breast or adrenal DLBCL support their inclusion within the IP-LBCL classification.

4 Diagnosis

4.1 Pathological examination

Pathological examination is considered the gold standard for diagnosing IP-LBCL. The combination of cytological, immunological, cytogenetic, and molecular biological assays enables a precise diagnosis of IP-LBCL. The pathological, molecular, and genetic changes of IP-LBCL are detailed in the Supplementary Table 1.

Stereotactic biopsy is the preferred approach for PCNSL. Approximately 95% of PCNSL have exhibited a DLBCL pathological subtype, predominantly of non-germinal center origin. The remaining cases include marginal zone lymphoma (MZL), anaplastic large cell lymphoma (ALCL), Burkitt lymphoma (BL), lymphoblastic lymphoma (LBL), mature T/NK-cell lymphoma (T/NK), and Hodgkin lymphoma (HL).

In the diagnosis of primary testicular lymphoma (PTL), orchiectomy is favored over fine needle aspiration and testicular biopsy due to the availability of intact tissue samples. Approximately 80% to 90% of PTL cases are classified as DLBCL; other pathologic types are predominantly Burkitt and Burkitt-like lymphoma (BL). Mantle cell, NK/T-cell, and follicular testicular lymphoma (FL) are observed less frequently.

PVRL is occasionally classified as a subtype of PCNSL. A vitreous biopsy is the preferred method for diagnosing PVRL. Lymph node or local lesion biopsy is the preferred method for diagnosing IVLBCL, primary cutaneous DLBCL leg-type, and primary breast or adrenal DLBCL.

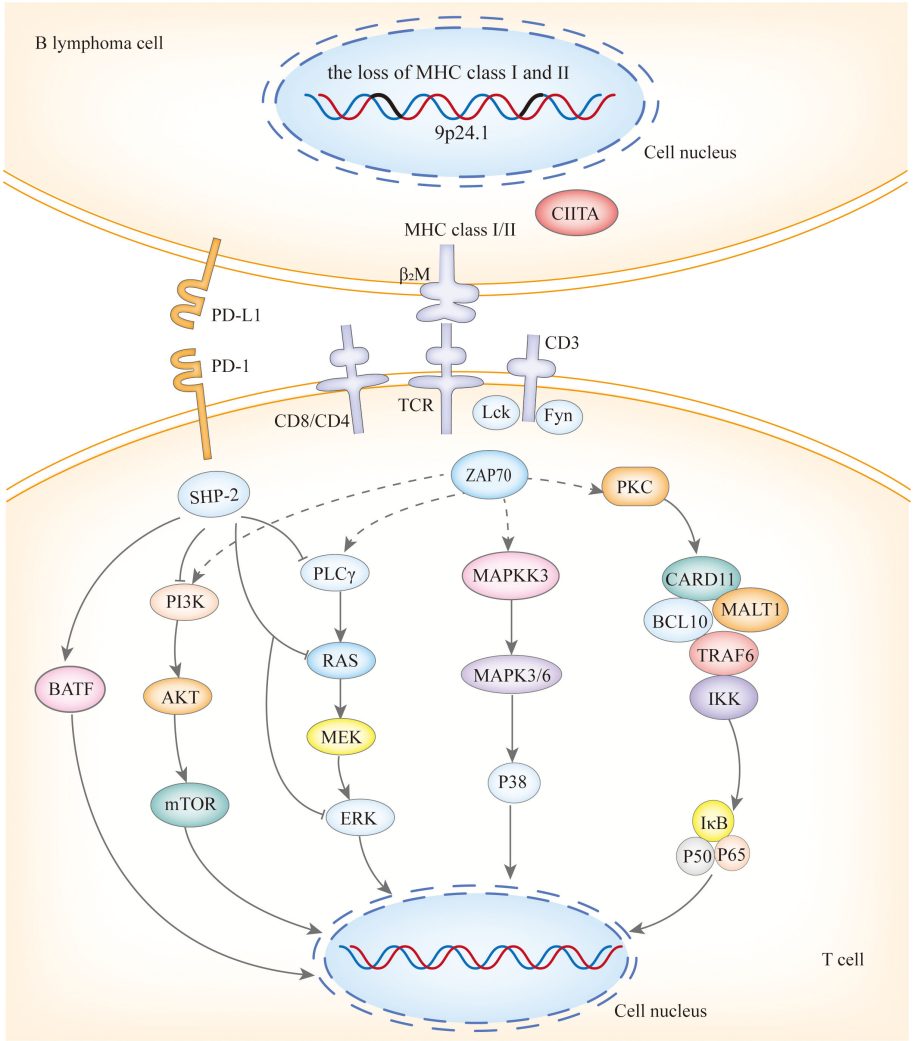

FIGURE 2
The immune escape mechanisms of IP-LBCL.

4.2 Laboratory examination

Research has demonstrated that a κ to λ free immunoglobulin light chains ratio exceeding 3.0 in Cerebrospinal Fluid (CSF) patients with PCNSL can be a provisional threshold for identifying clonal light chain restriction. Additionally, the CSF levels of cytokines IL-10, IL-6, IL-10/IL-6 ratio, and C-X-C chemokine ligand 13 (CXCL 13) have been identified as potential diagnostic markers for PCNSL. Studies have indicated that the diagnostic threshold value of IL-10 was 0.43 pg/mL, yielding a sensitivity of 96.3% and a specificity of 66.67%. While IL-6 alone was not significant for diagnosing PCNSL, the IL-10/IL-6 was significant, with a critical value of 0.21, a sensitivity of 81.48%, and a specificity of 80.95% (15). Furthermore, CXCL 13, which plays an essential role in B-cell homing, has been recognized as an independent diagnostic marker and can be utilized alone or in conjunction with IL-10 (16). A ROC curve analysis assessed the diagnostic potential of CXCL 13 as a biomarker for CNS lymphoma, revealing that CXCL 13 concentrations above 90 pg/mL had a sensitivity of 69.9% and a specificity of 92.7% for detecting CNS lymphoma.

IL-6 and IL-10 levels in the aqueous humor or vitreous body have been implicated in the diagnosis of PVRL (17). A systematic review has demonstrated that an IL-10/IL-6 ratio of 1 or higher is highly sensitive for identifying patients with PVRL (18). Notably, the diagnostic utility of the IL10 to IL6 ratio differs between PCNSL and PVRL, suggesting that further investigation is warranted to elucidate the underlying reasons for this discrepancy.

4.3 Imaging

For diagnosing PCNSL, contrast-enhanced magnetic resonance (MRI) and diffusion-weighted (DWI) are the preferred imaging modalities. Most PCNSL cases manifest as isolated supratentorial lesions affecting the white matter. However, multifocal disease,

involvement of the infratentorial compartments, and spinal cord involvement are also not uncommon occurrences (19). Research has shown that the notch sign, T2 necrosis sign, reef sign, and peritumoral white matter softening sign are closely associated with PCNSL (20). Concurrently, advanced MRI techniques, such as dynamic contrast-enhanced MRI and dynamic magnetic susceptibility contrast-perfusion MRI, offer distinctive insights into tumor biology.

Optical coherence tomography (OCT) is a valuable tool for accurately identifying the unique features and location of PVRL, which is essential for its diagnosis. OCT examinations reveal hyperreflective spots within the posterior vitreous cavity, with punctate or clustered hyperreflective foci that may infiltrate all layers. In severe cases, the retinal layers may become indistinguishable. Additionally, vertically oriented hyperreflective lesions within the retinal neuroepithelium are frequently observed. These lesions may also encircle the retinal pigment epithelium (RPE), creating a double layer between the RPE and Bruch's membrane.

Ultrasonography is the preferred diagnostic modality for PTL and can also be utilized for the exclusionary diagnosis of PVRL. PVRL is characterized by infiltration along the spermatic cord and gonadal veins to the retroperitoneum and diffuse thoracic and abdominal infiltrates (21).

Fundus autofluorescence (FA) and indocyanine green angiography (ICGA) are diagnostic tools PVRL patients use. Distinct clusters of round hypofluorescent foci are observed in both the early and late stages of FA, as reported by Venkatesh et al. Proposed capillary detachment is another feature of FA in PVRL (22). The primary characteristic of ICGA is hypoblue light (23), and small, round hypofluorescent foci may disappear in advanced stages. FA is a non-invasive test for PVRL, where tumor cells infiltrating the neuroretina exhibit high autofluorescence, and lesion regression can be tracked by hypofluorescence (22).

Enhanced computed tomography (CT) of the chest, abdomen, and pelvis is crucial for determining the extent of IP-LBCL and distinguishing between primary and secondary lesions. Compared to CT, 18F-fluorodeoxyglucose positron emission tomography (18F-FDG PET) has a higher diagnostic value. A meta-analysis of 967 patients from 29 studies revealed that the weighted mean combined sensitivity, specificity, positive predictive value, negative predictive value, and diagnostic ratio for 18F-FDG PET were 87% (95% CI, 83%–90%), 85% (95% CI, 81%–88%), 84% (95% CI, 81%–88%), 87% (95% CI, 84%–90%), and 29.78 (95% CI, 18.34–48.35), respectively (24). However, the diagnostic value of both tests is not without limitations. A large international multicenter cohort study indicated a false-positive rate of up to 5.8% for whole-body PET-CT in the preliminary diagnosis of extracranial invasion in CNS DLBCL patients (25). Kim et al. also found that 13.5% of PCNSL patients showed low FDG uptake on PET, which is associated with negative expression of MUM1, a critical regulatory protein in B cell development and tumorigenesis (26). Therefore, caution must be exercised regarding false positives and negatives when diagnosing PCNSL with PET-CT. Pathological examination remains the gold standard for diagnosis.

PET serves a dual role in assessing treatment efficacy and predicting patient outcomes in CNS lymphoma. A prospective multicenter study evaluated the utility of 18F-FDG PET in treating CNS lymphoma, revealing that baseline cerebellar metabolism and the sum of metabolized tumor volume (sumMTV) for up to five lesions were predictive of chemotherapy response in PCNSL patients. Higher average standardized uptake values (SUV) and lower sumMTV in the cerebellum were significantly associated with favorable response groups in the study (average SUV: 6.4 [5.7–7.5] vs. 5.4 [4.6–6.5], $p = 0.04$, and sumMTV: 5 [1.8–10.8] vs. 17.1 [5.3–19.9], $p = 0.01$, respectively) (27), This suggests that elevated average SUV and reduced sumMTV in the cerebellum are indicative of improved treatment outcomes. Additionally, another prospective study reported that a high maximum standardized uptake value (SUVmax) correlated with decreased progression-free survival (PFS), with a median PFS of 3.4 months for patients with SUVmax >20 and 10.8 months for those with SUVmax <20 (28).

4.4 Fundus photography

An accurate ophthalmologic evaluation can discern infiltrative patterns of cells within the vitreous, presenting as sheets or clumps, and multifocal creamy-white lesions in the outer retina, characteristic findings in PVRL (23).

4.5 Biomarkers

Circulating tumor DNAs (ctDNAs), which are DNA fragments deriving from apoptotic, necrotic, or secreted tumor cells, serve as biomarkers in oncological research (29) (14). Compared to traditional tissue biopsies, ctDNAs offer the advantages of being non-invasive, requiring only a tiny sample, real-time, and allowing for multiple tests, making them particularly suitable for patients from whom samples cannot be obtained. On the other hand, ctDNAs carry the genomic information of tumor cells, reflecting the status of IP-LBCL. Detection of ctDNAs facilitates the acquisition of IP-LBCL's genetic profiling, aiding in the selection of appropriate targeted therapies, but also enables real-time monitoring of tumor burden through changes in ctDNA levels, predicting tumor recurrence and surveillance of minimal residual disease. In brain tumor patients, the concentration of ctDNA in CSF exceeds that found in plasma, endowing it with heightened sensitivity for detecting CNS lesions (30). A CSF NGS analysis of 11 newly diagnosed PCNSL patients undergoing ibrutinib-based therapy demonstrated that ctDNAs could effectively monitor tumor burden and evaluate treatment response (29). Furthermore, the clinical utility of ctDNA in aqueous humor and vitreous fluid has also been established to diagnose and monitor PVRL (31). Similarly, changes in the microRNAs (miRNAs) levels also reflect crucial biological information about IP-LBCL, providing valuable reference information for evaluating treatment efficacy, assessing prognosis,

monitoring drug resistance, and personalized treatment, thereby supporting clinical management and evidence-based decision-making. Several studies have employed real-time quantitative polymerase chain reaction (qRT-PCR) quantified miRNAs in the CSF of PCNSL patients, identifying significantly elevated expression levels of miR-19b, miR-21, and miR-92a relative to controls (32). Moreover, studies have indicated that miR-326 was a key driver of B-cell proliferation, and miR-6513-3p had the potential to serve as an auxiliary tool for the diagnosis of PVRL (33).

Hernandez-Verdin's team conducted a comprehensive multi-omics analysis of PCNSL, encompassing whole-exome sequencing, RNA sequencing (RNA-seq), methylation sequencing, and clinical profiling. This analysis revealed four distinct prognostic molecular subtypes of PCNSL and developed algorithms for identification. Based on the multi-omics data classification, PCNSL was categorized into four clusters (CS). The CS1 and CS2 exhibited an immune-cold hypermethylated profile yet displayed distinct clinical behavior. The CS3 was characterized by meningeal infiltration and a high prevalence of HIST1H1E mutation; notably, only tumor cells from the CS3 were identified in the CSF in cases with meningeal infiltration, offering a potential diagnostic marker for PCNSL typing. The 'immune-hot' Cluster CS4 was enriched with mutations and exhibited increased JAK signal and NF-kB activity (34). These four molecular patterns, with their unique prognostic implications in PCNSL, lay the groundwork for future clinical stratification and the development of targeted interventions tailored to specific subtypes. Cluster CS3 may exhibit sensitivity to BTK inhibitors, while CS1 may derive therapeutic benefit from the loss of CDKN2A/B. The CS2 subtype potentially responds to the inhibition of IRF4, SPIB, MEIS1, and demethylation agents. Additionally, CS2 is characterized by elevated DNA methylation levels (34). Stratification based on distinct metabolic profiles can inform treatment strategies and potentially enhance prognostic outcomes.

4.6 Cognitive function assessment

Cognitive function in patients with CNS tumors can be compromised by both the cancer itself and the neurotoxic effects of treatment, resulting in a diminished quality of life and impaired social competence. Therefore, it is imperative to conduct essential cognitive screening and assessment for these patients using the Mini-Mental Status Examination (MMSE), a validated screening tool for cognitive function (35).

5 Treatment

5.1 Standard treatment

5.1.1 Induction therapy of PCNSL

NCCN and ESMO guidelines prioritize enrollment in clinical trials for patients newly diagnosed with PCNSL. For those who are not eligible for clinical trials, both NCCN and ESMO guidelines advocate for induction regiments incorporating high-dose methotrexate (HD-MTX), such as R-MT or R-MPV.

There are distinctions between the NCCN and ESMO guidelines regarding the recommended regimen and HD-MTX dosage (Table 1). The NCCN guidelines specify two points: 1. R-M/R-MT can serve as an induction regimen, requiring an MTX of $8g/m^2$; 2. If R-M is combined with additional chemotherapy agents (R-MPV/R-MT) and consolidation with whole brain radiotherapy (WBRT) consolidation is under consideration, the MTX dosage can be reduced to $3.5g/m^2$. In contrast, ESMO recommends R-M in combination with multiple chemotherapeutic agents for induction and sets the minimum MTX dosage at $3g/m^2$.

Patients who are intolerant to HD-MTX may consider alternative chemotherapy regimens. WBRT is suggested for patients who are ineligible for chemotherapy due to advanced age, poor performance status, or significant debilitation. For PCNSL patients who cannot tolerate chemotherapy, the ESMO guidelines recommend palliative strategies, including corticosteroids, oral alkylating agents such as temozolomide, carmustine, and procarbazine, with or without rituximab, WBRT, BTK inhibitors, and immunomodulators. In addition to intraocular chemotherapy, the NCCN guidelines also consider orbital radiotherapy (RT) for PCNSL patients exhibiting vitreoretinal involvement on ophthalmic examination who show no response to systemic therapy. The NCCN guidelines further recommend intra-CSF systemic treatment for patients with positive CSF findings who cannot tolerate systemic chemotherapy. Moreover, for patients with positive CSF or spinal MRI, the NCCN guidelines advocate focal spinal RT. Regarding intrathecal injection, the ESMO guidelines deem it appropriate for patients who are CSF-positive but cannot tolerate chemotherapy as a first-line treatment for those with persistent meningeal disease after initial CSF positivity.

5.1.2 Consolidation therapy of PCNSL

Patients who achieve complete remission (CR), partial remission (PR), or stable disease (SD) following induction therapy have options for consolidation therapy, which may include WBRT or autologous stem cell transplantation (ASCT). Table 1 delineates the distinctions between NCCN and ESMO guidelines regarding consolidation therapy approaches. The NCCN guidelines stipulate that ASCT should be considered only for patients who have attained CR or unconfirmed CR (uCR). In contrast, ESMO views ASCT as a viable option for patients who have not experienced disease progression and are otherwise eligible. For patients not eligible for ASCT post-CR, the ESMO guidelines suggest watchful waiting, WBRT, or lenalidomide maintenance therapy, given the intensive combination chemotherapy induction regimen typically utilized. Clinical trials are currently underway to assess lenalidomide and procarbazine as maintenance therapy in the R-MP regimen. Conversely, the NCCN guidelines do not endorse a wait-and-see approach; instead, they recommend a monthly MTX regimen ($3.5g/m^2$ ~ $8g/m^2$) with or without R or R/Temozolomide (TMZ) as standalone options.

TABLE 1 Comparison of NCCN and ESMO guidelines.

	NCCN	ESMO
Induction		
common		
	R-MT[1]/R-MPV[2]/R-MATRix[3]	
different		
	R-M (MTX 8.0g/m^2)	MATRix
		R ± MBVP[4]
		MPV
		(MTX ≥3.0g/m^2)
Consolidate and maintenance		
common		
	WBRT/ASCT	
different		
	HD-AraC ± etoposide	Watchful waiting**
	TMZ (after WBRT)	Maintenance therapy(lenalidomide)
	R-M based regimen*	
	Best supportive care	
R/R		
common		
	Retreat with HD-MTX	
	HD-AraC/Lenalidomide/Ibrutinib/TMZ	
different		
	Systemic and/or intra-CSF	HD-ifosfamide-based chemotherapy
	Focal irradiation	HD-Arac-based chemotherapy
	Involved-field RT	
	Rituximab + TMZ	
	Lenalidomide + rituximab	
	Pemetrexed	
	Pomalidomide	
	R-MBVP	

*Continue monthly for up to 1 y; **Patients not suitable for ASCT after CR.
1. R-MT, Rituximab + HD-MTX + Temozolomide;
2. R-MPV, Rituximab + HD-MTX + Procarbazine + Vincristine;
3. R-MATRix, Rituximab + HD-MTX + HD-AraC+ Thiotepa;
4. R ± MBVP, Rituximab ± HD-MTX + Carmustine + Teniposide +Methylprednisolone.

5.1.3 Recurrent/refractory PCNSL

NCCN and ESMO guidelines prioritize enrollment in clinical trials for both R/R PCNSL and newly treated PCNSL. HD-MTX reinduction is acknowledged as an effective strategy for patients experiencing advanced recurrence, defined as ≥12 months post-HD-MTX-based chemotherapy by NCCN. For patients with early recurrence occurring within < 12 months or those with refractory treatment, alternative non-MTX regiments, such as HD-AraC chemotherapy, are recommended by the NCCN. The NCCN and ESMO guidelines endorse ibrutinib, TMZ, or lenalidomide for treating R/R PCNSL. Additionally, ESMO advocates for HD-ifosfamide-based chemotherapy. In contrast, the NCCN tailors its regimen recommendations to various conditions, including prior WBRT, prior HD-MTX-based regimen without prior RT, and ASCT, as detailed in Table 1.

5.1.4 PTL

The CSCO guidelines utilize the 2014 Lugano staging criteria for the stratification of PTL. The preferred treatment for PTL, according to these guidelines, is radical orchiectomy followed by 6 to 8 cycles of R-CHOP and prophylactic RT (25 to 30Gy) to the contralateral scrotum. When orchiectomy is not feasible, involved site radiotherapy becomes an alternative treatment approach. Given the high propensity for CNS relapse in PTL, CNS prophylaxis is also recommended. This includes intrathecal injections of methotrexate, with or without cytarabine, and two cycles of HD-MTX. A distinction is made between stages III and IV and stages and IIE, where DLBCL-like therapy is favored. For R/R PTL, clinical trials should be considered the first-line option. For those who do not meet the eligibility criteria for clinical trials, DLBCL-like therapy, Bruton's tyrosine kinase inhibitors (BTKi), lenalidomide, Programmed cell death receptor 1 (PD-1) monoclonal antibody, chimeric antigen receptor T-cell therapy (CAR-T), and ASCT are viable treatment options.

5.1.5 PVRL

The ESMO guidelines advocate for a treatment approach for PVRL that mirrors the regimen used for PCNSL, complemented by intravitreal injection of MTX to expedite the remission of intraocular disease. Patients who attain CR or PR may benefit from further consolidation with orbital radiotherapy. For patients who are intolerant to chemotherapy, oral temozolomide in conjunction with orbital radiotherapy or intravitreal MTX injection is recommended. For R/R PVRL, treatment options include R-DHAP (Rituximab-Dexamethasone-Cytarabine-Cisplatin) or R-ICE(Rituximab-Ifosfamide-Carboplatine-Toposide) regimens, followed by thiotepa-based consolidation with HDC-ASCT therapy. For patients with R/R PVRL who are generally in poor condition, alternative treatment options include topical therapy, ibrutinib, lenalidomide, or temozolomide.

5.2 Targeted drug

BTKi, immune checkpoint inhibitors, immunomodulatory agents, CD20 monoclonal antibodies, and CAR-T cell therapies targeting CD19 have been proven to have significant anti-tumor effects, with their blood-brain barrier penetration rates shown in Table 2.

BTKi are a class of small molecules capable of traversing physiological barriers to specifically bind and inhibit the activity of BTK, thereby blocking downstream signal transduction pathways (Figure 3), including the NF-κB pathways. Among them, the My-T-BCR is a site for NF-κB activation and is extremely sensitive to BTK

TABLE 2 BBB penetration rate of the targeted drug.

Representative drug	Target	BBB penetration rate(%)
Zanubrutinib	BTK	2.39 ± 1.71[a](people[1]) (61) 3.58[b](SD rat) (62)
Tirabrutinib		8.5[b](SD rat) (62)
Nivolumab	PD-1	0.88-1.9[c](people) (63)
Lenalidomide	Ikaros	1.3-2.4[c](people) (64)
Pomalidomide	Aiolos	39[d](CD-IGS rat) (65)
Rituximab	CD20	0.1[c](people) (40)
Tisagenlecleucel	CD19	–

[1]Zanubrutinib protein binding rates were as high as 94%, and the adjusted BBB penetration ratio was 42.7% ± 27.7%.
[a]Penetration rate (%) =C median, CSF/C median, plasma.
[b]Penetration rate (%) =C max, brain/C max, plasma.
[c]Penetration rate (%) =C CSF/C plasma.
[d]Penetration rate (%) =AUC ratio (Brain: Blood).

inhibition (possibly due to the autophagy of mutated MYD88 by BTK inhibitors), especially when there are concurrent mutations in MYD88 and CD79B, where the benefit of combining BTK inhibitors with chemotherapy is maximized. First-generation BTKi exhibit specific off-target inhibition effects, which has led to the preferential use of second-generation BTKi. Apart from acalabrutinib, which is currently under clinical investigation, both zanubrutinib and tirabrutinib have demonstrated efficacy and safety in PCNSL and PVRL, as shown in Table 3. Orelabrutinib has shown efficacy only in PCNSL. There are no reports on the application of orelabrutinib in PVRL or the use of BTK inhibitors in PTL. The programmed cell death receptor 1 (PD-1) and its ligand (primarily PD-L1) are expressed by tumor and microenvironmental cells. They mediate immune evasion of tumors by dampening the PTEN-PI3K-Akt and RAS-MEK-ERK signaling pathways and upregulating the expression of transcription factors such as Basic Leucine Zipper Transcriptional Factor ATF-like (BATF) (36), as shown in Figure 3. Drugs targeting PD-1/PD-L1 rejuvenate exhausted T cells in the TME. Apart from PVRL, both PCNSL and PTL have shown clinical and radiological responses following PD-1 blockade. A clinical trial investigated the effectiveness of the anti-PD-1 antibody Nivolumab in four patients with R/R PCNSL and one patient with PTL CNS relapse. The results indicated that all five patients exhibited clinical and radiographic responses to PD-1 blockade (37).

Immune modulators lenalidomide and pomalidomide exert their effects by binding to the cereblon protein within the E3 ubiquitin ligase complex, leading to the ubiquitination and degradation of specific proteins such as Ikaros and Aiolos, as shown in Figure 3. The degradation of these proteins plays a crucial role in regulating immunity and tumor cell growth. Additionally, lenalidomide has the ability to cross the blood-brain barrier and exhibits single-agent activity (38). Pomalidomide is 10 times more potent than lenalidomide, yet there are no clinical studies to assess its ability to cross the blood-brain barrier. However, research has shown that after a single oral administration of ^{14}C-labeled pomalidomide to rats, radioactivity can be detected in the spinal cord and brain 3 hours later (39). Lenalidomide has demonstrated clinical activity in PCNSL, PTL, and PVRL, while pomalidomide has shown efficacy only in PCNSL and PVRL, as reported in Table 3. Its efficacy in PTL remains to be investigated.

The monoclonal antibody targeting CD20 (see Figure 3), rituximab, has been incorporated into guidelines. Although only 0.1% can cross the BBB (Table 2) (40), it plays a positive role in IP-LBCL (Table 3).

CD19-targeting CAR-T cell therapy (Figure 3) offers a novel option for IP-LBCL patients, introducing a new treatment paradigm that demonstrates unprecedented efficacy and significantly improves the prognosis of IP-LBCL patients. It has been reported that CD19 CAR-T cells can cross the BBB, but the extent of BBB penetration requires further investigation. A retrospective study leveraging the LOC network database demonstrated significantly improved clinical outcomes in the CAR-T cell therapy cohort relative to controls, with median progression-free survival (PFS) of 3 months versus not reported (NR) in controls ($p < 0.001$), and median overall survival (OS) of 4.7 months versus NR. Of the 25 CAR-T recipients, 23 (92%) developed cytokine release syndrome (CRS), while neurotoxicity events occurred in 17 patients (68%), 5 of whom (20%) experienced grade 3 or higher adverse events (41). A meta-analysis evaluating the toxicity and efficacy of CAR-T cell therapy in PCNSL revealed that 70% of PCNSL patients developed cytokine release syndrome (CRS) of any grade, including 13% with grade 3-4 severity, while 53% experienced immune effector cell-associated neurotoxicity syndrome (ICANS), with 18% classified as grade 3-4. Clinically, 56% of patients achieved complete remission (CR) and 37% maintained remission at 6 months. These findings suggest that the toxicity profile of anti-CD19 CAR-T cell therapy in PCNSL aligns with that reported in systemic diffuse large B-cell lymphoma (DLBCL), without evidence of elevated neurotoxicity. Furthermore, the therapy demonstrated robust efficacy with high rates of durable responses, supporting its safety and effectiveness in this patient population (42). Additionally, some patients experience disease progression or lack of response to CAR-T cells during infusion, relapse, or succumb to severe adverse reactions post-infusion. Enhancing the persistence of CAR-T cells *in vivo*, increasing their tumor cell-killing capacity, and reducing CRS and ICANS are current challenges that need to be addressed. There is an urgent need to develop new CAR-T products to overcome these limitations. Some clinical trials on CAR-T are detailed in Table 4.

5.3 Potential targeted drugs

Small molecule inhibitors of ROR1, bispecific antibodies, antibody-drug conjugates (ADCs), and carriers for large molecular substances have not yet been applied to IP-LBCL, but all show great clinical potential.

ROR1 small molecule inhibitors, such as KAN0441571C (Figure 3), target ATP-binding sites within the ROR1 TK domain (43) and down-regulate ROR1 signaling pathways, including non-classical Wnt pathways (PKC and PI3Kδ/AKT/mTOR) and classical Wnt/β-catenin pathways, which have been shown to

10.3389/fimmu.2025.1533444

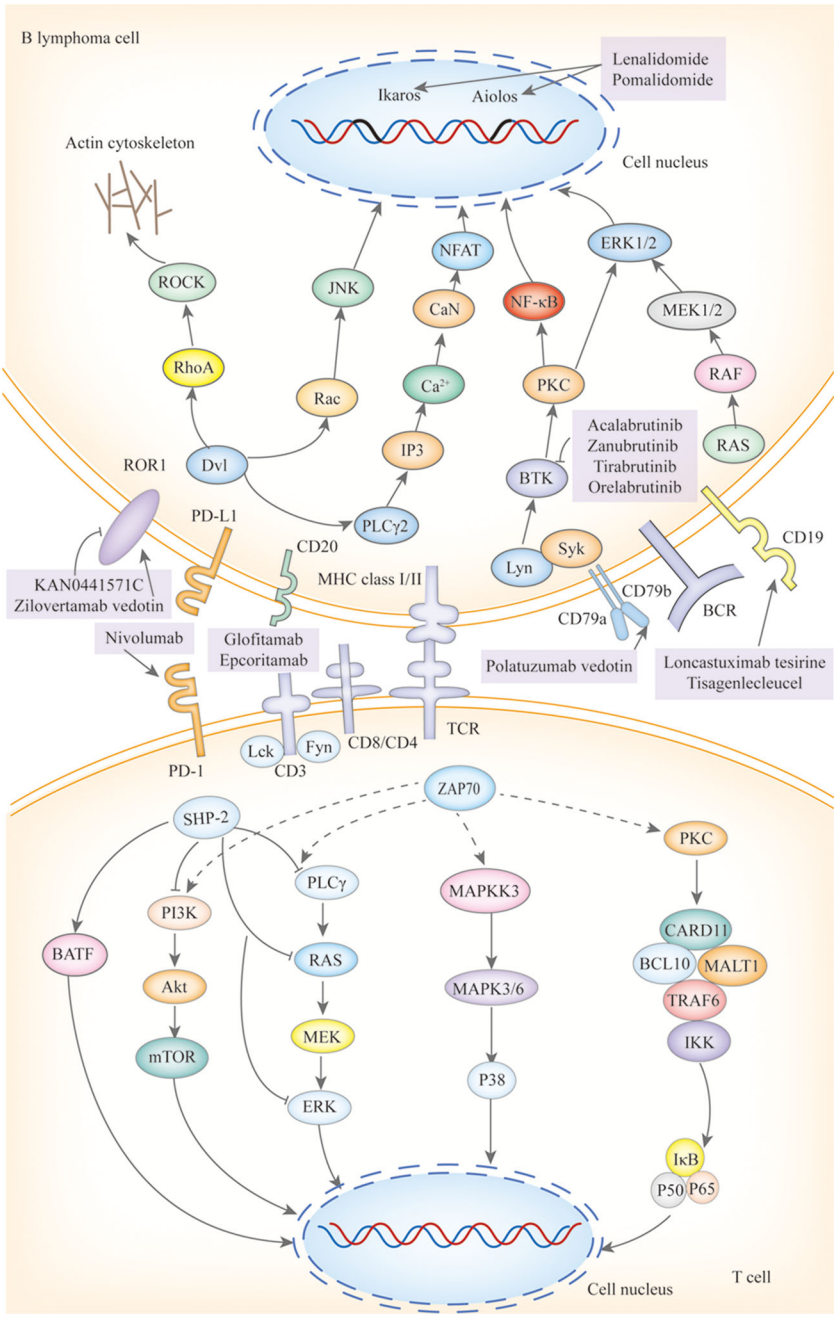

FIGURE 3
The mechanisms of action of targeted drugs and potential targeted drugs in IP-LBCL. ROR1, Receptor Tyrosine Kinase-Like Orphan Receptor 1; BCR, B-Cell Receptor; Dvl, Dishevelled; RhoA, Ras Homolog Family Member A; ROCK, Rho-Associated Coiled-Coil Kinase; Rac, Ras-Related C3 Botulinum Toxin Substrate; JNK, C-Jun N-Terminal Kinase; GSK3β, Glycogen Synthase Kinase 3 β; PI3K, Phosphatidylinositol3 kinase; Akt, Protein Kinase B; CaN, Calcineurin; PIP2, Phosphatidylinositol 4,5-Bisphosphate 3-Kinase; IP3:Inositol Triphosphate; NFAT; Nuclear Factor of Activated T Cells; Lyn, Tyrosine-Protein Kinase Lyn; Syk, Spleen Tyrosine Kinas; BTK, Bruton tyrosine kinase; PLCγ, Protein-Activated Phosphatidylinositol-Specific Phospholipase Cγ; BLNK1, B-Cell Linker Protein 1; VAV, Vav Guanine Nucleotide Exchange Factor; GRB2, Growth Factor Receptor-Bound Protein 2; SOS, Guanylate Release Factor; RAS, Rat Sarcoma; RAF, Rapidly Accelerated Fibrosarcoma; MEK1/2, Mitogen-Activated Protein Kinase Kinase 1 and 2; ERK1/2, Extracellular Regulated Protein Kinases; DAG, diglyceride; PKC, Protein Kinase C; CARD11, Caspase Recruitment Domain Containing Protein 11; BCL10, B-Cell Lymphoma 10 Protein; MALT1, Mucosa-Associated Lymphoid Tissue Lymphoma 1; TRAF, Tumor Necrosis Factor Receptor-Associated Factor; TAB2, Transforming Growth Factor-β Activated Kinase 1 Binding Protein 2; TAK1, Transforming Growth Factor Beta-Activated Kinase 1; IκB, Inhibitor of Kappa B; IKK, IκB Kinase; P50/65, NF-κB Subunits p50/p65; P100/52, NF-Kappa B Subunits p100/p52; TLR, Toll-Like Receptor; TRAM, Recombinant Translocation Associated Membrane Protein 1; MYD88, Myeloiddifferentiationfactor; IRAK, Interleukin 1 Receptor Associated Kinase; IAP, Inhibitor of Apoptosis Protein; NIK, NF-κB Inducing Kinase; JAK, Janus Kinase; STAT, Signal Transducer and Activator of Transcription; BAFF, B-cell Activating Factor of the TNF Family; IL-10R1, Interleukin-10 Receptor 1; CD, B-Cluster of Differentiation; Cluster of Differentiation 30/40; TNFR, Tumor Necrosis Factor Receptor; C-myc, Myelocellular Leukemia Oncogene; CyclinD1, Cyclin Dependent Kinase 1; PTEN, Phosphatase and Tensin Homolog; PD-L1, Programmed Cell Death Receptor 1; mTOR, MammalianTarget of Rapamycin; CIITA, MHC class II transactivator; β2M, β2-Microglobulin; ZAP70, Zeta-Chain Associated Protein Kinase 70; TCR, T-Cell Receptor; Lck, Lymphocyte-Specific Protein Tyrosine Kinase; Fyn, Src family tyrosine kinase; SHP-2, SH2 domain-containing protein-tyrosine phosphatase-2; MAPKK, Mitogen-Ativated Protein Kinase Kinase; MAPK, Mitogen-Activated Protein Kinase.

TABLE 3 Clinical Trials of Targeted Therapies for IP-LBCL.

Study	Time	Regimen	Median follow-up	Patients (n)	ORR (%)	CR (%)	OS	PFS
Bai et al. (66)	2024	BTKi combination therapy	28.7m**	26	96.2	76.9	NR* (median)	NR* (median)
Yang et al. (67)	2022	Orelabrutinib lenalidomide immunochemo-therapy	219d***	15	86.7	73.3	NR* (median)	9.8m** (median)
Maet al. (68)	2022	Pemetrexed lenalidomide	18m**	38	68.4	39.5	18m** (median)	6m** (median)
Yonezawa et al. (69)	2024	Tirabrutinib	37.1m**	44	63.6	20.5	NR* (median)	2.9m** (median)
Fox et al. (70)	2021	Thiotepa ifosfamide etoposide rituximab	21m**	27	52.0	14.8	5m**	3m** (median)
Han et al. (71)	2018	pomalidomide dexamethasone	16.5m**	25	48	20.7	-	5.3m**
Ghesquieres et al. (72)	2019	Lenalidomide rituximab	19.2m**	45	35.6	28.9	17.7m**	7.8m**

*NR: not reached; **m: months; ***d: days.

induce apoptosis of ROR1-positive DLBCL cell lines. The high ROR1 expression in IP-LBCL suggests its potential as a novel therapeutic target for IP-LBCL (11). Further research in this area is ongoing.

Bispecific antibodies (Figure 3) bridge CD3 on T cells and tumor antigens. They guide T cells to the tumor site to form an immunological synapse, triggering a cascade reaction of perforin, granzyme, and cytokine release, thereby lysing tumor cells. This reaction is independent of the interaction between MHC and T cells (43). Therefore, bispecific antibodies may still have a cytotoxic effect for IP-LBCL, which often lacks MHC and causes immune escape. The CD20×CD3 bispecific antibody glofitamab can partially penetrate the blood-brain barrier. Although the average concentration in cerebrospinal fluid is only 0.1-0.4% (40) of that in peripheral blood, it is sufficient to induce clinical and radiological responses in patients with PCNSL. Godfrey and colleagues enrolled four patients with DLBCL involving the central nervous system and administered glofitamab (median number of cycles, 6.5). Glofitamab was detected in the CSF of all four patients, with concentrations ranging from 0.00632 to 0.0296 g/mL. Moreover, CSF samples from three patients significantly induced T-cell activation (upregulation of CD25 and CD69), enhancing T-cell cytotoxicity (40).

ADCs, such as loncastuximab tesirine (an anti-CD19 antibody conjugated with a potent pyrrolobenzodiazepine), zilovertamab vedotin (an anti-ROR1 antibody conjugated with monomethyl auristatin E (MMAE)), and polatuzumab vedotin (an anti-CD79 antibody conjugated with MMAE), represent an innovative therapeutic approach that combines the targeting capability of monoclonal antibodies with the potent cytotoxicity of small molecule drugs. These ADCs induce apoptosis through four processes: targeted binding (Figure 3), internalization, toxin release, and cell killing. Currently, no ADCs have been specifically studied for IP-LBCL. IP-LBCL is a rare B-cell lymphoma with

TABLE 4 The clinical trials of CAR-T.

Study	Time	Median follow-up	Patients (n)	ORR (%)	CR (%)	OS	PFS	CRS (%)	CRS≥3 (%)	Median CRS onset	ICANS (%)	ICANS≥3 (%)	Median ICANS onset
Yu et al. (73)	2024	316d	22	90.9	68.2	NR***	NR	72.7	4.5	4d	36.4	4.5	8d
Mercadal et al. (74)	2024	26m	24	61	48	–	–	66.7	0	3.5d	33	8	6d
Frigault et al. (75)	2022	12.2m*	12	58.3	50	–	–	58.3	0	4d**	50	8	5d
Choquet et al. (41)	2024	20.8m	25	56	8	21.2m (median)	8.4m (median)	92	–	1d	68	20	1d
Karschnia et al. (76)	2023	12m	18	39	33	–	3.5m (median)	–	–	–	44.4	16.7	2.5d
Lacan et al. (77)	2023	12m	13	38	31	20m (median)	3m (median)	–	–	–	–	–	–

*m: months; **d: days; ***NR: not reached.

10.3389/fimmu.2025.1533444

TABLE 5 New prognostic model of PCNSL.

Model	Factors	Risk stratification	Prognostic value	
			median OS	median PFS
IESLG (49)	Age LDH ECOG CSF protein Deep brain structure	Low-risk	89m*	18m
		Medium-risk	23m	7m
		High-risk	6m	4m
MSKCC (49)	Age KPS	Low-risk	NR**	8.5m
		Medium-risk	23m	8.5m
		High-risk	12m	4.5m
POD18-IELSG (46)	POD18 Age Ratios to upper limits of normal for LDH ECOG CSF protein Deep brain structure	Low-risk	–	–
		Intermediate-risk		-
		High-risk		–
IELSG-M index (47)	PD-1 expression on TAMs M2/M1 Age LDH ECOG CSF protein Deep brain structure	Low-risk	NR	NR
		Intermediate-risk	29.9m	29.57m
		High-risk	11.7m	11.57m
The novel PCNSL LLR scoring system (34)	LLR Age KPS	Low-risk	74m	–
		Intermediate-risk	33m	-
		High-risk	17m	–
The Xijing model (49)	Lesion number β2-MG SIRI KPS	Low-risk	48m	10m
		Medium-risk	19m	5.5m
		High-risk	5m	3m
The two–factor prognostic model (50)	ECOG PS Albumin	Low-risk	55m	–
		Intermediate-risk	46m	–
		High-risk	23m	–
The Taipei Score (51)	Age ECOG Deep brain lesions	Low-risk	NR	3.9y***
		Intermediate-risk	3.1y	1.7y
		High-risk	NR	0.7y
		Very high-risk	NR	0.1y
The prognostic risk scoring system (52)	KPS Six mutated genes (BRD4, EBF1, BTG1, CCND3, STAG2, and TMSB4X)	Low-risk	-	-
		High-risk	–	–
The NCCS-NNI score (53)	Age Pre-steroids NLR Post-steroids NLR	Low-risk	-	-
		Medium-risk	–	–
		High-risk	-	-
Multi-omic grouping (34)	Immune state	CS1	–	–
		CS2	-	-
		CS3	–	–
		CS4	-	-

*m: months; **NR: not reached; ***y: years.

similar biological characteristics to DLBCL so that ADCs may have potential therapeutic value. Efficacy and safety data from DLBCL can provide a reference for treating IP-LBCL.

Penetrating the BBB to cross physiological barriers and enter immune-privileged sites is challenging in developing immunotherapeutic drugs for IP-LBCL. Carriers such as the transferrin receptor (TfR), CD98hc, and gold nanoparticles (AuNPs) (44) that form tight junctions have paved the way for significant molecular substances to enter these privileged areas. TfR and CD98hc are molecules expressed by brain vascular endothelium, and animal experiments have proven that TfR and CD98hc can promote the transcytosis of significant molecular substances across the BBB (45). AuNPs can temporarily increase BBB permeability through local biophysical effects generated by their interaction with laser pulses. Monoclonal antibodies, bispecific antibodies, and even ADCs in combination with TfR, CD98hc, or AuNPs seem to offer a solution to the challenge of drug penetration through the blood-brain barrier.

6 Prognosis

For PCNSL, the current recommended prognostic scoring systems are derived from the International Extranodal Lymphoma Working Group (IELSG) and the Model for Memorial Sloan-Kettering Cancer Centre (MSKCC). However, these models have their limitations. In practical clinical settings, the IELSG score may be challenging to apply for some patients due to the contraindications of lumbar puncture or the unavailability of lactate dehydrogenase (LDH) data, hindering practical prognosis evaluation. The MSKCC risk stratification, which relies solely on age and Karnofsky Performance Status (KPS), may be biased, leading to potentially inaccurate prediction outcomes. Consequently, modifications have been made to the IELSG and MSKCC scoring models. New prognostic factors have been incorporated, including 18-month progression of disease (POD18), tumor-associated macrophages, LDH levels, and lymphocyte ratios. The combination of POD18 with an improved IELSG score (age≥54 years, ECOG≥2, deep brain structure involvement, elevated CSF protein, LDH ratios above the upper limits of normal > 0.75) demonstrated robust discriminability (C-index=0.828), significantly outperforming the standard IELSG score (C-index=0.625). Similarly, the AUC for this combined model was higher than that of the IELSG (46). To validate the prognostic significance of combined tumor-associated macrophage (TAMs) related biomarkers, the expression PD-1 on TAMs and the ratio of alternatively activated macrophage (M2) to classically activated macrophages (M1) were integrated into the IELSG, resulting in the IELSG-M index. Kaplan-Meier plots indicated that the IESLG-M index more effectively stratified patients into low-, intermediate-, and high-risk prognosis subgroups than the IELSG. The areas under the receiver operating characteristic curves for IELSG-M were 0.844 for OS, surpassing the IELSG model's 0.580 (47). Furthermore, studies have revealed that while there is a significant difference in the OS rates among low-, intermediate-, and high-risk groups according to the MSKCC scoring system, the 5-year OS rate is 33.3%, 40.9% and 11.6%, respectively, the validation cohort's low - and intermediate-risk groups could not be distinguished. The novel PCNSL lactate-dehydrogenase-to-lymphocyte ratio (LLR) scoring system successfully differentiated patients in the validation cohort into low-, intermediate- and high-risk groups, with 5-year OS rates of 61.9%, 30.2%, and 11.6%, respectively (48).

Researchers have proposed several new prognostic models for PCNSL, including the Xijing model, the two-factor prediction model, the Taipei score, and the NNI-NCCS score (Table 5). The Xijing model incorporates four variables: number of lesions, β2-microglobulin (β2-MG), systemic inflammatory response index (SIRI), and KPS. Patient scores are calculated by assigning different points to these variables. A cut-off value is determined to stratify the risk. When applied to a cohort study of 72 PCNSL patients, the Xijing model demonstrated that the median OS was 48, 19, and 5 months in the low-, medium-, and high-risk groups, respectively, and the median PFS was 10, 5.5, and 3 months, respectively. These values were shorter than those obtained through IELSG and MSKCC score stratification, suggesting that the Xijing model may offer more refined prognostic stratification (49). The two-factor prognostic model is based on Eastern Cooperative Oncology Group (ECOG) PS and albumin levels (ECOG PS >1 and albumin ≤4.1), with each parameter assigned a point, categorizing newly diagnosed PCNSL patients into three risk groups (Low-risk group: 0 points; Intermediate-risk group: 1 point; High-risk group: 2 points). The 5-year survival rates for these groups were 47.5%, 36.9%, and 11.9%, respectively, showing significant OS differences. Unlike the MSKCC scoring system, which showed no statistical difference in OS between the low- and intermediate-risk groups, this two-factor model provides a simple yet effective prognostic tool for newly diagnosed PCNSL patients (50). The Taipei score is based on three risk factors: age≥80, deep brain lesions, and ECOG≥2, with each factor assigned one point. The model was used to evaluate 101 newly diagnosed PCNSL patients, with median PFS in the low-, intermediate, high-, and very high-risk groups being 3.9, 1.7, 0.7, and 0.1 years, respectively. The higher the score, the worse the OS (51). The Taipei score retains factors with prognostic value in assessing OS and PFS: Age and deep brain lesions, with 80 years as the age dividing line (50 years for MSKCC and 60 years for IELSG), and significantly differentiates the validation risk group while providing prognostic stratification for PFS and OS compared to the IELSG and MSKCC. A novel PCNSL prognostic risk-scoring system has been proposed based on KPS and six mutant genes (BRD4, EBF1, BTG1, CCND3, STAG2, and TMSB4X). Using a calculated cut-off value, patients are divided into low-risk (≤0.504) and high-risk (>0.504) groups, with the high-risk group showing significantly lower OS (52). This system enriches the understanding of the genetic mechanisms of PCNSL and offers a new method for assessing the prognostic risk. In the rituximab era, the MSKCC had a poor concordance index of 0.57. The NCCS-NNI score classifies patients into low-, medium-, and high-risk groups based on age and post-steroid neutrophil-lymphocyte ratio (NLR) and pre-steroid NLR. The 2-year mortality rates were 5%, 38% i, and 73% for the low-, medium-, and high-risk groups, respectively

(53). An increase in post-steroid NLR may serve as a biomarker for prolonged survival and a lower rate of progression after chemotherapy initiation. The NCCS-NNI score is more discriminating and better calibrated in internal validation than MSKCC and aligns more closely with modern healthcare and treatment options. Furthermore, by integrating genome-wide data from multiple omics, researchers have identified four molecular patterns in PCNSL with unique prognostic effects labeled CS1-CS4. OS was significantly different among these groups, with patients in CS4 having the most prolonged survival, substantially longer than those with CS2 and CS3, and slightly longer than those with CS1. These differences remained significant after adjusting for age and KPS. CS4 was also independently relevant when considering PFS (34). This provides a basis for future clinical stratification and targeted interventions based on subtypes.

The International Prognostic Index (IPI) is limited in its ability to stratify the prognostic of patients with PTL, necessitating the development of a more refined prognostic model. Current research has identified several factors associated with poor prognosis in PTL patients: the presence of B symptoms, specific genetic alterations such as BTG2 mutation (54), TP53 mutation, HLA deletion, a serum LDH to CSF LDH ratio of6.5 or higher (55), loss of 5-hydroxymethylcytosine (56), low T lymphocyte content or low expression of T lymphocyte characteristic genes in TME, and p53 immunohistochemical overexpression (defined as positive immunohistochemical staining of at least 50% of tumor cells in testicular tissue (57)). A molecular analysis of 25 PTL patients revealed that those with HLA mutations had a significantly worse prognosis than those with TP53 mutations (58). Leivonen et al. categorized patients into high, medium, and low groups based on the expression of 121 T lymphocyte characteristic genes. Cox multivariate analysis showed that the low expression of these genes was an independent prognostic factor, significantly correlating with poor PFS, OS, and disease-specific survival (DSS), with hazard ratios of 2.810, 3.267, and 2.910, respectively (59).

Research on the prognosis of PVRL is limited. However, one study suggested that patients with lower serum IgA levels had a higher relapse rate and lower survival rates compared to those with higher IgA levels (60).

7 Outlook

Recent research advancements have provided new perspectives for the diagnosis and treatment of IP-LBCL. The integration of genomics, proteomics, metabolomics, immunology, and radiomics with clinical features is anticipated to facilitate the development of novel, specific predictive and diagnostic biomarkers. Utilizing AI to develop new prognostic models will aid in guiding clinical decision-making.

Exploring potential therapeutic targets such as ROR1 provides direction for the development of new targeted drugs; designing and developing new antibody-based drugs based on the distinct antigen expression profiles that may exist in different types of IP-LBCL; and facilitating the transport of large molecular drugs across the BBB using carriers like TfR, CD98hc, and exosomes, or by optimizing drug molecular structures and administration methods, can all increase drug concentration and activity in immune-privileged sites. Further optimizing the structural design of CAR-T cells to enhance their targeting and persistence in immune-privileged areas and developing dual-target and multi-target CAR-T cells to overcome drug resistance and broaden the therapeutic spectrum will offer more effective treatment options for IP-LBCL patients, significantly improving their survival rates.

By combining various treatment modalities such as targeted therapy, immune checkpoint inhibitors, CAR-T cell therapy, and antibody-based drugs in a rationally personalized manner according to the genetic, protein, and immune microenvironmental characteristics of IP-LBCL patients, the combination of BTK inhibitors with PD-1/PD-L1 inhibitors may synergistically overcome tumor immune escape, enhancing the efficacy and reducing adverse reactions in IP-LBCL patients.

Given the rarity of the other three types of IP-LBCL, a comprehensive and systematic summary of these subtypes is lacking, which represents a limitation of this review.

In summary, breaking the immune escape of IP-LBCL and developing effective therapeutic strategies will pave new avenues and demonstrate a promising future for the treatment of IP-LBCL!

Author contributions

LW: Conceptualization, Data curation, Formal Analysis, Funding acquisition, Investigation, Methodology, Project administration, Resources, Software, Supervision, Validation, Visualization, Writing – original draft, Writing – review & editing. MG: Conceptualization, Data curation, Formal Analysis, Investigation, Methodology, Project administration, Resources, Software, Supervision, Validation, Visualization, Writing – original draft, Writing – review & editing. SH: Conceptualization, Data curation, Formal Analysis, Investigation, Methodology, Project administration, Resources, Software, Supervision, Validation, Visualization, Writing – review & editing.

Funding

The author(s) declare that financial support was received for the research, authorship, and/or publication of this article. This work was supported by the Fundamental Research Program of Shanxi Province (202103021223404 to LW and 202403021221260 to SH) and Research and Innovation Team Project for Scientific Breakthroughs at Shanxi Bethune Hospital (2024AOXIANG04 to LW).

Acknowledgments

All authors thank the patient's participation and agreement to publish the report.

Conflict of interest

The authors declare that the research was conducted in the absence of any commercial or financial relationships that could be construed as a potential conflict of interest.

Generative AI statement

The author(s) declare that no Generative AI was used in the creation of this manuscript.

Publisher's note

All claims expressed in this article are solely those of the authors and do not necessarily represent those of their affiliated organizations, or those of the publisher, the editors and the reviewers. Any product that may be evaluated in this article, or claim that may be made by its manufacturer, is not guaranteed or endorsed by the publisher.

Supplementary material

The Supplementary Material for this article can be found online at: https://www.frontiersin.org/articles/10.3389/fimmu.2025.1533444/full#supplementary-material

SUPPLEMENTARY TABLE 1
Pathological, molecular, and genetic changes of IP-LBCL. *DLBCL accounted for 95% of PCNSL, and the remaining pathological types accounted for 5%. **DLBCL accounted for 80-90% of PCNSL, and the remaining pathological types accounted for 10-20%.

References

1. Roschewski M, Phelan JD, Jaffe ES. Primary large B-cell lymphomas of immune-privileged sites. *Blood*. (2024) 144(25):2593–603. doi: 10.1182/blood.2023020911

2. Bairey O, Lebel E, Buxbaum C, Porges T, Taliansky A, Gurion R, et al. A retrospective study of 222 patients with newly diagnosed primary central nervous system lymphoma-outcomes indicative for improved survival overtime. *Hematol Oncol*. (2023) 41:838–47. doi: 10.1002/hon.3198

3. Ferreri AJM, Calimeri T, Cwynarski K, Dietrich J, Grommes C, Hoang-Xuan K, et al. Primary central nervous system lymphoma. *Nat Rev Dis Primers*. (2023) 9:29. doi: 10.1038/s41572-023-00439-0

4. Liu KT, Chang YC, Lin YC, Chang JL. Unusually aggressive primary testicular diffuse large B-cell lymphoma initially presenting as systemic disseminating metastases in older adult men: A case report. *Ann Med Surg (2012)*. (2023) 85:4106–11. doi: 10.1097/ms9.0000000000001018

5. Shah S, Sreenivasan S, Kancharla P, Khan C, Samhouri Y. Primary testicular lymphoma: single center experience. *Cancer Diagn Prognosis*. (2023) 3:139–44. doi: 10.21873/cdp.10192

6. Soussain C, Malaise D, Cassoux N. Primary vitreoretinal lymphoma: A diagnostic and management challenge. *Blood*. (2021) 138:1519–34. doi: 10.1182/blood.2020008235

7. Petrova TV, Koh GY. Biological functions of lymphatic vessels. *Sci (New York N.Y.)*. (2020) 369(6500):eaax4063. doi: 10.1126/science.aax4063

8. Kumaria A. Insights in primary central nervous system lymphoma: A role for glymphatics? *Brain Tumor Pathol*. (2021) 38:290–91. doi: 10.1007/s10014-021-00414-1

9. Radke J, Ishaque N, Koll R, Gu Z, Schumann E, Sieverling L, et al. The genomic and transcriptional landscape of primary central nervous system lymphoma. *Nat Commun*. (2022) 13:2558. doi: 10.1038/s41467-022-30050-y

10. Pollari M, Leivonen SK, Leppä S. Testicular diffuse large B-cell lymphoma-clinical, molecular, and immunological features. *Cancers*. (2021) 13(16):4049. doi: 10.3390/cancers13164049

11. Ghaderi A, Daneshmanesh AH, Moshfegh A, Kokhaei P, Vågberg J, Schultz J, et al. Ror1 is expressed in diffuse large B-cell lymphoma (Dlbcl) and a small molecule inhibitor of ror1 (Kan0441571c) induced apoptosis of lymphoma cells. *Biomedicines*. (2020) 8(6):170. doi: 10.3390/biomedicines8060170

12. Minderman M, Amir A, Kraan W, Schilder-Tol EJM, Oud M, Scheepstra CG, et al. Immune evasion in primary testicular and central nervous system lymphomas: hla loss rather than 9p24.1/pd-L1/pd-L2 alterations. *Blood*. (2021) 138:1194–97. doi: 10.1182/blood.2021011366

13. Twa DDW, Mottok A, Savage KJ, Steidl C. The pathobiology of primary testicular diffuse large B-cell lymphoma: implications for novel therapies. *Blood Rev*. (2018) 32:249–55. doi: 10.1016/j.blre.2017.12.001

14. Bonzheim I, Sander P, Salmerón-Villalobos J, Süsskind D, Szurman P, Gekeler F, et al. The molecular hallmarks of primary and secondary vitreoretinal lymphoma. *Blood Adv*. (2022) 6:1598–607. doi: 10.1182/bloodadvances.2021004212

15. Li J, Tang X, Luo X, Liu L, Li D, Yang L. Clinicopathological analysis and specific discriminating markers of interleukin detection in cerebrospinal fluid with primary central nervous system lymphoma: results from a retrospective study. *Ann Hematol*. (2023) 102:2153–63. doi: 10.1007/s00277-023-05301-7

16. Sun X, Lv L, Wu Y, Cui Q, Sun S, Ji N, et al. Challenges in the management of primary central nervous system lymphoma. *Crit Rev Oncology/hematol*. (2023) 188:104042. doi: 10.1016/j.critrevonc.2023.104042

17. Kuo DE, Wei MM, Knickelbein JE, Armbrust KR, Yeung IYL, Lee AY, et al. Logistic regression classification of primary vitreoretinal lymphoma versus uveitis by interleukin 6 and interleukin 10 levels. *Ophthalmology*. (2020) 127:956–62. doi: 10.1016/j.ophtha.2020.01.042

18. Huang RS, Mihalache A, Popovic MM, Cruz-Pimentel M, Pandya BU, Muni RH, et al. Diagnostic methods for primary vitreoretinal lymphoma: A systematic review. *Survey Ophthalmol*. (2024) 69:456–64. doi: 10.1016/j.survophthal.2023.12.001

19. Ambady P, Hu LS, Politi LS, Anzalone N, Barajas RFJr. Primary central nervous system lymphoma: advances in mri and pet imaging. *Ann Lymphoma*. (2021) 5:27. doi: 10.21037/aol-20-53

20. Han Y, Wang ZJ, Li WH, Yang Y, Zhang J, Yang XB, et al. Differentiation between primary central nervous system lymphoma and atypical glioblastoma based on mri morphological feature and signal intensity ratio: A retrospective multicenter study. *Front Oncol*. (2022) 12:811197. doi: 10.3389/fonc.2022.811197

21. Kumar Madaan P, Jain P, Sharma A, Malik A, Nair Misra R. Imaging of primary testicular lymphoma with unusual intraabdominal spread along the spermatic cord and gonadal vein. *Radiol Case Rep*. (2021) 16:419–24. doi: 10.1016/j.radcr.2020.12.003

22. Takase H, Arai A, Iwasaki Y, Imai A, Nagao T, Kawagishi M, et al. Challenges in the diagnosis and management of vitreoretinal lymphoma - clinical and basic approaches. *Prog Retinal Eye Res*. (2022) 90:101053. doi: 10.1016/j.preteyeres.2022.101053

23. Melli B, Gentile P, Nicoli D, Farnetti E, Croci S, Gozzi F, et al. Primary vitreoretinal lymphoma: current diagnostic laboratory tests and new emerging molecular tools. *Curr Oncol (Toronto Ont.)*. (2022) 29:6908–21. doi: 10.3390/curroncol29100543

24. Gupta T, Manjali JJ, Kannan S, Purandare N, Rangarajan V. Diagnostic performance of pretreatment 18f-fluorodeoxyglucose positron emission tomography with or without computed tomography in patients with primary central nervous system lymphoma: updated systematic review and diagnostic test accuracy meta-analyses. *Clin Lymphoma Nyeloma Leukemia*. (2021) 21:497–507. doi: 10.1016/j.clml.2021.03.011

25. Hyun Suh C, Kim HS, Ahn SS, Seong M, Han K, Park JE, et al. Body ct and pet/ct detection of extracranial lymphoma in patients with newly diagnosed central nervous system lymphoma. *Neuro-oncology*. (2022) 24:482–91. doi: 10.1093/neuonc/noab234

26. Kim HO, Kim JS, Kim S-O, Chae SY, Oh SJ, Seo M, et al. Clinicopathological characteristics of primary central nervous system lymphoma with low 18f-fludeoxyglucose uptake on brain positron emission tomography. *Medicine*. (2020) 99(20):e20140. doi: 10.1097/md.0000000000020140

27. Rozenblum L, Galanaud D, Houillier C, Soussain C, Baptiste A, Belin L, et al. 18f] Fdg pet-mri provides survival biomarkers in primary central nervous system lymphoma in the elderly: an ancillary study from the blocage trial of the loc network. *Eur J Nucl Med Mol Imaging*. (2023) 50:3684–96. doi: 10.1007/s00259-023-06334-w

28. Barajas RF, Politi LS, Anzalone N, Schöder H, Fox CP, Boxerman JL, et al. Consensus recommendations for mri and pet imaging of primary central nervous system lymphoma: guideline statement from the international primary cns lymphoma

collaborative group (Ipcg). *Neuro-oncology*. (2021) 23:1056–71. doi: 10.1093/neuonc/noab020

29. Zhai Y, Zhou X, Wang X. Novel insights into the biomarkers and therapies for primary central nervous system lymphoma. *Ther Adv Med Oncol*. (2022) 14:17588359221093745. doi: 10.1177/17588359221093745

30. Bobillo S, Crespo M, Escudero L, Mayor R, Raheja P, Carpio C, et al. Cell free circulating tumor DNA in cerebrospinal fluid detects and monitors central nervous system involvement of B-cell lymphomas. *Haematologica*. (2021) 106:513–21. doi: 10.3324/haematol.2019.241208

31. Wang X, Su W, Gao Y, Feng Y, Wang X, Chen X, et al. A pilot study of the use of dynamic analysis of cell-free DNA from aqueous humor and vitreous fluid for the diagnosis and treatment monitoring of vitreoretinal lymphomas. *Haematologica*. (2022) 107:2154–62. doi: 10.3324/haematol.2021.279908

32. Zajdel M, Rymkiewicz G, Sromek M, Cieslikowska M, Swoboda P, Kulinczak M, et al. Tumor and cerebrospinal fluid micrornas in primary central nervous system lymphomas. *Cancers*. (2019) 11(11):1647. doi: 10.3390/cancers11111647

33. Minezaki T, Usui Y, Asakage M, Takanashi M, Shimizu H, Nezu N, et al. High-throughput microrna profiling of vitreoretinal lymphoma: vitreous and serum microrna profiles distinct from uveitis. *J Clin Med*. (2020) 9(6):1844. doi: 10.3390/jcm9061844

34. Hernández-Verdin I, Kirasic E, Wienand K, Mokhtari K, Eimer S, Loiseau H, et al. Molecular and clinical diversity in primary central nervous system lymphoma. *Ann Oncol*. (2023) 34:186–99. doi: 10.1016/j.annonc.2022.11.002

35. Chen T, Liu Y, Wang Y, Chang Q, Wu J, Wang Z, et al. Evidence-based expert consensus on the management of primary central nervous system lymphoma in China. *J Hematol Oncol*. (2022) 15:136. doi: 10.1186/s13045-022-01356-7

36. Ai L, Xu A, Xu J. Roles of pd-1/pd-L1 pathway: signaling, cancer, and beyond. *Adv Exp Med Biol*. (2020) 1248:33–59. doi: 10.1007/978-981-15-3266-5_3

37. Nayak L, Iwamoto FM, Lacasce A, Mukundan S, Roemer MGM, Chapuy B, et al. Pd-1 blockade with nivolumab in relapsed/refractory primary central nervous system and testicular lymphoma. *Blood*. (2017) 129:3071–73. doi: 10.1182/blood-2017-01-764209

38. Goldfinger M, Xu M, Bertino JR, Cooper DL. Checking in on lenalidomide in diffuse large B cell lymphoma. *Clin Lymphoma Nyeloma Leukemia*. (2019) 19:e307–e11. doi: 10.1016/j.clml.2019.02.012

39. Gozzetti A, Cerase A. Novel agents in cns myeloma treatment. *Cent Nervous Syst Agents Ned Chem*. (2014) 14:23–7. doi: 10.2174/1871524914999140818111514

40. Godfrey JK, Gao L, Shouse G, Song JY, Pak S, Lee B, et al. Glofitamab stimulates immune cell infiltration of cns tumors and induces clinical responses in secondary cns lymphoma. *Blood*. (2024) 144:457–61. doi: 10.1182/blood.2024024168

41. Choquet S, Soussain C, Azar N, Morel V, Metz C, Ursu R, et al. Car T-cell therapy induces a high rate of prolonged remission in relapsed primary cns lymphoma: real-life results of the loc network. *Am J Hematol*. (2024) 99:1240–49. doi: 10.1002/ajh.27316

42. Cook MR, Dorris CS, Makambi KH, Luo Y, Munshi PN, Donato M, et al. Toxicity and efficacy of car T-cell therapy in primary and secondary cns lymphoma: A meta-analysis of 128 patients. *Blood Adv*. (2023) 7:32–9. doi: 10.1182/bloodadvances.2022008525

43. Li L, Huang W, Ren X, Wang Z, Ding K, Zhao L, et al. Unlocking the potential: advancements and future horizons in ror1-targeted cancer therapies. *Sci China Life Sci*. (2024) 67(12):2603–16. doi: 10.1007/s11427-024-2685-9

44. Li X, Vemireddy V, Cai Q, Xiong H, Kang P, Li X, et al. Reversibly modulating the blood-brain barrier by laser stimulation of molecular-targeted nanoparticles. *Nano Lett*. (2021) 21:9805–15. doi: 10.1021/acs.nanolett.1c02996

45. Pornnoppadol G, Bond LG, Lucas MJ, Zupancic JM, Kuo YH, Zhang B, et al. Bispecific antibody shuttles targeting cd98hc mediate efficient and long-lived brain delivery of iggs. *Cell Chem Biol*. (2024) 31:361–72.e8. doi: 10.1016/j.chembiol.2023.09.008

46. Du KX, Shen HR, Pan BH, Luthuli S, Wang L, Liang JH, et al. Prognostic value of pod18 combined with improved ielsg in primary central nervous system lymphoma. *Clin Trans Oncol*. (2024) 26:720–31. doi: 10.1007/s12094-023-03292-5

47. Sun X, Wang C, Chen C, Huang J, Wu X, Wang Y, et al. Combined tumor-associated macrophages biomarker predicting extremely poor outcome of patients with primary central nervous system lymphoma. *Hematol Oncol*. (2021) 39:625–38. doi: 10.1002/hon.2926

48. Gao Y, Wei L, Kim SJ, Wang L, He Y, Zheng Y, et al. A novel prognostic marker for primary cns lymphoma: lactate dehydrogenase-to-lymphocyte ratio improves stratification of patients within the low and intermediate mskcc risk groups. *Front Oncol*. (2021) 11:696147. doi: 10.3389/fonc.2021.696147

49. Wu Z, Wang C, Lyu Y, Lin Z, Lu M, Wang S, et al. A novel inflammation-related prognostic model for predicting the overall survival of primary central nervous system lymphoma: A real-world data analysis. *Front Oncol*. (2023) 13:1104425. doi: 10.3389/fonc.2023.1104425

50. Wei L, Gao Y, Prochazka KT, Liu R, Wang L, Liu B, et al. A novel prognostic model based on pretreatment serum albumin and ecog ps for primary cns lymphoma: an international, multi-center study. *J Neuro-oncol*. (2023) 163:301–11. doi: 10.1007/s11060-023-04337-z

51. Liu CJ, Lin SY, Yang CF, Yeh CM, Kuan AS, Wang HY, et al. A new prognostic score for disease progression and mortality in patients with newly diagnosed primary cns lymphoma. *Cancer Med*. (2020) 9:2134–45. doi: 10.1002/cam4.2872

52. Yuan X, Yu T, Zhao J, Jiang H, Hao Y, Lei W, et al. Analysis of the genomic landscape of primary central nervous system lymphoma using whole-genome sequencing in chinese patients. *Front Med*. (2023) 17:889–906. doi: 10.1007/s11684-023-0994-x

53. Lo YT, Lim VY, Ng M, Tan YH, Chiang J, Chang EWY, et al. A prognostic model using post-steroid neutrophil-lymphocyte ratio predicts overall survival in primary central nervous system lymphoma. *Cancers*. (2022) 14(7):1818. doi: 10.3390/cancers14071818

54. Guo D, Hong L, Ji H, Jiang Y, Lu L, Wang X, et al. The mutation of btg2 gene predicts a poor outcome in primary testicular diffuse large B-cell lymphoma. *J Inflammation Res*. (2022) 15:1757–69. doi: 10.2147/jir.S341355

55. Liu YZ, Luo P, Liu C, Xue K, Jin J, Xia ZG, et al. Prognostic significance of ldh ratio in serum/cerebral spinal fluid of patients with primary testicular diffuse large B-cell lymphoma. *OncoTargets Ther*. (2019) 12:10469–75. doi: 10.2147/ott.S228746

56. Shen Y, Wang L, Ou J, Wang B, Cen X. Loss of 5-hydroxymethylcytosine as a poor prognostic factor for primary testicular diffuse large B-cell lymphoma. *Int J Med Sci*. (2022) 19:225–32. doi: 10.7150/ijms.65517

57. Hatzl S, Posch F, Schulz E, Gornicec M, Deutsch A, Beham-Schmid C, et al. The role of immunohistochemical overexpression of P53 as adverse prognostic factor in primary testicular diffuse large B cell lymphoma. *Pathol Oncol Res: POR*. (2020) 26:2831–33. doi: 10.1007/s12253-020-00864-6

58. Zhang W, Yang P, Yang Y, Liu S, Xu Y, Wu C, et al. Genomic landscape and distinct molecular subtypes of primary testicular lymphoma. *J Trans Med*. (2024) 22:414. doi: 10.1186/s12967-024-05140-8

59. Leivonen SK, Pollari M, Brück O, Pellinen T, Autio M, Karjalainen-Lindsberg ML, et al. T-cell inflamed tumor microenvironment predicts favorable prognosis in primary testicular lymphoma. *Haematologica*. (2019) 104:338–46. doi: 10.3324/haematol.2018.200105

60. Tsubota K, Usui Y, Goto H. Identification of prognostic markers in patients with primary vitreoretinal lymphoma by clustering analysis using clinical data. *J Clin Med*. (2020) 9(7):2298. doi: 10.3390/jcm9072298

61. Zhang Y, Li Y, Zhuang Z, Wang W, Wei C, Zhao D, et al. Preliminary evaluation of zanubrutinib-containing regimens in dlbcl and the cerebrospinal fluid distribution of zanubrutinib: A 13-case series. *Front Oncol*. (2021) 11:760405. doi: 10.3389/fonc.2021.760405

62. Yu H, Kong H, Li C, Dong X, Wu Y, Zhuang Y, et al. Bruton's tyrosine kinase inhibitors in primary central nervous system lymphoma-evaluation of anti-tumor efficacy and brain distribution. *Trans Cancer Res*. (2021) 10:1975–83. doi: 10.21037/tcr-21-50

63. Van Bussel MTJ, Beijnen JH, Brandsma D. Intracranial antitumor responses of nivolumab and ipilimumab: A pharmacodynamic and pharmacokinetic perspective, a scoping systematic review. *BMC Cancer*. (2019) 19:519. doi: 10.1186/s12885-019-5741-y

64. Ogiya D, Murayama N, Kamiya Y, Saito R, Shiraiwa S, Suzuki R, et al. Low cerebrospinal fluid-to-plasma ratios of orally administered lenalidomide mediated by its low cell membrane permeability in patients with hematologic Malignancies. *Ann Hematol*. (2022) 101:2013–19. doi: 10.1007/s00277-022-04893-w

65. Li Z, Qiu Y, Personett D, Huang P, Edenfield B, Katz J, et al. Pomalidomide shows significant therapeutic activity against cns lymphoma with a major impact on the tumor microenvironment in murine models. *PloS One*. (2013) 8:e71754. doi: 10.1371/journal.pone.0071754

66. Bai S-J, He J-X, Zheng Y-J, Geng Y, Gao Y-N, Zhang C-X, et al. Clinical characteristics and prognosis of patients with newly diagnosed primary central nervous system lymphoma: A multicenter retrospective analysis. *Ann Hematol*. (2024) 103(11):4649–60. doi: 10.1007/s00277-024-05797-7

67. Yang C, Cui Y, Ren X, Li M, Yu K, Shen S, et al. Orelabrutinib combined with lenalidomide and immunochemotherapy for relapsed/refractory primary central nervous system lymphoma: A retrospective analysis of case series. *Front Oncol*. (2022) 12:901797. doi: 10.3389/fonc.2022.901797

68. Ma J, Lin Z, Ding T, Li Q, Zhang M, Kang H, et al. Pemetrexed plus lenalidomide for relapsed/refractory primary central nervous system lymphoma: A prospective single-arm phase ii study. *Front Oncol*. (2022) 12:938421. doi: 10.3389/fonc.2022.938421

69. Yonezawa H, Narita Y, Nagane M, Mishima K, Terui Y, Arakawa Y, et al. Three-year follow-up analysis of phase 1/2 study on tirabrutinib in patients with relapsed or refractory primary central nervous system lymphoma. *Neuro-oncol Adv*. (2024) 6:vdae037. doi: 10.1093/noajnl/vdae037

70. Fox CP, Ali AS, Mcilroy G, Thust S, Martinez-Calle N, Jackson AE, et al. A phase 1/2 study of thiotepa-based immunochemotherapy in relapsed/refractory primary cns lymphoma: the tier trial. *Blood Adv*. (2021) 5:4073–82. doi: 10.1182/bloodadvances.2021004779

71. Tun HW, Johnston PB, Deangelis LM, Atherton PJ, Pederson LD, Koenig PA, et al. Phase 1 study of pomalidomide and dexamethasone for relapsed/refractory primary cns or vitreoretinal lymphoma. *Blood*. (2018) 132:2240–48. doi: 10.1182/blood-2018-02-835496

72. Ghesquieres H, Chevrier M, Laadhari M, Chinot O, Choquet S, Moluçon-Chabrot C, et al. Lenalidomide in combination with intravenous rituximab (Revri) in relapsed/refractory primary cns lymphoma or primary intraocular lymphoma: A multicenter prospective 'Proof of concept' Phase ii study of the french oculo-cerebral

lymphoma (Loc) network and the lymphoma study association (Lysa)†. *Ann Oncol*. (2019) 30:621–28. doi: 10.1093/annonc/mdz032

73. Yu W, Huang L, Mei H, Li Y, Niu T, Zou D, et al. Real-world experience of commercial relmacabtagene autoleucel (Relma-cel) for relapsed/refractory central nervous system lymphoma: A multicenter retrospective analysis of patients in China. *J Immunother Cancer*. (2024) 12(5):e008553. doi: 10.1136/jitc-2023-008553

74. Mercadal S, Ahn KW, Allbee-Johnson M, Ganguly S, Geethakumari PR, Hong S, et al. Outcomes of patients with primary central nervous system lymphoma following cd19-targeted chimeric antigen receptor T-cell therapy. *Haematologica*. (2024) 110 (1):218–21. doi: 10.3324/haematol.2024.285613

75. Frigault MJ, Dietrich J, Gallagher K, Roschewski M, Jordan JT, Forst D, et al. Safety and efficacy of tisagenlecleucel in primary cns lymphoma: A phase 1/2 clinical trial. *Blood*. (2022) 139:2306–15. doi: 10.1182/blood.2021014738

76. Karschnia P, Arrillaga-Romany IC, Eichler A, Forst DA, Gerstner E, Jordan JT, et al. Neurotoxicity and management of primary and secondary central nervous system lymphoma after adoptive immunotherapy with cd19-directed chimeric antigen receptor T-cells. *Neuro-oncology*. (2023) 25:2239–49. doi: 10.1093/neuonc/noad118

77. Lacan C, Caron J, Tarantino N, Fouquet B, Cherai M, Parizot C, et al. Car T-cell therapy for central nervous system lymphomas: blood and cerebrospinal fluid biology, and outcomes. *Haematologica*. (2023) 108:3485–90. doi: 10.3324/haematol.2023.282875

frontiers | Frontiers in Immunology

TYPE Case Report
PUBLISHED 08 May 2025
DOI 10.3389/fimmu.2025.1567149

OPEN ACCESS

EDITED BY
Hamid Reza Mirzaei,
University of Texas MD Anderson Cancer Center, United States

REVIEWED BY
Reshmi Parameswaran,
Case Western Reserve University, United States
Roman H. Khadka,
University of Pennsylvania, United States

*CORRESPONDENCE
Hong Liu
hongliu63@126.com
Han Wang
wwhh1991@aliyun.com

RECEIVED 26 January 2025
ACCEPTED 14 April 2025
PUBLISHED 08 May 2025

CITATION
Huang Y, Gong Y, Liu X, Ruan H, Lu J, Kouros-Mehr H, Liu H and Wang H (2025) Case Report: Bispecific CD20/CD30-targeted chimeric antigen receptor T-cell therapy for non-Hodgkin's lymphoma.
Front. Immunol. 16:1567149.
doi: 10.3389/fimmu.2025.1567149

Case Report: Bispecific CD20/CD30-targeted chimeric antigen receptor T-cell therapy for non-Hodgkin's lymphoma

Yuejiao Huang[1], Yiming Gong[2], Xiang Liu[2], Huaying Ruan[3], Jinhua Lu[2], Hosein Kouros-Mehr[4], Hong Liu[1*] and Han Wang[5*]

[1]Department of Hematology, Affiliated Hospital of Nantong University, Nantong, China, [2]TriArm Therapeutics (Shanghai), Shanghai, China, [3]Shanghai First Song Therapeutics, Shanghai, China, [4]TriArm Inc., San Mateo, CA, United States, [5]Department of General Surgery, Affiliated Hospital of Nantong University, Nantong, China

CD19-directed CAR T-cell therapy is a breakthrough immunotherapy for B-cell malignancies. However, CD19 loss-mediated relapsed/refractory disease continues to pose a significant challenge, highlighting the urgent need for CAR T cells targeting alternative antigens. To address this issue, we developed a CD20-directed CAR T incorporated with an additional CD30-directed binder to enhance cytotoxicity toward cancer cells. Here, we report that a patient with bulky transformed follicular lymphoma was successfully treated with CD20/CD30-directed CAR-T cells. The patient received two doses of anti-CD20/CD30-CAR-T therapy administered one month apart. Complete metabolic remission was achieved 1 month after the first infusion without evidence of cytokine release syndrome (CRS) or immune effector cell-associated neurotoxicity syndrome (ICANS). The second dose was given as a consolidation therapy with sustained disease-free survival exceeding 12 months to date. The report underscores the promising therapeutic potential and safety profile of CD20/CD30-directed CAR T-cell therapy.

Clinical Trial Registration: https://www.clinicaltrials.gov, identifier NCT06756321.

KEYWORDS

CAR T-cell therapy, transformed follicular lymphoma, CD20, CD30, bispecific CAR T

Introduction

Chimeric antigen receptor (CAR) T-cell therapy has transformed the clinical landscape of hematologic malignancies. Currently, FDA has approved 5 CAR T-cell products for the management of B-cell malignancies, demonstrating remarkable efficacy with an overall remission of 71-81% in B-cell acute lymphoblastic leukemia (1–3), and 52-97% in B-cell

non-Hodgkin lymphoma (B-NHL) (4–10). Despite the high initial response rate, relapsed or refractory disease following CAR T still represents a challenge, with subsequent salvage treatments providing less than 3 months of progression-free survival benefit (11). The loss of CD19 antigen, which is the target of all 5 commercial products, was reported as one of the major contributors to disease relapse (12–16), emphasizing the need for alternative targets to be explored.

CD20 is a B cell marker universally expressed on the surface of normal B cells and most mature B-cell malignancies. For several years, CD20-targeted therapy involving monoclonal antibodies and T cell engagers have served as the cornerstone in the management of B-NHL. In clinical trials, CD20-targeted CAR T-cell therapies have exhibited potent anti-lymphoid effect in various B-NHL cancers (17–22), particularly in cases of relapsed or refractory disease following CD19-directed CAR T treatment (17, 22). In one study, anti-CD20 CAR T-cell therapy generated a complete remission rate of 57.1% even after failure of anti-CD19 CAR-T treatment (17), which is comparable to the efficacy in CAR T-naïve NHLs (4, 7, 9). The above studies suggested that CD20 could be a promising target for CAR T development.

CD30 is mostly found to express in a subset of activated lymphocytes and lymphomas, including classical Hodgkin lymphoma (cHL), anaplastic large-cell lymphoma (ALCL) (23, 24). Brentuximab Vedotin (BV), a CD30-targeted antibody drug conjugate, has been approved for the treatment and maintenance of cHL, and for combo therapy with lenalidomide and rituximab against large B-cell lymphoma. Given its success in various lymphoid malignancies, CD30 has emerged as a promising target for CAR T-cell therapy. Most anti-CD30-CAR T-cell studies have demonstrated remarkable efficacy against $CD30^+$ lymphomas, with objective response rates ranging from 37.5% to 91.7% (25–29). Notably, Kochenderfer et al. reported a 43% transient anti-lymphoid response in $CD30^+$ lymphomas, with extensive rash and prolonged hematologic toxicities (30). Despite these challenges, anti-CD30-CAR-T have shown clinical responses in some $CD30^+$ lymphomas, solidifying CD30 as a compelling target for further CAR T-cell development.

Multi-specific CAR T is a potential strategy to enhance the potency of CAR T-cell therapies. By targeting 2 or more antigens on tumor cells, tumor microenvironment (TME), or immune cells, multi-specific CAR design can potentially prevent antigen escape-mediated relapse (12, 31–36), remodel the tumor microenvironment (37–39), boost CAR T-cell expansion (40), and enhance CAR T-cell function (41). In 2019, Aben et al. reported that co-targeting of CD30 in CEA- and TAG72-targeted CAR T cells enhanced T cell activity against CD30-negative tumor cells via elimination of $CD30^+$ T cells, which suppress the cytotoxic T cell response. Moreover, CD30 is expressed in 10-30% of NHL cancers (42–44). Beyond the direct activity against $CD30^+$ NHL, BV combined therapy with rituximab, a CD20-targeted agents, produce robust clinical response in large B-cell lymphoma regardless of CD30 expression (45, 46), suggesting a potential synergistic antitumor effects with CD20/CD30 dual targeting therapies. The dual-targeting strategy may improve therapeutic outcomes and reduce the risk of relapse due to antigen escape.

Therefore, we developed a CAR T-cell product targeting both CD20 and CD30, for patients with relapsed/refractory B-cell non-Hodgkin lymphoma, including patients who progressed following conventional CD19-targeted CAR T cells. Here we report a case using the CD20/CD30 bispecific CAR T to treat a bulky transformed follicular lymphoma.

Case description

A 60-year-old female patient with extensive lymphadenopathy (cervical, supraclavicular and abdominal nodes) was diagnosed with grade 1 follicular lymphoma (stage III) in January 2019 (Figure 1A). She was first treated with 6 cycles rituximab combined with cyclophosphamide, pirarubicin, vincristine, and prednisone (R-CHOP) and then obtained a partial response by CT-scan. As the patient had no symptoms at the time, she refused further treatment.

The first relapse occurred approximately 3 months after the last chemotherapy. She developed right inguinal lymphadenopathy, and further core needle aspiration revealed a B cell lymphoma with the following immunohistochemistry (IHC) results: CD20+ (3+), CD30-, Bcl-2+ (3+), Bcl-6+ (3+), Ki-67+ (40%+), and MUM1-. She was subsequently treated with R-GemOx (consisting of rituximab, gemcitabine and oxaliplatin). Two months into her treatment, her abdominal lymph nodes have significantly reduced in size, but there has been little change in the lesions in other areas. Unfortunately, PET-CT scans after 7 cycles R-GemOx demonstrated progressive disease with enlarged lymph nodes and increased FDG uptake (Deauville 5) in left cervical, left supraclavicular, left axilla, para-aortic, presacral, left obturator, right inguinal, and left gluteal intermuscular area. The treatment was then switched to R-DHAP (Rituximab, Dexamethasone, High-dose Cytarabine, Cisplatin) but was discontinued due to intolerance. Rituximab combined with lenalidomide (R2 regimen) was then administered for 5 cycles. No further treatment or evaluation was performed.

Approximately 1.5 years later, the patient was admitted with left gluteal pain and limited physical activity for 7 months. Her MRI scan showed an occupying lesion (73×66 mm) in the left gluteus maximus and partial mid-arm muscle area. The third pathological investigation revealed non-germinal center B cell like (GCB) diffuse large B cell lymphoma (DLBCL) with invasion of striated muscle tissue, positive for Bcl-2 (90%+), Bcl-6 (60%+), CD20 (3+), Ki67 (80%+), MUM1 (80%+) and c-myc (50%+). PET-CT showed a bulky mass (68×64×101mm) in the left buttocks with increased SUV uptake (SUVmax=30) and an enlarged left inguinal lymph node with slightly increased SUV uptake (SUVmax=5.6). Similarly, the extremely high LDH concentration (>3 × upper limit of normal) also reflected an extensive tumor burden. In light of the patient's history of FL, this DLBCL was diagnosed as a transformed lymphoma.

Due to ineffective treatment approaches, the patient visited the affiliated hospital of Nantong University in search of a CAR

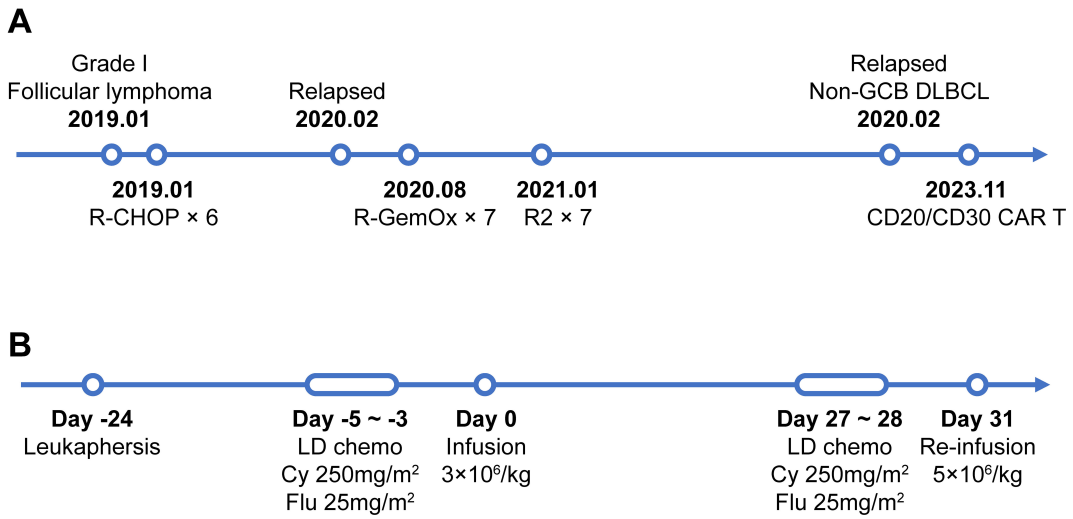

FIGURE 1
The timeline of patients' treatment and trial intervention. **(A)** Flow chart of the disease process and therapeutic modalities before CAR T treatment. **(B)** The timeline of CAR T preparation and administration from leukapheresis to the 2nd dose of CAR T infusion. Abbreviations: Non-GCB DLBCL, Non-germinal center diffuse large B cell lymphoma; LD chemo, lymphodepleting chemotherapy; Cy, cyclophasphomide; Flu, fludarabine.

T-cell therapy. Immunohistochemistry (IHC) analysis revealed diffuse positivity for CD20, partial positivity (80%) for CD19, and scattered/weak positivity for CD30 in the tumor cells (Supplementary Figure S1). Following a comprehensive discussion of available therapies, the patient opted to participate in an investigator-initiated clinical trial of tandem anti-CD20/CD30 CAR T-cell therapy (NCT No.: NCT06756321) instead of pursuing CD19-directed CAR T-cell therapy. Leukapheresis was successfully performed and peripheral blood mononuclear cells (PBMCs) were collected for manufacturing the 3rd generation tandem anti-CD20/CD30 CAR T-cells (The CAR construct and characterization is given in Supplementary Figure S2). After a mild lymphodepleting chemotherapy (cyclophosphamide 250mg/m^2 d1-d3, fludarabine 25mg/m^2 d1-d3), a total dose of 1.7×10^8 CAR T-cells (3×10^6/kg) were then infused (Figure 1B).

Following the infusion, her left gluteal pain was soon relieved and no longer affected her daily life. In parallel, the serum LDH remarkably decreased and returned to normal range within 2 weeks (Figure 2A). At month 1 after infusion, PET-CT showed a clear regression of FDG uptake in the left buttocks and inguinal lymph node (Figure 3). Notably, the patient did not experience cytokine release syndrome (CRS) or neurotoxicity or notable changes in inflammatory markers or cytokines (Figures 2B–D) despite a rapid therapeutic response. Except hematologic toxicity (Grade 4 lymphocytopenia and grade 3 neutropenia), no other adverse events were observed.

After T cell infusion, CAR T expansion was analyzed at the indicated time points via quantitative polymerase chain reaction (qPCR). As demonstrated in Figure 4A, CAR T-cells began to expand *in vivo* after 3 days, peaked on day 7 and then gradually decreased, with a Cmax of 11,228.9 CAR copies/μg DNA. Meanwhile, circulating B cells remained at extremely low levels after infusion.

At month 1, the patient experienced complete metabolic response and had hypometabolic lesions (Deaville score 3). Considering that circulating CAR T cells were no longer detectable at month 1 and the patient still experienced mild edema in the left gluteus maximus (with the possibility of residual tumor), an additional 2.8×10^8 CAR T-cells (5×10^6/kg) were given as a consolidative treatment following a reduced-dose LD regimen (cyclophosphamide 250mg/m^2 d1-d2, fludarabine 25mg/m^2 d1-d2) (Figure 1B). Although the patient developed mild fever and fatigue after reinfusion, the 2nd CAR T failed to engraft with minimal levels of CAR copies detected in the peripheral blood (Figure 4A). B cells, neutrophils, and lymphocytes began to rebound 1 month after the 2nd CAR T re-infusion (Figures 4B, C). At month 2, the patient continued to have complete metabolic response which was maintained for approximately 12 months following initial CAR T infusion (Figure 3).

Discussion

Here we report the treatment of a relapsed/refractory transformed follicular lymphoma patient with anti-CD20/CD30 bispecific CAR T-cells. The treatment was well tolerated with no CRS or ICANS and expected hematologic toxicities. Peak levels of CAR-T cells occurred on day 7 following CAR T-cell infusion and the patient reached CMR at 1 month, which was maintained for over 12 months following infusion.

In this case, while the 1st CAR T infusion expanded significantly *in vivo*, the 2nd consolidative CAR T cells appeared to fail to engraft. While re-infusion often exhibiting poor expansion and suboptimal efficacy (47, 48), CAR T-cell expansion is in general related with

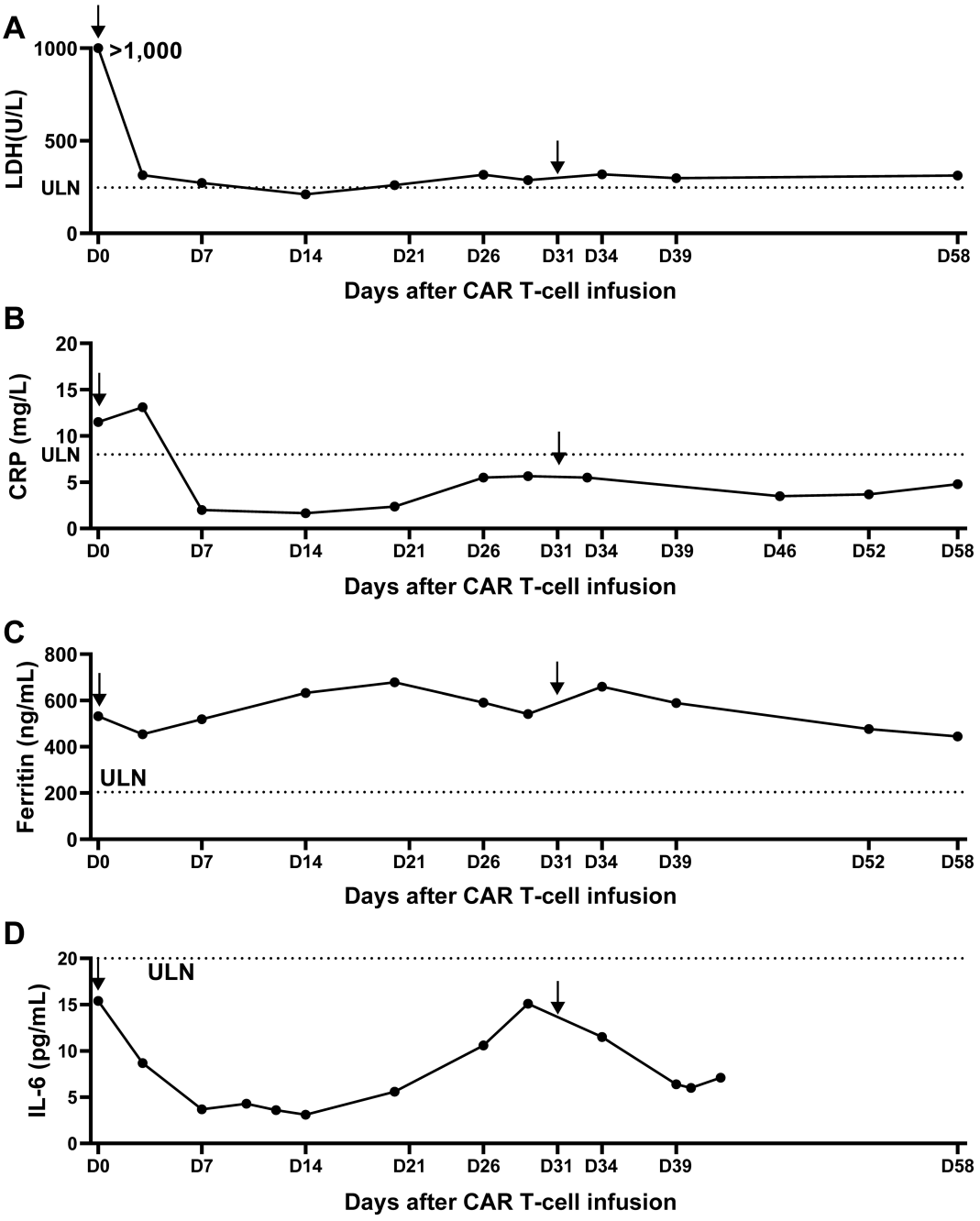

FIGURE 2
Measurement of lactate dehydrogenase and CRS-related indicators over 2 months after anti-CD20/CD30-CAR-T infusion. **(A)** The serum lactate dehydrogenase (LDH) was remarkably decreased after CAR T infusion. **(B-D)** Serum C-reactive protein **(B)**, serum ferritin **(C)** and IL-6 **(D)** showed no significant changes over the first 2 months after CAR T infusion, consistent with the absence of CRS. Arrow indicates the timepoint of CAR T infusion and the doted lines indicate the lower limits of normal ranges.

various factors, including target antigen burden and CAR design. Following the 1st CAR T dosed, the patient experienced rapid resolution of symptoms, accompanied by normalization of LDH levels within 2 weeks. The PET-CT scan confirmed a complete metabolic response at Month 1. The absence of target antigen may explain both the failed expansion of the 2nd CAR T dose and the rapid disappearance of the 1st CAR T cells from Day 14 to Month 1. Furthermore, CD30 has been reported to be expressed on activated T cells (24). The introduction of an additional anti-CD30 CAR might have induced fratricide during late-phase of CAR T expansion, contributing to their poor persistence. Notably, the suboptimal CAR T persistence did not compromise tumor control in this case - a finding seemingly contradictory to the conventional paradigm that durable tumor control requires long-

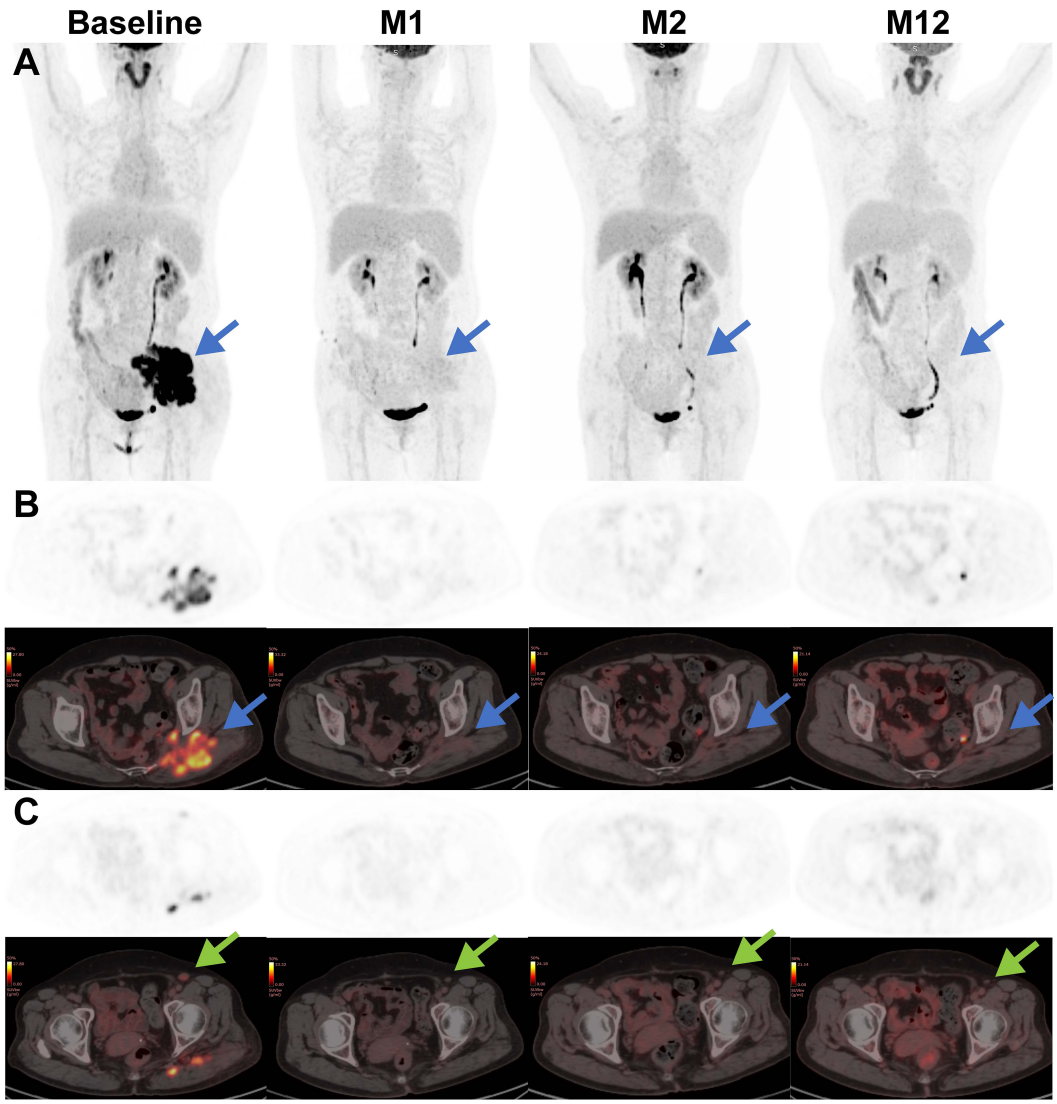

FIGURE 3
Representative coronal-view and axial-view images of serial 18F-FDG PET/CT scans before and after CAR T treatment. The baseline PET-CT shows a bulky mass (blue arrow) in the left buttocks with SUVmax of 30 and an enlarged left inguinal lymph node (green arrow) with SUVmax of 5.6. After CAR T infusion, the lymphoma lesions showed a rapid decrease in metabolic activity and a slow reduction in size, supporting the conclusion of complete remission. **(A)** Maximum intensity projection PET images; **(B)** axial images of lymphoma lesion in the left buttocks; **(C)** axial images of enlarged left inguinal lymph node.

term CAR T persistence. Further studies may provide more insights on expansion and persistence of anti-CD20-CD30 CAR T cells vs clinical responses.

It has been well-established that CD30 is a biomarker of classic Hodgkin lymphoma (cHL) (49). In contrast, CD30 expression can be detected at various frequencies in NHL, including primary mediastinal B-cell lymphoma (PMBCL) (50) and mediastinal gray-zone lymphoma (MGZL) (51). BV monotherapy in NHL has been disappointing. However, the combination of BV and rituximab plus lenalidomide had a significant improvement in overall survival compared with rituximab and lenalidomide plus placebo in patients with relapsed and refractory DLBCL (45, 46). The overall survival benefit suggests potential synergy of CD20- and CD30-targeted treatment in NHL. The quick metabolic response in our case after bispecific anti-CD20-CD30 CAR T cell infusion seems consistent with this hypothesis.

Bispecific CAR T has several advantages over monospecific CAR-T. First, bispecific anti-CD20 and -CD30 CAR-T can be administered to patients with NHL and HL because expression of CD20 and CD30 can be detected in both diseases. Second, multi-specific CAR-T may potentially mitigate antigen escape mediated tumor relapse (52, 53), which is frequently observed after

10.3389/fimmu.2025.1567149

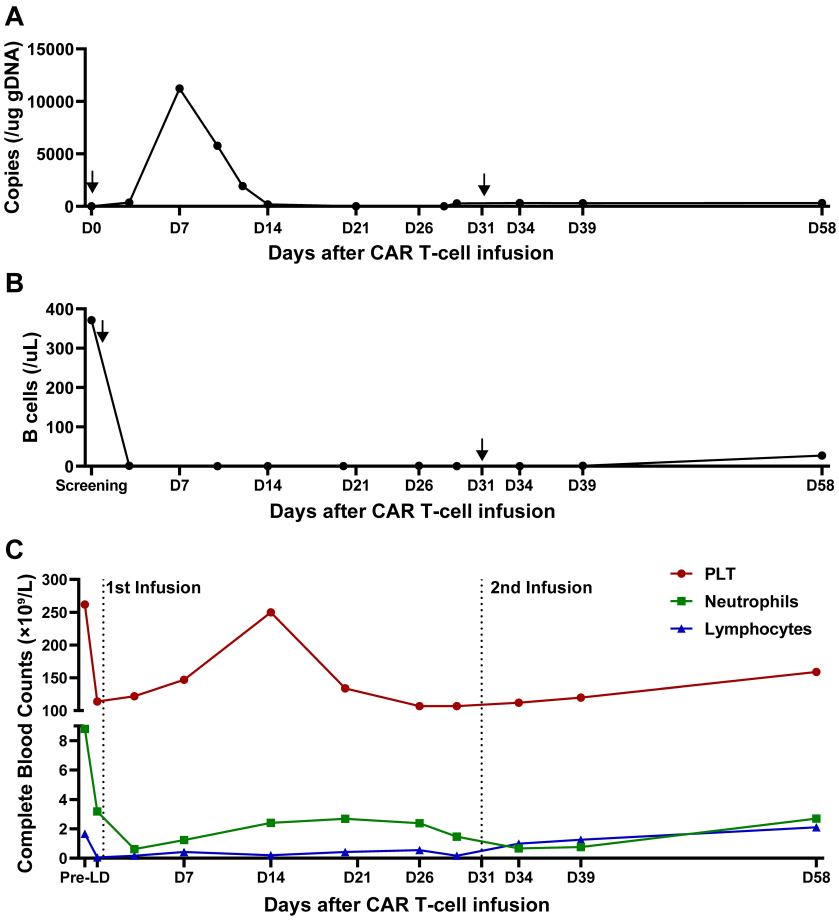

FIGURE 4
CAR T cells and other blood cells dynamics after infusion. **(A)** Quantification of anti-CD20/CD30 CAR copies detected by qPCR after infusion. Arrows indicate the timepoint of CAR T infusion. **(B)** B cell reconstitution after CAR T infusion. Data is shown as B cell counts detected by flow cytometry in peripheral blood. Arrows indicate the timepoint of CAR T infusion. **(C)** The recovery of platelet counts, absolute neutrophil counts and absolute lymphocyte counts during CAR T treatment. Dot lines indicate the timepoint of CAR T infusion.

monospecific CAR T treatment in clinical trials. However, multi-targeting CAR-T may also have its drawbacks. The clinical efficacy of dual-targeting CAR T-cell therapy has been inconsistent. Several studies have reported that CD19/CD22 dual-targeting CAR T cells exhibit non-superior objective response rates and shorter response durations in ALL or LBCL, potentially due to inadequate CAR T-cell persistence or pharmacokinetics (12, 54, 55). Furthermore, multi-targeting CAR T-cell may potentially result in the loss of multiple targetable antigens (12, 56, 57), thereby restricting further therapeutic options. Another concern is that conventional dual-targeting CAR T strategies often rely on co-transduction with separate viral vectors, which may lead to large burden of vector integration and increase genotoxicity concerns. To mitigate these risks, our study utilizes a tandem CAR design delivered via a single vector, substantially minimizing potential safety issues.

A caveat of the study is that the patient did not receive a CD19-targeted therapy before CAR T-cell infusion. Although CD19 CAR-T has been approved for the treatment of NHL, up to 30% patients relapse due to antigen loss, mutation, or other reasons. We aim to investigate the efficacy of anti-CD20/CD30 bispecific CAR T-cells in patients who relapse after CD19 CAR T therapy. We also plan to evaluate escalating doses of bispecific CD20/CD30 CAR T-cells in future.

Conclusion remarks

This case report demonstrates the safety and efficacy of CD20/CD30 CAR-T cell therapy in the treatment of transformed follicular lymphoma. Our results provide evidence that bispecific CAR T-cell therapy may be a promising strategy for relapsed and refractory B-cell malignancy. Further research efforts will focus on potential efficacy in patients with heterogenous expression of CD20 and CD30 and with prior CD19-directed CAR T-cell treatment.

Data availability statement

The original contributions presented in the study are included in the article/Supplementary Material. Further inquiries can be directed to the corresponding authors.

Ethics statement

The studies involving humans were approved by Institutional Ethics Committee of the Affiliated Hospital of Nantong University. The studies were conducted in accordance with the local legislation and institutional requirements. The participants provided their written informed consent to participate in this study. Written informed consent was obtained from the individual(s) for the publication of any potentially identifiable images or data included in this article.

Author contributions

YH: Writing – review & editing. YG: Writing – review & editing. XL: Writing – review & editing. HR: Conceptualization, Funding acquisition, Project administration, Resources, Supervision, Writing – original draft. JL: Writing – review & editing. HK: Writing – review & editing. HL: Conceptualization, Funding acquisition, Project administration, Resources, Supervision, Writing – review & editing. HW: Writing – review & editing.

Funding

The author(s) declare that financial support was received for the research and/or publication of this article. This study was supported by Shanghai First Song Therapeutics and grants from the Nantong Health Commission Project (QN2023007).

Acknowledgments

We thank the patient and her family along with the staff at Affiliated Hospital of Nantong University for the participation in this study.

Conflict of interest

The authors disclose the following: HR: Employee of Shanghai First Song Therapeutics; HK-M: Employee of TriArm Inc.; YG, XL, and JL: Employee of TriArm Therapeutics Shanghai.

The remaining authors declare that the research was conducted in the absence of any commercial or financial relationships that could be construed as a potential conflict of interest.

The authors declare that this work received funding from Shanghai First Song Therapeutics. The funder was involved in the preparation of the manuscript.

Generative AI statement

The author(s) declare that no Generative AI was used in the creation of this manuscript.

Publisher's note

Supplementary material

The Supplementary Material for this article can be found online at: https://www.frontiersin.org/articles/10.3389/fimmu.2025.1567149/full#supplementary-material

References

1. Shah BD, Ghobadi A, Oluwole OO, Logan AC, Boissel N, Cassaday RD, et al. Kte-X19 for relapsed or refractory adult B-cell acute lymphoblastic le ukaemia: phase 2 results of the single-arm, open-label, multicentre zu. *Lancet (London England)*. (2021) 398(10299):491–502. doi: 10.1016/S0140-6736(21)01222-8

2. Maude SL, Laetsch TW, Buechner J, Rives S, Boyer M, Bittencourt H, et al. Tisagenlecleucel in children and young adults with B-cell lymphoblastic leukemia. *N Engl J Med*. (2018) 378:439–48. doi: 10.1056/NEJMoa1709866

3. Roddie C, Sandhu KS, Tholouli E, Logan AC, Shaughnessy P, Barba P, et al. Obecabtagene autoleucel in adults with B-cell acute lymphoblastic leukemia. *N Engl J Med*. (2024) 391:2219–30. doi: 10.1056/NEJMoa2406526

4. Neelapu SS, Locke FL, Bartlett NL, Lekakis LJ, Miklos DB, Jacobson CA, et al. Axicabtagene ciloleucel car T-cell therapy in refractory large B-cell lymphoma. *N Engl J Med*. (2017) 377:2531–44. doi: 10.1056/NEJMoa1707447

5. Jacobson CA, Chavez JC, Sehgal AR, William BM, Munoz J, Salles G, et al. Axicabtagene ciloleucel in relapsed or refractory indolent non-hodgkin lymphoma (Zuma-5): A single-arm, multicentre, phase 2 trial. *Lancet Oncol*. (2022) 23:91–103. doi: 10.1016/S1470-2045(21)00591-X

6. Wang M, Munoz J, Goy A, Locke FL, Jacobson CA, Hill BT, et al. Kte-X19 car T-cell therapy in relapsed or refractory mantle-cell lymphoma. *N Engl J Med*. (2020) 382:1331–42. doi: 10.1056/NEJMoa1914347

7. Abramson JS, Palomba ML, Gordon LI, Lunning MA, Wang M, Arnason J, et al. Lisocabtagene maraleucel for patients with relapsed or refractory large B-cell lymphomas (Transcend nhl 001): A multicentre seamless design study. *Lancet*. (2020) 396:839–52. doi: 10.1016/s0140-6736(20)31366-0

8. Morschhauser F, Dahiya S, Palomba ML, Martin Garcia-Sancho A, Reguera Ortega JL, Kuruvilla J, et al. Lisocabtagene maraleucel in follicular

lymphoma: the phase 2 transcend fl study. *Nat Med*. (2024) 30:2199–207. doi: 10.1038/s41591-024-02986-9

9. Schuster SJ, Bishop MR, Tam CS, Waller EK, Borchmann P, McGuirk JP, et al. Tisagenlecleucel in adult relapsed or refractory diffuse large B-cell lymphoma. *N Engl J Med*. (2019) 380:45–56. doi: 10.1056/NEJMoa1804980

10. Fowler NH, Dickinson M, Dreyling M, Martinez-Lopez J, Kolstad A, Butler J, et al. Tisagenlecleucel in adult relapsed or refractory follicular lymphoma: the phase 2 elara trial. *Nat Med*. (2022) 28:325–32. doi: 10.1038/s41591-021-01622-0

11. Di Blasi R, Le Gouill S, Bachy E, Cartron G, Beauvais D, Le Bras F, et al. Outcomes of patients with aggressive B-cell lymphoma after failure of anti-cd19 car T-cell therapy: A descar-T analysis. *Blood*. (2022) 140:2584–93. doi: 10.1182/blood.2022016945

12. Spiegel JY, Patel S, Muffly L, Hossain NM, Oak J, Baird JH, et al. Car T cells with dual targeting of cd19 and cd22 in adult patients with recurrent or refractory B cell Malignancies: A phase 1 trial. *Nat Med*. (2021) 27:1419–31. doi: 10.1038/s41591-021-01436-0

13. Sotillo E, Barrett DM, Black KL, Bagashev A, Oldridge D, Wu G, et al. Convergence of acquired mutations and alternative splicing of cd19 enables resistance to cart-19 immunotherapy. *Cancer Discov*. (2015) 5:1282–95. doi: 10.1158/2159-8290.Cd-15-1020

14. Pan J, Tan Y, Deng B, Tong C, Hua L, Ling Z, et al. Frequent occurrence of cd19-negative relapse after cd19 car T and consolidation therapy in 14 tp53-mutated R/R B-all children. *Leukemia*. (2020) 34:3382–7. doi: 10.1038/s41375-020-0831-z

15. Schneider D, Xiong Y, Wu D, Nölle V, Schmitz S, Haso W, et al. A tandem cd19/cd20 car lentiviral vector drives on-target and off-target antigen modulation in leukemia cell lines. *J Immunother Cancer*. (2017) 5:42. doi: 10.1186/s40425-017-0246-1

16. Plaks V, Rossi JM, Chou J, Wang L, Poddar S, Han G, et al. Cd19 target evasion as a mechanism of relapse in large B-cell lymphoma treated with axicabtagene ciloleucel. *Blood*. (2021) 138:1081–5. doi: 10.1182/blood.2021010930

17. Li P, Liu W, Zhou L, Ye S, Zhu D, Huang J, et al. C-car066, a novel fully human anti-cd20 car-T therapy for relapsed or refractory large B-cell lymphoma after failure of anti-cd19 car-T therapy: A phase I clinical study. *Am J Hematol*. (2024) 99:2306–12. doi: 10.1002/ajh.27488

18. Cheng Q, Tan J, Liu R, Kang L, Zhang Y, Wang E, et al. Cd20-specific chimeric antigen receptor-expressing T cells as salvage therapy in rituximab-refractory/relapsed B-cell non-hodgkin lymphoma. *Cytotherapy*. (2022) 24:1026–34. doi: 10.1016/j.jcyt.2022.05.001

19. Shadman M, Caimi PF, O'Brien SM, Reagan PM, Dezube B, Navaratnarajah P, et al. Efficacy and safety of a third generation cd20 car-T (Mb-106) for treatment of relapsed/refractory indolent B-cell non-hodgkin lymphoma: phase-1 results from a multicenter trial. *Blood*. (2023) 142:2102. doi: 10.1182/blood-2023-175007

20. Shadman M, Yeung C, Redman MW, Yun Lee S, Hoon Lee D, Ra S, et al. P1097: cd20 car-T therapy with mb-106 for btk inhibitor-refractory waldenstrÖm macroglobulinemia (Wm)/lymphoplasmacytic lymphoma (Lpl) – single institution study. *HemaSphere*. (2023) 7:e68877ca. doi: 10.1097/01.HS9.0000971284.68877.ca

21. Shadman M, Yeung C, Redman M, Lee SY, Lee DH, Ra S, et al. S207: efficacy and safety of a third generation cd20 cart (Mb-106) for treatment of relapsed/refractory follicular lymphoma (Fl). *HemaSphere*. (2022) 6:108–9. doi: 10.1097/01.HS9.0000843720.23634.a9

22. Xue F, Zheng P, Yang F, Liu R, Feng S, Guo Y, et al. Salvage cd20-sd-cart therapy in aggressive B-cell lymphoma after cd19 cart treatment failure. *Front Oncol*. (2024) 14:1376490. doi: 10.3389/fonc.2024.1376490

23. Schwab U, Stein H, Gerdes J, Lemke H, Kirchner H, Schaadt M, et al. Production of a monoclonal antibody specific for hodgkin and sternberg-reed cells of hodgkin's disease and a subset of normal lymphoid cells. *Nature*. (1982) 299:65–7. doi: 10.1038/299065a0

24. Horie R, Watanabe T. Cd30: expression and function in health and disease. *Semin Immunol*. (1998) 10:457–70. doi: 10.1006/smim.1998.0156

25. Ramos CA, Ballard B, Zhang H, Dakhova O, Gee AP, Mei Z, et al. Clinical and immunological responses after cd30-specific chimeric antigen receptor-redirected lymphocytes. *J Clin Invest*. (2017) 127:3462–71. doi: 10.1172/jci94306

26. Ramos CA, Grover NS, Beaven AW, Lulla PD, Wu MF, Ivanova A, et al. Anti-cd30 car-T cell therapy in relapsed and refractory hodgkin lymphoma. *J Clin Oncol*. (2020) 38:3794–804. doi: 10.1200/jco.20.01342

27. Sang W, Wang X, Geng H, Li T, Li D, Zhang B, et al. Anti-pd-1 therapy enhances the efficacy of cd30-directed chimeric antigen receptor T cell therapy in patients with relapsed/refractory cd30+ Lymphoma. *Front Immunol*. (2022) 13:858021. doi: 10.3389/fimmu.2022.858021

28. Wang CM, Wu ZQ, Wang Y, Guo YL, Dai HR, Wang XH, et al. Autologous T cells expressing cd30 chimeric antigen receptors for relapsed or refractory hodgkin lymphoma: an open-label phase I trial. *Clin Cancer Res*. (2017) 23:1156–66. doi: 10.1158/1078-0432.Ccr-16-1365

29. Tschernia NP, Heiling H, Deal AM, Cheng C, Babinec C, Gonzalez M, et al. Patient-reported outcomes in cd30-directed car-T cells against relapsed/refractory cd30+ Lymphomas. *J Immunother Cancer*. (2023) 11:e006959. doi: 10.1136/jitc-2023-006959

30. Brudno JN, Natrakul DA, Karrs J, Patel N, Maass-Moreno R, Ahlman MA, et al. Transient responses and significant toxicities of anti-cd30 car T cells for cd30+ Lymphomas: results of a phase 1 trial. *Blood Adv*. (2024) 8:802–14. doi: 10.1182/bloodadvances.2023011470

31. Shah NN, Johnson BD, Schneider D, Zhu F, Szabo A, Keever-Taylor CA, et al. Bispecific anti-cd20, anti-cd19 car T cells for relapsed B cell Malignancies: A phase 1 dose escalation and expansion trial. *Nat Med*. (2020) 26:1569–75. doi: 10.1038/s41591-020-1081-3

32. Tong C, Zhang Y, Liu Y, Ji X, Zhang W, Guo Y, et al. Optimized tandem cd19/cd20 car-engineered T cells in refractory/relapsed B-cell lymphoma. *Blood*. (2020) 136:1632–44. doi: 10.1182/blood.2020005278

33. Schneider D, Xiong Y, Wu D, Hu P, Alabanza L, Steimle B, et al. Trispecific cd19-cd20-cd22-targeting duocar-T cells eliminate antigen-heterogeneous B cell tumors in preclinical models. *Sci Transl Med*. (2021) 13:eabc6401. doi: 10.1126/scitranslmed.abc6401

34. Zhang Y, Wang Y, Liu Y, Tong C, Wang C, Guo Y, et al. Long-term activity of tandem cd19/cd20 car therapy in refractory/relapsed B-cell lymphoma: A single-arm, phase 1–2 trial. *Leukemia*. (2022) 36:189–96. doi: 10.1038/s41375-021-01345-8

35. Zurko JC, Fenske TS, Johnson BD, Bucklan D, Szabo A, Xu H, et al. Long-term outcomes and predictors of early response, late relapse, and survival for patients treated with bispecific lv20.19 car T-cells. *Am J Hematol*. (2022) 97:1580–8. doi: 10.1002/ajh.26718

36. Ghorashian S, Lucchini G, Richardson R, Nguyen K, Terris C, Guvenel A, et al. Cd19/cd22 targeting with cotransduced car T cells to prevent antigen-negative relapse after car T-cell therapy for B-cell all. *Blood*. (2024) 143:118–23. doi: 10.1182/blood.2023020621

37. Li D, Qin J, Zhou T, Li Y, Cheng X, Chen Z, et al. Bispecific gpc3/pd−1 car−T cells for the treatment of hcc. *Int J Oncol*. (2023) 62:53. doi: 10.3892/ijo.2023.5501

38. Zannikou M, Duffy JT, Levine RN, Seblani M, Liu Q, Presser A, et al. Il15 modification enables car T cells to act as a dual targeting agent against tumor cells and myeloid-derived suppressor cells in gbm. *J Immunother Cancer*. (2023) 11:e006239. doi: 10.1136/jitc-2022-006239

39. Hou AJ, Shih RM, Uy BR, Shafer A, Chang ZL, Comin-Anduix B, et al. Il-13rα2/tgf-β Bispecific car-T cells counter tgf-β-mediated immune suppression and potentiate anti-tumor responses in glioblastoma. *Neuro Oncol*. (2024) 26:1850–66. doi: 10.1093/neuonc/noae126

40. Chen N, Pu C, Zhao L, Li W, Wang C, Zhu R, et al. Chimeric antigen receptor T cells targeting cd19 and gcc in metastatic colorectal cancer: A nonrandomized clinical trial. *JAMA Oncol*. (2024) 10:1532–6. doi: 10.1001/jamaoncol.2024.3891

41. Hombach AA, Rappl G, Abken H. Blocking cd30 on T cells by a dual specific car for cd30 and colon cancer antigens improves the car T cell response against cd30(-) tumors. *Mol Ther*. (2019) 27:1825–35. doi: 10.1016/j.ymthe.2019.06.007

42. Gardner LJ, Polski JM, Evans HL, Perkins SL, Dunphy CH. Cd30 expression in follicular lymphoma. *Arch Pathol Lab Med*. (2001) 125:1036–41. doi: 10.5858/2001-125-1036-ceifl

43. Campuzano-Zuluaga G, Cioffi-Lavina M, Lossos IS, Chapman-Fredricks JR. Frequency and extent of cd30 expression in diffuse large B-cell lymphoma and its relation to clinical and biologic factors: A retrospective study of 167 cases. *Leuk Lymphoma*. (2013) 54:2405–11. doi: 10.3109/10428194.2013.778407

44. Hu S, Xu-Monette ZY, Balasubramanyam A, Manyam GC, Visco C, Tzankov A, et al. Cd30 expression defines a novel subgroup of diffuse large B-cell lymphoma with favorable prognosis and distinct gene expression signature: A report from the international dlbcl rituximab-chop consortium program study. *Blood*. (2013) 121:2715–24. doi: 10.1182/blood-2012-10-461848

45. Bartlett NL, Hahn U, Kim WS, Fleury I, Laribi K, Bergua JM, et al. Brentuximab vedotin combination for relapsed diffuse large B-cell lymphoma. *J Clin Oncol*. (2025) 43(9):1061–72. doi: 10.1200/jco-24-02242

46. Jacobsen ED, Sharman JP, Oki Y, Advani RH, Winter JN, Bello CM, et al. Brentuximab vedotin demonstrates objective responses in a phase 2 study of relapsed/refractory dlbcl with variable cd30 expression. *Blood*. (2015) 125:1394–402. doi: 10.1182/blood-2014-09-598763

47. Gauthier J, Bezerra ED, Hirayama AV, Fiorenza S, Sheih A, Chou CK, et al. Factors associated with outcomes after a second cd19-targeted car T-cell infusion for refractory B-cell Malignancies. *Blood*. (2021) 137:323–35. doi: 10.1182/blood.2020006770

48. Holland EM, Molina JC, Dede K, Moyer D, Zhou T, Yuan CM, et al. Efficacy of second car-T (Cart2) infusion limited by poor cart expansion and antigen modulation. *J Immunother Cancer*. (2022) 10:e004483. doi: 10.1136/jitc-2021-004483

49. Dürkop H, Latza U, Hummel M, Eitelbach F, Seed B, Stein H. Molecular cloning and expression of a new member of the nerve growth factor receptor family that is characteristic for hodgkin's disease. *Cell*. (1992) 68:421–7. doi: 10.1016/0092-8674(92)90180-k

50. Higgins JP, Warnke RA. Cd30 expression is common in mediastinal large B-cell lymphoma. *Am J Clin Pathol*. (1999) 112:241–7. doi: 10.1093/ajcp/112.2.241

51. Hutchinson CB, Wang E. Primary mediastinal (Thymic) large B-cell lymphoma: A short review with brief discussion of mediastinal gray zone lymphoma. *Arch Pathol Lab Med*. (2011) 135:394–8. doi: 10.5858/2009-0463-rsr.1

52. Hamieh M, Dobrin A, Cabriolu A, van der Stegen SJC, Giavridis T, Mansilla-Soto J, et al. Car T cell trogocytosis and cooperative killing regulate tumour antigen escape. *Nature*. (2019) 568:112–6. doi: 10.1038/s41586-019-1054-1

53. Hegde M, Corder A, Chow KK, Mukherjee M, Ashoori A, Kew Y, et al. Combinational targeting offsets antigen escape and enhances effector functions of adoptively transferred T cells in glioblastoma. *Mol Ther*. (2013) 21:2087–101. doi: 10.1038/mt.2013.185

54. Larson SM, Walthers CM, Ji B, Ghafouri SN, Naparstek J, Trent J, et al. Cd19/cd20 bispecific chimeric antigen receptor (Car) in naive/memory T cells for the treatment of relapsed or refractory non-hodgkin lymphoma. *Cancer Discov*. (2023) 13:580–97. doi: 10.1158/2159-8290.Cd-22-0964

55. Shalabi H, Qin H, Su A, Yates B, Wolters PL, Steinberg SM, et al. Cd19/22 car T cells in children and young adults with B-all: phase 1 results and development of a novel bicistronic car. *Blood*. (2022) 140:451–63. doi: 10.1182/blood.2022015795

56. Dai H, Wu Z, Jia H, Tong C, Guo Y, Ti D, et al. Bispecific car-T cells targeting both cd19 and cd22 for therapy of adults with relapsed or refractory B cell acute lymphoblastic leukemia. *J Hematol Oncol*. (2020) 13:30. doi: 10.1186/s13045-020-00856-8

57. Zhang Y, Li S, Wang Y, Lu Y, Xu Y, Rao Q, et al. A novel and efficient cd22 car-T therapy induced a robust antitumor effect in relapsed/refractory leukemia patients when combined with cd19 car-T treatment as a sequential therapy. *Exp Hematol Oncol*. (2022) 11:15. doi: 10.1186/s40164-022-00270-5

frontiers | Frontiers in Immunology

TYPE Original Research
PUBLISHED 22 May 2025
DOI 10.3389/fimmu.2025.1579483

OPEN ACCESS

EDITED BY
Michael John Robertson,
Indiana University Bloomington, United States

REVIEWED BY
Xianggui Yuan,
Zhejiang University, China
Derya Koyun,
Ankara University School of Medicine, Türkiye

*CORRESPONDENCE
Lanfang Li
lilanfangmeng@163.com
Xianhuo Wang
tjzlyy_xianhuow@163.com
Huilai Zhang
zhlwgq@126.com

†These authors have contributed equally to this work

RECEIVED 19 February 2025
ACCEPTED 05 May 2025
PUBLISHED 22 May 2025

CITATION
Wang W, Wang B, Sun Y, Qiu L, Qian Z, Zhou S, Song Z, Li W, Li L, Wang X and Zhang H (2025) Clinical outcomes of newly diagnosed PCNSL treated with rituximab-methotrexate-cytarabine with or without ibrutinib: a retrospective study. *Front. Immunol.* 16:1579483. doi: 10.3389/fimmu.2025.1579483

Clinical outcomes of newly diagnosed PCNSL treated with rituximab-methotrexate-cytarabine with or without ibrutinib: a retrospective study

Wenhua Wang[1,2†], Bingyi Wang[1,2†], Yifei Sun[1,2], Lihua Qiu[1,2], Zhengzi Qian[1,2], Shiyong Zhou[1,2], Zheng Song[1,2], Wei Li[1,2], Lanfang Li[1,2*], Xianhuo Wang[1,2*] and Huilai Zhang[1,2*]

[1]State Key Laboratory of Druggability Evaluation and Systematic Translational Medicine, Department of Lymphoma, Tianjin Medical University Cancer Institute and Hospital, National Clinical Research Center for Cancer, Tianjin's Clinical Research Center for Cancer, Tianjin, China, [2]Key Laboratory of Cancer Prevention and Therapy, The Sino-United States Center for Lymphoma and Leukemia Research, Tianjin, China

Objective: This study aimed to evaluate the efficacy and safety of rituximab, methotrexate, cytarabine with or without ibrutinib in newly diagnosed primary central nervous system lymphoma (PCNSL) and explore the correlation between efficacy and genomic alterations.

Methods: From March 2013 to October 2022, data from 88 patients with newly diagnosed PCNSL were retrospectively collected and analyzed. Fifty-nine patients received rituximab, methotrexate and cytarabine (RMA, group A), and twenty-nine patients received the same RMA combined with ibrutinib (RMA + Ibrutinib, group B).

Results: At a median follow-up of 27.7 months, the complete response rate (CRR), overall response rate (ORR) and overall survival (OS) in group B superior to group A (41.4% versus 16.9% for CRR, P=0.013; 86.2% versus 59.3% for ORR, *P*=0.011; P=0.036 for OS). The ORR, progression-free survival (PFS) and OS of RMA + ibrutinib +deep lesions (group C) were better than those of RMA + deep lesions (group D) (*P*=0.027 for ORR, *P*=0.046 for PFS, *P*=0.004 for OS). Patients in group B had no more toxicities than those in group A and the most common adverse events in the two groups were primarily grade 1-2. Sequencing of tumor tissues from 22 patients showed that *MYD88* mutations were the most frequent genetic alterations, two patients with *CARD11* mutation did not respond to treatment and three patients without an *MYD88* or *CD79B* had response after treatment.

Conclusions: RMA in combination with ibrutinib regimen improved response rates and survival in newly diagnosed PCNSL with no serious adverse effects. Mutations in *CARD11* gene may provide directions for patients to select targeted drugs.

KEYWORDS

central nervous system, lymphoma, ibrutinib, retrospective, methotrexate

Introduction

Primary central nervous system lymphoma (PCNSL) is an extranodal non-Hodgkin lymphoma that occurs in the brain, leptomeninges, spinal cord, central nerves and eyes (1). Most PCNSL tumors are nongerminal center B-cell-like (non-GCB) subtypes of diffuse large B-cell lymphoma (DLBCL) (2, 3). PCNSL accounts for less than 1% of all lymphomas, 3% of all central nervous system (CNS) tumors and 4%-6% of all extranodal lymphomas. Immunodeficiency is the primary risk factor for the occurrence of PCNSL (4). In recent years, the incidence of this disease has increased, especially in elderly individuals (5, 6). The treatment of PCNSL includes induction and consolidation therapy, and there are no standard regimens. Multidrug chemotherapy based on high-dose methotrexate (HD-MTX) is usually deemed the standard induction method. Consolidation regimens include autologous stem cell transplantation (ASCT) and whole-brain radiotherapy (WBRT) (7–10). Although therapeutic progress for PCNSL has been achieved, 15%-25% of patients have refractory disease, and 25%-50% of patients relapse after initially having a response (11–13). Notably, elderly individuals are more likely to relapse than others, although age is not a factor in a poor prognosis (14).

Bruton's tyrosine kinase (BTK) is the crucial component linked with the B-cell antigen receptor (BCR), Toll-like receptor (TLR) and nuclear factor kappa B (NF-κB) signaling pathways. Mutations in myeloid differentiation primary response 88 (*MYD88*) and *CD79B* activate the BCR, TLR and NF-κB signaling pathways, disturb the cell cycle, facilitate immune escape, and inhibit B-cell apoptosis (15–17). Compared with systemic DLBCL, alterations in BCR signaling pathways occur more frequently in PCNSL (18). Therefore, BTK is an attractive treatment target for PCNSL. Ibrutinib, a first-in-class BTK inhibitor, has activity in refractory/relapsed (R/R) PCNSL through reducing NF-κB pathway activity (18). Studies have suggested that Ibrutinib has potential efficacy in R/R PCNSL patients (18–20). In addition, ibrutinib has been included in the National Comprehensive Cancer Network (NCCN) guidelines for R/R PCNSL treatment. However, studies on ibrutinib in patients with newly diagnosed PCNSL are rare. In this study, we retrospectively compared and analyzed the efficacy and safety of rituximab-methotrexate-cytarabine with or without ibrutinib in newly diagnosed PCNSL patients to explore whether ibrutinib is beneficial for the first-line treatment of PCNSL and to explore the correlation between efficacy and genomic alterations.

Materials and methods

Patients and treatment

From March 2013 to October 2022, 88 newly diagnosed PCNSL patients from Tianjin Medical University Cancer Institute & Hospital (TMUCIH) were retrospectively enrolled and analyzed. Eighty-eight patients received the two study regimens: rituximab 375 mg/m^2 (intravenous infusion) on day 0, methotrexate 3.5 g/m^2 (0.5 g/m^2 in 15 min, followed by 3 g/m^2 in a six h infusion) on day 1 and cytarabine 1.0 g/m^2 (1 h infusion, every 12 h) on days 2–3 every 28 days, for four cycles in total (RMA; group A), or the same rituximab-methotrexate-cytarabine combined with ibrutinib (560 mg/d) (RMA + Ibrutinib; group B). Ibrutinib was suspended on HD-MTX infusion days and restarted after HD-MTX clearance. Ibrutinib was administered each day uninterruptedly after induction therapy until intolerable toxicity, disease progression or death occurred. After induction therapy, patients received consolidation therapy including thiotepa-containing conditioning regimen and ASCT, followed by maintenance therapy with ibrutinib (560mg/d) or lenalidomide (10mg/d). We defined groups C, D, E and F: group C = deep lesions in R-MA; group D = deep lesions in R-MA + ibrutinib; group E = multiple lesions in R-MA; group F = multiple lesions in R-MA+ ibrutinib. Figure 1 shows the study flowchart. The study was approved by the institutional review board of the Tianjin Medical University Cancer Institute and Hospital. Informed consent was obtained from all patients.

Assessment of efficacy and adverse events

The efficacy of treatment was evaluated according to the International PCNSL Collaborative Group (IPCG) Response Criteria (21). The response was identified by changes in tumor volume on MRI every two cycles and cerebrospinal fluid (CSF) cytology. The best response after treatment was assessed, and the overall response rate (ORR) was calculated, in which the ORR was defined as the sum of patients with a complete response (CR; the disappearance of all lymphoma diseases) and patients with a partial response (PR; 50% or more significant reduction in tumor volume). The total tumor volume was the sum of the disease volume (6 or fewer CNS compartments) calculated by its maximum longitudinal diameter multiplied by its vertical diameter on the same MRI scan. Adverse events (AEs) were recorded via physical examination; laboratory tests such as a hematological panel, plasma biochemical panel and electrocardiograms; and classification of AEs was made following the National Cancer Institute Common Terminology Criteria for Adverse Events (CTCAE, version 5.0) (22).

Sample collection

Baseline tumor samples from 22 patients were analyzed by targeted sequencing of a 307 lymphoma-associated panel. The non-GCB and germinal center B-cell-like (GCB) *Hans's* classification determined subtype.

Statistical analysis

SPSS25 (IBM, Chicago, IL) and R statistical programming environment (v4.0; The R Project for Statistical Computing, Vienna, Austria) software were used for statistical analyses. The χ^2 test or Fisher's exact test was used to compare characteristics and response

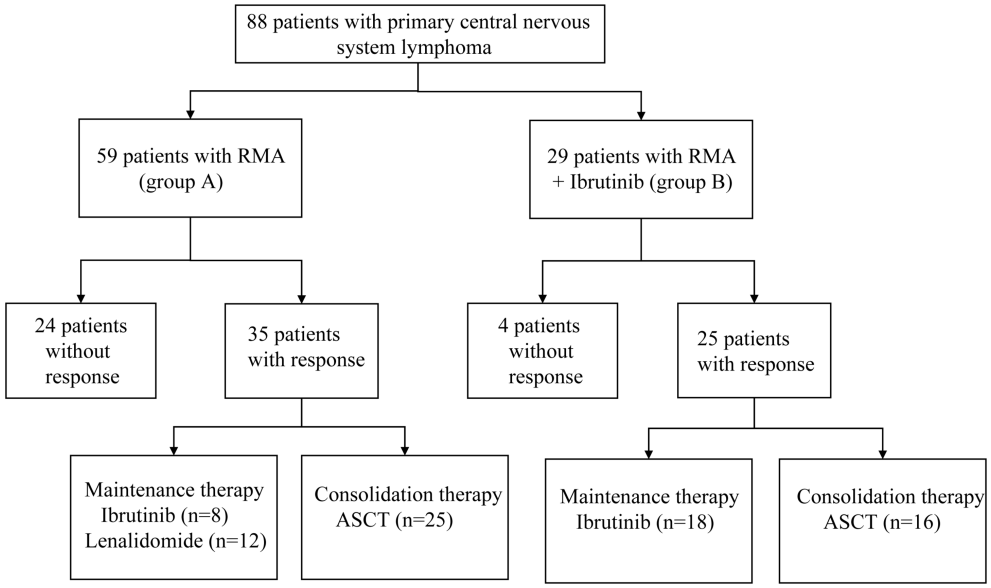

FIGURE 1
This study profile.

rates between therapeutic groups. Mann–Whitney tests were used to compare quantitative and ordinal variables. Progression-free survival (PFS) was calculated as the time from diagnosis to disease progression, death or last follow-up. Overall survival (OS) was calculated as the time from the diagnosis to death or the last follow-up. Survival curves were generated via the Kaplan–Meier method, and comparisons were performed via the log-rank test. All *P* values were two-sided, and $P<0.05$ was considered a significant difference.

Results

Patient population

The clinical and pathological characteristics of the RMA (group A) and RMA + Ibrutinib (group B) groups are shown in Table 1. The median age of the 88 patients was 59 (19-82) years, and 40 (45.5%) patients were male. Forty-two (47.7%) patients had an Eastern Cooperative Oncology Group (ECOG) performance status greater than or equal to 2. Twenty (22.7%) and 12 (13.6%) patients had elevated lactate dehydrogenase (LDH) and β2-microglobulin (β2-MG) levels, respectively. Thirty-four (38.6%) patients had multiple lesions at the first registration, and 47 (53.4%) patients had lesions in deep intracranial areas. The Memorial Sloan–Kettering Cancer Center (MSKCC) risk score was low for 20 (22.7%) patients and high for 14 (15.9%). Sixty-three (71.6%) patients were diagnosed with the non-GCB subtype. Group B had more patients with multiple lesions at the first registration than in group A ($P=0.007$). The groups were well-balanced in terms of patient characteristics, such as age, sex, and ECOG PS, none of which differed significantly between group A and group B.

TABLE 1 Baseline characteristics of patients in the group A and group B.

Characteristics	RMA (group A, n=59)	RMA+ Ibrutinib (group B, n=29)	*p* Value
Age (years)			0.113
≤60	35 (59.3)	12 (41.4)	
>60	24 (40.7)	17 (58.6)	
Sex			0.590
Male	28 (47.5)	12 (41.4)	
Female	31 (52.5)	17 (58.6)	
ECOG PS			0.703
0-1	30 (50.8)	16 (55.2)	
2-4	29 (49.2)	13 (44.8)	
Serum LDH level at diagnosis			0.825
Normal	46 (78.0)	22 (75.9)	
Elevated	13 (22.0)	7 (24.1)	
Serum β2-MG level at diagnosis			0.520
Normal	52 (88.1)	24 (82.8)	
Elevated	7 (11.9)	5 (17.2)	
Lesion at first registration			**0.007**
Single	42 (71.2)	12 (41.4)	
Multiple	17 (28.8)	17 (58.6)	

(Continued)

TABLE 1 Continued

Characteristics	RMA (group A, n=59)	RMA+ Ibrutinib (group B, n=29)	*p* Value
Invasion of deep intracranial areas			0.254
Yes	29 (49.2)	18 (62.1)	
No	30 (50.8)	11 (37.9)	
Pathological subtype			0.260
GCB	19 (32.2)	6 (20.7)	
Non-GCB	40 (67.8)	23 (79.3)	
Bcl-6			0.186
≥50%	44 (74.6)	18 (62.1)	
<50%	6 (10.2)	6 (20.7)	
unknown	9 (15.3)	5 (17.2)	
c-myc			0.625
≥40%	26 (44.1)	18 (62.1)	
<40%	15 (25.1)	8 (27.6)	
unknown	18 (30.5)	3 (10.3)	
MSKCC score (Risk)			0.628
1 (Low)	13 (22.0)	7 (24.1)	
2 (Intermediate)	38 (64.4)	16 (55.2)	
3 (High)	8 (13.6)	6 (20.7)	

RMA, rituximab + methotrexate + cytarabine; ECOG PS, Eastern Cooperative Oncology Group performance status; LDH, lactate dehydrogenase; β2-MG, β2-microglobulin; GCB, germinal B cell-like; MSKCC, Memorial Sloan–Kettering Cancer Center. Bold values: $P < 0.05$.

Treatment responses

All patients completed induction therapy. Twenty-five and 16 patients in Groups A and B underwent ASCT as consolidation therapy, respectively. Within Group A, 12 and 8 patients received lenalidomide and ibrutinib as maintenance therapies, respectively. In contrast, 18 patients in Group B were treated with ibrutinib as a maintenance therapy. Ten (16.9%) patients in group A and 12 (41.4%) patients in group B achieved a CR, with a significantly increased CR rate (CRR) in favor of group B, while 25 (42.4%) patients in group A and 13 (44.8%) patients in group B achieved a PR (Figure 2). The ORR was 59.3% in group A and 86.2% in group B, with a significantly increased ORR in favor of group B (Table 2). In a median follow-up of 27.7 (range 2.5–87.1) months of 88 patients, 36 (40.9%) patients were progression free, 19 (52.8%) of whom were in group A and 17 (47.2%) of whom were in group B. The 2-year PFS rates were 45.1% for group A, 56.7% for group B, and the 3-year OS rates were 56.3% for group A and 75.1% for group B. The median PFS and OS in group A were 18.6 (95% confidence interval (CI): 8.80-28.50) months and 38.7 (95% CI: 33.98-43.48) months, respectively. The median PFS and OS in group B were not reached (Figure 2).

Five (17.2%) patients in R-MA + deep lesions (group C) and 6 (33.3%) patients in R-MA + ibrutinib + deep lesions (group D) achieved a CR, while 12 (41.4) patients in R-MA + deep lesions (group C) and 10 (55.6%) patients in R-MA + ibrutinib + deep lesions (group D) achieved a PR. The ORR was 58.6% in R-MA + deep lesions (group C) and 88.9% in R-MA + ibrutinib + deep lesions (group D), with a significantly increased ORR in favor of R-MA + ibrutinib + deep lesions (group D) (Supplementary Table S1, Supplementary Figure S1). The 2-year PFS rate was 44.8% in R-MA + deep lesions (group C) and 64.9% in R-MA + ibrutinib + deep lesions (group D), with a median PFS of 19.63 (95%CI 12.77-26.49) months for R-MA + deep lesions (group C). The 3-year OS rate was 50.2% in R-MA + deep lesions (group C) and 85.6% in R-MA + ibrutinib + deep lesions (group D), with a median OS of 36.2 (95% CI 16.38-56.02) months for R-MA + deep lesions (group C). The median OS of R-MA + ibrutinib + deep lesions (group D) was not achieved. The PFS and OS in R-MA + ibrutinib + deep lesions (group D) were significantly better than those in R-MA + deep lesions (group C) (Figure 3).

Three (17.6%) of the 17 patients in R-MA + multiple lesions (group E) and 6 (35.3%) of the 17 patients in R-MA + ibrutinib + multiple lesions (group F) achieved a CR, while 7 (41.2%) of the 17 patients in R-MA + multiple lesions (group E) and 8 (47.1%) of the 17 patients in R-MA + ibrutinib + multiple lesions (group F) achieved a PR, with no significant difference between R-MA + multiple lesions (group E) and group F (Supplementary Table S2, Supplementary Figure S1). The 2-year PFS rates were 47.1% in R-MA + multiple lesions (group E) and 57.8% in R-MA + ibrutinib + multiple lesions (group F), with a median PFS of 21.20 (95%CI 2.98-39.43) months for R-MA + multiple lesions (group E). The 3-year OS rates were 63.5% in R-MA + multiple lesions (group E) and 87.5% in R-MA + ibrutinib + multiple lesions (group F), with a median OS of 40.1 (95%CI 33.86-46.28) months for R-MA + multiple lesions (group E). The PFS and OS of R-MA + multiple lesions (group E) and R-MA + ibrutinib + multiple lesions (group F) did not differ significantly (Figure 3).

Adverse events

All 88 patients were included in the AE analysis. The more common AEs in group A and group B included hematological toxicities such as leukopenia (66.1% for group A, 55.2% for group B), anemia (69.5% for group A, 72.4% for group B), thrombocytopenia (64.4% for group A, 62.1% for group B) and nonhematological toxicities such as electrolyte imbalance (37.3% for group A, 44.8% for group B), hepatotoxicity (42.4% for group A, 31.0% for group B), and mucositis (18.6% for group A, 24.1% for group B) (Table 3). Accordingly, the most common hematological and nonhematological toxicities were anemia and electrolyte imbalance, respectively. Notably, nonhematological toxicities were

10.3389/fimmu.2025.1579483

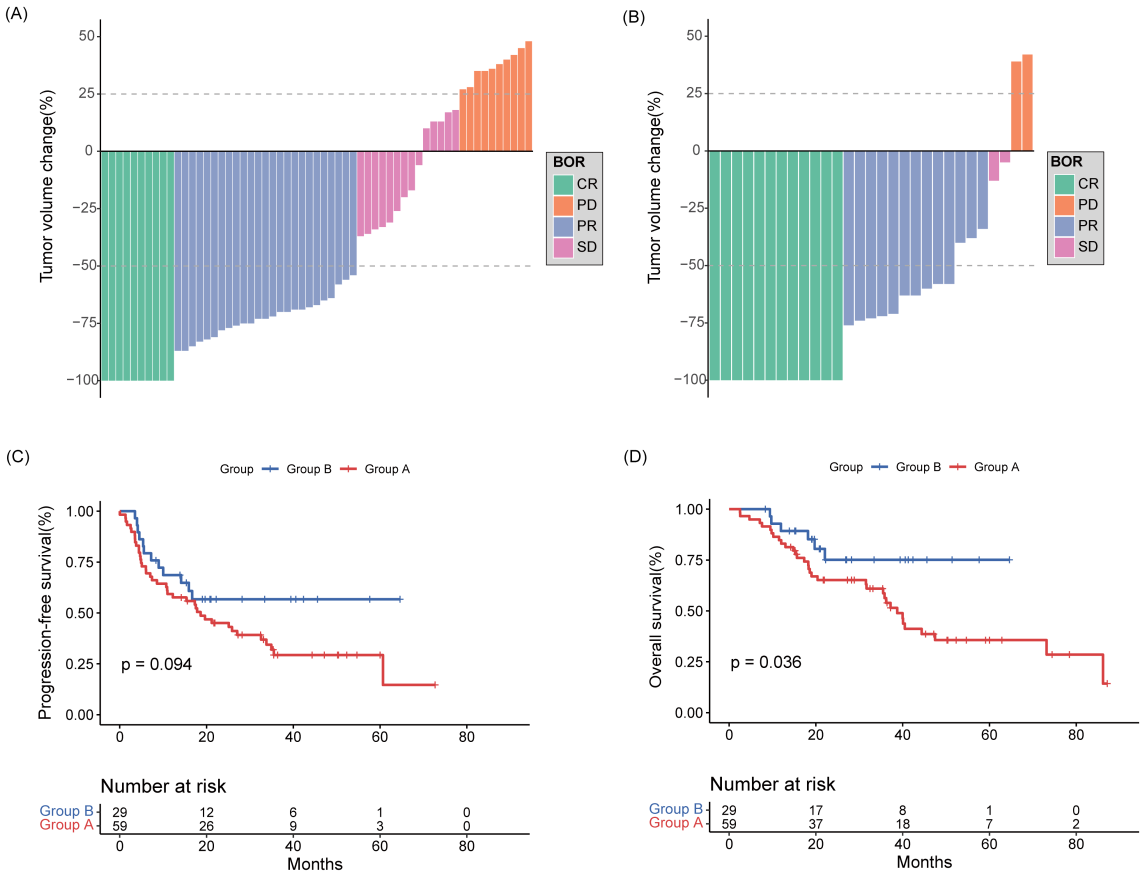

FIGURE 2
Best response to rituximab-methotrexate-cytarabine **(A)** and rituximab-methotrexate-cytarabine plus ibrutinib **(B)**. Percentage change of the total tumor volume from baseline was determined by MRI images. **(C)** Progression-free survival and **(D)** overall survival curves of collected patients divided according to induction treatment group.

mainly grade 1–2 and were usually mild. As expected for ibrutinib, grade 3–4 hepatotoxicity, electrolyte imbalance and digestive tract toxicity were more common in patients treated with R-MA + ibrutinib (group B) but cardiotoxicity was similar in the two groups. Grade 3–4 leukopenia, anemia and thrombocytopenia were increased in the R-MA group (group A) compared with those in the R-MA + ibrutinib group (group B). Treatment-related deaths were not observed in this study. After 2.5–87.1 months of follow-up, Thirty-nine patients died: 32 (82.1%) patients died from progressive disease, 3 (7.7%) from infection, 1 (2.6%) from renal failure, and 3 (7.7%) for unclear reasons.

TABLE 2 Response rate of group A and group B.

Response status	RMA (group A, n=59)	RMA+ Ibrutinib (group B, n=29)	*p* Value
CR	10 (16.9)	12 (41.4)	**0.013**
PR	25 (42.4)	13 (44.8)	0.827
SD	14 (23.7)	2 (6.9)	0.054
PD	10 (16.9)	2 (6.9)	0.323
ORR	35 (59.3)	25 (86.2)	**0.011**

RMA, rituximab + methotrexate + cytarabine; CR, complete response; PR, partial response; SD, stable disease; PD, progressive disease; ORR, overall response rate.
Bold values: $P < 0.05$.

Relationships between clinical efficacy and gene mutations

Sequencing data were available for twenty-two patients in group B, and the gene mutation status was shown in Figure 4. Of the 22 patients, 19 were the non-GCB subtype and 3 were the GCB subtype. *MYD88* (73%) was the most common mutation in primary tumor tissues, followed by the mutation of *PIM1*(64%) and *CD79B* (55%). The predominant type of mutation is of the missense type, and the variant type was mainly single-nucleotide polymorphism (SNP). Among the patients with *MYD88* mutation and *CD79B* mutation, two patients had *CARD11* mutation simultaneously, and these two patients did not respond to treatment. The remaining patients with *MYD88* mutation and *CD79B* mutation all had remission after treatment, and the two patients with *CARD11* mutation did not respond to treatment. Notably, the three patients without an *MYD88* or *CD79B* had response after treatment.

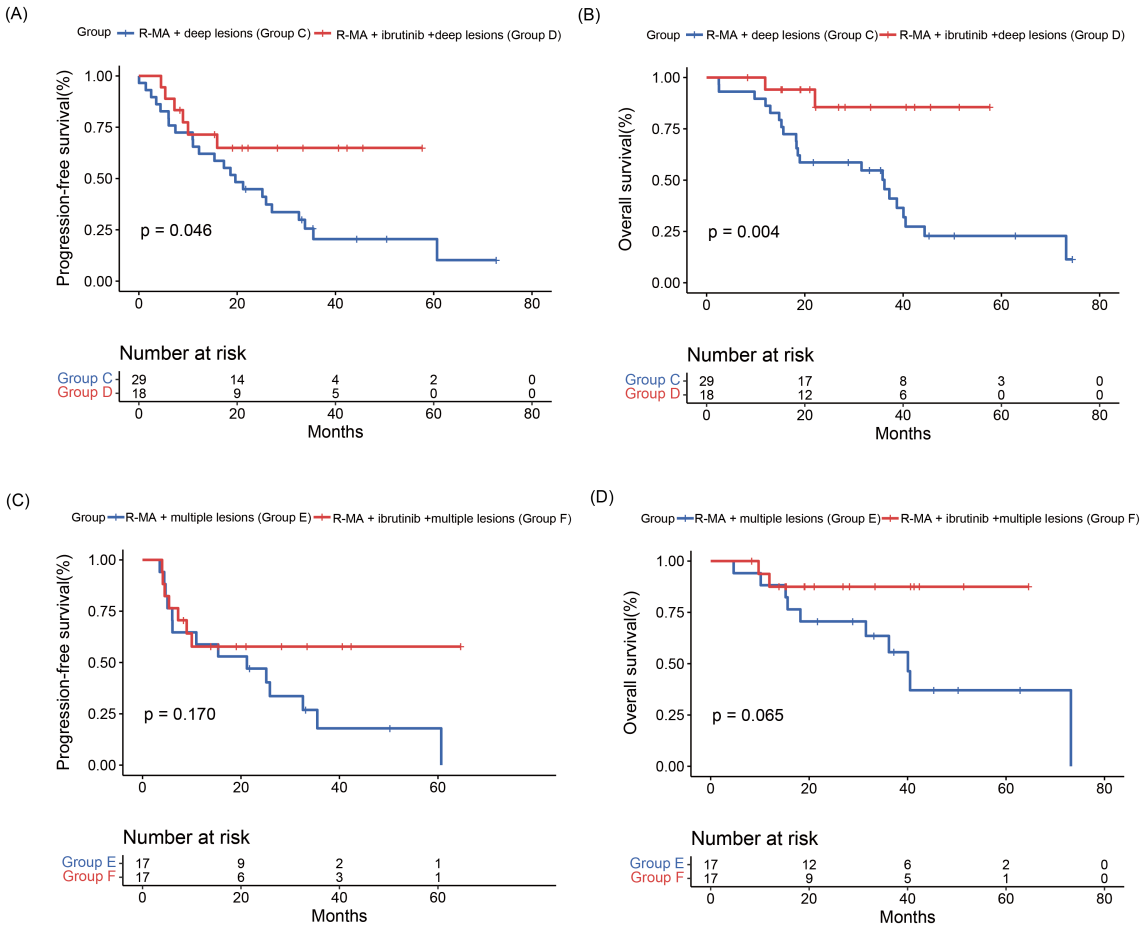

FIGURE 3
(A) Progression-free survival and **(B)** overall survival curves of patients in R-MA + deep lesions (group C) and R-MA + ibrutinib + deep lesions (group D). **(C)** Progression-free survival and **(D)** overall survival curves of patients in R-MA + multiple lesions (group E) and R-MA + ibrutinib + multiple lesions (group F).

Discussion

In recent years, the treatment of PCNSL has developed, and HD-MTX is the backbone of first-line treatment. Multi-drug chemoimmunotherapy regimens containing HD-MTX are considered to have better efficacy. Many researchers have suggested that ibrutinib has better efficacy and safety in patients with relapsed/refractory (R/R) PCNSL (19, 20, 22). However, studies on ibrutinib in newly diagnosed PCNSLs are rare. Therefore, we retrospectively analyzed the efficacy and safety of RMA and RMA plus ibrutinib regimens in newly diagnosed PCNSL patients. The results suggested that the RMA plus ibrutinib regimen increased the CRR, ORR and OS of newly diagnosed patients, and these regimens have better safety profiles in this patient population. More importantly, we found that RMA plus ibrutinib regimen may have better efficacy in the treatment of patients with newly diagnosed PCNSL with invasion of deep intracranial areas.

Marion Alcantara et al. (23) conducted a phase IB/II clinical trial to assess the efficacy and safety of rituximab, methotrexate, procarbazine, vincristine, and prednisone (RMVP) in combination with ibrutinib or lenalidomide for newly diagnosed PCNSL. After four cycles of induction therapy, the ORR for the lenalidomide and ibrutinib groups were 76.9% and 83.3%, respectively. The study observed a total of four dose-limiting toxicities (DLTs): one case of aspergillosis and pneumocystosis, one case of catheter-related infection, and two cases of elevated alanine aminotransferase levels (23). A retrospective study evaluated the efficacy and mutational profiles of HD-MTX combined with zanubrutinib in nineteen newly diagnosed PCNSL patients, the ORR, 2-year PFS and 2-year OS rate were 84.2%, 75.6% and 94.1%, respectively (24). The ORR of nine patients with ASCT as consolidation therapy was 88.9%, and the ORR of 10 patients with zanubrutinib as maintenance therapy was 80%. Chen et al. (25). analyzed data from real-world experience in treating newly diagnosed PCNSL with HD-MTX plus ibrutinib; 9 of 11 (82%) patients achieved a CR or PR, 7 of 11 (64%) patients achieved a CR, and the therapeutic approach was well tolerated. In our study, adding ibrutinib to the RMA combination was correlated with significant increases in the CRR, ORR and OS but not in PFS. The possible reasons for the tendency of the PFS curves to separate are as follows: first, the number of patients in the two treatment groups was inconsistent, and the number of patients in the whole cohort was small. Second, ibrutinib has been available for clinical use only recently, resulting in a limited follow-up time for patients in the RMA plus ibrutinib group. In this

TABLE 3 Main adverse events in group A and group B.

Adverse events	RMA (group A, n=59)			RMA+ Ibrutinib (group B, n=29)			*p* Value
Grade	0	1-2	3-4	0	1-2	3-4	
Hematological							
Leukopenia	20 (33.9)	22 (37.3)	17 (28.8)	13 (44.8)	10 (34.5)	6 (20.7)	0.287
Anemia	18 (30.5)	31 (52.5)	10 (16.9)	8 (27.6)	17 (58.6)	4 (13.8)	0.984
Thrombocytopenia	21 (35.6)	24 (40.7)	14 (23.7)	11 (37.9)	12 (41.4)	6 (20.7)	0.761
Non-hematologic							
Hepatotoxicity	34 (57.6)	23 (39.0)	2 (3.4)	20 (69.0)	7 (24.1)	2 (6.9)	0.400
Nephrotoxicity	48 (81.4)	9 (15.3)	2 (3.4)	22 (75.9)	6 (20.7)	1 (3.4)	0.565
Electrolyte imbalance	37 (62.7)	17 (28.8)	5 (8.5)	16 (55.2)	9 (31.0)	4 (13.8)	0.437
Mucositis	48 (81.4)	9 (15.3)	2 (3.4)	22 (75.9)	6 (20.7)	1 (3.4)	0.565
Digestive tract toxicity	40 (67.8)	17 (28.8)	2 (3.4)	21 (72.4)	6 (20.7)	2 (6.9)	0.753
Infection	48 (81.4)	6 (10.2)	5 (8.5)	26 (89.7)	1 (3.4)	2 (6.9)	0.346
Cardiotoxicity	57 (96.6)	2 (3.4)	0	27 (93.1)	2 (6.9)	0	0.460

RMA, rituximab + methotrexate + cytarabine.

study, the ORR of RMA combined with ibrutinib group was 86.4%, and the 2-year PFS and 3-year OS rates were 56.7% and 75.1%, respectively, similar to previous studies. Notably, the cytarabine dose in this study (1 g/m^2/day × 2 days) is lower than the IELSG32 trial (2 g/m^2/day × 2 days) (9). The CRR and ORR in the R-MA group (16.9% and 54.2%) are notably inferior to those in IELSG32's Arm B (CRR: 30, ORR: 74%). The reduced cytarabine dose possibly contributed to inferior efficacy and poorer outcomes. Several potential factors such as patient selection and supportive care also influence the efficacy and clinical outcomes. Most adverse events in our study were grade 1–2 and mild, consistent with findings of previous studies. More importantly, compared with the RMA regimen, the addition of ibrutinib to RMA was associated with similar toxicities. It is worth noting that, despite similar overall incidence of adverse events between the two groups, the incidence of grade 3–4 hematologic toxicities was higher in the R-MA group (group A) compared to the R-MA + ibrutinib group (group B) (leukopenia, 28.8% vs 20.0%; anemia, 16.9% vs 13.8%; thrombocytopenia, 23.7% vs 20.7%). This suggests that the addition of ibrutinib to the R-MA regimen primarily induces Grade 1–2 hematologic adverse events, which are generally well-tolerated by patients. Those results indicated that RMA plus ibrutinib regimen can increase the CRR, ORR and OS in patients with newly diagnosed PCNSL without additional toxicity.

The IELSG (26) score and Memorial Sloan Kettering Cancer Center (MSKCC) (27) prognostic score are typically used to stratify and evaluate the prognosis of PCNSL. The IELSG score consists of five factors, namely, age, ECOG PS, LDH level, cerebrospinal fluid (CSF) protein level and deep brain invasion, and each factor is worth one point. A score of 0 to 1 corresponds to low risk, 2 to 3 corresponds to intermediate risk, and 4 to 5 corresponds to high risk. The stratification of low, intermediate, and high risk correlates with 2-year survival rates of 80%, 48%, or 15%, respectively (28). The MSKCC score distinguishes three groups according to two factors: age and Karnofsky performance status (KPS). The median OS of PCNSL patients with age ≤ 50 years, age > 50 years and KPS ≥ 70, age ≥ 50 years and KPS < 70 were 8.5, 3.2 and 1.1 months, respectively (27). We analyzed the efficacy of R-MA+ deep lesions (group C) and R-MA+ ibrutinib + deep lesions (group D) and found that R-MA+ ibrutinib + deep lesions (group D) could significantly improve the ORR, PFS and OS of patients. In addition, the comparison of characteristics between the group A and group B revealed a more significant proportion of newly diagnosed PCNSL patients with multiple lesions in the group B. Therefore, we further compared the efficacy of R-MA+ multiple lesions (group E) and R-MA + ibrutinib + multiple lesions (group F) and found that neither the response rates (CR rate, PR rate and ORR) nor the PFS and OS differed significantly between the groups. The possible reason for these negative results is the small number of group patients. However, the above results suggest that combining of RMA and ibrutinib increases the response rates and improves the prognosis of newly diagnosed PCNSL with adverse prognostic factors, such as deep brain involvement. Furthermore, no adjustment for multiple comparisons was performed despite numerous subgroup analyses including deep lesions and multiple lesions, thus the results of the subgroup analyses are exploratory. A large sample and prospective study should be carried out to explore this issue.

In recent years, studies on pathomechanistic genomic alterations have made significant progress. Genomic studies indicate that the emergence of lymphoma is driven mainly by disorders of the TLR, BCR, JAK-STAT and NF-κB signaling pathways, resulting in NF-κB inactivation (29, 30). In addition, the most commonly altered genes in the TLR and BCR signaling pathways are *MYD88*, *CD79B* and *CARD11* (31, 32). Therefore, upstream and downstream inhibitors of NF-κB, such as BTK inhibitors, are considered to inhibit BTK (the important element of BCR signaling) (19, 20). Currently, the molecular mechanisms of known resistance to ibrutinib in CNSL remains insufficiently understood. *CARD11*, a down-stream component of the

10.3389/fimmu.2025.1579483

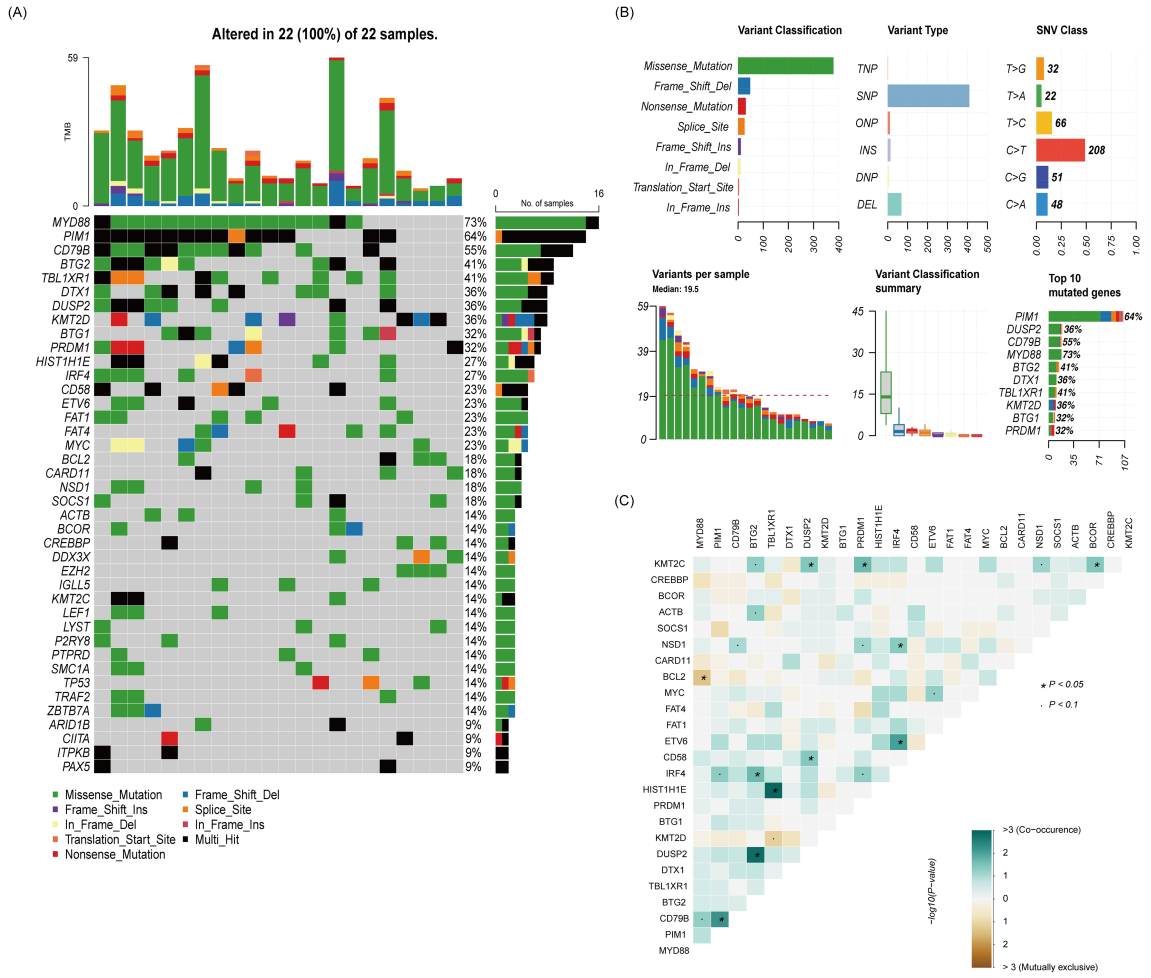

FIGURE 4
The relationship between clinical response and genetic characteristics in 22 patients treated with rituximab-methotrexate-cytarabine plus ibrutinib. **(A)** The gene mutation spectrum. **(B)** The whole picture of the mutation. **(C)** Analysis of gene co-mutation and mutual exclusion.

BCR pathway, has been correlated with resistance to ibrutinib in B-cell malignancies (33, 34). A real-world study of ibrutinib combination therapy in the treatment of newly diagnosed PCNSL was conducted by Chen et al. (25), and the results showed that 9 patients who achieved ORR had mutations in BCR pathway genes (*MYD88*, 77.8%; *CD79B*, 33.3%; *CARD11*, 33.3%). Three patients with *CARD11* mutations also responded to ibrutinib combination therapy. A phase Ib clinical trial was initiated to explore the combination of ibrutinib with HD-MTX and rituximab in patients with CNSL (18). Twelve of 15 (80%) CNSL patients had mutations in ≥1 BCR pathway member (*MYD88*, 53%; *CD79B*, 47%; *CARD11*, 40%; *TNFAIP3*, 7%), 4 of 5 (80%) patients with *CARD11* mutations achieved responses after ibrutinib-based treatment. In addition, patients without detectable mutations in members of the BCR pathway still responded to ibrutinib-based treatment. In our study, fourteen of twenty-two (63.6%) PCNSL patients with a *MYD88* and (or) *CD79B* mutation responded to treatment, whereas four of twenty-two (18.2%) patients with a *CARD11* mutation did not respond to treatment. Therefore, whether *CARD11* is the main factor of ibrutinib resistance still needs further exploration and analysis. Notably, three of twenty-two (13.6%) patients with wild-type *MYD88* and *CD79B* in this study also had remission after treatment, which is consistent with the findings of Chen et al. (25). In PCNSL patients with wild-type *MYD88* and *CD79B*, several mechanisms may still allow for a response to ibrutinib. First, other signaling pathways may compensate for the lack of *MYD88* and *CD79B* mutations. For example, the NF-κB pathway, which is often activated downstream of BCR signaling, may still be active through alternative mechanisms (33). This can lead to ibrutinib sensitivity even in the absence of the typical *MYD88*/*CD79B* mutations. Second, ibrutinib is known to inhibit not only BTK but also other kinases such as ITK and TEC (33). These additional targets may contribute to its therapeutic effect in PCNSL patients, independent of *MYD88* and *CD79B* mutations. In addition, other factors, such as the specific subtype of PCNSL or the characteristics of individuals, may play a role.

We provide *post hoc* power calculation for PFS and OS. For the PFS endpoint, the ORR of RMA + ibrutinib (group B) was better than that of RMA (group A) (P=0.01), and the ORR of RMA + ibrutinib + deep lesions (group D) was superior to that of RMA + deep lesions (group C) ($P < 0.05$). For the OS endpoint, the ORR was similarly higher in RMA + ibrutinib (group B) than in RMA (group A) (P=0.01).

However, there was no significant difference in ORR between RMA + deep lesions (group C) and RMA + ibrutinib + deep lesions (group D) ($P > 0.05$). The results demonstrated that this study was adequately powered to detect clinically meaningful differences.

In general, this study has several limitations. First, our study is a retrospective and small cohort study, and the small number of cases in the subgroup analysis led to significant negative differences between the therapeutic groups. And the treatment allocation was non-randomized, potentially introducing selection bias such as group B had more patients with multiple lesions (P=0.007). This baseline imbalance can mask the true differences in efficacy between RMA (group A) and RMA + ibrutinib (group B). Even if a treatment has potential benefits for all patients, the presence of more severe patients in group B may make the efficacy differences between the groups appear less significant. Second, the follow-up time of the group B was shorter, and the follow-up times of the group A and group B differed. Third, sequencing data are available for twenty-two patients, and the data of some patients are incomplete. Therefore, only a simple descriptive analysis can be conducted on the basis of the sequencing data; it is impossible to analyze the whole genomic characteristics of PCNSL and the relationship with therapeutic effects owing to the absence of large-scale sequencing data.

In conclusion, our retrospective study indicated that the addition of ibrutinib to RMA can clinically benefit newly diagnosed PCNSL patients and may improve the prognosis of PCNSL with adverse prognostic factors. On the basis of these results, we propose several exploratory analyses, such as the possibility that patients without mutations in BCR pathway members may respond to ibrutinib-based combination therapy through other mechanisms. However, studies with many patients and prospective clinical trials are needed to confirm these findings.

Data availability statement

The raw data supporting the conclusions of this article will be made available by the authors, without undue reservation.

Ethics statement

The studies involving humans were approved by The institutional review board of the Tianjin Medical University Cancer Institute and Hospital. The studies were conducted in accordance with the local legislation and institutional requirements. Written informed consent for participation in this study was provided by the participants' legal guardians/next of kin.

Author contributions

WW: Formal analysis, Writing – original draft. BW: Data curation, Writing – review & editing. YS: Data curation, Writing – review & editing. LQ: Data curation, Writing – review & editing. ZQ: Data curation, Writing – review & editing. SZ: Data curation, Writing – review & editing. ZS: Data curation, Writing – review & editing. WL: Data curation, Formal analysis, Writing – review & editing. LL: Conceptualization, Funding acquisition, Writing – review & editing. XW: Supervision, Writing – review & editing. HZ: Conceptualization, Supervision, Writing – review & editing.

Funding

The author(s) declare that financial support was received for the research and/or publication of this article. This study was supported by CACA-BeiGene Lymphoma Research Foundation (CORP-117), State Key Laboratory of Druggability Evaluation and Systematic Translational Medicine (QZ23-6; QZ23-4), Haihe Yingcai (Tianjin) Project (TJSJMYXYC-D2-039) and Tianjin Key Medical Discipline (Specialty) Construction Project grant (TJYXZDXK-009A).

Acknowledgments

We thank the Department of Pathology of Tianjin Medical University Cancer Institute and Hospital for providing pathological diagnosis.

Conflict of interest

The authors declare that the research was conducted in the absence of any commercial or financial relationships that could be construed as a potential conflict of interest.

The author(s) declared that they were an editorial board member of Frontiers, at the time of submission. This had no impact on the peer review process and the final decision.

Generative AI statement

The author(s) declare that no Generative AI was used in the creation of this manuscript.

Publisher's note

Supplementary material

The Supplementary Material for this article can be found online at: https://www.frontiersin.org/articles/10.3389/fimmu.2025.1579483/full#supplementary-material

SUPPLEMENTARY FIGURE 1
Best response of patients in R-MA + deep lesions (group C) **(A)** or R-MA + ibrutinib + deep lesions (group D) **(B)**. Best response of patients in R-MA + multiple lesions (group E) **(C)** or R-MA + ibrutinib + multiple lesions (group F) **(D)**.

References

1. Ferreri AJM, Calimeri T, Cwynarski K, Dietrich J, Grommes C, Hoang-Xuan K, et al. Primary central nervous system lymphoma. *Nat Rev Dis Primers*. (2023) 9:29. doi: 10.1038/s41572-023-00439-0

2. Deckert M, Engert A, Brück W, Ferreri AJ, Finke J, Illerhaus G, et al. Modern concepts in the biology, diagnosis, differential diagnosis and treatment of primary central nervous system lymphoma. *Leukemia*. (2011) 25:1797–807. doi: 10.1038/leu.2011.169

3. Batchelor T, Carson K, O'Neill A, Grossman SA, Alavi J, New P, et al. Treatment of primary CNS lymphoma with methotrexate and deferred radiotherapy: a report of NABTT 96-07. *J Clin Oncol*. (2003) 21:1044–9. doi: 10.1200/JCO.2003.03.036

4. Hoang-Xuan K, Deckert M, Ferreri AJM, Furtner J, Gallego Perez-Larraya J, Henriksson R, et al. European Association of Neuro-Oncology (EANO) guidelines for treatment of primary central nervous system lymphoma (PCNSL). *Neuro Oncol*. (2023) 25:37–53. doi: 10.1093/neuonc/noac196

5. van der Meulen M, Dinmohamed AG, Visser O, Doorduijn JK, Bromberg JEC. Improved survival in primary central nervous system lymphoma up to age 70 only: a population-based study on incidence, primary treatment and survival in the Netherlands, 1989-2015. *Leukemia*. (2017) 31:1822–5. doi: 10.1038/leu.2017.128

6. Mendez JS, Ostrom QT, Gittleman H, Kruchko C, DeAngelis LM, Barnholtz-Sloan JS, et al. The elderly left behind-changes in survival trends of primary central nervous system lymphoma over the past 4 decades. *Neuro Oncol*. (2018) 20:687–94. doi: 10.1093/neuonc/nox187

7. Ferreri AJM, Cwynarski K, Pulczynski E, Fox CP, Schorb E, Celico C, et al. Long-term efficacy, safety and neurotolerability of MATRix regimen followed by autologous transplant in primary CNS lymphoma: 7-year results of the IELSG32 randomized trial. *Leukemia*. (2022) 36:1870–8. doi: 10.1038/s41375-022-01582-5

8. Schorb E, Fox CP, Kasenda B, Linton K, Martinez-Calle N, Calimeri T, et al. Induction therapy with the MATRix regimen in patients with newly diagnosed primary diffuse large B-cell lymphoma of the central nervous system - an international study of feasibility and efficacy in routine clinical practice. *Br J Haematol*. (2020) 189:879–87. doi: 10.1111/bjh.16451

9. Ferreri AJ, Cwynarski K, Pulczynski E, Ponzoni M, Deckert M, Politi LS, et al. Chemoimmunotherapy with methotrexate, cytarabine, thiotepa, and rituximab (MATRix regimen) in patients with primary CNS lymphoma: results of the first randomisation of the International Extranodal Lymphoma Study Group-32 (IELSG32) phase 2 trial. *Lancet Haematol*. (2016) 3:e217–27. doi: 10.1016/S2352-3026(16)00036-3

10. Fox CP, Phillips EH, Smith J, Linton K, Gallop-Evans E, Hemmaway C, et al. Guidelines for the diagnosis and management of primary central nervous system diffuse large B-cell lymphoma. *Br J Haematol*. (2019) 184:348–63. doi: 10.1111/bjh.15661

11. Houillier C, Soussain C, Ghesquières H, Soubeyran P, Chinot O, Taillandier L, et al. Management and outcome of primary CNS lymphoma in the modern era: An LOC network study. *Neurology*. (2020) 94:e1027–e39. doi: 10.1212/WNL.0000000000008900

12. Houillier C, Taillandier L, Dureau S, Lamy T, Laadhari M, Chinot O, et al. Radiotherapy or autologous stem-cell transplantation for primary CNS lymphoma in patients 60 years of age and younger: results of the intergroup ANOCEF-GOELAMS randomized phase II PRECIS study. *J Clin Oncol*. (2019) 37:823–33. doi: 10.1200/JCO.18.00306

13. Ambady P, Holdhoff M, Bonekamp D, Wong F, Grossman SA. Late relapses in primary CNS lymphoma after complete remissions with high-dose methotrexate monotherapy. *CNS Oncol*. (2015) 4:393–8. doi: 10.2217/cns.15.34

14. Langner-Lemercier S, Houillier C, Soussain C, Ghesquières H, Chinot O, Taillandier L, et al. Primary CNS lymphoma at first relapse/progression: characteristics, management, and outcome of 256 patients from the French LOC network. *Neuro Oncol*. (2016) 18:1297–303. doi: 10.1093/neuonc/now033

15. Chen R, Zhou D, Wang L, Zhu L, Ye X. MYD88(L265P) and CD79B double mutations type (MCD type) of diffuse large B-cell lymphoma: mechanism, clinical characteristics, and targeted therapy. *Ther Adv Hematol*. (2022) 13:20406207211072839. doi: 10.1177/20406207211072839

16. Schaff L, Nayak L, Grommes C. Bruton's tyrosine kinase (BTK) inhibitors for the treatment of primary central nervous system lymphoma (PCNSL): current progress and latest advances. *Leuk Lymphoma*. (2024) 65:882–94. doi: 10.1080/10428194.2024.2333985

17. Lionakis MS, Dunleavy K, Roschewski M, Widemann BC, Butman JA, Schmitz R, et al. Inhibition of B cell receptor signaling by ibrutinib in primary CNS lymphoma. *Cancer Cell*. (2017) 31:833–43.e5. doi: 10.1016/j.ccell.2017.04.012

18. Grommes C, Tang SS, Wolfe J, Kaley TJ, Daras M, Pentsova EI, et al. Phase 1b trial of an ibrutinib-based combination therapy in recurrent/refractory CNS lymphoma. *Blood*. (2019) 133:436–45. doi: 10.1182/blood-2018-09-875732

19. Soussain C, Choquet S, Blonski M, Leclercq D, Houillier C, Rezai K, et al. Ibrutinib monotherapy for relapse or refractory primary CNS lymphoma and primary vitreoretinal lymphoma: Final analysis of the phase II 'proof-of-concept' iLOC study by the Lymphoma study association (LYSA) and the French oculo-cerebral lymphoma (LOC) network. *Eur J Cancer*. (2019) 117:121–30. doi: 10.1016/j.ejca.2019.05.024

20. Grommes C, Pastore A, Palaskas N, Tang SS, Campos C, Schartz D, et al. Ibrutinib unmasks critical role of bruton tyrosine kinase in primary CNS lymphoma. *Cancer Discovery*. (2017) 7:1018–29. doi: 10.1158/2159-8290.CD-17-0613

21. Abrey LE, Batchelor TT, Ferreri AJ, Gospodarowicz M, Pulczynski EJ, Zucca E, et al. Report of an international workshop to standardize baseline evaluation and response criteria for primary CNS lymphoma. *J Clin Oncol*. (2005) 23:5034–43. doi: 10.1200/JCO.2005.13.524

22. Freites-Martinez A, Santana N, Arias-Santiago S, Viera A. Using the common terminology criteria for adverse events (CTCAE - version 5.0) to evaluate the severity of adverse events of anticancer therapies. *Actas Dermosifiliogr (Engl Ed)*. (2021) 112:90–2. doi: 10.1016/j.ad.2019.05.009

23. Alcantara M, Chevrier M, Jardin F, Schmitt A, Houillier C, Oberic L, et al. Phase IB part of LOC-R01, a LOC network non-comparative randomized phase IB/II study testing R-MPV in combination with escalating doses of lenalidomide or ibrutinib for newly diagnosed primary central nervous system lymphoma (PCNSL) patients. *J Hematol Oncol*. (2024) 17:86. doi: 10.1186/s13045-024-01606-w

24. Wang N, Chen FL, Pan L, Teng Y, Wei XJ, Guo HG, et al. Clinical outcomes of newly diagnosed primary central nervous system lymphoma treated with zanubrutinib-based combination therapy. *World J Clin Oncol*. (2023) 14:606–19. doi: 10.5306/wjco.v14.i12.606

25. Chen F, Pang D, Guo H, Ou Q, Wu X, Jiang X, et al. Clinical outcomes of newly diagnosed primary CNS lymphoma treated with ibrutinib-based combination therapy: A real-world experience of off-label ibrutinib use. *Cancer Med*. (2020) 9:8676–84. doi: 10.1002/cam4.3499

26. Ferreri AJ, Blay JY, Reni M, Pasini F, Spina M, Ambrosetti A, et al. Prognostic scoring system for primary CNS lymphomas: the International Extranodal Lymphoma Study Group experience. *J Clin Oncol*. (2003) 21:266–72. doi: 10.1200/JCO.2003.09.139

27. Abrey LE, Ben-Porat L, Panageas KS, Yahalom J, Berkey B, Curran W, et al. Primary central nervous system lymphoma: the Memorial Sloan-Kettering Cancer Center prognostic model. *J Clin Oncol*. (2006) 24:5711–5. doi: 10.1200/JCO.2006.08.2941

28. Grommes C, DeAngelis LM. Primary CNS lymphoma. *J Clin Oncol*. (2017) 35:2410–8. doi: 10.1200/JCO.2017.72.7602

29. Braggio E, Van Wier S, Ojha J, McPhail E, Asmann YW, Egan J, et al. Genome-wide analysis uncovers novel recurrent alterations in primary central nervous system lymphomas. *Clin Cancer Res*. (2015) 21:3986–94. doi: 10.1158/1078-0432.CCR-14-2116

30. Nayyar N, White MD, Gill CM, Lastrapes M, Bertalan M, Kaplan A, et al. MYD88 L265P mutation and CDKN2A loss are early mutational events in primary central nervous system diffuse large B-cell lymphomas. *Blood Adv*. (2019) 3:375–83. doi: 10.1182/bloodadvances.2018027672

31. Bödör C, Alpár D, Marosvári D, Galik B, Rajnai H, Bátai B, et al. Molecular subtypes and genomic profile of primary central nervous system lymphoma. *J Neuropathol Exp Neurol*. (2020) 79:176–83. doi: 10.1093/jnen/nlz125

32. Radke J, Ishaque N, Koll R, Gu Z, Schumann E, Sieverling L, et al. The genomic and transcriptional landscape of primary central nervous system lymphoma. *Nat Commun*. (2022) 13:2558. doi: 10.1038/s41467-022-30050-y

33. Wilson WH, Young RM, Schmitz R, Yang Y, Pittaluga S, Wright G, et al. Targeting B cell receptor signaling with ibrutinib in diffuse large B cell lymphoma. *Nat Med*. (2015) 21:922–6. doi: 10.1038/nm.3884

34. Wu C, de Miranda NF, Chen L, Wasik AM, Mansouri L, Jurczak W, et al. Genetic heterogeneity in primary and relapsed mantle cell lymphomas: Impact of recurrent CARD11 mutations. *Oncotarget*. (2016) 7:38180–90. doi: 10.18632/oncotarget.9500

Frontiers in Immunology

Explores novel approaches and diagnoses to treat immune disorders.

The official journal of the International Union of Immunological Societies (IUIS) and the most cited in its field, leading the way for research across basic, translational and clinical immunology.

Discover the latest Research Topics

See more →

Frontiers

Avenue du Tribunal-Fédéral 34
1005 Lausanne, Switzerland
frontiersin.org

Contact us

+41 (0)21 510 17 00
frontiersin.org/about/contact